Topology in finite chiral structures

Thesis submitted for doctor of philosophy degree

The University of Sheffield,
Department of Physics and Astronomy

Maxine Maryam McCarthy

May 2024

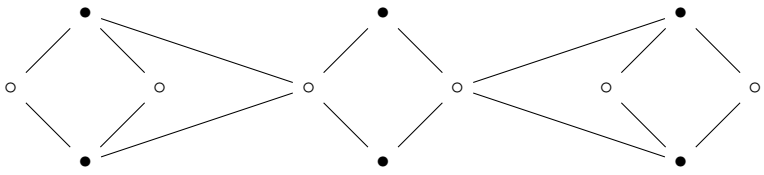

To Georgie, the eccentric and excitable dog
we lost at the beginning of my PhD.
Love you and miss you.

Abstract

Topological phenomena in solid state physics are conventionally studied under the assumption of an infinite or large system. This allows the study of topological properties of the bulk, which may be related to observable phenomena with the bulk-boundary correspondence. This has resulted in the very successful prediction of a large variety of unusual and novel phases in such systems. Due to their topological nature, boundary properties of such phases are resistant to disorder, however this is only exact in the infinite limit. For a finite structure there is a finite disorder where boundary phenomena are lost. We study exact topological properties in finite chiral structures, where we wish to allow arbitrary continuous hopping disorder. Our methods allow for studying topology where the bulk-boundary correspondence no longer holds. In particular, we study topological protection and topological phase transitions in such finite media. We propose a definition of topological protection when topologically robust states are not protected by a bulk. We then go on to study topological phase transitions and reveal a rich classification in finite chiral structures when allowing for arbitrary continuous hopping disorder. Allowing some hopping terms to be constrained, we then study sequences of topological phase transitions, where the number of states which close around a gap are iteratively increased. Throughout our work we experimentally verify some of our predictions using a flexible coaxial cable platform to create arbitrary real tight binding Hamiltonians. First we demonstrate this platform by experimentally observing topological protection and a phase transition in a Su-Schrieffer-Heeger chain. We also demonstrate a deep connection between the localisation properties of a topologically marginal finite chiral structure, nut graphs, and core graphs and study nut graphs experimentally, giving an experimental observation of omni-conduction.

Acknowledgements

I don't think I really had an exact understanding of what a PhD would be like before I began. It has been difficult, and came with a lot of emotional ups and downs, but it was also exciting, and deeply fulfilling, and I am sad that it is soon coming to an end. I wouldn't trade these last few years for anything.

I couldn't have done this without the help of my family and friends who have always been there throughout my PhD. There are so many people I want to thank for their help on this journey, and many I haven't had the space to name here, but I am enormously grateful to you too.

First and foremost I wish to thank my supervisor David Whittaker, who has helped guide me on my first scientific path, and through showing me how to question and think like a scientist, how to get back on this path when wandering too close to the shadows. I have learned so much from you David! You have shown me what it truly means to try and understand physics, and for this I will always be grateful.

I want to thank those who have been here for me throughout this journey – when I started in 2020, during the pandemic. I remember the first time I met people from the office in April that year, it was quite nerve-wracking, but once I met the residents of E13a, I knew I didn't need to be nervous. Thank you for making the office such an inclusive and welcoming place!

I have many fond memories of my time in E13a. From our tour of interesting different foods, to the many chips at the University Arms, and watching the sunset on even the cloudiest and coldest of days but feeling an inner peace and calm that comes with it, and for just being such a supportive network that I felt I could endlessly rely on (and still do) thank you, Elena Callus, Armanda Quintavalle, Marta Marchese, and Alice Cullen.

The office has continued to support my attempts to try and do physics, and I don't know what I would have done without you all! I am endlessly grateful to those who have been there for me during the final parts of my PhD – Ben Kinvig, Subhrajit Modak, Mateusz Duda, and Benny Kuo.

Thank you also to Patrick Fowler and Barry Pickup, who showed me a wonderful side of chemistry, and introduced me to the beautiful and absorbing world of graphs! I will never forget the many enjoyable moments we had discussing graph theory.

My work would also have not been possible without the help of my wonderful and expert experimentalist collaborator – Qingqing Duan – you taught me what it means to do an experiment, and I really loved our conversations while making and measuring coaxial cable networks. Our experiments always seemed to run better when we were working together! I also wish to extend my deep gratitude to Belle Darling and Phillip Graham who always managed to find space for us to run so many experiments.

And of course I want to thank my family, who decided I have been doing a 'PhD in shapes'. Your endless support and love, especially when times have been tough, have really made this all possible.

None of this would have been possible without any of you. Your kindness, your friendship, and your support has been the true topological invariant during my PhD. I don't know what I would have done without you.

Declaration

I, Maxine M. McCarthy, declare that I am the sole author of this thesis, and the results in this thesis are largely my own. Anywhere I present results from others I reference this appropriately in this work.

Publications and conferences

Much of this work is based on results detailed on the following publications:

1. D. M. Whittaker, Maxine M. McCarthy, and Qingqing Duan, "Observation of a Topological Phase Transition in Random Coaxial Cable Structures with Chiral Symmetry". In: *arXiv:2311.11040* (2023). `https://arxiv.org/abs/2311.11040`
2. Patrick W. Fowler, Maxine M. McCarthy, Barry T. Pickup, and D. M. Whittaker, "Topologically protected nullity in weighted graphs". Under preparation.
3. Maxine M. McCarthy, and D. M. Whittaker, "A Topological Classification of Finite Chiral Structures using Complete Matchings". Submitted to arXiv, (2024).
4. Maxine M. McCarthy, D. M. Whittaker, Patrick W. Fowler, and Barry T. Pickup, "Experimental realisation of nut graphs with coaxial cable networks". Under preparation.

And have been discussed at the following conferences and events:

1. Maxine M. McCarthy, and D. M. Whittaker, "Topological Physics in Finite Graphene Structures: Theory and Experiment", talk, CMD29 (2022).
2. Maxine M. McCarthy, and D. M. Whittaker, "A topological classification of finite chiral structures – theory and experiment", talk, CMQM 2023 (2023).
3. Maxine M. McCarthy, and D. M. Whittaker, "Measuring spectral properties of nut graphs with coaxial cable networks", talk, IWONT 2023 (2023).
4. Maxine M. McCarthy, and D. M. Whittaker, "The emergence of topological phases and protected states in finite chiral structures", talk, CMD30 (2023).
5. Maxine M. McCarthy, and D. M. Whittaker, "Counting topological phases in finite chiral structures", talk, Northem Quantum Meeting IX (2023).
6. Maxine M. McCarthy, and D. M. Whittaker, "A physically motivated topological classification of weighted bipartite graphs", talk, NetSciX 2024 (2024).

Contents

Chapter 1

Introduction

1.1 Topology and physics

Topology is the study of properties of shapes and spaces that are invariant under continuous deformation. Topology has a long history in physics. One of the first applications of topology to physics was an attempt to understand the (at the time, thought to be immutable) elements of the periodic table [1] by modelling atoms as mathematical knots. (Rather wonderfully non-trivial knots have now been realised in an atomic system [2]). There are many applications of topology to physics: any physical system whose description lives in a parameter space may have interesting topological properties. Remarkably changes in topological properties of a space describing a physical system can alter observable physical phenomena, giving rise to topological phase transitions.

In solid state physics, topology is most often used to study how properties of the bulk alter physics at the boundary of a material. This has led to a wonderful and weird set of materials which have gapless boundary modes [3], whose propagation may be protected [4], can be superconducting [5], and may provide a robust platform for quantum computating [6], all despite a possibly gapped bulk.

Excitement in topological phenomena has been enhanced by an often fast paced interaction between theory and experiment. For instance, the quantum Hall effect was predicted in 1975 [7] and found experimentally in 1978 [8] before it was discovered to be topological in 1982 [9]. More recently the quantum spin Hall effect was predicted in 2005 [10] and experimentally found just 2 years later in 2007 [11].

Underpinning topological phenomena, are equivalence classes of Hamiltonians which define distinct topological phases. Materials that host a number of topological phases are surprisingly common, with around 90% of all materials in the Bilboa material database predicted to have non-trivial topological phases [12–14].

It is an exciting time to see the developments in topological physics.

1.2 Outline of thesis

Many topological phenomena are described by the bulk-boundary correspondence [15] which relates topological indices associated to an infinitely periodic crystal to observable physics on the boundary of a material. This allows topological phenomena to be predicted with topological indices in the bulk or (for example) using local real space markers that, via unit cell averaging, predict topologically non-trivial properties of the bulk [16, 17]. Boundary properties are generally asymptotic to the thermodynamic limit [18] so that in finite structures, there is a finite disorder at which boundary properties are not retained [19]. This opens up the question of what is topology in structures which, under significant disorder or an unusual network topology, have effectively lost the bulk boundary correspondence?

At low disorder non-trivial topology is still well predicted with a bulk-boundary correspondence in even quite small structures [20, 21], and no matter the size of a structure, use of a periodic supercell [22, 23] can be used to predict topological phase transitions in disordered finite media, so long as they occur at zero momentum. This means the bulk-boundary approach may still be used in finite structures, but phenomena are sometimes made opaque: there may be fewer topological phases than predicted with a bulk calculation, or there may be more topologically distinct phases which have the same bulk index. This motivates a completely finite approach, where distinct topological phases are defined using the finite structure alone.

In this thesis we study exact finite topological phenomena in structures with arbitrary hopping disorder, that have chiral symmetry. We then experimentally verify some of our predictions using a coaxial cable network as a platform for tight binding structures.

We begin in chapter 2 where we discuss literature relating to our work and give a discussion of the theoretical and experimental background to this thesis. In chapter 3 we give an experimental study of topological physics in coaxial cable networks, and experimentally observe a topological phase transition and topological protection in the Su-Schrieffer-Heeger model [24].

In chapter 4 we propose a definition for topologically protected states in finite media, where topology of the bulk does not provide topological protection. We then discuss some physical properties of such states and relate these to the network topology of the underlying structure, as well as experimentally verify such topological protection in a small graphene structure.

We propose a classification of topological phases in finite chiral structures in chapter 5, as well as predict a set of physical consequences in the localisation of zero energy states. Using such consequences, we demonstrate a deep connection between finite topological phase transitions and nut graphs, and experimentally verify our classification in graphene.

We then demonstrate an experimental realisation of nut graphs in chapter 6 and confirm a prediction of the transport properties of nut graphs.

Finally, we discuss the topology of finite structures where we start to allow constrained hopping terms, and study topological phenomena with an increasing number of zero energy states. We uncover (up to a few simple considerations) a universal sequence of phase

transitions, which correspond to novel localisation phenomena. Using this localisation we then experimentally confirm this sequence in a coaxial cable network.

In chapter 8 we conclude and give an outlook on potential future work.

1.3 Notation and definitions guide

Notation	Meaning	Definition
$A \cup B$	The union of two sets A, B	-
$A \cap B$	The intersection of the sets A, B	-
$A \setminus B$	The set A excluding any point also in B	-
$A \subset B$	The set A is a subset of B	-
$A \hookrightarrow B$	An embedding/inclusion from $A \to B$ such that $A \subset B$	-
$A \to B$	A map from the set A to the set B	-
$\lvert \cdot \rvert$	The determinant, or absolute value	-
$\mathrm{Sign}(\cdot)$	The sign of a number	-
G	An unweighted graph	2.1.3
H	Tight binding Hamiltonian defined on a graph G	2.1.5
g	An induced[a] subgraph g of G	2.1.9
h	A Hamiltonian on a subgraph g of G	-
A	The adjacency matrix of a graph G	2.1.4
Q	The biadjacency matrix of a bipartite graph G	2.1.6
q	The biadjacency matrix of a bipartite induced subgraph g	-
$[H]$	An equivalence class of tight binding Hamiltonians H	-
ε	An energy eigenvalue of a tight binding Hamiltonian	-
ω	Coaxial cable driving frequency	-
τ	Coaxial cable transmission time	-
$M(\varepsilon)$	A transfer matrix at energy ε	-
$g_{i,j}$	Greens function for a coaxial cable network (CCN)	2.2.2
$G_{i,j}$	Greens Function for a (CCN) connected to a vector network analyser	2.2.2
$Z_{i,j}$	Cable impedance between a site i and a site j in a CCN	-
$H_{i,j}$	A hopping term between a site i and a site j in a CCN[b]	-
$\mathbb{Z}$	The additive group of integers	-
$\mathbb{Z}_2$	A two element group[c]	-
$N\mathbb{Z}_2$	Short hand for a direct sum $\bigoplus^N \mathbb{Z}_2 = \mathbb{Z}_2 \oplus \mathbb{Z}_2 \oplus \cdots$	-
$\delta_{i,j}$	Dirac delta function	-
x	A variable with value in real space	-
k	A variable with value in momentum space	-

[a] Often we wish to refer to a special type of induced subgraph which we call a section. This is defined explicitely in chapter 5.

[b] We often use lower case Roman letters to denote hopping terms.

[c] Often we use this as short hand to denote two equivalence classes, but it only becomes a cyclic group for an infinite structure.

Notation	Meaning	Definition
$\mathbb{F}$	A field, generally taken to be the complex or real numbers	-
X_i	A topological space[a]	2.1.16
τ	A topology τ on a topological space X	2.1.16
ξ	A parameter space defined for H on G	2.1.17
$\pi(X)$	The zeroth homotopy group of a space X	2.1.18
$\mathcal{P}(X_i)$	The zeroth homotopy group of a specific subspace of X_i	7.3.17
V or v	A voltage in a CCN	-
I	A current in a CCN	-
s_{11}	Measured reflectance of a CCN	-
s_{21}	Measured transmission of a CCN[b]	-
$\lvert s_{21}\rvert$	Measured transmittance of a CCN	-
Γ or γ	A loss term on a CCN from connecting to a VNA	2.2.2
Z or Z_s	The measured local impedance of a CCN	2.2.2
CV	A vertex of a graph that supports a zero energy state	4.1.3
CFV	A vertex of a graph which does not support a zero energy state	4.1.3
TCV	A vertex of a graph that supports a zero energy state for almost all hopping terms	4.1.6
TCFV	A vertex of a graph that does not support a zero energy state for almost all hopping terms	4.1.6
TA	A vertex adjacent to a TCV	-
TR	A vertex not adjacent to a TCV	-
$C_{i,j}$	A block matrix that connects two diagonal blocks q_i and q_j of a matrix Q	5 & 7
$\mathcal{N}(H)$	The nullity of a matrix H	5.3.5
q^k	The k-th column of a matrix q	5.3.6
$q^{l\neq k}$	A submatrix of q where the k-th column has been deleted	5.3.6

[a] Note that sometimes the index is dropped.

[b] Note that the convention for transmission vs. transmittance seems to be different for optics and radio frequency engineering, so we have used this convention.

Notation	Meaning	Definition
b	A constraint map defined as the solution to a polynomial which is a restriction from a subspace $X_i \to X_j$	7.1.1 & 7.3.13
ψ_j^i	The support of a nullstate[a] on a block q_j originating from a block q_i	7.1.14
c_j^{2n}	A map from a subspace $X_j \subset \xi$ with $2n$ zero energy states to a subspace $X_k \subset \xi$ with $2n+2$ zero energy states	7.3.12

Table 1.3.0.1: A notation and definition guide for this thesis. Most of the frequently used notation is included here.

[a] The Greek letter used is sometimes different.

Chapter 2

Background

This section is split in to two main subsections. The first focusses on the theoretical background of our work, and the second is a discussion of the experimental methods we used in this work.

Throughout sections 2.1.2, 2.1.2.2, 2.1.2.3, and 2.1.2.4 we will give a brief overview of some of the previous work on topological classification, mostly focussing on classification in non-interacting Hamiltonians. With this in mind we will give a short discussion on tight binding models (and Hückel theory), and electronic band structure in section 2.1.1. In section 2.1.4 we will discuss chiral symmetry, and the structure of a chiral symmetric Hamiltonian when allowing for arbitrary continuous hopping disorder. Much of this thesis uses some notions from graph theory and topology, so in section 2.1.5 we give a brief outline of some of the preliminary details of graph theory and topology that we use in this work.

A small number of the theoretical predictions we make are verified experimentally using a coaxial cable network to create tight binding structures. In section 2.2 we will discuss the experimental basis for our experiments, first by demonstrating a map between coaxial cable networks in section 2.2.1, and then discussing experimental measurements and experimental techniques in section 2.2.2. In section 2.2.2.1 we also give a brief overview of topological classification in terms of transfer matrices — a convenient formalism for transmission experiments.

2.1 Topology and materials

Topology studies properties of a space X which are unchanged under some continuous deformation of the space X. Loosely speaking, this means the space may not be torn, or have new holes introduced. One of the main questions of topology is, given two topological spaces X and Y, can X be continuously deformed to the space Y? To answer such a question in complete generality is very difficult, but can be simplified by considering certain properties of the space. A ubiquitous approach is to calculate a topological invariant for the space X and the space Y. If they are distinct, then you can be certain the two spaces may not be continuously deformed to one another.

One example of a topological invariant is the number of ways a circle may be mapped

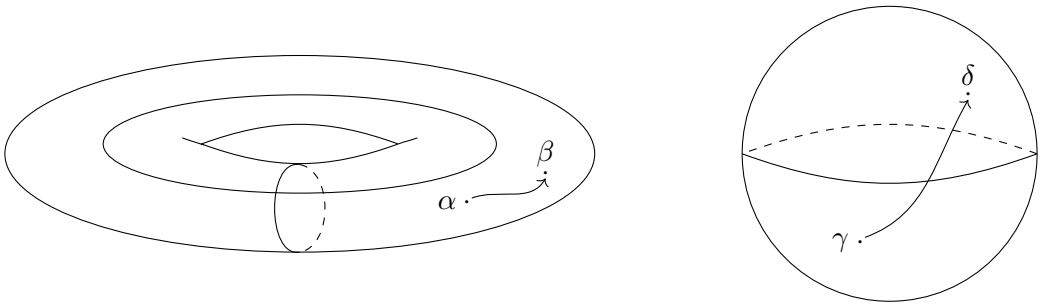

Figure 2.1.1: Roughly speaking the first homotopy group counts the number of ways a circle may be drawn on a surface, and the zeroth homotopy group counts the number of ways a point may be drawn on a surface. The torus has a first homotopy group of $\mathbb{Z} \times \mathbb{Z}$. It has two generators, corresponding to the circles drawn on the surface. Each circle may be wound around the torus an integer number of times, resulting in a first homotopy group of $\mathbb{Z} \times \mathbb{Z}$. For a sphere every circle may be continuously mapped to a point, so the first homotopy group is trivial. For both the torus and the sphere, any point may be mapped to any other (for example $\alpha \mapsto \beta$ for the torus, $\gamma \mapsto \delta$ for the sphere) so both the torus and the sphere have a trivial zeroth homotopy group. So a distinct topological invariant is sufficient to show two spaces are topologically distinct, but not necessary.

to a space, such that the circle does not undergo a discontinuous change. That is, if you have two surfaces X and Y and X has $\mathbb{Z} \times \mathbb{Z}$ different ways to draw a circle, but Y has 1 equivalent way, then we know X and Y must be topologically distinct. Such an example is illustrated in Fig. 2.1.1. Roughly speaking, counting the number of ways a circle may be drawn on a space is the first homotopy group of that space. One may also ask how many different ways a point may be drawn on a space (the zeroth homotopy group). For the example in Fig. 2.1.1 both a torus and a sphere have one way to do this. That is, a topological invariant can be used to tell two spaces apart, but if they have the same invariant, it does not mean the two spaces are topologically the same.

Broadly speaking questions of topology arise quite naturally in physical systems. In a material context, we often have a Hamiltonian, with a certain set of physically defined parameters. There are many topological properties here already: the Hamiltonian has an Eigenspace and is acting in a Hilbert space. We may ask what are the topological properties of this Eigenspace? Or even what the topological properties are of its full Hilbert space? If we allow our physically defined parameters to change, what happens to the topological properties of this space? Or perhaps as is more interesting in a physical context, if we drive our system to undergo a topological change, does this have physical consequences?

Remarkably, physical properties of a system can be very dependent on the systems underlying topological properties. The localisation and transport of electronic states [4, 25–28] for instance, can often be related to the topological invariant associated to a particular Hamiltonian. We say, if a topological invariant associated to a Hamiltonian changes, then the system has undergone a topological phase transition.

In this work we wish to study exact topological properties in finite tight binding models.

2.1.1 Tight binding approximation

Suppose we wish to describe the electronic properties of a system with N atoms. To write down and solve the full Hamiltonian, in complete generality, is often not analytically possible. Using steady state approximations gives a system which is a little more approachable. Assuming nuclear contributions to such a system are negligible (the Born-Oppenheimer approximation [29]), many numerical ab initio approaches have been developed to get highly accurate descriptions of the electronic structure of a system from first principle. For instance, Hartree-Fock [30, 31] and the highly successful density function theory [32], and even (more recently) approaches using machine learning [33]. One of the simplest methods to approximating the electronic structure of an N atom system is with the tight binding approximation, also known as Hückel theory in quantum chemistry [34–36]. We now present an overview of the tight binding approximation in real and momentum space.

In the tight binding approach, it is assumed that on each atom there is a steady state Hamiltonian with a set of orbitals n and that the overlap of eigenstates on two different atoms is negligible. That is, each orbital of the atom is orthonormal and orbitals on neighbouring atoms are orthogonal so that

$$\langle \psi(x,n) | \psi(y,m) \rangle = \delta_{x,y}\delta_{n,m}. \tag{2.1.2}$$

where x, y denote atom positions and n, m denote atomic orbitals. To simplify notation, let $|i\rangle = |\psi(x,n)\rangle$. Labelling the probability of an electron hopping from $|i\rangle$ to $|j\rangle$ with $|h_{i,j}|^2$ gives a tight binding Hamiltonian

$$H = \sum_i E_i \left|i\right\rangle \left\langle i\right| + \sum_{i,j} h_{i,j} \left|i\right\rangle \left\langle j\right|. \tag{2.1.3}$$

where E_i is an onsite energy and $h_{i,j} = h^*_{j,i}$.

The bulk Hamiltonian is defined on an infinitely periodic lattice $\mathcal{L}$. This approximation works well for a large enough physical system where the electronic properties away from the boundaries behave as though they are in an infinitely periodic structure. A bulk Hamiltonian may be defined in real or momentum space. This corresponds to defining H on $\mathcal{L}$ directly, or on its reciprocal lattice $\mathcal{R}$. For the set of primitive lattice vectors R_i, the reciprocal lattice is defined by a set of vectors K_i such that $K_i \cdot R_j = 2\pi\delta_{i,j}$.

To see that the reciprocal lattice takes values in momentum space, consider a translation operator $T_\alpha : \mathcal{L} \to \mathcal{L}$ with eigenvalue t_α which translates a wavefunction $\psi(x)$ by some lattice vector $\alpha = n_1 R_1 + n_2 R_2 + \cdots$ with integers n_i defined on $\mathcal{L}$. If the structure is periodic on m unit cells in the α direction, then

$$T_{m\alpha}\psi(x) = T^m_\alpha \psi(x) = t^m_\alpha \psi(x) = \psi(x). \tag{2.1.4}$$

So eigenvalues of the translation operator are roots of unity $t_\alpha = e^{ia}$ [34] where $a = 2\pi\frac{n_1+n_2+\cdots}{m}$. As α is a lattice vector, we may decompose $a = \frac{K\cdot\alpha}{m}$ where $K = K_1 + K_2 + \cdots$ on $\mathcal{R}$ or equivalently $a = \frac{1}{m}(n_1K_2 + n_2K_2 + \cdots)\cdot(R_1 + R_2 + \cdots) = k\cdot(R_1 + R_2 + \cdots)$. This defines a Fourier series between functions on $\mathcal{L}$ and functions on $\mathcal{R}$ so K_i, R_i are the canonical variables momentum and position.

The unit cell of the reciprocal lattice defines the Brillouin zone (BZ) of $\mathcal{L}$. As a consequence of periodicity, all values of k are periodic on $\mathcal{R}$ so are defined up to the periodicity of the lattice. That is

$$k = 2\pi\left(\frac{n_1}{m_1}, \frac{n_2}{m_2}, \cdots\right) \tag{2.1.5}$$

where each $n_i \in \{0, 1, \cdots, m_i - 1\}$ where m_i is the periodicity of the lattice in the ith direction. For an N-dimensional lattice this defines the Brillouin torus T^N. For an infinite crystal, when $\lim m \to \infty$ each entry to k takes on a continuous value in the range $[0, 2\pi)$.

As the Hamiltonian is periodic on $\mathcal{L}$ the eigenstates $\psi(x)$ of H are eigenstates of the translation operator T so they are periodic up to a phase factor. That is,

$$\psi_k(x + R) = e^{ik\cdot R}\psi_k(x) \tag{2.1.6}$$

where k labels the value taken in the BZ. This is Bloch's theorem [37], and means eigenstates may be defined in terms of periodic functions on $\mathcal{L}$.

Definition 2.1.1. A Bloch state of a periodic structure with Hamiltonian H is given by

$$\psi_k(x) = e^{ik\cdot x}u_k(x) \tag{2.1.7}$$

where the crystal momentum k takes values in BZ of the reciprocal lattice and u is periodic on the lattice $\mathcal{L}$, so that for any lattice translation a, $u_k(x + a) = u_k(x)$.

The band structure of a bulk Hamiltonian is defined by Fourier transforming a Hamiltonian from real space to momentum space. This gives a Hamiltonian $H(k)$ with energy levels $E(k)$ corresponding to its spectrum. For an infinite crystal the BZ is continuous, so each $E(k)$ defines a function from momentum space to $\mathbb{R}$.

The Bloch states may be transformed to real space giving a localised real space basis for the eigenstates of H. This defines the Wannier functions [38].

Definition 2.1.2. The Wannier functions of a Bloch state $\psi_k(x)$ are given by

$$W_x = \frac{1}{\sqrt{N}}\sum_{k\in BZ} e^{-ik\cdot x}\psi_k(x). \tag{2.1.8}$$

Or in the infinite limit

$$W_x = \frac{1}{V}\int_{k\in\mathrm{BZ}} dk e^{-ik\cdot x}\psi_k(x) \tag{2.1.9}$$

where V is the volume of the BZ.

The Wannier functions form a complete orthonormal basis for the eigenstates of H [22, 23, 34, 38] and because they are localised in real space they provide an alternative basis for the real space tight binding Hamiltonian.

The Bloch functions are unique up to a phase transformation, however the localisation of Wannier functions may be altered by such a transformation. There has been a lot of research in finding maximally localised Wannier functions [22, 23]. Using Wannier functions an exact tight binding Hamiltonian may be found, so maximally localised Wannier functions define an ideal basis for a tight binding Hamiltonian. Maximally localised Wannier functions are typically defined by minimising the sum of variances of the position operator for each Wannier function [22, 23]. Under this approach the maximally localised Wannier functions are also unique.

2.1.2 Development of topology in tight binding systems

Topology has a long history as a tool to understand physics. One of the first applications of topology to physics occurred in the mid 19th century with W. Thomson proposing a model of elements as non-trivial knots [1]. Since then, many physical phenomena have been explained as having a topological origin [39, 40] for instance Van Hove singularities were first predicted as a consequence of the topological properties of differentiable functions defined on the Brillouin torus [41]. One of the first topological materials appeared with the discovery of the quantum Hall effect [7, 8] which after its discovery was realised to be a topological phenomenon [9]. The quantum Hall effect has been shown to relate to the Berry phase [42] — a topological invariant of the Brillouin zone. We will discuss the Berry phase in more detail in section 2.1.2.1.

2.1.2.1 Adiabatic evolution

The band structure of a material is particularly important for describing the electronic properties of a periodic system. The band structure is found by taking a cyclic path through the Brillouin zone and at each point k finding the spectrum of a Hamiltonian $H(k)$. Parametrising k as a function of time, we can understand finding the eigendecomposition of $H(k(t))$ as solving the instantaneous Schrödinger equation. Under slow evolution we may approximate solutions to the (time dependent) Schrödinger equation using instantaneous solutions via the adiabatic theorem [43]. As we will discuss below, the way in which the solutions to the Schrödinger equation are changed under a cyclic path through the Brillouin zone has significant consequences on topological properties of a structure.

Consider a time dependent Schrödinger equation with a Hamiltonian $H(t)$ and an instantaneous eigenbasis $|n(t)\rangle$. If the Hamiltonian is evolving very slowly, then we can approximate solutions to the Schrödinger equation with instantaneous solutions so that

$$H(t)\,|\psi(t)\rangle = E\,|\psi(t)\rangle = i\hbar\frac{\partial}{\partial t}\,|\psi(t)\rangle \tag{2.1.10}$$

where $|\psi(t)\rangle = \sum c_n(t)\,|n(t)\rangle$. Solving this equation reveals that a phase is picked up on each instantaneous basis state — the adiabatic theorem [43]. That is, an eigenstate at a time t is related to the eigenbasis at a time 0 by

$$|\psi(t)\rangle = \sum c_n(0)\exp\left(i\gamma_n(t) + i\theta_n(t)\right)|n(t)\rangle\,. \tag{2.1.11}$$

The phase θ_n is a dynamic phase, caused by a change in the eigenvalues between $H(0)$ and $H(t)$. That is

$$\theta_n(t) = \frac{-i}{\hbar}\int_0^t E_n(T)dT \tag{2.1.12}$$

where T parametrises time at each point between 0 and t. Of significant interest to this work is the geometric phase, given by

$$\gamma_{n,m}(t) = i\int_0^t \langle n(t)|\,\partial_t\,|m(t)\rangle\cdot dT. \tag{2.1.13}$$

The dynamical phase corresponds to changes in eigenvalues of $H(t)$ while the geometric phase corresponds to changes in the eigenbasis $|n(t)\rangle$.

Now consider a time $t+\epsilon$ very close to t. Then it is likely that solutions to $H(t+\epsilon)$ are quite similar to solutions to $H(t)$. In such a case we may assume the eigenbasis between t and $t+\epsilon$ are related by

$$\langle n(t \pm \epsilon)|m(t)\rangle \approx \alpha \delta_{n,m} \tag{2.1.14}$$

where $|\alpha| = 1$. In such an instance the geometric phase is diagonal, so that $\langle n(t)| \partial_t |m(t)\rangle = 0$ for $n \neq m$. This assumption holds so long as there are no degenerate eigenvalues, or equivalently that bands remain gapped throughout the path through the BZ. We refer to evolution that satisfies the adiabatic approximation and has a diagonal geometric phase as adiabatic evolution.

Consider adiabatic evolution for a Hamiltonian $H(k)$ in a BZ, where the crystal momentum $k(t)$ is time dependent. Adiabatically evolving the Hamiltonian through a cyclic path $\mathscr{C}$ in the BZ defines the Berry phase

$$\gamma_n = i \oint_{\mathscr{C} \in \mathrm{BZ}} \langle n| \nabla_k |n\rangle \cdot dk \tag{2.1.15}$$

where ∇_k is the grad operator. Under non-cyclic adiabatic evolution, the geometric phase may always be removed under a suitable phase transformation $e^{i\phi_n(t)}$ of each Bloch state $|n(t)\rangle$. But for cyclic adiabatic evolution where $H(t+T) = H(t)$, then any phase transformation must satisfy $e^{i\phi_n(t)} = e^{i\phi_n(t+T)}$, so that $\phi(t+T) = \phi(t) + 2\pi m$ for some integer m. Consequently, $\gamma_n \bmod 2\pi$ cannot be removed by any such phase transformation.

For certain systems, the Berry phase becomes quantized, and is a topological invariant of momentum space. For instance, consider a two site periodic structure, with a unit cell depicted in Fig. 2.1.2 (a) (this structure is the famed Su-Schrieffer-Heeger model [24] which we will discuss more in Chapter 3). This structure has a momentum space Hamiltonian of

$$H(k) = \begin{pmatrix} 0 & t_1 + t_2 e^{ikx} \\ t_1 + t_2 e^{-ikx} & 0 \end{pmatrix} = (t_1 + t_2 \cos kx)\sigma_x + i t_2 \sin(kx)\sigma_y \tag{2.1.16}$$

where σ_x, σ_y are Pauli matrices. Taking a path that maps $k \mapsto k + 2\pi$ induces cyclic evolution of $H(k)$ and its eigenbasis $|n\rangle$ over the BZ. The Berry phase calculates a winding number around the origin (this special case of the Berry phase is also called Zak's phase [44]), so is both quantised and represents a topological invariant of the BZ. An example of the different evolution in the instantaneous eigenbasis for a trivial Berry phase, and Berry phase of π is illustrated in Fig. 2.1.3.

A change in the winding number also corresponds to an unavoidable gap closure. To see this, observe that the band structure is given by

$$E_k^{\pm} = \pm\sqrt{t_1^2 + t_2^2 + 2t_1 t_2 \cos kx}. \tag{2.1.17}$$

By continuously evolving the hopping terms t_1 and t_2 it is possible to change the winding number from zero to one by evolving from $t_1 > t_2$ to $t_1 < t_2$. The origin passes through the

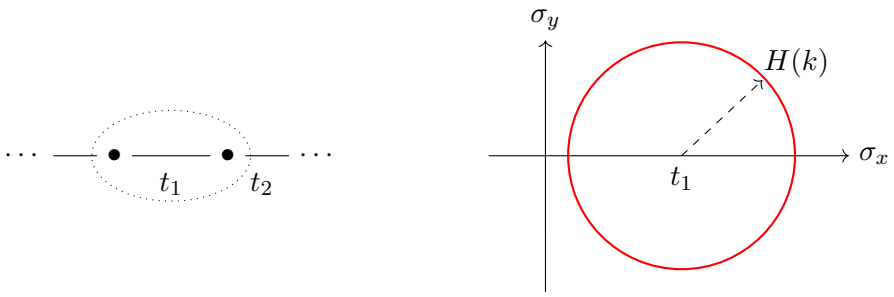

(a) (b)

Figure 2.1.2: (a) A periodic structure with 2 sites in a unit cell, denoted by the dotted circle. Hopping terms are indicated with t_1, t_2 where t_1 is an intracellular hopping term and t_2 is an intercellular hopping term. The Brillouin zone for this 1D structure is a 1 dimensional torus, represented as the red circle drawn in (b) parametrised by the dependence on the Pauli matrices in equation (2.1.16). Fixing the hopping terms, a cyclic path through the BZ corresponds to evolving $H(k) = t_1 + t_2 e^{ikx}$ along the red circle, and the Berry phase calculates the winding number around the origin and is zero if $t_1 > t_2$ or one if $t_1 < t_2$.

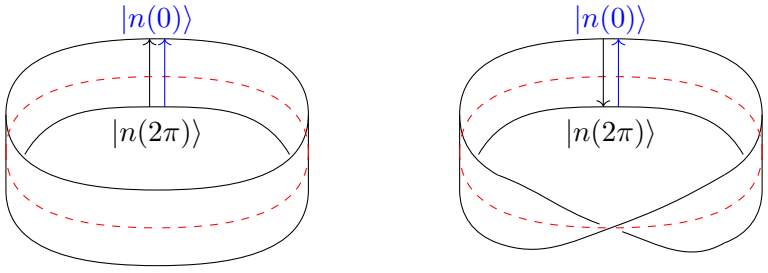

(a) (b)

Figure 2.1.3: The instantaneous eigenbasis of a 1D Hamiltonian $H(k)$ that is undergoing cyclic evolution, as depicted in Fig. 2.1.2. (a) Denotes a Berry phase of 0, and (b) denotes a Berry phase of π. The path is illustrated by the red dashed line. For every k, $H(k)$ has an instantaneous eigenbasis $|n(k)\rangle$, defining a vector space at each k.

BZ when $t_1 = t_2$ and corresponds to a gap closure, $E_k^+ = E_k^-$, at $k = \pi$ — so a topological change coincides with unavoidable non-adiabatic evolution.

If the BZ is an even dimension, then integrating the Berry phase over all k is also quantised. To see this we consider a 2 dimensional Brillouin torus so we may use the standard Stokes theorem, but this holds for the generalised Stokes theorem as well. Defining the Berry connection as $\mathcal{A}_n = \langle n| \nabla_k |n\rangle$ then we may define the Berry curvature $\Omega_n = \nabla \times \mathcal{A}_n$ so that

$$\gamma_n = i \int_S dS \cdot \Omega_n \tag{2.1.20}$$

where the surface S is the entire 2 dimensional Brillouin torus. We may evaluate γ_n by integrating around a contractable closed path $\mathscr{C}$, and contracting this path to a point. That is

$$\gamma_n = i \lim_{\mathscr{C}\to 0} \left[\int_{S<\mathscr{C}} dS \cdot \Omega_n + \int_{S>\mathscr{C}} dS \cdot \Omega_n \right] \tag{2.1.21}$$

where $\mathscr{C}$ cuts the BZ along a contractable closed path, $S < \mathscr{C}$ is the BZ on the side of the path being contracted, and $S > \mathscr{C}$ is the BZ on the other side of the path. In the limit of $\mathscr{C} \to 0$ the path maps the eigenbasis to itself, so by the definition of the BZ this has solutions for $|n(k_x, k_y)\rangle = |n(k_x + 2\pi n, k_y + 2\pi m)\rangle = e^{2\pi i(n+m)} |n(k_x, k_y)\rangle$, and the Berry phase must take values of $2\pi p$ where $p = n + m$ is an integer value. The integer p is the Chern number [45], which is a topological invariant of an even dimensional BZ. A material that can have a non-zero Chern number is known as a Chern insulator.

To see why the Chern number is a topological invariant, observe that with Gauss' theorem we may evaluate equation (2.1.22) as

$$\gamma_n = i \int_V dV \ \nabla \cdot \Omega_n \tag{2.1.22}$$

where V is the volume enclosed by the surface S. So the Chern number can only be non-zero if there are singularities of Ω_n contained in S, the number of which is a topological invariant.

We may interpret Ω_n as an analogue magnetic field in momentum space. As such the value γ_n in equation (2.1.22) corresponds to the flux of Ω_n through S with singularities in Ω_n corresponding to monopoles enclosed by S. In order to change the Berry phase we must pass singularities in Ω_n through the surface of the Brillouin torus, this results in a necessary gap closure in $H(k)$. To see that a singularity in Ω_n corresponds to a gap closure in the spectrum, we expand the Berry curvature as,

$$\Omega_n = \nabla \times \langle n| \nabla |n\rangle = \langle \nabla n| \times |\nabla n\rangle = \sum_m \langle \nabla n|m\rangle \times \langle m|\nabla n\rangle \,. \tag{2.1.23}$$

Using Levi-Civita notation, $\langle \nabla n|m\rangle \times \langle m|\nabla n\rangle = \left\langle \frac{\partial}{\partial k^\mu} n \middle| m \right\rangle \left\langle m \middle| \frac{\partial}{\partial k^\nu} n \right\rangle - \left\langle \frac{\partial}{\partial k^\nu} n \middle| m \right\rangle \left\langle m \middle| \frac{\partial}{\partial k^\mu} \right\rangle$ thus $\langle \nabla n|n\rangle \times \langle n|\nabla n\rangle = 0$, so we can restrict the sum in equation (2.1.23) to $m \neq n$. Finally, we note that $\langle m|\nabla n\rangle = \frac{\langle m|\nabla H|n\rangle}{\varepsilon_n - \varepsilon_m}$ so that

$$\Omega_n = \sum_{m\neq n} \frac{\langle n| \nabla H |m\rangle \times \langle m| \nabla H |n\rangle}{(\varepsilon_n - \varepsilon_m)^2} \tag{2.1.24}$$

which has singularities whenever $\varepsilon_n = \varepsilon_m$. That is, the Berry phase is only possible to alter by taking a gap closure through S on the Brillouin torus, meaning adiabatically equivalent Hamiltonians (with a 2 dimensional BZ) all have the same Berry phase.

Examples of Chern insulators (which may have a non-zero Chern number) include materials which exhibit the quantum Hall effect — for a 2D material in a magnetic field, due to cyclotron motion of the electrons, electronic transport is localised to the edge of the material. The resulting conductance is quantised and exactly proportional to the materials Chern number [9, 46].

More formally we may understand the band structure as a type of vector bundle. Loosely speaking a vector bundle consists of some manifold $\mathcal{M}$ such that for every point $m \in \mathcal{M}$ there is a vector space $V(m)$ along with some structure[1] to ensure that there exists an open neighbourhood U around m where for every $m+\varepsilon \in U$ then $\lim_{\epsilon \to 0} V(t+\varepsilon) = V(t)$. In the band structure the manifold is given by the Brillouin torus, and a vector space is defined for each k with a bulk Hamiltonian $H(k)$. The topological classification of momentum space Hamiltonians is therefore very closely related to the topological classification of vector bundles on the Brillouin zone. The Berry phase is itself often a topological invariant of a vector bundle. For instance in the above 1D example the Berry phase corresponds to a winding number, and in the 2D case related to the Chern number [47] of the Brillouin torus.

There are many physical properties which may only be changed by non-adiabatic evolution [45]. For instance, a protected band crossing cannot be removed without a gap closure [48]. This can lead to protected chiral transport [4] localised to the materials boundaries which is robust even in finite structures [20, 21]. The connection between the quantum Hall effect and the Berry phase also ensures that the quantisation in the quantum Hall effect is robust up to adiabatic evolution. So there is a strong physical motivation to define equivalence classes for all Hamiltonians, where two Hamiltonians are in different equivalence classes if they may not be related by adiabatic evolution.

For the purposes of this thesis two Hamiltonians H_1 and H_2 (in real or momentum space) are considered topologically distinct if and only if there exists no adiabatic path between them.

2.1.2.2 Bulk-boundary correspondence

Physically any real system must be finite, and so a bulk Hamiltonian does not fully describe the physical system. For a topologically non-trivial system, boundary modes (whose behaviour is dictated by the topological index of the material) exist localised to the boundary. The rigorous foundations for the bulk boundary correspondence are quite complicated and are often formalised in terms of K-theory [15] and for disordered infinite systems can be made rigorous with the use of non-commutative geometry [19, 49]. That said, the physical premise behind the bulk boundary correspondence is quite intuitive.

Consider two semi-infinite d dimensional topological materials t_1 and t_2. The bulk is

[1] Note that this structure is quite technical, and is not too necessary to understand the work we present in this thesis, so we omit the full definition of a vector bundle here.

well defined for each material, due to their semi-infinite nature. Suppose we choose for the topological indices of each material to be different. If we sew the two materials together along their $d-1$ dimensional boundary, then we can imagine taking a path from somewhere deep in the bulk of t_1 to somewhere deep in the bulk of t_2. When far in the bulk of either material it seems reasonable to approximate the local structure as being entirely within the bulk of t_1 or t_2, so the topology in either location approximately corresponds to the topology deep in the bulk (this can be made rigorous with the use of local topological indices [16, 17, 50, 51]). As we follow the path from our position far in t_1 to a position far in t_2 the topological index must change at some point. From the previous discussion in section 2.1.2.1 a topological index may only change with a gap closure, so somewhere along the path there is a boundary, with degenerate modes corresponding to a topological phase transition.

A similar argument holds for a single material with one bulk topological index. The vacuum may (roughly speaking) be considered a trivial topological material. In this case our sample, with a single bulk index, will have degenerate modes localised to its boundaries [3]. Other properties of the boundary modes are also dictated by bulk topological indices, for instance protected (and quantised) transport [4].

In Hermitian systems the bulk boundary correspondence is well understood when the material is taken to the infinite (thermodynamic) limit [15]. Furthermore, the bulk boundary correspondence has been demonstrated to hold in the presence of arbitrary boundary conditions [52, 53] assuming the system otherwise has no disorder.

2.1.2.3 Momentum space and the 10 fold way

We may choose to restrict adiabatic evolution of the Hamiltonian to ensure a certain symmetry is satisfied. For this section we consider the Altland Zirnbauer symmetries [54] that define the fundamental symmetries of random matrix theory:

$$\begin{aligned} CHC^\dagger &= -H \qquad \text{chiral symmetry,} \\ THT^{-1} &= H \qquad \text{time reversal symmetry,} \\ PHP^{-1} &= -H \qquad \text{particle-hole symmetry,} \end{aligned} \tag{2.1.25}$$

where C is a unitary and T and P are antiunitary matrices. Note that particle-hole symmetry arises when a Hamiltonian acts symmetrically on particles excited above the Fermi energy and the hole (created by the excitation) below the Fermi energy.

As mentioned in section 2.1.2.1 we may understand the Brillouin zone as a vector bundle defined on the Brillouin torus. That is, for every point k in the Brillouin torus there is a Hamiltonian $H(k)$ defining a vector space. The topological classification of bulk Hamiltonians is therefore deeply connected to the topological classification of vector bundles on a torus. We can impose constraints to ensure perturbations to vector bundles satisfy certain symmetries.

We can imagine taking a bulk Hamiltonian and asking what happens to the topological classification upon the addition of topologically trivial bands — that is, bands in the BZ that have a trivial topological index. Topological properties that remain stable under an

Symmetry		Dimension			
AZ	(T,P,C)	0	1	2	3
AIII	(0,0,1)	0	$\mathbb{Z}$	0	$\mathbb{Z}$
BDI	(1,1,1)	$\mathbb{Z}_2$	$\mathbb{Z}$	0	0
DIII	(-1,1,1)	0	$\mathbb{Z}_2$	$\mathbb{Z}_2$	$\mathbb{Z}$
CII	(-1,-1,1)	0	$2\mathbb{Z}$	0	$\mathbb{Z}$
CI	(1,-1,1)	0	0	0	$2\mathbb{Z}$

Table 2.1.2.1: The Altland Zirnbeaur classes that have chiral symmetry. Most of the results in this thesis apply to classes AIII and BDI.

arbitrary addition of trivial bands falls in to the study of K-theory [15, 47, 55], and is the origin of *stable* topological invariants [56].

From the perspective that adding or removing trivial bands (as much as one may desire) does not change a topological classification, bulk Hamiltonians may all be characterised by their fundamental symmetries. Combining symmetries in different ways leads to the famous periodic table of topological insulators [56]. The periodicity of the table is a consequence of Bott periodicity in the homotopy groups of vector bundles [47, 55].

The standard momentum space approach does not hold for strongly disordered systems. This is because the bulk Hamiltonian may not well approximate the infinite system — a consequence of the loss of translational invariance. One approach around this is the use of non-commutative geometry [19, 49].

Non-commutative geometry allows for the study of spaces corresponding to non-commutative algebras. The idea behind using non-commutative geometry is that translational invariance was previously defined using a translation operator on an infinite lattice. The translation operator is defined in a commutative algebra on the lattice. Under the loss of translation invariance, a translation operator may be defined in a non-commutative algebra [19]. Much like the use of a translation operator led to a commutative Brillouin zone, the non-commutative translation operator leads to a non-commutative Brillouin zone.

Remarkably with the use of non-commutative geometry (in the infinite limit) it has even been proven that topological properties remain for arbitrary disorder, for every entry of the periodic table [57]. From the perspective of the 10 fold way, this gives a complete picture of stable topological matter in infinite media.

2.1.2.4 Other approaches to classification

There are subtleties to the classification that even non-commutative geometry is unable to resolve without further considerations. These include fragile topological materials. These are materials such that the addition of trivial bands can change the topological classification [58]. Furthermore, the presence of crystal symmetries, for instance the C_3 symmetry of graphene, can also affect topological classification. For example, this can lead to the very rich classifications of higher order topology such as multipole topological insulators [59]. Finally (and the most relevant to this thesis) is the properties of topology in finite

systems.

For systems with crystal symmetry — crystalline topological insulators — the underlying space group becomes important. This is because the maximally localised Wannier functions that form a basis for electronic functions of the crystal depend on the irreducible representations (irreps) of the underlying space group [12]. Furthermore, any AZ symmetries may also combine with crystalline symmetries to reveal a very rich classification (for example in second order topological insulators [60]).

One very successful approach is to compute the irreps of the underlying space group, to predict if the maximally localised Wannier functions may be adiabatically localised to the atomic limit [12–14]. It has been shown that if and only if the maximally localised Wannier functions may be localised to atomic orbitals, then the Brillouin torus has a trivial Chern number [61]. That is the irreps may be used to indicate the presence topologically robust electronic states. This approach has been applied to the Bilbao material database, and using DFT calculations, indicates around 90% of materials in the database have a topologically non-trivial band structure.

There have also been a number of approaches to classification in finite media, often using (in some way) the bulk boundary correspondence. One approach is to use a topological index which may be defined locally in real space [17, 62]. For instance, local Chern numbers [50, 51] have been used to predict the number of approximately topologically robust modes in finite systems (the last two also using the non-existence of an atomic limit of the maximally localised Wannier functions to predict non-trivial topological bands). Local invariants are useful in calculating an index for finite systems, however finite size effects mean topological degeneracy is not exact [18]. It has also been demonstrated that (for low disorder) a rich phase diagram is realised for systems with inversion symmetry [21] giving a larger number of topological indices as a direct result of finite size effects. Time reversal symmetry has also been demonstrated to give non-trivial topology in finite structures [20].

2.1.3 The focus of this work

In finite media, topologically robust properties of the bulk are asymptotic to the infinite limit. This means that even exact properties associated to topological phase transitions, such as spectral gap closures and boundary properties, may be lost at sufficient disorder [18]. The relationship between bulk topology and boundary physics may also be lost when the network topology does not admit a clean definition of what constitutes a bulk and what constitutes a boundary, for instance in random graphs.

In this thesis we propose a rigorous approach to the classification of finite media, where we only consider gap closures topological if they remain for arbitrary (symmetry respecting) continuous hopping disorder. As a result, our approach is entirely finite, with some connection between our work and infinite media discussed throughout the thesis. That is, we are interested in the exact topological properties of finite structures. Our approach also allows for the consideration of arbitrary network topology, allowing for classification beyond the bulk boundary correspondence.

We consider three main problems in this thesis. The first is the problem of topological

protection. We consider a state to be topologically protected only if its eigenvalue is exactly robust to hopping disorder. That is, it has an eigenvalue that is constant for any continuous perturbation on the system. In finite systems this gives a direct connection between the structure of the system, and the number of topologically protected states it may host. We present a method for finding the number of topologically protected states in chapter 4 and also discuss how this relates to the underlying network topology of a structure.

We then give an approach to classifying topological phase transitions in finite media with chiral symmetry. In finite systems, boundary properties protected by a bulk index converge exponentially in the thermodynamic limit [19]. For example, a gap opens splitting zero energy boundary modes in a finite chiral structure, with the gap size dependant on disorder strength [18]. Furthermore, a gap closure separating topological phases in the bulk does not necessarily indicate an exact gap closure in the finite sample. That is, at sufficient disorder and small enough size, the bulk boundary correspondence is effectively lost. Using a graph theoretic approach, we define topologically distinct equivalence classes of finite Hamiltonians separated by *exact* energy gap closures. This allows us to relate a structures network topology to its topological classification. We discuss this classification and experimental confirmation of our classification in chapter 5.

The final main problem we consider is the topology of chiral Hamiltonians where we begin to allow control of individual hopping terms. This allows us to study topology as the number of degenerate states is sequentially increased. We give some general results demonstrating topology in constrained chiral systems with exact gap closures is quite universal. This leads to some sequences of topological phase transitions that may occur in finite structures. Such sequences alter the localisation of degenerate modes undergoing such a phase transition, which we also confirm experimentally. This is discussed in chapter 7.

Throughout this thesis we present experimental measurements using a coaxial cable network, corroborating some of our predictions. A coaxial cable platform, starting with the SSH model is discussed in chapter 3. We also find many deep connections between our classification and nut graphs, discussed in chapters 5 and 6. Using this platform we experimentally confirm some predictions of the behaviour of nut graphs in chapter 6. A definition and discussion of the literature surrounding nut graphs is given in this chapter also.

2.1.4 Chiral symmetry

In this thesis we present results primarily relating to the classification of finite tight binding models with chiral symmetry, at arbitrary continuous hopping disorder. We now present some properties of chiral symmetry that we will use throughout this work.

As discussed in section 2.1.2.1 a Hamiltonian H has chiral symmetry if for some unitary C

$$CHC^{\dagger} = -H. \tag{2.1.26}$$

As a consequence, H and $-H$ have the same eigenvalues, and so for any state with the non-zero energy ε then there is also an eigenstate with the energy $-\varepsilon$. Furthermore, if H

is a structure with an odd number of sites, then to maintain chiral symmetry there must be at least one zero energy state. Similarly, if H has an even number of sites, then the number of zero energy states is also even.

We are interested in chiral Hamiltonians with arbitrary hopping disorder. To allow this, we define each non-zero hopping term $h_{i,j}$ to be algebraically independent from all other hopping terms. It may be shown (with the use of the Harary Sachs theorem [63, 64]) that this requires that the sites of the Hamiltonian may be permuted to give a basis of the form

$$H = \begin{pmatrix} 0 & Q \\ Q^\dagger & 0 \end{pmatrix}. \tag{2.1.27}$$

A Hamiltonian with this structure allows chiral symmetry to be interpreted in terms of sublattices of the Hamiltonian, an example of which is given in Fig. 2.1.4. As will be discussed in section 2.1.5.1 this means we can interpret a chiral structure as being a bipartite graph.

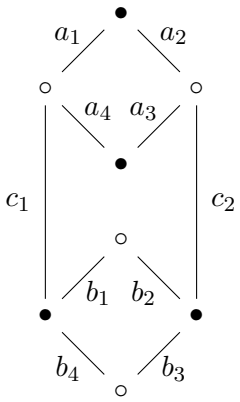

Figure 2.1.4: An example chiral structure, with two sublattices — a black sublattice and a white sublattice, where white sites may only connect to black sites and black sites may only connect to white sites. Each labelled hopping term is algebraically independent.

In chapters 5 and 7 we will make a lot of use of the fact that for a chiral structure an even number of sites ensures that zero energy states come in pairs. From the form of H in equation (2.1.27) it follows that $\operatorname{rank}(H) = 2\operatorname{rank}(Q)$. This ensures we can study the block Q to infer properties about the Hamiltonian, for instance in finding unavoidable gap closures in the energy spectrum of H at zero energy.

Using the block Q to study the presence of unavoidable gap closures in the full Hamiltonian has a few advantages, but also has some subtle difficulties compared to using the full Hamiltonian directly. This is because Q is not a normal matrix.

The first issue is the loss of Hermiticity. The Hamiltonian itself is Hermitian, so is unitarily diagonalisable ensuring all eigenstates are necessarily orthogonal, however Q is not. It is in chapter 7 where the consequences of this become most apparent, where Q may not be diagonalisable, and the left and right eigenspace of Q may have quite different properties.

A matrix Q is not diagonalisable if it has defective eigenvalues. This occurs when there are $n \geq 2$ degenerate eigenvalues, but there are not n linearly independent eigenvectors of that eigenvalue. For example, the matrix

$$Q = \begin{pmatrix} 1 & 2 \\ 0 & 1 \end{pmatrix} \tag{2.1.29}$$

has two eigenvalues of 1 but only one corresponding eigenvector of $(1, 0)^T$.

A second issue is that two eigenvectors of Q may be linearly independent, but might not be orthogonal. For instance, for

$$Q = \begin{pmatrix} 1 & 2 \\ 0 & 3 \end{pmatrix} \tag{2.1.30}$$

there are two linearly independent (unnormalised) eigenvectors,

$$\begin{pmatrix} 1 \\ 0 \end{pmatrix}, \begin{pmatrix} 2 \\ 1 \end{pmatrix}. \tag{2.1.31}$$

There is no linear combination of one that will give the other.

Orthogonality of eigenvectors does appear in another sense, however. Consider a non-defective matrix Q. Then we have the eigendecomposition

$$\begin{aligned} A^{-1}QA &= \Lambda \\ A^\dagger Q^\dagger (A^\dagger)^{-1} &= \Lambda^* \end{aligned} \tag{2.1.32}$$

where A diagonalises Q and Λ is a diagonal matrix with eigenvalues λ of Q on the diagonal. That is, the columns of $(A^\dagger)^{-1}$ are the eigenvectors of $Q^\dagger$. The requirement that $A^{-1}A = I$ ensures that — when Q is not defective — each eigenvector of Q is orthogonal to all but one eigenvector of $Q^\dagger$ (where we consider the eigenvectors $|a\rangle, |b\rangle$ to be orthogonal if $\langle a|b\rangle = 0$). We use this orthogonality in chapter 7 to find ways of evolving hopping terms of H to get large numbers of zero energy states.

2.1.5 Mathematical background

In this thesis we study topological properties of particular finite tight binding models, where we only allow continuous hopping evolution. To study these structures in full generality, we make use of some graph theory and topology. Some of the basic notions of graph theory and topology that we use throughout this thesis are reviewed in section 2.1.5.1 and section 2.1.5.2 respectively.

2.1.5.1 Some notions in graph theory

In this thesis we study topological materials using a graph theoretic approach. As such, we give a short discussion of some results in graph theory that we use throughout this thesis.

Definition 2.1.3. A graph G is a pair $\{V, L\}$ where V is a set of vertices, and L a set of edges between the vertices. The number of edges that connect to an individual vertex we refer to as *vertex degree* or *vertex order*.

Remark. In this thesis we will refer to vertices as sites or vertices. Here they are used synonymously.

We will be studying, mostly, simple graphs which have at most one edge between two vertices, and no edges that loop to the same vertex. That said, we sometimes relax the restriction on loops in chapter 4 and section 5.6.

Occasionally we also wish to restrict to chemical graphs (in chapter 6). These are graphs where each vertex has at most three nearest neighbours. Such graphs are theoretically realisable with carbon nanostructures, such as benzenoids and nanographenes.

To see the connection between a graph and a tight binding model, we need to define an adjacency matrix of G.

Definition 2.1.4. An adjacency matrix A of a graph G with N vertices is an $N \times N$ matrix where

$$A_{i,j} := \begin{cases} 1 & \text{if vertex } i \text{ and } j \text{ share an edge} \\ 0 & \text{otherwise.} \end{cases} \tag{2.1.33}$$

A related matrix, H, is the weighted adjacency matrix. In this matrix every edge is labelled with a weight, so that

$$H_{i,j} := \begin{cases} h_{i,j} & \text{if vertex } i \text{ and } j \text{ share an edge} \\ 0 & \text{otherwise.} \end{cases} \tag{2.1.34}$$

A tight binding model is a weighted adjacency matrix where entries to the matrix are given by hopping terms, and $h_{i,j} = h^*_{j,i}$ so that $H^\dagger = H$.

Remark. For many systems it is assumed there is only one orbital per atom. This means that the graph G is also the chemical structure of the system. If a system has more than one orbital for any atom, then G is no longer the chemical structure of the system.

Throughout this work we frequently wish to relate how a graph is connected to the topological classification of a Hamiltonian defined on it. In order to do this we define two objects of interest for every structure: a graph of the structure, and a Hamiltonian on the graph.

Definition 2.1.5. A Hamiltonian H is defined on a graph G where a non-zero hopping term $h_{i,j}$ is associated to each edge of the graph G.

As discussed in section 2.1.4 to allow, with full generality, hopping disorder in our tight binding model, chiral symmetry is only present for Hamiltonians with the form

$$H = \begin{pmatrix} 0 & Q \\ Q^\dagger & 0 \end{pmatrix}. \tag{2.1.35}$$

We can partition the edges of such a weighted graph in to two partite sets: a black set b, and a white set w. This defines a *bipartite graph* where the black set and white set of sites each correspond to a *partite set*.

Definition 2.1.6. A bipartite graph is a graph G which has two partite sets such that edges may only be drawn between the partite sets. This leads to an adjacency matrix of the form

$$A = \begin{pmatrix} 0 & B \\ B^T & 0 \end{pmatrix} \tag{2.1.36}$$

with Hamiltonians of the form

$$H = \begin{pmatrix} 0 & Q \\ Q^\dagger & 0 \end{pmatrix}. \tag{2.1.37}$$

We refer to the matrix B and Q as the *biadjacency matrix* of G and/or H.

More generally we often wish to make more arbitrary partitions of a graph. To do this we just define sets of vertices, each corresponding to a different partition, and label each vertex based on which set it is in.

Throughout this work we sometimes wish to consider permutations of H or A such maps take the graph from itself to itself, and correspond to a graph automorphism.

Definition 2.1.7. A map $H_1 \to H_2$ such that the underling structure G is the same defines a *graph automorphism.*

It is often useful to consider distinct vertices and edges that may be mapped to one another under a graph automorphism. When allowing arbitrary edge weights such maps are very rare, but for unweighted graphs G they are quite frequent. An example of such an automorphism is given by mapping any vertices of the same colour (black, white, or green) to one another in Fig. 2.1.5 (a).

Definition 2.1.8. Under a graph automorphism $G \to G$ any two different edges or vertices that may be mapped to one another are in the same *orbit.* That is, let P be the permutation group of G and $p \in P$ be an element of P. Then the orbit is given by

$$P(o) := \{po \in G | p \in P\}. \tag{2.1.38}$$

where o is an object (an edge or vertex) of the graph G.

We also often wish to study particular subgraphs of a structure, especially in chapters 4, 5, and 7.

Definition 2.1.9. An *induced subgraph* g of G is a graph defined on a subset of vertices v of G such that every edge between a vertex in v is present in g and G.

An example of such a subgraph is given in Fig. 2.1.5 (b). Note that most of the subgraphs we study in this thesis are induced subgraphs. We will sometimes refer to a different subgraph (in chapter 7) which we call an effective subgraph, but we will explicitly refer to such a subgraph as an effective subgraph. As such we will drop the term induced, and every time we refer to a subgraph without declaring it effective we mean an induced subgraph. The definition of an effective subgraph is quite technical, so we do not define this here.

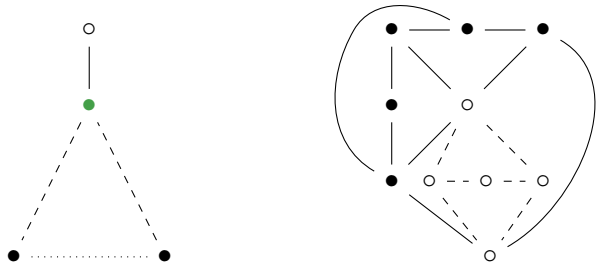

(a) (b)

Figure 2.1.5: (a) A graph where vertex orbits are indicated by the colour of the vertex, and edge orbits are indicated by the solid, dashed, and dotted lines. A graph automorphism maps any vertex or edge to another vertex or edge in the same orbit. (b) An example of an induced subgraph g of G. The subgraph g is indicated with the dashed edges and white sites, whereas G is the entire graph. Notice how every edge between a vertex of g is also precisely the edges in G between the same subset of vertices.

In chapter 6 we wish to look at the properties that relate to a bridge between two (connected) induced subgraphs. A bridge is a set of vertices that connect two subgraphs such that the vertex degree of each vertex is two. And in chapter 5 we consider to properties that relate to branches. A branch is a set of vertices such that it is terminated by a vertex with degree one, and every vertex connecting this set has degree two. An example of a bridge and a branch is given in Fig 2.1.6 (a) and (b) respectively.

A result we will use a lot in chapters 4, 5 and 7 is the Harary-Sachs theorem [63, 64]. This gives a connection between the way a graph is connected — its network topology — and the terms that appear in its determinant. To discuss the Harary-Sachs theorem, we need to make a few definitions about how vertices are connected. We then give a simple proof of the Harary-Sachs theorem for a weighted bipartite graph in 2.1.13.

Definition 2.1.10. If two vertices of a graph G share an edge, we say there is a *matching* between the vertices, or that the two vertices may be *matched*, or that the two vertices are possible to *match*. An example of such a matching is given in Fig. 2.1.7.

Definition 2.1.11. If every vertex of a graph G is possible to match, such that each matching is between a disjoint pair of sites, then we say G has a *perfect matching*. In this thesis we also often refer to such a matching as a *cover*.

Definition 2.1.12. If a graph G has no perfect matching, we call a matching of the largest subgraph which has a perfect matching the *largest matching* of the graph.

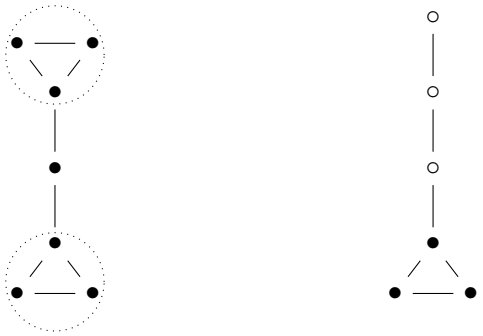

(a) (b)

Figure 2.1.6: (a) An example of a bridge in a graph. The two induced subgraphs connected by a bridge are encircled with ellipses. (b) An example of a branch in a graph, indicated by the white vertices.

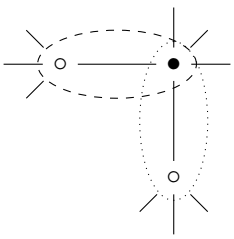

Figure 2.1.7: Part of a graph, where there exists a (dashed) matching between the black site and one of the white sites, and a (dotted) matching between the black site and a second white site. The two white sites are not connected, so do not have a matching.

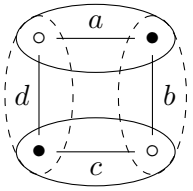

$$Q = \begin{pmatrix} a & b \\ d & c \end{pmatrix} \Rightarrow |Q| = ac - bd$$

Figure 2.1.8: There are two matchings of this graph, with the biadjacency matrix Q, the solid matching (with hopping terms a and c) and the dashed matching (with hopping terms b and d). By the Harary-Sachs theorem, every term in the determinant of the biadjacency matrix, corresponds to the product of hopping terms in a complete matching, as is indicated by computing $|Q|$.

Theorem 2.1.13. *In a weighted bipartite graph with biadjacency matrix Q and a set of perfect matchings $\{m\}$, then each term of $|Q|$ is given by a sum of the product of each edge weight that appears in a perfect matching m.*

Proof. Consider the matrix

$$H = \begin{pmatrix} 0 & Q \\ Q^\dagger & 0 \end{pmatrix} \tag{2.1.42}$$

on a graph G. A perfect matching corresponds to a bijective map between one partite set to the other partite set, labelled by edges. This is exactly any set of terms in Q that may be permuted to be on a non-zero diagonal of Q.

Any non-zero term in Q corresponds to the product of a set of terms which may be permuted to be on the diagonal of Q, therefore every non-zero term in $|Q|$ corresponds to a perfect matching. That is

$$|Q| = \sum_m \pm \prod_i h_{m,i} \tag{2.1.43}$$

where $h_{m,i}$ is the set of hopping terms on any edge in the matching m and the sign of the product depends on the number of permutations to put this matching on the diagonal of Q. □

The Harary-Sachs theorem is particularly important to allow us to relate the determinant of a structure to it's underlying connectivity. This is because, to study a particular structure with arbitrary hopping disorder, we often leave hopping terms as indeterminates within some field (for instance the real numbers). As such, the determinant of the Hamiltonian is a polynomial of these indeterminates. Using theorem 2.1.13 we are able to relate the structures connectivity to the determinant. An example of the correspondence between the perfect matchings of a bipartite graph and the determinant of it's biadjacency matrix is illustrated in Fig. 2.1.8.

Another property we wish to make use of throughout this thesis is that when randomly selecting edge weights for a graph G from some continuous field, if the graph can be non-singular, then the graph is almost always non-singular.

Proposition 2.1.14. For a weighted graph G where we independently and randomly select edge weights, then if there exist a set of edge weights such that G is non-singular, then with randomly selected edge weights the graph is almost always non-singular graph.

Proof. Let H denote the weighted adjacency matrix of G. If there exists edge weights such that G is non-singular, then to get a singular graph requires solving $|H| = 0$. If solutions to $|H| = 0$ exist, they constrain at least one edge weight of the graph. Fix all but one hopping term h in the expansion of $|H|$, such that $|H|$ is a non-constant polynomial. Solutions to $|H| = 0$ correspond to individual points. Therefore, if h is selected from a continuous field, such solutions are almost always avoided. This is true regardless of the choice of which hopping terms are fixed or not, so for randomly selected hopping terms from a continuous field $|H|$ is almost always non-zero. □

In chapters 5, 6 and 7 we often wish to study graphs where every vertex has non-zero support of a nullstate — a vector in the nullspace of that graph. And in chapter 6 and section 5.6 we also wish to study such graphs that have only one nullstate.

Definition 2.1.15. A graph G with N nullstates such that every vertex in the graph has non-zero support of a nullstate is an N-core graph [65]. A nut graph is a core graph of nullity 1 [66].

Nut graphs were first described by Irene Sciriha [66, 67], and have had numerous applications in chemistry [68–71] as we will discuss in more detail in chapter 6.

2.1.5.2 Some notions of topology

In this thesis we wish to study exact topological properties in finite tight binding models. To this end, we give a brief introduction to topology. As indicated in section 2.1 in order to study topology we need to define a topological space. A topological space consists of some set X with additional structure — a *topology* τ — on X. A topology allows for some notion of closeness between two points x and y in X without distance necessarily being defined. Loosely speaking a continuous change to the space X only changes the distance between any two points, so a topology allows us to study properties that are invariant up to continuous changes to X.

A topology on a space X allows us to understand how different subspaces of X are connected to one another, which may be done by defining subsets of X. For instance, we may define X as the set of all vegetables and fruit. Culinary fruit and vegetables are distinct, for example the set of fruit contains oranges, apples, and pears, and the set of vegetables contains tomatoes, potatoes, and carrots. In culinary terms, we might suggest that oranges are closer to apples then carrots are to apples. We may do this by defining a subset of $\{$oranges, apples, pears$\} \subset X$ and the subset $\{$tomatoes, potatoes, carrots$\} \subset X$. Because the subset of vegetables and fruit are disjoint in the culinary sense, then under the culinary topology X is a disconnected space. Alternatively, we may define the subsets of X in terms of their botanical definition. In this case many culinary vegetables are fruits, but all edible parts of a plant define a vegetable, so we may consider all vegetables as equally

close to one another. In this sense we may only allow one subset of X, which is X itself. Under this botanical topology (with a little extra structure this the trivial topology) we can never find a fruit that is not a vegetable, and so X is not disconnected. That is, the choice of topology will change how we understand the topological properties of the space X.

In chapters 5 and 7 we need to define a topology on certain subspaces, in such a way that the topological invariants we are interested in correspond to distinct topological phases. This can either be done by careful choice of a topology (which we will remark on briefly later in this section) or else by carefully defining your subspace of interest and using a quite standard choice of topology. We have favoured the latter in this thesis, but we anticipate the former also has advantages.

A topology on a space X may be defined in terms of open subsets (a definition first proposed by Hausdorff [72]) but can also be defined in many other (equivalent) ways, for example with closed subsets (using De Morgan's laws). For our purposes I think the definition in terms of open subsets is the most intuitive, as in chapter 7 we explicitly calculate topological invariants of open subspaces X_i that are entirely contained within other open subspaces X_j.

Definition 2.1.16. A topological space X is given by the pair (X, τ) where τ is the topology on X. A topology τ is given by a collection of sets of X where

1. The empty set $\varnothing \subset \tau$ and the whole space $X \subset \tau$.
2. For any subsets $U \subset \tau$ and $V \subset \tau$ then the union $U \cup V \subset \tau$.
3. For any subsets $U \subset \tau$ and $V \subset \tau$ then the intersection $U \cap V \subset \tau$.

Subsets that combine according to these axioms we define as open.

Remark. Note that a closed subset of X is a subset whose complement is open.

We will make use of the so called usual topology on a space X, although I think our approach to the classification problem may be (quite naturally) formulated in terms of a Zariski-like topology where closed subsets are defined as solutions to the coefficients of the secular equation of a Hamiltonian [73, 74]. The usual topology on an n dimensional space X has open subsets defined in terms of open n-balls, as well as the empty set and X itself [75]. An open n-ball in X consists of all points at a distance $x < r$ around a point in X.

In order to study the exact topological properties of a finite tight binding model H we define a parameter space ξ of which each H defines a point.

Definition 2.1.17. Let H be a tight binding Hamiltonian defined on a connected graph G with algebraically independent non-zero hopping terms $h_{i,j} \in \mathbb{F} \setminus 0$ for some field (often the real or complex numbers) $\mathbb{F}$. Let $(h_{i,j})$ be the tuple of hopping terms of H. This tuple defines the parameter space ξ of G with the dimension of the number of edges of G.

Remark. Every Hamiltonian H on G with specific hopping terms defines a point in ξ. A continuous map between two Hamiltonians $H_1, H_2 \in \xi$ involves continuous evolution of the hopping terms which defines a path in ξ.

If two Hamiltonians H_1 and H_2 are topologically distinct, then any continuous path between them involves a non-adiabatic change to the Hamiltonian. This allows us to define a collection of disjoint open subsets of ξ with each subset corresponding to a topologically distinct Hamiltonian. As will be discussed in chapters 5 and 7 we will define subspaces X of ξ in which these collections of subsets become disconnected. The number of topological phases is then found by counting the number of disconnected components of X. That is if there exists an open n-ball in X that connects two points then the two points represent topologically equivalent Hamiltonians.

The number of disconnected subspaces of a space X can be understood in terms of the number of ways to map a point x to X. Formally this is the zeroth homotopy group of X.

Definition 2.1.18. Let X be a topological space with the topology τ. Let $x \in X$ be a point in X. Let S^0 denote a point. The zeroth homotopy group $\pi(X)$ is the set of equivalence classes of maps $f : S^0 \to X$ such that for $a \in S^0$

$$f(a) = x \tag{2.1.45}$$

where $f_1(a)$ and $f_2(a)$ are in the same equivalence class if there exists a continuous map $g : X \to X$ such that $g(f_1(a)) = f_2(a)$. We denote this as $f_1(a) \sim f_2(a)$.

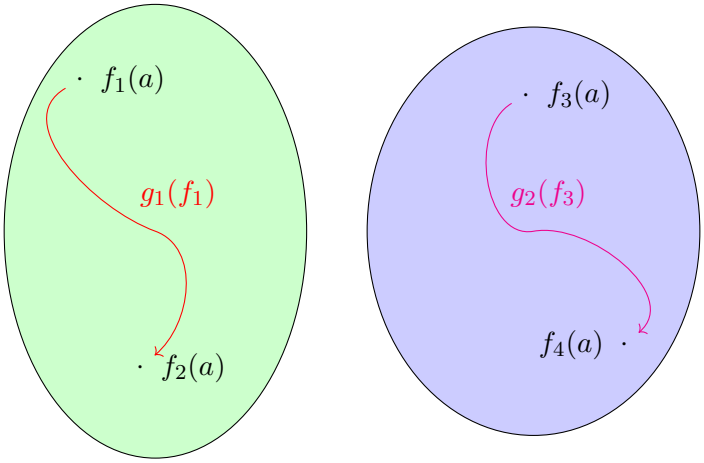

Figure 2.1.9: A space X with two disconnected components, giving two equivalence classes of the zeroth homotopy group $\pi(X)$. If this space X represented the number of topological phases a particular structure has, then this would give a $\mathbb{Z}_2$ classification.

Remark. All of the zeroth homotopy groups we calculate are of the form $\bigoplus^N \mathbb{Z}_2$ which we denote by $N\mathbb{Z}_2$. Elements of this group may be represented with an N-dimensional vector $(a, b, c, \cdots)$ where each a, b, c takes values in $\mathbb{Z}_2$.

In chapter 7 we wish to have an iterative way to define the subspaces of ξ. We can map between a subspaces of ξ by some map $f_{i,j} : X_i \to X_j$. As we will define many different subspaces of ξ it is convenient to represent this as a commutative diagram where each arrow corresponds to a different map.

Definition 2.1.19. A commutative diagram consists of a set of objects with a collection of maps between them represented by arrows. If the starting point is an object A then following any directed path that takes you to an object B will give the same image and preimage. Note that an inverse of a particular arrow may not be defined.

Following multiple arrows corresponds to taking a composition of maps. As an example, the following is a commutative diagram. This is taken from an example in section 7.7 of a structure we study experimentally.

$$\begin{array}{ccccc} E_0 & \xrightarrow{c_0^1} & E_2 \cap X_1 & \xrightarrow{c_2^2} & E_4 \cap X_2 \\ \downarrow & & \downarrow & & \downarrow \\ X_0 & \xrightarrow{|q_1|=0} & X_1 & \xrightarrow{|q_2|=0} & X_2 \end{array}$$

The rows denote different subspaces of ξ, with arrows indicating maps between these subspaces, and the maps labelled on the arrow. Here we have represented by E_{2n} a subspace of ξ with exactly $2n$ zero energy states. By X_i we denote subspaces defined by solutions to certain polynomials (which will be explained and defined in chapter 7). The hooked arrows denote inclusion maps, that is $E_{2n} \cap X_i$ is a proper subset of X_i. We refer to such a map as an inclusion or an embedding. A map from $X_i \to E_{2n} \cap X_i$ or $X_i \to X_j$ where $j > i$ we will refer to as a restriction.

We also often wish to represent maps from spaces to zeroth homotopy groups. We will represent these with arrows, but the general theory of such maps is outside the scope of this thesis (and are described by category theory). From the same example, such maps are represented as

$$\begin{array}{ccccc} X_0 & \xrightarrow{|q_1|=0} & X_1 & \xrightarrow{|q_2|=0} & X_2 \\ \downarrow & & \downarrow & & \downarrow \\ 3\mathbb{Z}_2 & \longrightarrow & \mathbb{Z}_2 & \longrightarrow & 0 \end{array}$$

where the bottom row represents a sequence of zeroth homotopy groups. Much of chapters 5 and 7 will revolve around computing these maps.

2.2 Coaxial cable networks as an experimental platform

In this work we often wish to observe topological phase transitions, and physical properties that occur at topological criticality directly on some structure. To do this we use coaxial cable networks, which are represented by tight binding models where cables correspond to edges and junctions correspond to sites [76–78] (although it is possible to represent sites with the centre of cables, which are connected at junctions [79]).

Topological phase transitions have been directly observed in tunable topological insulators by altering lattice parameters and chemical properties of the structure [80] changing the filling [81, 82] and even direct control of hopping terms in linear polariton devices [28, 82] and microwave arrays [83], as well as by creating multiple structures with different hopping parameters [26]. Order-disorder topological phase transitions have also been observed

in 2d photonic crystals [27] by detuning on site energy terms using sites with different refractive indices.

One difficulty in observing topological phase transitions on a particular graph is that its hard to change values of hopping terms independently, or without a significant change to the connectivity of the maximally localised Wannier functions. This makes direct observations of topological phase transitions on graphs difficult to experimentally observe without a discontinuous change to the underlying structure, or changing a symmetry of the Hamiltonian.

Coaxial cable networks can be used to create structures which are modelled by a tight binding model [76–79]. In these systems sites correspond to junctions in the network and cables correspond to hopping terms. The value of a hopping term between two sites is directly related to the impedance of the cable between the same two sites, allowing for hopping terms to be changed while maintaining exactly the same underlying structure. This allows for a very flexible platform for topological physics experiments.

Coaxial cable networks as an experimental platform have been used in a number of experimental settings. Including to make quantum graphs [84–88], to study edge states in graphene [78], and have been proposed as a good system for the study of topological phenomena in large structures [79]. In this thesis we primarily use them to experimentally study topological phase transitions in systems with arbitrary hopping disorder.

We may make two main measurements on a coaxial cable network using a vector network analyser (VNA). The first is a single port measurement, which can be used to find the local density of states (LDOS) (for example in chapters 3, 4, 5, 6, and 7). The second is a transmission measurement, which relates the phase and amplitude of an eigenstate on one site to that of another. We can use transmission to map out entire eigenvectors (as we use in chapter 6), and we can also use transmission to give signatures of delocalisation corresponding to topological phase transitions (as we use in chapters 3, 5, and 7).

This section is organised as follows. In section 2.2.1 we discuss a general mapping discovered by David Whittaker between coaxial cable networks and tight binding models [76, 77]. We then discuss experimental measurements of a coaxial cable network in section 2.2.2, and discuss a transfer matrix approach to classification, which helps tie together signatures of a topological phase transition to transmittance measurements. The details we discuss about experimental measurements of a coaxial cable network are based on results of David Whittaker, much of which are also detailed in the supplementary material of [76].

2.2.1 An equivalence of tight binding models & coaxial cable networks

A coaxial cable consists of an inner conductor, an outer conductor, and a dielectric between them. Due to their geometry coaxial cables are shielded which prevents interference from neighbouring electromagnetic signals (see Fig. 2.2.1 for an example of the cross section of a coaxial cable). When operating a coaxial cable, a current passes through the inner and outer conductor, typically the same current which is antiparallel in the two conductors. This results in an electromagnetic field in the dielectric through which transverse electromagnetic modes may propagate.

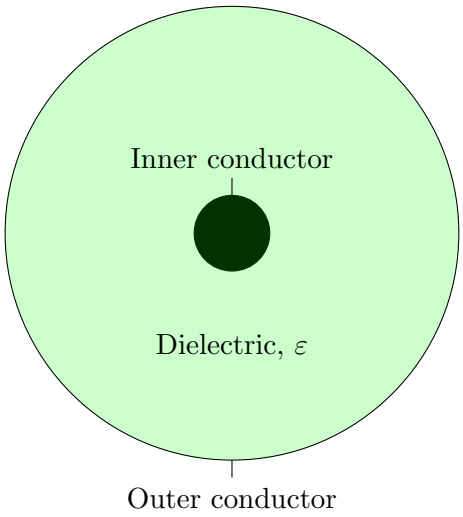

Figure 2.2.1: A cross section of a coaxial cable.

Assuming lossless cables, and approximating a 1d system the frequency response in a coaxial cable may be described by the Telegraphers' equations

$$\begin{aligned} \frac{d}{dx}V(x) &= iZ\omega\kappa I(x) \\ \frac{d}{dx}I(x) &= \frac{i}{Z}\omega\kappa V(x) \end{aligned} \tag{2.2.47}$$

where $I(x), V(x)$ are current and voltage, Z is the cable impedance, ω is the current frequency and κ^{-1} is the propagation velocity. Solving these equations yield

$$\begin{aligned} V(x) &= V(0)\cos\omega\kappa x + iZI(0)\sin\omega\kappa x \\ I(x) &= I(0)\cos\omega\kappa x + \frac{i}{Z}V(0)\sin\omega\kappa x. \end{aligned} \tag{2.2.48}$$

This defines the voltage and current at a point x in a cable (as illustrated in Fig. 2.2.2).

Using equation (2.2.48) it is convenient to relate $I(x), V(x)$ to $I(0), V(0)$ with a transfer matrix, so that

$$\begin{pmatrix} V(x) \\ I(x) \end{pmatrix} = \begin{pmatrix} \cos\omega\kappa x & iZ\sin\omega\kappa x \\ \frac{i}{Z}\sin\omega\kappa x & \cos\omega\kappa x \end{pmatrix} \begin{pmatrix} V(0) \\ I(0) \end{pmatrix} = M \begin{pmatrix} V(0) \\ I(0) \end{pmatrix}. \tag{2.2.49}$$

We make significant use of this transfer matrix in studying the topology of an SSH chain in chapter 3. This formalism can also be extended to more complex networks as discussed in section 2.2.2.1. We make use of this generalisation in chapters 5 and 7.

We wish to make coaxial cable networks which are more complex than a linear chain where, for every cable the transmission time $\tau = \kappa x$ is the same. That is, we wish to relate the voltage and current at any site in the network. Such a problem can be solved with a standard eigenproblem. We may do this by considering Kirchhoff's current rule — at any site the sum of currents in the network is zero, so we can write

$$\cos\omega\tau \sum_n i\frac{V_j}{Z_{n,j}} = \sum_n i\frac{V_n}{Z_{n,j}} \tag{2.2.52}$$

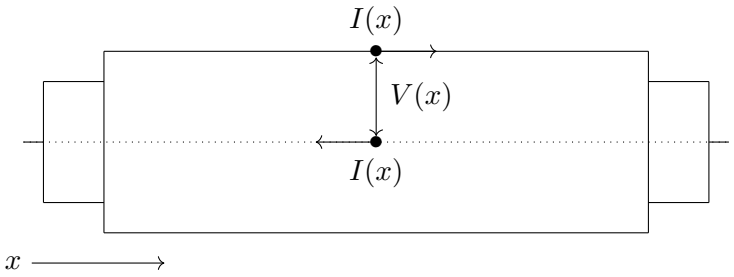

Figure 2.2.2: The current $I(x)$ and voltage $V(x)$ at a position x of the coaxial cable.

where the sum is taken over the n nearest neighbours of the site j, $Z_{n,j}$ denotes the impedance of a cable between site n and site j and V_n is the voltage at a site n. This is a general eigenproblem with an eigenvector consisting of voltages v, diagonal matrix p, and a matrix H,

$$\cos(\omega\tau)pv = Hv. \tag{2.2.53}$$

Let 'energy' be denoted $\varepsilon = \cos\omega\tau$. We may turn this in to a standard eigenproblem with the map

$$\varepsilon\bar{v} = p^{-\frac{1}{2}}Hp^{-\frac{1}{2}}\bar{v} \tag{2.2.54}$$

where $\bar{v} = p^{\frac{1}{2}}v$. The scaling is given by a diagonal matrix with entries given by

$$p_{j,j}^{-\frac{1}{2}} = \left(\sum_n \frac{1}{Z_{n,j}}\right)^{-\frac{1}{2}} \tag{2.2.55}$$

where the sum is taken over the nearest neighbours of the site j.

Remark. Note that unless the transmission time for every cable is the same, or at least integer multiples of one another, then the energy ε is not separable in the general eigenproblem. This makes the interpretation of energy in a system that lacks a constant transmission time difficult, so we require all the networks we experimentally study in this work to have the same transmission time τ (or an integer multiple of this).

We now have a standard eigenproblem which is equivalent to a Schrödinger equation

$$\varepsilon\bar{v} = \bar{H}\bar{v} \tag{2.2.56}$$

where $\bar{H} = p^{-\frac{1}{2}}Hp^{-\frac{1}{2}}$ is Hermitian and defines a tight binding Hamiltonian with hopping terms given by

$$\bar{H}_{i,j} = \left(\sum_n \frac{1}{Z_{n,i}}\right)^{-\frac{1}{2}} \left(\sum_m \frac{1}{Z_{m,j}}\right)^{-\frac{1}{2}} \frac{1}{Z_{i,j}}. \tag{2.2.57}$$

That is we may make arbitrary tight binding Hamiltonians with a coaxial cable network. The scaled and unscaled Hamiltonian $\bar{H}, H$ are related by a non-singular diagonal matrix so they are adiabatically equivalent and the topological properties of $\bar{H}$ and H are the same.

Remark. Note that throughout this thesis we will typically drop the bar, and just refer to the scaled Hamiltonian of the coaxial cable network as H.

The characteristic impedance of a coaxial cable may take complex values when they have sufficient loss or capacitance or inductance. Although we will use only cables which have an approximately real characteristic impedance at the frequencies we use for experiments in this thesis. This allows us to experimentally probe topological physics in systems with positive real hopping terms.

2.2.2 Measuring a coaxial cable network

As mentioned above, we make use of two main measurements on a coaxial cable network. We are using a two port vector network analyser (depending on the experiment this is a NanoVNA V2 Plus 4 or a NanoVNA V2 Plus 4 Pro) which has an input port and an output port so we can directly measure reflectance and transmission in a structure. The VNA itself measures the input and output amplitudes of power waves in the coaxial cable network.

A VNA measures the scattering parameters of a coaxial cable network. In particular, s_{11} is reflectance and s_{21} is transmission. These are given in terms of the left and right moving power waves in the network. Power waves are defined in terms of the left and right moving planar waves that form solutions to the telegrapher's equations. That is

$$\begin{aligned} a_{\text{in}} &= \frac{1}{2\sqrt{Z}}(V + IZ) \\ a_{\text{out}} &= \frac{1}{2\sqrt{Z}}(V - IZ) \end{aligned} \tag{2.2.58}$$

where Z is the (real) load on the port a of the VNA. The scattering parameters are then given by

$$\begin{aligned} s_{11} &= \frac{a_{\text{out}}}{a_{\text{in}}} \\ s_{21} &= \frac{b_{\text{out}}}{a_{\text{in}}} \end{aligned} \tag{2.2.59}$$

where a and b are the input and output ports of the VNA, respectively. Note that the input waves of a are moving in the same direction as the output waves of b. Furthermore, the input and output impedances are matched so

$$s_{21} = \frac{V_b}{V_a}. \tag{2.2.60}$$

To understand how these measurements relate to the states in the tight binding Hamiltonian, we need to model a coaxial cable system with input and output ports attached. The following discussion follows similar lines to the supplementary material of [76]. The VNA itself undergoes a calibration procedure (outlined in section 2.2.2.3) to correct the port impedance to 50Ω. The circuit diagrams for connecting the VNA to the structure are illustrated in Fig. 2.2.3.

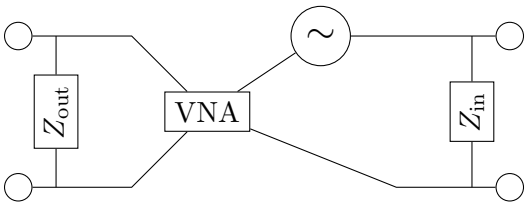

Figure 2.2.3: A simplified circuit diagram for the input and output ports. The input port is denoted with a signal generator to represent an inhomogeneous driving term. The two circles on each port denotes the connection to the inner and outer conductor of the coaxial cable.

Connecting an output port to the structure at a site j will result in the port drawing a current $I = \frac{V_j}{Z_{\text{port}}}$. By Kirchhoff's current rule the sum of currents on a site is zero, so this alters the onsite voltage by

$$V_j \left(\frac{-i}{Z_{\text{out}}} + \varepsilon \sum_n \frac{1}{Z_{n,j}} \right) = \left(\sum_n i \frac{V_n}{Z_{n,j}} \right) \tag{2.2.62}$$

where n is summed over the neighbours of the site connected to the VNA. This adds an imaginary onsite term to the unscaled Hamiltonian. Scaling reveals an onsite term of

$$-i\gamma = -ip_{j,j}^{-1}. \tag{2.2.63}$$

So connecting the VNA directly to the network gives a scaled Hamiltonian of the form

$$H + i\Gamma \tag{2.2.64}$$

where Γ is a diagonal matrix with non-zero terms representing an onsite imaginary energy for each port connected to the VNA.

On the input port, there is also a driven voltage V_d, and the port draws a current so connecting the input to site j yields $V_j = V_d - IZ_{\text{in}}$ where Z_{in} is the impedance of the input port. This is an inhomogeneous driving term so we may write

$$(H + i\Gamma)v = \varepsilon v + V_{\text{in}} \tag{2.2.65}$$

where v is an eigenvector of $H + i\Gamma$ and V_{in} is a vector with one non-zero term corresponding to the site j where $V_{\text{in}} = ip_{j,j}^{\frac{1}{2}} \frac{V_d}{Z_{\text{in}}}$.

The Greens functions of $H + i\Gamma$ relate a voltage on a site k to the site j connected to the input site by

$$v_k = G_{k,j} V_{\text{in}}. \tag{2.2.66}$$

The physical voltages (corresponding to those of the unscaled system) are then related by

$$p_{k,k}^{\frac{1}{2}} V_k = i \frac{p_{j,j}^{\frac{1}{2}}}{Z_{\text{in}}} G_{k,i} V_d. \tag{2.2.67}$$

So the transmission measurement is related to the Greens functions by

$$\frac{V_k}{V_d} = i\frac{p_{j,j}^{\frac{1}{2}}}{Z_{\text{in}} p_{k,k}^{\frac{1}{2}}} G_{k,j}. \tag{2.2.68}$$

The reflectance measurement is most useful to find the LDOS of H. This is because a large resonance in the structure may be indicated by a large loss (analogously to loss increasing with amplitude in an oscillating mechanical system). The loss in a coaxial cable network is indicated with the real part of the impedance, which we may calculate with the reflectance.

To see how the local impedance is related to the s_{11} measurement we make use of the power wave basis and the fact $I_{\text{in}} = \frac{V_{\text{in}}}{Z_s}$ on an input port. Therefore

$$Z_s = Z_{\text{in}} \frac{1 + s_{11}}{1 - s_{11}} \tag{2.2.69}$$

where Z_s is the impedance of the structure on that site.

To see that the LDOS is proportional to Z_s we look to the Greens functions of H and the Greens functions of $H + i\Gamma$ for a single port measurement. A diagonal term of the Greens functions of H is given by

$$g_{j,j}(\varepsilon) = \sum_k |u_k^j|^2 \frac{1}{\varepsilon - \varepsilon_k} \tag{2.2.70}$$

where the sum is over the eigenstates u^k with an entry u_k^j on site j and eigenvalues ε_k. In the limit as $\varepsilon \to \varepsilon_k$ the Greens function is dominated by the term with eigenvalue ε_k therefore

$$g_{j,j}(\varepsilon_k) = \sum_k |u_k^j|^2 \delta(\varepsilon - \varepsilon_k) \tag{2.2.71}$$

which is the local density of states. Note that we will use G for a Greens function of $H + i\Gamma$ and g for a Greens function of H.

To relate impedance of the structure to the LDOS, we compare the Greens functions when connecting one port to the network to the Greens functions of H. Using the Sherman-Morrison formula the Greens function when connecting a single port to the VNA is related to $g_{j,j}$ by

$$\frac{V_j}{V_d} = i p_{j,j}^{\frac{1}{2}} G_{j,j} = \frac{i p_{j,j}^{\frac{1}{2}} g_{j,j}}{Z_{\text{in}} + i p_{j,j}^{\frac{1}{2}} g_{j,j}}. \tag{2.2.72}$$

Viewing the coaxial cable network as an impedance in series with the input impedance reveals that

$$\frac{V_j}{V_d} = \frac{Z_s}{Z_{\text{in}} + Z_s} \tag{2.2.73}$$

and so $Z_s = i p_{j,j}^{\frac{1}{2}} g_{j,j}$. When driving the structure the onsite imaginary term $-i\gamma$ that is a consequence of connecting the VNA to the structure means $-\text{Im}[g_{j,j}]$ corresponds to the LDOS. That is

$$-\text{Re}[Z_s] = p_{j,j}^{\frac{1}{2}} \sum_k |u_k^j|^2 \delta(\varepsilon - \varepsilon_k). \tag{2.2.74}$$

Using the reflectance to calculate the local impedance therefore gives us an experimental measurement of the LDOS of the structure.

2.2.2.1 A transfer matrix approach

In many experiments we wish to measure the two site transmission of a coaxial cable network. Generally, we make use of transmission measurements because properties of the transfer matrix may be used to indicate a topological phase transition [76, 89, 90] (and as we use in chapters 3, 5, and 7). It is also very useful for finding the phase relationship between two sites, as we use in chapter 6.

To see the relationship between a phase transition and the transfer matrix consider an infinite periodic structure with a transfer matrix of $M(\varepsilon)$ for some slice of the structure. Due to periodicity when a transfer matrix has an eigenvalue of $e^{i\phi}$ for some phase factor ϕ then there is a state with energy ε at $k = \phi$ in the Brillouin zone.

For a finite system we consider a transfer matrix defined for the complete structure. In order to do this, we need to cut an individual site to make an input and output site (as indicated in Fig. 2.2.4). In this structure if there is an eigenvalue of 1 then there is an eigenstate which satisfies the boundary conditions of the uncut structure, so at $\varepsilon = 0$

$$|M(\varepsilon = 0) - I| = 0 \Leftrightarrow |H| = 0. \tag{2.2.75}$$

For an uncut chiral structure that does not have topologically protected states, then this indicates a closed gap. It is this property that we use to study topological phase transitions experimentally.

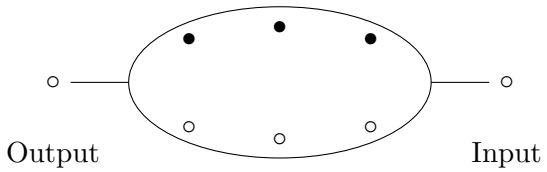

Figure 2.2.4: An example of a structure cut for a transmission experiment. The edges connecting sites in the ellipse are not drawn in so as to represent an arbitrary chiral structure. The input and output ports of the VNA are then each connected to a cut site.

The transfer matrix also indicates if an eigenstate is delocalised in a structure. Consider a chiral structure with an even number of sites. Cutting the structure on a site introduces an imbalance in the number of black sites n_b and the number of white sites n_w. This creates a zero energy state on the cut structure. As in equation (2.2.60) measuring transmittance then gives the relative magnitude of this state on the input and output sites. Because the cut input and output sites are now quite distant from one another, support of the created nullstate is the largest on both sites when the state is delocalised. The relationship between delocalisation and transmittance has a few subtleties to it, as we discuss further in chapters 3, 5, and 7.

In chapter 6 we wish to make use of transmission experiments to experimentally find the complete nullspace of a selection of nut graphs. Nut graphs have all real eigenvectors,

so we wish to use these measurements to find the relative sign of a nullstate on two sites.

The transmission is related to the Greens functions as in equation (2.2.68), so we can experimentally probe the phase relationship of $H + i\Gamma$ on two sites with a transmission measurement. We can relate these to the nullspace of the structure itself by using the Woodbury matrix identity, giving

$$G_{a,b} = \frac{g_{a,b}}{1 + \gamma_{\text{in}}\gamma_{\text{out}}(1-\varepsilon^2)(g_{a,b}g_{b,a} - g_{a,a}g_{b,b}) + i(1-\varepsilon^2)^{\frac{1}{2}}(\gamma_{\text{in}}g_{a,a} + \gamma_{\text{out}}g_{b,b})}. \tag{2.2.77}$$

For a nut graph, which has all real eigenvectors and has only one zero energy state $g_{a,b}g_{b,a} - g_{a,a}g_{b,b} = 0$. So we can relate the two Greens functions by

$$G_{a,b} = g_{a,b}(1 + \alpha i)^{-1} \tag{2.2.78}$$

where $\alpha \in \mathbb{R}$. This alters the transmission by a phase factor in $\left(-\frac{\pi}{2}, \frac{\pi}{2}\right)$ so the real part of the transmission can be used to get the sign dependence of an eigenstate on two sites.

2.2.2.2 Vector Network Analyser

A VNA measures the amplitude and phase of power waves that propagate a coaxial cable network at a particular frequency. The basic working principle behind a VNA is to have a signal generator to drive a structure and measure a frequency response of the network. This response is then compared with a reference signal.

Roughly speaking the VNA we use has one driven input, and so the signal generator is connected only to the input port. This is then split in to two arms, one to drive the network and the other to measure the input signal. The arm which drives the network is connected to a directional coupler — a resonator which is shorted on one end. This allows the signal returning to the input port to be isolated from the signal driving the network. The input and output signal are then compared to a reference oscillator, giving the s_{11} measurement.

The undriven port does not have an input on the structure, so only the output signal is measured. This is connected to a directional coupler. The output of this coupler is connected to the same reference oscillator, allowing measurement of the s_{21} term.

In combination this allows the frequency dependence of the reflectance and transmission to be measured. A simplified diagram of this is illustrated in Fig. 2.2.5. It should be noted that the NanoVNA itself uses a different architecture, where a careful use of switches allows for only one directed coupled in the device. The working principle is still the same, however.

2.2.2.3 Experimental protocols

The VNA was operated with the software NanoVNA-Saver version 0.5.5. The software runs a calibration procedure with a short-open-load measurement on the input port and a through and isolated (both ports are shorted) measurement for a two port calibration. The calibration itself is based on a direct reverse calibration measurement, as detailed in [91].

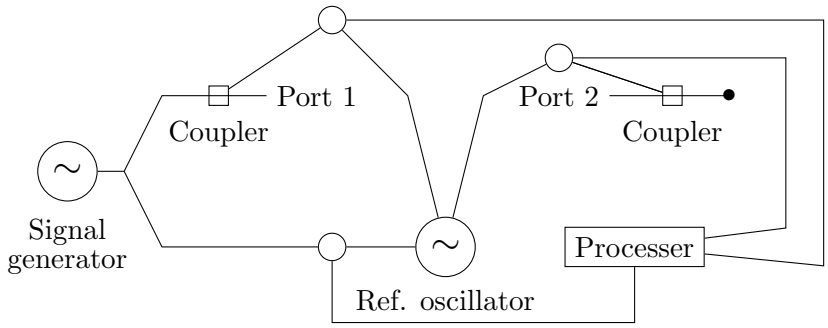

Figure 2.2.5: A highly simplified circuit diagram for a 2-port VNA, to measure s_{11} and s_{21} parameters. Each coupler is a directed coupler to extract the incoming wave amplitude on each port.

2.2.2.4 Experimental techniques

Making coaxial cable networks that represent arbitrary real tight binding models comes with a few difficulties. We begin by discussing issues relating to manufacturing cables, before detailing some experimental challenges of the networks themselves.

As discussed in section 2.2.1 one crucial aspect of making a coaxial cable network which represents a TB model is to ensure that the transmission time of every cable is the same. Of course, in practice this is not possible. Instead, we have a procedure for making two cable types, each with a specific transmission time as close to the desired transmission time as possible. The two cable types we use in our experiments are RG58 cables and RG62 cables, with a characteristic impedance of 50 Ω and 93 Ω respectively.

The coaxial cable networks are made with SMA connectors — one female end and one male end. The commercial standard for such connectors is that they have a 50Ω characteristic impedance. The length of the connectors alters the transmission time of the complete cables. To get around this, for each cable type we attached with a male or female connector to one end and left the other end as a cut cable. We then measured the transmission time and attached a final female or male connector to the other end and repeated the measurement. This gave us an experimental measurement of the transmission time of each connector. We also compared this to the length of the connectors as detailed in the relevant specification sheets for the connectors.

The connectors used were Amphenol RF132240 and Amphenol RF132231 for female and male RG62 SMA connectors, and Telegartner J01151A0491 and Multicomp Pro 19-03F-4-TGG for female and male RG58 SMA connectors.

Using the transmission time of a connector, we can calculate the required transmission time of a cable connected with just a male end, to ensure the final complete cable has the correct transmission time. Cable manufacturing then followed this procedure:

1. Cut a length of coaxial cable to roughly the right length (but intentionally slightly too long).

2. Connect a male connector to the cable.

3. Measure the transmission time, and iteratively cut the cable to the appropriate length, until the measured transmission time matches the required time.

4. Attach the female connector to the cable.

5. Measure the final transmission time to ensure the cable has the appropriate length.

A completed cable was then characterised with a single port and two port measurement, to ensure it was within a suitable range of the ideal transmission time, and its transmission properties were suitable. Data were collected in a database, allowing for very precise simulations of the networks. Note that most of the simulations we used to compare to experimental data did not take in to account the specific cables, once we had a good enough ensemble of individual cables.

In terms of making coaxial cable networks there are a few problems mainly relating to measurements, and connections within the network.

Connecting a port of the VNA to a network introduces an extra length in the structure, which results in a slightly off site measurement. This connection can be modelled as a short coaxial cable which, as per equation (2.2.49), has the transfer matrix

$$M_c = \begin{pmatrix} \cos\omega\kappa_c d_c & iZ_c \sin\omega\kappa_c d_c \\ \frac{i}{Z_c}\sin\omega\kappa_c d_c & \cos\omega\kappa_c d_c \end{pmatrix} \tag{2.2.80}$$

where d_c is the length, κ_c^{-1} is the transmission speed, Z_c is the impedance all of the connector, and ω is the driving frequency. This acts as a phase shift on the voltage and current before and after the connector, and so the transmittance $|s_{21}|$ is unaffected by measuring slightly off site.

For a single port measurement local impedance is related to the transfer matrix of the complete structure by

$$Z_m = -\frac{M_{22}}{M_{12}}. \tag{2.2.81}$$

Taking in to account the connector when connecting the network to a single port of the VNA results in a shift of the impedance by

$$Z_m = \frac{-M_{c_{22}} + M_{c_{22}} Z_s}{M_{c_{11}} - M_{c_{12}} Z_s} \tag{2.2.82}$$

where Z_m is the measured impedance, and Z_s is the impedance of the structure on the site. Finding Z_s allows us to effectively calibrate out the connector forcing an off site measurement.

Connections within a network also need to be accounted for. This can be most effectively dealt with in a linear structure. The finite length of a connector alters the effective length of 50Ω coaxial cable, which we can simply account for by increasing the length of 93Ω coaxial cable. The sites are then located where a change of impedance occurs. We also allowed for double lengths of 93Ω cable without including a small 50Ω region by making double length cables. To prevent a connector at the unconnected end affecting the measurement, we made two cables which terminated without a connector. These allowed us to

terminate the structure exactly on a site.

For a more complicated network we may need to connect n nearest neighbours to a particular site. Commercially only 3 port connectors are available[2] (higher number of ports are commercially available, but these distribute the power equally to each port which we want to avoid in our structures). To reach higher connectivity we simply attached multiple T-connectors to one another.

With T-connectors also being 50Ω this results in two problems. The first is that it is not possible to have 93Ω connectors between two such sites, and the second is that connecting several T-connectors shifts the location of a particular site. Our approach here was to maintain the transmission time of each complete cable (with SMA connectors attached). To first order this results in a small on site energy, which was generally not sufficient to affect measurements enormously and was not accounted for in data analysis. It may be possible to have a more optimal approach, but this is not a trivial problem, and is currently being worked on by colleagues. The second problem may be improved by manufacturing custom connectors, although we do not address this approach here, and this also being looked in to by colleagues.

There are also some issues which arise from the quality of a connection when the coaxial cable network is completely connected. Sometimes in making the cables, or repeated plugging and unplugging of the connectors the internal pins can shift and no longer reach the ideal point of a connector. This can result in a capacitive effect at the junction. At the low radio frequencies we are running experiments this causes significant losses. To account for this, once a cable is known to have connection issues it is characterised once again and removed from the ensemble of cables used to make structures. This does not give a great way to detect damaged cables, but any experimental data were compared with numerics to ensure the structure was behaving as expected.

[2]Note that this means the most ideal graphs to make with a coaxial cable network are in the class of chemical graphs, much to the pleasure and amusement of our chemist collaborators.

Chapter 3

Exploring topological physics in coaxial cable networks: the Su-Schrieffer-Heeger model

As discussed in section 2.2, at radio frequencies, a coaxial cable network can be modelled with a tight binding model [76, 78, 79]. Furthermore, coaxial cables are flexible, allowing a simple method to make structures with a tight binding model of non-planar graphs, which (up to the constraints of engineering suitable connectors) may have any geometry or connectivity.

Coaxial cable networks can also be designed to have exact chiral symmetry. In many systems it is difficult to exactly control the hopping terms between sites, while simultaneously letting them evolve. As discussed in section 2.2 this makes it hard to engineer systems with exact symmetries. One significant advantage of coaxial cable networks is the ability to exactly control the neighbours of individual sites, as well as hopping terms between them, allowing exact symmetries — such as chiral symmetry — to be maintained. This makes coaxial cable networks a promising platform for disordered topological photonics experiments.

As an example of a coaxial cable network representing a topological system, we present an experimental study of a Su-Schriefer-Heeger (SSH) model [24]. We demonstrate a topological phase transition, along with a topologically protected state of the kind that will be discussed more in chapter 4.

The SSH model was originally developed as a model for a polyacetylene molecule (see Fig. 3.0.1) which consists of a linear chain, with two sites in a unit cell. It is a tight binding model with the Hamiltonian

$$H = \sum_i t_{i_1} |2i+1\rangle \langle 2i| + t_{i_2} |2i+2\rangle \langle 2i+1| + \text{H.c.} \tag{3.0.1}$$

where t_{i_1}, t_{i_2} are hopping terms, and H.c. denotes the Hermitian conjugate. The intracell hopping is given by t_{i_1}, while the intercell hopping is given by t_{i_2}. When $t_{i_1} = t_{j_1}$ and $t_{i_2} = t_{j_2}$ for every $i \neq j$ the SSH model has no disorder.

The SSH model has two sublattices, so it has chiral symmetry. As discussed in section 2.1.4, sublattice symmetry satisfies the requirement for chiral symmetry to survive when allowing arbitrary continuous hopping disorder.

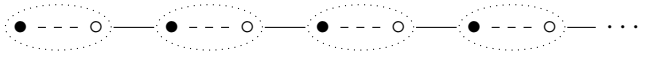

Figure 3.0.1: The structure of the SSH model. Notice the two sets of sites (black and white) corresponding to the two sub lattices. A unit cell is indicated by the dotted ellipse, with the solid line an intercell hopping and the dashed line an intracell hopping.

In [76] we discuss experimental results corroborating the observation of a topological phase transition, and a topologically protected state in a disordered SSH model. I gratefully acknowledge Prof. David M. Whittaker who devised the project and also wrote [76]. I contributed to the experimental work with the insightful and expert help of Dr. Qingqing Duan, and I contributed a little to the development of the theory by helping to uncover the relationship between the determinant of the SSH model, and the eigenvalues of the transfer matrix. I also helped to solve several experimental problems with using coaxial cables, as outlined below.

In [76] we observe a phase transition in a disordered SSH chain by using two methods. In both cases we use a probability distribution to generate hopping terms, which may be biased to take a structure away from a topological phase boundary. We then take the structure through a phase transition by altering how this distribution is biased.

The first method we used to observe a phase transition was by direct measurement of the LDOS in a looped SSH chain. This allowed us to detect a gap closure around zero energy as we varied the probability distribution of hopping terms in an ensemble of randomly generated SSH chains. To confirm the structure has two zero energy states at topological criticality, the LDOS was measured on a site of both sublattices. Recall from section 2.1.4 that for a chiral structure a zero energy state may be localised to each sublattice, so confirming non-zero support on both sublattices corroborates the presence of two zero energy states. This was further demonstrated by a small energy splitting between the two states, verifying the sublattices hosted distinct zero energy states.

Secondly, we cut the looped chain to create an open chain with an odd number of sites. Measuring transmittance of the cut structure allowed us to observe a topological phase transition, present in the equivalent looped structure. As discussed in section 2.2.2.1, at zero energy the measured transmittance in the cut chain is a maximum when the looped chain is topologically marginal. This is because — neglecting losses in the coaxial cables — at zero energy, a topologically marginal looped chain corresponds to a cut structure that has a transfer matrix with unit eigenvalues. As the chain is driven away from topological criticality (by altering the values of hopping terms) the eigenvalues of the transfer matrix are no longer one and the transmittance reduces. So by measuring the transmittance for an ensemble of disordered SSH chains which were either topologically marginal, or on one side of the phase boundary, we were able to observe a topological phase transition in the structure. The experimentally measured transmittance for the ensemble of the SSH chains

agreed well with the predicted transmittance from the transfer matrix treatment at zero energy.

To observe a topologically protected state we measured the LDOS of the cut structure (which, having an odd number of sites, has a topologically protected state) using the same ensemble of structures as in the transmittance experiments. We demonstrated a very robust zero energy state, with a standard deviation of 0.2% over the ensemble.

To achieve this demonstration of a topological phase transition and topological protection in a coaxial cable network, required overcoming a few experimental problems (as detailed in section 2.2.2.4). Largely these issues are a result of the finite junction lengths that are necessary to connect two cables. We first recall issues with measuring the network, and then discuss problems with how the network itself is connected. Furthermore, as mentioned in section 2.2 it is difficult to independently change hopping terms in a structure without changing the connectivity of the maximally localised Wannier functions. As a coaxial cable network allows for exact control of connectivity, we wished to unambiguously demonstrate such a phase transition in a disordered structure, so we wanted to try and overcome these issues as best as we could.

Ideally experimental measurements would be made exactly on a lattice site. However, the finite size of the ports of the vector network analyser (VNA) mean measurements are inherently made off site.

With a two port VNA we can make two measurements on a structure — reflectance and transmission measurements. Because the topological properties we are most interested in occur at zero energy ($\varepsilon = \cos\omega\tau = 0$) it is useful to know how measuring off site affects reflectance and transmission near zero energy. For the purposes of studying the SSH model, transmittance and reflectance are the two most useful measurements. As demonstrated in section 2.2.2.4 transmission undergoes a phase shift with an off-site measurement, so transmittance is not affected by measuring slightly off-site.

We use the reflectance data to find the local impedance, which (as shown in [76] and discussed in section 2.2.2) has peaks corresponding to the LDOS. As discussed in section 2.2.2.4 we chose the sites of the SSH chain to correspond to where the impedance changes in the structure. As a consequence the finite length of SMA connectors ensures all measurements are made off-site, as illustrated in Fig. 3.0.2. Measuring off-site results in a shift in the LDOS. As we demonstrated in section 2.2.2.4 this shift has a simple functional form, and we are able to account for this by transforming the data by

$$Z_s = \frac{-Z\cos(\omega l_a) + iZ_a\sin(\omega l_a)}{-\cos(\omega l_a) + i\frac{Z}{Z_a}\sin(\omega l_a)} \tag{3.0.3}$$

where Z_a is the impedance of the connector, ω is the frequency, l_a is the distance off the site (it is positive when measuring off an RG62 cable, and negative when measuring off an RG58 cable), and Z is the impedance calculated from the raw data. This transformation allows us to infer the LDOS exactly on a lattice site.

If a cable does not terminate with a site this also leads to a shift in the measured LDOS. To account for this we made special cables which are cut to the right length to terminate the chain exactly on a lattice site.

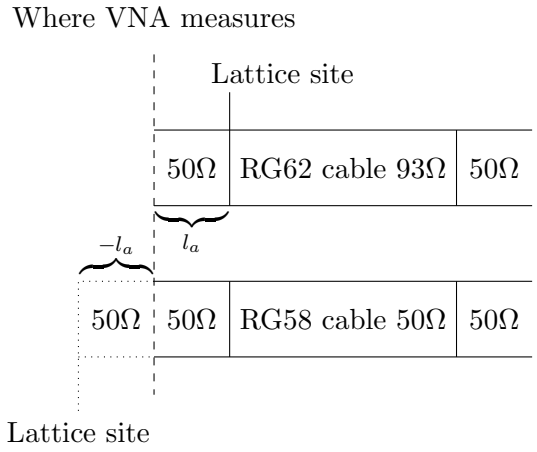

Figure 3.0.2: To account for the 50Ω characteristic impedance of the SMA connectors, the coaxial cables are made so that a change in impedance matches a site in the structure. When connecting to the VNA this forces the measurement to be taken slightly off-site, by a length l_a. For an RG62 cable this puts the ideal place to measure away from the VNA, and for an RG58 cable this puts the ideal place to measure inside the VNA port. We can account for this shift with equation (3.0.3) to infer the LDOS on the actual site.

Another issue, as also mentioned in section 2.2.2.4, is that the connectors between any two cables are of a finite size. Commercial SMA connectors are typically 50Ω. In this work we used two types of cables: 50Ω (RG58) cables and 93Ω (RG62) cables. For linear structures we we may get around this by using the connector lengths as an extension of the 50Ω cables. In this case, the lattice sites are located where the impedance shifts from 93Ω to 50Ω. To account for this effective increase in the length of 50Ω cables the RG62 cables were made slightly longer.

As we have discussed, cables were made using the VNA to benchmark the transmission time of each cable, before both ends of the cable were fastened in place. This is much more convenient to do when the complete cables (transmission line and the connectors) both have the same transmission time, which is the approach we used for more complex networks. However, the change in length of the complete cable (with the fastened ends) means the complete RG62 cable is longer than the RG58 cable. To account for this we measured the shift in transmission time of both cable types upon the addition of a female connector. Using these data we were able to know the exact transmission time required of each finished cable type. In combination with the cable manufacturing protocol discussed in section 2.2.2.4 this allowed us to make ensembles of cables each with a standard deviation of 2mm of the ideal length for our experiments[1].

Another issue that arises from the 50Ω connectors is that if two RG62 cables neighbour each other, then there will necessarily be a small 50Ω region between them. To solve this we made double length RG62 cables, and restricted the distribution of structures so that no more than two cables of the same type will neighbour each other.

[1]Calculated from the characterisation of the manufactured cables.

Finally, there was a problem arising from the measured transmittance in certain structures. This resulted in a non-zero variance of measurements around what the simplest transfer matrix approximation would reveal. However, by including losses in numerical modelling resulted in states that were localised differently to when not considering losses. This altered the transmittance, but we were able to predict the exact transmittance of a particular structure very accurately in numerics when accounting for such losses. This was generally an issue more for structures away from a phase transition.

3.1 Linear paper

Observation of a Topological Phase Transition in Random Coaxial Cable Structures with Chiral Symmetry

D. M. Whittaker and Maxine M. McCarthy
Department of Physics and Astronomy, University of Sheffield, Sheffield S3 7RH, UK.

Qingqing Duan
Wenzhou Institute and Wenzhou Key Laboratory of Biophysics, University of Chinese Academy of Sciences, Wenzhou, Zhejiang 325001, China.

(Dated: April 24, 2024)

We report an experimental study of the disordered Su-Schrieffer-Heeger (SSH) model, implemented in a system of coaxial cables, whose radio frequency properties map on to the SSH Hamiltonian. By measuring multiple chains with random hopping terms, we demonstrate the presence of a topologically protected state, with frequency variation of less than 0.2% over the ensemble. Connecting the ends of the chains to form loops, we observe a topological phase transition, characterised by the closure of the band gap and the appearance of states which are delocalised, despite the strong disorder.

The Su-Schrieffer-Heeger (SSH) model[1], originally a description of the electronic states in polyacetylene, is one of the simplest systems of topological physics. It consists of a chain of sites, representing carbon atoms, connected by hopping terms which alternate in strength, corresponding to the bonds of the dimerised molecule. In this periodic form, it has a band gap which closes when the two hopping strengths are the same. The gap closure separates two topological phases, determined by the relative magnitudes of the hopping amplitudes. With appropriate termination, SSH chains can support localised boundary states which are said to be topologically protected, because their energy is independent of disorder in the hopping amplitudes. These non-trivial topological properties are a consequence of the chiral, or sublattice, symmetry of the SSH model: the sites can be divided into two sublattices, such that there are only hopping terms connecting the two types.

The topology of the SSH model is robust in the presence of disorder, provided that the chiral symmetry is not broken. A chain with a random sequence of hopping amplitudes can still be assigned to one of two topological phases. We can thus talk about a topological phase transition in an ensemble of random SSH loops, driven by varying the parameters in the probability distribution from which the hopping amplitudes are drawn[2]. The theory of such random chains, with off-diagonal disorder, has a long history, dating back to work by Dyson[3–5] and continuing through modern scaling theories of the Anderson transition[6–10]. If the probability distribution for each hopping term is the same, leading to structures which are close to the topological phase boundary, the states at zero energy are predicted to be delocalised. Measurements of the localisation properties can thus provide a signature of a topological phase transition. In an infinite chain, the transition is also predicted to be accompanied by a singularity in the density of states.

There have been numerous experimental studies of implementations of the SSH model using electromagnetic waves, in photonic and microwave structures[11–15], and discrete electronics[16, 17]. It is generally hard to control all the couplings in these systems so as to maintain chiral symmetry with sufficient accuracy to observe the effects we discuss, particularly while introducing controlled disorder. This is has been achieved in cold-atom systems[18], where delocalisation at a topological phase boundary has been observed[19] for a momentum-space SSH structure.

Coaxial cable networks are a very simple electromagnetic system which can be used to investigate disorder[20] and topological[21, 22] physics. We have shown[23] that cable structure can be fabricated with radio frequency properties which map very accurately onto the SSH Hamiltonian. The hopping amplitudes are determined by the impedances of the corresponding cables, so it is easy to make a random ensemble of chains with full chiral symmetry. In this letter, we use cable structures to investigate experimentally the properties of random SSH chains. By the use of impedance and transmission measurements, we demonstrate very precise topological protection of a state, and show the delocalisation and closing of the gap at the phase transition.

The derivation of the matrix description of a coaxial cable network is given in the Supplementary Materials, S1. We consider a network consisting of a set of sites, labelled n, connected by sections of coaxial cable, all of which have the same transmission time, τ, the length divided by the transmission speed. The cable connecting sites n and n' has electrical impedance $Z_{nn'}$. The network has radio frequency resonances which are determined by a matrix eigenvalue equation $Hv = \varepsilon v$, where the dimensionless 'energy', ε, is related to the frequency, ω, by $\varepsilon = \cos\omega\tau$. The components of the vector v are the voltages at the sites, scaled such that the actual voltage is $V_n = \sigma_n v_n$. Here $\sigma_n = (\sum_{n'} Z_{nn'}^{-1})^{-1/2}$, with the sum taken over the sites n' directly connected to n. The matrix elements of the 'Hamiltonian' are then the hopping amplitudes

$$H_{nn'} = \sigma_n Z_{nn'}^{-1} \sigma_{n'} \ . \tag{1}$$

This one-to-one mapping from cables connecting sites to hopping amplitudes means it is possible to create a net-

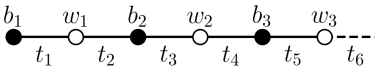

FIG. 1. Sublattice colouring of an SSH chain, with black and white sites labelled b_n and w_n, as in Eq.(2). The hopping amplitudes, t_n, follow Eq.(3).

work corresponding to any finite real matrix Hamiltonian, though in practice this is limited by the availability of cables with arbitrary impedances.

We measure the radio frequency properties of the cable structures using a vector network analyser (VNA). Two sorts of measurement are useful. A single port reflection measurement of the S_{11} parameter gives us the impedance of the structure measured at a given site. We show, in Supplementary Materials S2, that the real part of this is proportional to the local density of states, broadened only by losses in the cables. This enables us accurately to determine the frequencies of the resonances of the structure. Two port transmission measurements (S_{21}) provide information about the spatial extent of the states, allowing us to detect the delocalisation which occurs around the phase transition.

A Hamiltonian has chiral symmetry if the sites can be divided into two sublattices, which we call 'black' and 'white', Fig.1, such that there is only hopping between sites on different sublattices. There can be no intra-sublattice terms, including on-site energies. If this is the case, ordering the basis such that all the black sites proceed the white sites gives an anti-diagonal form:

$$H\begin{pmatrix} b \\ w \end{pmatrix} = \begin{pmatrix} 0 & Q \\ Q^\dagger & 0 \end{pmatrix}\begin{pmatrix} b \\ w \end{pmatrix} = \varepsilon \begin{pmatrix} b \\ w \end{pmatrix} . \qquad (2)$$

From this we obtain $(Q^\dagger Q)w = \varepsilon^2 w$, so the eigenvalues must either be zero, or occur in symmetric pairs with opposite signs. It immediately follows that for a chain with an odd number of sites there must be at least one zero energy state. Since this conclusion does not depend on the values of the hopping amplitudes which form the matrix elements of Q, the zero-energy state is topologically protected against disorder. More generally, for a chiral network with n_b black sites and n_w white sites, there are at least $|n_b - n_w|$ protected states.

Fig.2 shows the local density of states measurement for a number of structures consisting of sequences of 16 cables connected end-to-end. The individual cables are randomly selected from two impedances: 50Ω and 93Ω. The structures thus map onto finite length SSH chains with randomised hopping terms. More details of the cables are given in the Supplementary Materials S3. Fig.2(a) shows unlooped chains, with the measurement on a site at the end of the structure. The 16 cables correspond to 17 lattice sites, so we see, as expected, a topologically protected $\varepsilon = 0$ state, at a frequency of approximately 114MHz. The topological protection is very good: the inset shows combined results for this state in 41 random structures. The standard deviation of the resonance energy is approximately 0.22MHz, which we believe is due to small errors in the lengths of the cables.

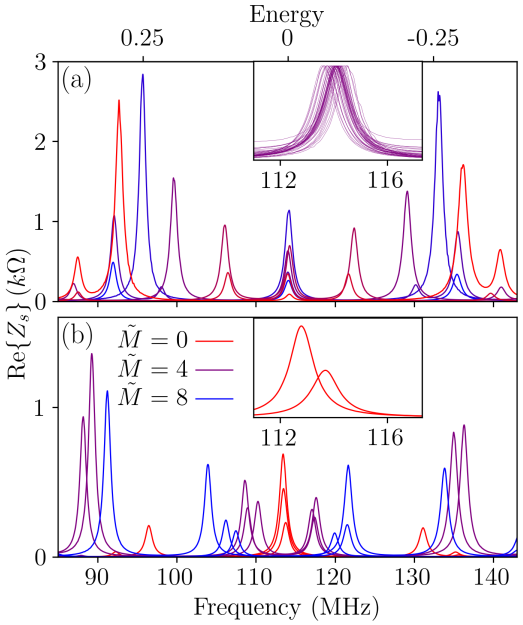

FIG. 2. (a) Measured impedance spectra (local density of states) for a selection of unlooped length $N = 16$ random SSH chains. The colours are an aid to distinguishing curves. The spectra show the expected symmetry about the chiral frequency (∼ 114MHz), which corresponds to zero energy in the SSH Hamiltonian. The topological protection of the state at $\varepsilon = 0$ is apparent. The inset shows, expanded and normalised, the protected state in an ensemble of 41 unlooped chains, demonstrating the minimal chiral symmetry breaking in our cable structures. (b) Impedance spectra for looped length 16 random cables with various reduced lengths, Eq.(5): $\tilde{M} = 0$ (red), $\tilde{M} = 2$ (purple) and $\tilde{M} = 4$ (blue). Reducing $\tilde{M}$ closes the gap, leading to a doubly degenerate state at the chiral frequency for the topologically marginal $\tilde{M} = 0$ structures. The inset shows spectra for $\tilde{M} = 0$ around $\varepsilon = 0$ measured on adjacent sites, revealing the two states, one localised on each sublattice. Compared to (a), there is more chiral symmetry breaking, and a slight lowering of the chiral frequency, due to the extra length of the T-connector inserted in the loop to make the measurement.

A topological phase transition is signalled by the presence of a pair of degenerate states at zero energy, equivalent to the gap-closure in a periodic structure. When $n_b = n_w$, this corresponds to the condition that the determinant $|Q| = 0$[25]. For our structures, $|Q|$ is a simple product of hopping amplitudes, the first term in Eq.(3), which cannot be made zero without cutting the chain, so there is, trivially, just one topological phase. However, by joining the ends of the chains to form loops, we can observe a transition between the two phases of the SSH model, using measurements of the local density of states. For chiral symmetry, the loops must consist of an even number of sites, and thus be made from an even number of cables. In a loop with N cables, labelling hopping amplitudes rather than the sites, $t_1, t_2, \ldots t_N$ (Fig.1), we

obtain

$$|Q| = t_1 t_3 \dots t_{N-1} - (-1)^{(N/2)} t_2 t_4 \dots t_N \ . \qquad (3)$$

However, since the t_n contain the scaling factors σ as well as the cable impedances Z_n, Eq.(1), it is convenient to look at the quotient of the two terms, where these cancel, and define a quantity

$$M = 2 \ln \left(\frac{Z_1 Z_3 \dots Z_{N-1}}{Z_2 Z_4 \dots Z_N} \right) . \qquad (4)$$

For our structures, where the impedances are taken from a binary distribution, Z_a or Z_b, there are typically cancellations in the ratio of the impedances, and we can write

$$M = \tilde{M} \ln \left(Z_a / Z_b \right) , \qquad (5)$$

where $\tilde{M}$ is an even integer, which we call the 'reduced length' of the structure. For a loop where the length N is an even multiple of 2, $N = 4, 8 \dots$, $|Q| = 0$ when M is zero. The sign of M is thus a topological invariant: the impedances, and corresponding hopping amplitudes, are real, so if they were changed continuously, it would not be possible to flip the sign of M without passing through a marginal structure with $|Q| = 0$. For odd multiples of 2, $N = 2, 6 \dots$, the two terms in the expansion of $|Q|$ have the same sign, so, though M can be zero, to make a topologically marginal structure would require a negative hopping amplitude in the loop.

If, instead of making a loop, the chain is infinitely repeated to form a periodic structure, we find that the topological classification from the sign of the reduced length always agrees the generalised Berry phase[24] and winding number invariants obtained from Brillouin zone based calculations. These methods also predict a phase transition when $M = 0$ in a chain with an odd number of pairs. In a periodic structure this is correct, because there are gap closures somewhere in the Brillouin zone for both even and odd numbers of pairs. The two cases differ because, for an even number of pairs, the closure is at wavenumber $k = 0$ where the state is the same at the end of each period, corresponding to the boundary condition for a loop. For an odd number of pairs, the closure is at $k = \pi$, so the loop boundary condition is not satisfied. However, as we show below, the delocalisation associated with the phase transition can be seen for both even and odd numbers of pairs. The $M = 0$ condition also corresponds to the phase boundary found in Ref.[2] and observed experimentally in Ref.[19]; the unusual reentrant shape of the boundary in these works is due to the particular choice of rectangular probability distribution from which the hopping amplitudes are drawn.

In Fig.2(b), we plot the local density of states for some random looped chains with length $N = 16$ and different values of the reduced length $\tilde{M}$. As expected, there is always a gap around $\varepsilon = 0$, except in the marginal case $\tilde{M} = 0$, where the degenerate pair of zero energy states is found. From this pair, it is always possible to make states which are localised entirely on separate sublattices. In the inset, this is demonstrated experimentally by comparing spectra from two adjacent sites, one on each sublattice. The peaks correspond to two distinct states, as can be seen by the small energy difference.

In order to explore the localisation of the zero energy states, we make use of transmission measurements on the unlooped chains. These are most simply described using a transfer matrix treatment, which relates the currents and voltages entering and leaving the structure. At zero energy, the transfer matrix, Supplementary Materials Eq.(S5), for a single cable is

$$\begin{pmatrix} V_{\text{out}} \\ I_{\text{out}} \end{pmatrix} = \mathcal{M}_n \begin{pmatrix} V_{\text{in}} \\ I_{\text{in}} \end{pmatrix} = \begin{pmatrix} 0 & iZ_n \\ i/Z_n & 0 \end{pmatrix} \begin{pmatrix} V_{\text{in}} \\ I_{\text{in}} \end{pmatrix} \qquad (6)$$

The matrix representing a sequence of N cables is then just the product of the $\mathcal{M}_n$ for each cable, $\mathcal{M} = \mathcal{M}_N \mathcal{M}_{N-1} \dots \mathcal{M}_1$. The non-zero elements of $\mathcal{M}$ are the same ratios of impedance products as appear in M, Eq.(4), so we write, for even N,

$$\mathcal{M} = (-1)^{(N/2)} \begin{pmatrix} e^{-M/2} & 0 \\ 0 & e^{M/2} \end{pmatrix} . \qquad (7)$$

The measured transmission amplitude, S_{21}, at $\varepsilon = 0$ is then

$$S_{21} = \operatorname{sech} \left(\frac{M}{2} \right) = \operatorname{sech} \left(\frac{\tilde{M}}{2} \ln \left(\frac{Z_a}{Z_b} \right) \right) . \qquad (8)$$

For our binary distribution, this is the same as the transmission for a periodic chain, $Z_a Z_b Z_a Z_b \dots$, in which the number of cables is equal to the reduced length $\tilde{M}$ (for negative $\tilde{M}$ the sequence starts with Z_b). This follows because, at $\varepsilon = 0$, the transfer matrix for an adjacent pair of cables with the same impedance is just minus the unit matrix, so in calculating S_{21} we can iteratively remove such pairs from the structure until it is reduced to a periodic chain.

Eq.(8) shows that the transmission at $\varepsilon = 0$ depends only on the value of M, and has a value of unity in chains with $M = 0$, which are topologically marginal when joined to form a loop or repeated periodically. The topologically protected states in the marginal cables are completely delocalised[4, 5], having the same amplitude at either end. Away from $M = 0$, the state is localised, with a larger amplitude at one or the other end, depending on the sign of M, and thus the topological phase. The simple treatment leading to Eq.(8) does not account for the small resistive losses occurring in the cables, though this easily included numerically. The losses always reduce the transmission, but they also cause some spread of the $\varepsilon = 0$ values for a given value of M.

Experimental transmission results for our length 16 chains are shown in Fig.3, where we plot $|S_{21}|$ as a function of frequency for different values of the reduced length $\tilde{M}$. The spectra consist of peaks which correspond to the states found in the S_{11} measurements of Fig.2, but with much greater broadening, a result of losses due to the finite (50Ω) input and output impedances of the VNA.

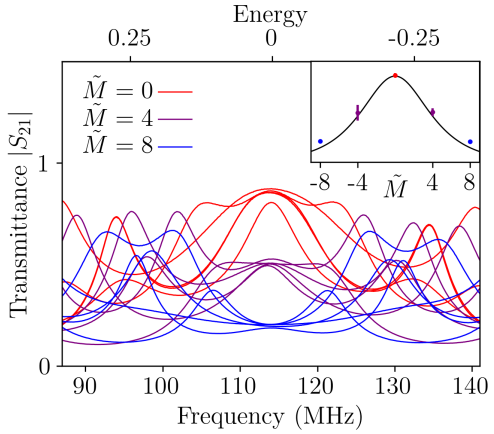

FIG. 3. Measured transmission spectra, $|S_{21}|$ for a selection of random unlooped chains with length $N = 16$. The curves are coloured according to the reduced length of the structures, Eq.(5): $\tilde{M} = 0$ (red), $\tilde{M} = 2$ (purple) and $\tilde{M} = 4$ (blue), as in Fig.2. The transmission at zero energy (top scale) is, neglecting losses, predicted to depend only on $\tilde{M}$. The inset shows the dependence of this transmission on reduced length (points), averaging over 7 to 9 structures for each $\tilde{M}$. The error bars show the standard deviation of the measured values. The solid line is the behaviour predicted in Eq.(8), with a constant scaling to account for losses.

As predicted, the value at $\varepsilon = 0$ is fairly similar for all structures with the same $\tilde{M}$. In the inset, the average of $|S_{21}|$ at $\varepsilon = 0$ is plotted as a function of $\tilde{M}$, along with the hyperbolic secant dependence predicted in Eq.(8), scaled by a constant factor to account for losses in the cables. With this scaling, the agreement is good, and both the absolute values and the spread are consistent with numerics using values for the losses deduced from the measured broadening of the peaks in Fig.2.

In addition to the delocalisation which we have demonstrated, Refs.[4–10]. predict a singular peak, the Dyson singularity, in the density of states, $\rho(\varepsilon)$, around $\varepsilon = 0$ for topologically marginal random structures of infinite length. This has a functional form $\rho(\varepsilon) \sim |\varepsilon(\ln \varepsilon)^3|^{-1}$. However, in finite structures this singularity is replaced by a broader peak, which narrows as N increases. The situation is further complicated by our use of cables with only two impedances, which quantises the value of M, producing gaps in the density of states on either side of $\varepsilon = 0$, as is apparent in the spectra of Fig.2. Numerical simulations suggest that, with our choice of impedances, an ensemble of structures with 50-100 cables would be required to see a strong, reasonably narrow peak in the averaged density of states.

We have shown that when a looped chiral structure is split, the transmission through the corresponding chain has unit value, in the absence of losses, if the original loop was topologically marginal. Such perfect transmission is thus an experimental signature of a topological phase boundary. The result generalises, with some caveats, to more complicated networks with chiral symmetry. If we start from a balanced structure, having equal numbers of sites on each sublattice, and break a loop by unplugging a cable, we split a site, creating an imbalance, and thus a topologically protected state through which transmission can occur. The transfer matrix which determines the transmission between the the two sides of the break will always be diagonal at zero energy, like Eq.(7), of the form

$$\mathcal{M} = \begin{pmatrix} \lambda & 0 \\ 0 & \lambda^{-1} \end{pmatrix} . \tag{9}$$

As we have seen, this leads to perfect transmission when $\lambda = 1$[26]. However, this is also the condition for the unsplit structure to be topologically marginal; then the voltages and currents on either side of the break are identical, which is the boundary condition which must be satisfied to obtain a zero energy state when they are joined[27].

The connection between topological phase boundaries and perfect transmission is not, however, universal. In more complicated networks, there are cases where a structure is marginal but it can be split in such a way that the transmission between the ends is less than one, sometimes zero. Though a full discussion is beyond the scope of the present paper, this occurs when, in the split structure, either the topologically protected state has zero amplitude on the input or output site, or there is more than one zero energy state on the same sublattice.

To conclude, we have carried out an experimental study of the topological properties of a coaxial cable system which maps onto the SSH model. The accuracy of this mapping is demonstrated by the small variation in the frequencies of the topologically protected state in an ensemble of random structures. By varying the parameters in the random distribution, we have shown that looped structures can be taken through a topological phase transition, characterised by the closure of the gap and the appearance of a delocalised state at zero energy. Coaxial cable structures provide an excellent system for such topological physics experiments on finite structures. They can readily be generalised to networks representing more complicated Hamiltonians, where similar signatures of phase transitions are predicted to be observable.

Qingqing Duan's work is supported by the National Natural Science Foundation of China under Grant 12090052.

[1] W. P. Su, J. R. Schrieffer and A. J. Heeger, Phys. Rev. Lett. **42**, 1698 (1979).
[2] I. Mondragon-Shem, T. L. Hughes, J. Song and E. Prodan, Phys. Rev. Lett. **113**, 046802 (2014).
[3] F. J. Dyson, Phys. Rev. **92**, 1331 (1953).
[4] G. Theodorou and M. H. Cohen, Phys. Rev. B **13**, 4597 (1976).
[5] T. P. Eggarter and R. Riedinger, Phys. Rev. B **18**, 569 (1978).
[6] R. H. McKenzie Phys. Rev. Lett **77**, 4804 (1996).
[7] L. Balents and M. P. A. Fisher Phys. Rev. B**56**, 12970 (1997).

[8] P. W. Brouwer, C. Mudry and A. Furusaki Phys. Rev. Lett **84** 2913 (2000).
[9] M. Titov, P. W. Brouwer, A. Furusaki and C. Mudry Phys. Rev. B**63**, 235318 (2001).
[10] F. Evers and A. D. Mirlin, Rev. Mod. Phys **80**, 1355 (2008).
[11] N. Malkova, I. Hromada, X. Wang, G. Bryant and Z. Chen, Opt. Lett. **34**, 1633 (2009).
[12] T. Ozawa, H. M. Price, A. Amo, N. Goldman, M. Hafezi, L. Lu, M. C. Rechtsman, D. Schuster, J. Simon, O. Zilberberg and I. Carusotto, Rev. Mod. Phys. **91,** 015006 (2019).
[13] C. Poli, M. Bellec, U. Kuhl, F. Mortessagne and H. Schomerus, Nat. Commun. **6**, 6710 (2015).
[14] P. St-Jean, V. Goblot, E. Galopin, A. Lemaître, T. Ozawa, L. Le Gratiet, I. Sagnes, J. Bloch and A. Amo Nat. Photonics **11**, 651 (2017)
[15] F. Bleckmann, Z. Cherpakova, S. Linden and A. Alberti, Phys. Rev. B **96**, 045417 (2017).
[16] J. Ningyuan, C. Owens, A. Sommer and D. Schuster and J. Simon Phys. Rev. X, **5**, 021031 (2015).
[17] C. H. Lee, S. Imhof, C. Berger, F. Bayer, J. Brehm, L. W. Molenkamp, T. Kiessling and R. Thomale, Commun. Phys. **1** 39 (2018).
[18] M. Atala, M. Aidelsburger J. T. Barreiro, D. Abanin, T. Kitagawa, E. Demler and T. Bloch, Nat. Phys. **9**, 795-800 (2013).
[19] E. J. Meier, F. A. An, A. Dauphin, M. Maffei, P. Massignan, T. L. Hughes and B. Gadway, Science **362**, 929 (2018).
[20] Z. Q. Zhang, C. C. Wong, K. K. Fung, Y. L. Ho, W. L. Chan, S. C. Kan, T. L. Chan and N. Cheung, Phys. Rev. Lett. **81**, 5540 (1998).
[21] T. Jiang, M. Xiao, W-J. Chen, L. Yang, Y. Fang, W. Y. Tam, C. T. Chan, Nat. Commun. **10**, 434 (2019).
[22] Q. Guo, T. Jiang, R.-Y. Zhang, L. Zhang, Z.-Q. Zhang, B. Yang, S. Zhang and C. T. Chan, Nature **594**, 195 (2021).
[23] D. M. Whittaker and R. Ellis, arXiv:2102.03641.
[24] N. Marzari and D. Vanderbilt, Phys. Rev. B **56** 12847 (1997).
[25] In more complicated networks, it is also possible to have pairs of topologically protected states when $n_b = n_w$, in which case $|Q|$ is always zero. However, this does not occur in the simple structures considered here.
[26] There is also unit transmission when $\lambda = -1$, which corresponds to a phase transition when the network is periodically repeated, but not for the finite structure.
[27] I. C. Fulga, F. Hassler and A. R. Akhmerov, Phys. Rev. B **85**, 165409 (2012).

Chapter 4

Topology in finite chiral structures 1: topologically protected states

In the context of semi-infinite topological materials, topological protection conventionally refers to boundary modes that are resistant against disorder. In finite systems with a large amount of periodicity, and a sufficient size, such topological protection is well described by bulk indices. For instance, in a 1 dimensional chiral structure, two times the winding number indicates the number of topologically robust edge modes [92]. That is, topological protection can be changed under a topological phase transition.

In a finite system, these modes are not robust to arbitrary hopping disorder [18] and for sufficiently small systems the amount of disorder required to change the energy of topologically robust modes is often quite small (for instance random disorder of 2% of the largest hopping terms in an on site Zeeman field for some finite systems [21] is sufficient to shift energies of topologically robust states). Furthermore, in systems where there is not a well defined bulk or boundary, such as in random networks or graphs (and hence no bulk-boundary correspondence) it is not clear how to define topologically robust modes. In this chapter we instead consider topological protection not in terms of boundary modes protected by a bulk invariant, but in terms of zero energy states that have completely invariant energies under arbitrary continuous hopping evolution.

We do note, that through a super cell treatment, a bulk is possible to define for any random graph. Indeed, it may be sensible to do so using a partition that we will discuss in chapter 5, but at the scale of structures we are interested in, bulk protection is unlikely to be substantial for arbitrary hopping disorder.

Remark. Note that in this chapter we often refer to exact topological protection with the term exact, however often this is dropped to just refer to topological protection. For the purposes of this chapter, we do not mean states protected by a bulk invariant.

One example of exact topological protection occurs in an open SSH chain with an odd number of sites as we experimentally demonstrated in [76]. This occurs because of an excess in the number of sites in one sublattice over the other and results in the Hamiltonian having a minimum of 1 zero energy state (that is, for all values of hopping terms, the Hamiltonian has a minimum nullity of 1). This state is stable to any continuous hopping evolution.

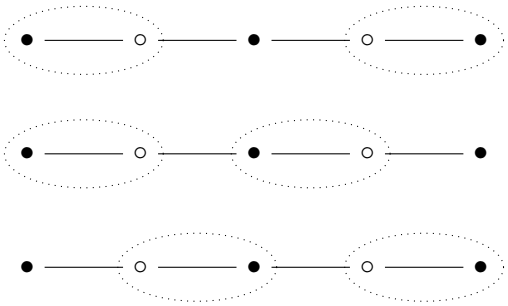

Figure 4.0.1: A finite SSH chain with an odd number of sites, displayed with three examples of the largest matchings of this chain. Notice that deleting any of the uncovered black site results in a structure with only one cover. This means every non-zero first minor of H cannot be set to zero and ensures a minimum and a maximum of one zero energy state in this structure.

It should be noted that in a finite system an exactly topologically protected state can still be localised — in a sense — to domain boundaries. For example, in the aforementioned topologically protected state, the LDOS will have a local maximum where the sign of the reduced length of one unit cell changes to the next unit cell. Recall that the reduced length of a unit cell is the log of the ratio of the intracell hopping term to the intercell hopping term to the next unit cell. When this sign changes, a local maximum in the LDOS will be measured on the sublattice which supports the topologically protected state. As the sign of the reduced length indicates the topological phase, we can interpret the topologically protected state has local maximum on the domain boundaries in the structure. However, although a topologically protected state may have local maxima on domain boundaries, as we will show in section 4.1, which sites have non-zero support of nullstates is a topological invariant of the graph, so not all domain boundaries will necessarily support the topologically protected state.

This example of topological protection in a finite disordered SSH chain is also quite special because it has a maximum nullity of 1. This is because every subgraph with a non-zero determinant has only one cover. So by the Harary Sachs theorem no such determinant can be set to zero, and the structure has a maximum nullity of 1. As a consequence, under any continuous evolution of the hopping terms, no spectral gaps can be closed around zero energy. Examples of the covers that result in this protection are illustrated in Fig. 4.0.1 for a small SSH chain.

For this chapter we focus on the minimum nullity a graph may have, although in chapter 7 the maximum nullity of a graph becomes of significant interest. This is considered an open problem in full generality, although there has been significant work on this problem in real weighted graphs [93, 94].

We consider systems with hopping terms defined in an arbitrary field[1], although we mostly consider complex or real hopping terms. Our conclusions hold for systems with any

[1]That is, a mathematical field consisting of a set and both an additive and multiplicative binary operator — with respective inverses — such as the field of real numbers.

symmetry, although in certain cases the number of exactly robust modes may be larger than for the results we give here (and is not a question we have explored in full generality, for example with Kramers degeneracy the number of topologically robust states may be larger). Our methods exactly predict the number of topologically protected zero energy states for bipartite and non-bipartite structure with either real and complex hopping terms when allowing for arbitrary hopping disorder. That is the symmetry classes A, AI, AIII, and BDI.

Remark. As in the bulk of this thesis, we consider a Hamiltonian H defined on a graph G where a non-zero hopping term is defined on each edge of G. A non-zero hopping term $h_{i,j}$ is not allowed to be set to zero, and a zero valued hopping term may not become non-zero. As such hopping terms take a value in some field of $h_{i,j} \in \mathbb{F} \setminus \{0\}$ with each hopping term defined algebraically independently.

For a chiral structure defined on a bipartite graph, with n_b black sites and n_w white sites, the minimum number of zero energy states is related to the maximum rank of the biadjacency matrix because $\operatorname{rank}(H) = 2\operatorname{rank}(Q)$. By the rank-nullity theorem this gives a lower bound on the number of topologically protected states as $|n_b - n_w|$.

In the graph theory literature, any zero eigenvalue beyond $|n_b - n_w|$ for a bipartite graph is called a *supernumerary zero*. This is defined with all hopping terms equal to 1, though coincidentally many supernumerary zeros also happen to be topologically protected, such as those found in Clars goblet [95] (see Fig. 4.0.2). For chiral structures such topologically protected states are a consequence of there existing no covers of the structure. As we will show all topologically protected states are a result of a particular induced subgraph of the structure (which may itself be the entire graph) not having any covers. In the chemistry literature such structures are called non-Kekuléan.

The number of zero energy states in a chiral structure has been of interest in theoretical chemistry for a long time. In chemical graph theory one is usually interested in the number of zero energy states for a structure with all unit eigenvalues and has most widely been applied to benzenoids [96] which are chiral structures formed out of benzene rings that are connected on one or two sites.

Interest in Kekuléan and non-Kekuléan structures dates back to the discovery of the structure of benzene [97, 98]. Benzene is stable due to having two covers, which for benzenoids is known as having two Kekuléan structures [96]. Kekuléan benzenoids have a number of convenient properties for making calculations of resonance energies, and the energies of delocalised electrons. It is also noted that, as a rule of thumb, the number of covers a benzenoid has increases its stability. This is because in a Kekuléan structure, the electrons resonate between different configurations of single and double bonds each of which are alternating. Due to the absence of a cover, a non-Kekuléan structure has no way to alternate single and double bonds. Due to an excess of electrons, this forces double bonds to neighbour one another, resulting in unstable electron configurations [96]. As such, it is only more recently non-Kekuléan benzenoids have been synthesised, with one of the first being that of Clar's Goblet [99].

In section 4.1 using a particular partition of a graph [100] along with some results of our

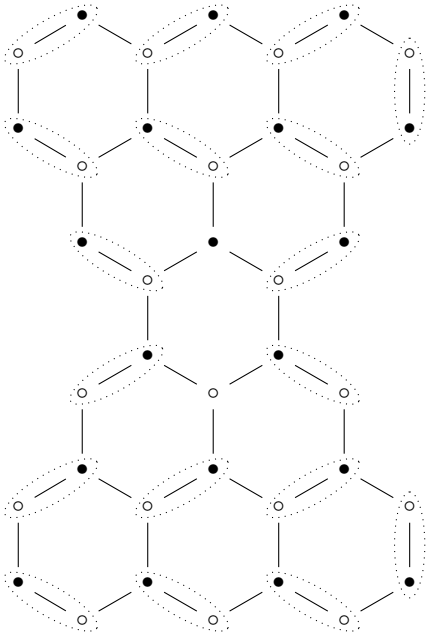

Figure 4.0.2: Clar's goblet [95] which has equal numbers of black and white sites yet has two zero energy states. In this structure it is a consequence of there being no covers, which results in 2 topologically protected zero energy states — at least two sites can never be included in a matching. An example of one of the largest possible matchings of this structure is drawn in.

collaborator Prof. Barry T. Pickup [101] we demonstrate how the number of exactly robust zero energy states is directly related to the network topology of a graph. We then show that localisation of exactly zero energy topologically protected states is an invariant for almost all hopping terms. Finally in section 4.2 we give some conclusions and limitations of our methods.

The work of this chapter was completed as part of a collaboration, for which I gratefully recognise and am enormously thankful to Prof. Barry T. Pickup, Prof. Patrick Fowler, and Prof. David Whittaker. I have tried to make clear when propositions are not my own, but to be completely unambiguous, propositions 4.1.1, 4.1.5, 4.1.8, and 4.1.9 are my own original work.

4.1 Numbers of topologically protected states and network topology

Exact topological protection is numerically quite simple to calculate, although it is harder to prove the number of zero energy states you calculate are all topologically protected. Consider a graph G with a Hamiltonian H defined on it. With randomly and independently selected hopping terms from a continuous field then H almost always has the minimum nullity. This is because the rank of H is given by the dimension of its largest non-singular sub-matrix. Recall from section 2.1.5.1 that if a matrix can be non-singular, it is almost always non-singular, so it follows that the largest sub-matrix of H that can be non-singular, is also almost non-singular.

Computationally it is not quite so simple as randomly generated numbers are discrete. However, the probability is still low that extra zero energy states will be found. So one may simply calculate the nullity for an ensemble of randomly generated Hamiltonians defined on G. Consider a matrix of indeterminates with a determinant that corresponds to an irreducible polynomial. For an n-bit number the probability that this matrix with randomly selected hopping terms satisfies the conditions for being singular is bounded above by

$$P \leq \left(\sum_{m=0}^{n} 2^m \right)^{-1} . \tag{4.1.3}$$

To see the origin of this bound, recall from Prop. 2.1.14 in section 2.1.5.1, that if the determinant of the matrix defines an irreducible polynomial, to satisfy the condition that it is singular restricts at least one hopping term to a particular fixed value. If this has solution, only one of the $\sum_{m=0}^{n} 2^m$ possible values of an n bit number satisfy this condition, giving the bound. Note that if the largest non-singular sub-matrix of a Hamiltonian defines a reducible polynomial, and has κ irreducible factors, then the hopping terms for each factor to be independently non-zero increase this probability to

$$P \leq 1 - \left(1 - \left(\sum_{m=0}^{n} 2^m \right)^{-1} \right)^{\kappa} . \tag{4.1.4}$$

However for the size of graphs we often consider $\kappa \ll n$ hence P is still quite small. Taking an ensemble of N randomly generated Hamiltonians H on G the probability that every single one has a nullity greater than the protected nullity is P^N which goes to zero quite rapidly.

Despite the simplicity of this calculation this approach is not exact. It would be nice to be able to prove that your approximate number of topologically protected states is exact. Furthermore, this approach also makes any physics quite opaque. For instance, how do these states localise? And how does this change as hopping terms are evolved? To answer these questions we look to connect exact topological protection to the structures network topology.

Remark. To avoid confusion, we will refer to the network topology of a graph as its connectivity. When referring to the topology of a structure, we will generally mean the topological properties of the parameter space ξ.

The connection between exact topological protection and connectivity of a graph is the simplest to understand in chiral structures. To see this connection, we first relate the covers of a graph to the topologically protected nullity.

Proposition 4.1.1. The number of topologically protected states in a finite chiral structure is the minimum number of sites which can not be included in a matching.

Proof. Recally from section 2.1.4 that because G is chiral and hopping terms are algebraically independent, then we can write

$$H = \begin{pmatrix} 0 & Q \\ Q^\dagger & 0 \end{pmatrix} \tag{4.1.5}$$

for some permutation of the sites of G. Therefore, the rank of $\operatorname{rank}(H) = 2\operatorname{rank}(Q)$. We can access any minor of Q as a primary minor of H so the largest non-singular subgraph of G necessarily corresponds to the largest non-singular sub-matrix of H.

If a subgraph of G has a cover, then this structure has no topologically protected states. Therefore, the largest subgraph with a cover gives the maximum rank. By the rank nullity theorem, the number of sites not in this cover is exactly the minimum nullity. □

As an example of topological protection, we display experimental results on a graphene torus (see Fig. 4.1.1) which has a vacancy introduced by removing one site. Removing one site created an imbalance in the number of black and white sites, therefore ensuring no cover exists of the structure. This results in one topologically protected state. The state is demonstrated to be a result of topological protection by measuring a sample of sites for an ensemble of structures with randomly selected hopping terms.

The subgraphs of G that have covers are dictated by which sites are connected, so proposition 4.1.1 gives a relationship between the connectivity of a graph and the number of topologically protected states. The relationship between connectivity and covers is still quite opaque in this form, but we can be much more explicit about topological protection and connectivity. To do this we present a proof given by Barry T. Pickup [101]

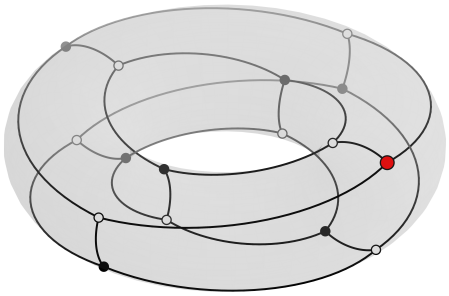

(a)

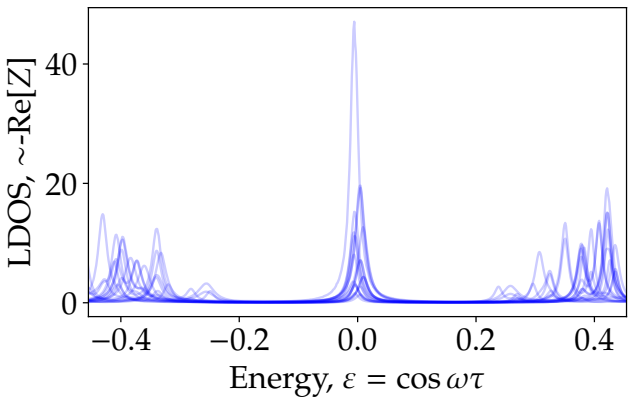

(b)

Figure 4.1.1: Topologically protected states in a coaxial cable network representing a small graphene torus as displayed in (a). Cable impedances were selected randomly from a binary distribution of 50Ω and 93Ω cables to generate an ensemble of random Hamiltonians defined on the structure in (a). On each Hamiltonian a site was then selected (for example, the red site), and the local density of states on three neighbouring sites was measured, with results displayed in (b). Topological protection was quite exact, with the states having a mean resonance at 114.0 MHz, and standard deviation of 0.4 MHz. This was sometimes repeated in the same structure, where a different site was deleted. An ensemble of four structures were measured for a total of 18 individual measurements, where hopping terms were selected randomly for each of the four structures.

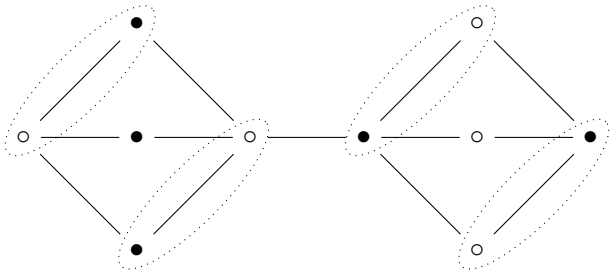

Figure 4.1.2: A chiral structure graph with no complete matching. An example of a largest matching is drawn. At least two sites can never be included in a matching of this graph.

demonstrating the sites which support topologically protected states may not connect to one another.

Proposition 4.1.2. If a graph has topologically protected states, then no vertices that have support for topologically protected states may be connected.

Proof. Let ε_i be an eigenvalue of H corresponding to an eigenvector $|\psi_i\rangle$. If this state is topologically protected, then under any change in a hopping term $h_{j,k}$ in H then ε_i is unchanged. That is, for all $h_{j,k}$ then

$$\frac{d}{dh_{j,k}}\varepsilon_i = \frac{d}{dh_{j,k}} \langle\psi_i| H |\psi_i\rangle = 0. \tag{4.1.7}$$

With the addition of a chemical potential, it is always possible to set a topologically protected state to have zero energy, so we can require this without altering the number of topologically protected states. As such for every j, k equation (4.1.7) reduces to

$$\begin{aligned} \langle\psi_i| \left(\frac{d}{dh_{j,k}} H\right) |\psi_i\rangle &= \langle\psi_{ij}| \left(\frac{d}{dh_{j,k}} h_{j,k}\right) |\psi_{ik}\rangle + \langle\psi_{ik}| \left(\frac{d}{dh_{j,k}} h_{k,j}\right) |\psi_{ij}\rangle \\ &= \langle\psi_{ij}|\psi_{ik}\rangle + \langle\psi_{ik}|\psi_{ij}\rangle = 0 \end{aligned} \tag{4.1.8}$$

where $|\psi_{ik}\rangle$ is support of the eigenstate $|\psi_i\rangle$ on site k. This is only generically possible if $|\psi_{ik}\rangle$ or $|\psi_{ij}\rangle$ is zero for every $h_{j,k}$. That is, no two vertices which support a topologically protected state may be neighbours. □

This proposition means there is a natural partition of the graph into sites that may support topologically protected states, and those which cannot. As we will see this partition is enormously useful because the set of sites that can host topologically protected states are topologically protected. That is, the localisation of exactly topologically protected nullstates is protected. To see this, it is useful to make a distinction between sites that can support zero energy states and those that cannot.

Definition 4.1.3. Let a *core vertex* (CV) be a vertex that has non-zero support of a null state. Let a *core forbidden vertex* (CFV) be a vertex which has no support of a nullstate.

Because it must be possible to write any nullspace vector in terms of any basis of nullspace vectors, it has been proven by Prof. Irene Sciriha in [65] that for a graph where all edge weights are fixed the core vertices are an invariant of the graph G. That is, the sites which have support of nullstates are invariant under a transformation of the nullspace. We will now show that for any H on G for which every minor of H that can be non-singular is non-singular, then the core vertices are always the same. That is, the nullstates of H are almost always localised to the same subset of sites.

Definition 4.1.4. Let a Hamiltonian H on G such that every minor of H that can be non-zero is non-zero be called *maximally non-zero*.

Proposition 4.1.5. Let G be a graph with a maximally non-zero Hamiltonian H on G with n topologically protected states. For every such graph the set CV of core vertices is the same.

Proof. Partition the graph G in to two sets of sites, a CV set and a CFV set. By proposition 4.1.2 this graph has an adjacency matrix of the form

$$\begin{pmatrix} 0 & Q \\ Q^\dagger & A \end{pmatrix}. \tag{4.1.10}$$

with all null vectors of the form $\begin{pmatrix} x \\ 0 \end{pmatrix}$ where x has all non-zero entries and $Q^\dagger x = 0$.

Assume, while H is maximally non-zero, that it is possible to choose hopping terms so that some vertices in CV do not host any nullstate. If this is the case then we may partition $Q^\dagger$ such that any nullstate x only has support on the same subset of CV. That is

$$Q^\dagger x = \begin{pmatrix} a & b \end{pmatrix} \begin{pmatrix} x_a \\ 0 \end{pmatrix} = 0. \tag{4.1.11}$$

Because every minor that can be non-zero is non-zero, then the nullity of a is topologically protected, so for every maximally non-zero H nullstates can always be restricted to a. However, the set CV is an invariant for a graph with fixed weights (proposition 3.1 in [65]) so this is a contradiction. Therefore, for any maximally non-zero H the set CV is exactly the same set of sites. □

Remark. Note that proposition 4.1.5 means that the support of nullstates is always non-zero on exactly the same subset of sites when H is maximally non-zero.

We note that when specifying certain hopping terms, it is possible to alter the localisation of nullstates. As a result, it is useful to make a distinction between generic core vertices and core vertices of maximally non-zero Hamiltonians. Because, for almost all hopping terms, a minor that can be non-zero is non-zero we give the following definition.

Definition 4.1.6. Let a *topological core vertex* (TCV) be a vertex that almost always has non-zero support of a null state. Let a *topological core forbidden vertex* (TCFV) be a vertex which almost always has no support of a nullstate. We sometimes refer to such vertices as topologically protected.

We may now extend proposition 4.1.1 to any graph, where the number of topologically protected states is given by the minimum number of sites that cannot be included in a cover of a particular subgraph. To do this it is convenient to define two sets of TCFV.

Definition 4.1.7. Let a TCFV which is adjacent to a TCV be denoted a *topological adjacent vertex* (TA). Let a TCFV which is not connected to a TCV be denoted a *topological removed vertex* (TR).

We can now define a TCV-TA-TR partition of the Hamiltonian,

$$H = \begin{pmatrix} 0 & Q & 0 \\ Q^\dagger & A & C \\ 0 & C^\dagger & R \end{pmatrix}. \tag{4.1.12}$$

This defines an analogue of the CAR partition [100] which is stable to allowing edge weights to vary continuously. Note that the use of the CAR partition is from our collaborator Barry T Pickup [101] who used this partition to show that the number of topologically protected states is $\geq n_{\mathrm{CV}} - n_{\mathrm{A}}$ where $n_{\mathrm{CV}}, n_{\mathrm{A}}$ are the number of (generic) core vertices and adjacent vertices. We now show the number of topologically protected states is exactly $n_{\mathrm{TCV}} - n_{\mathrm{TA}}$ where $n_{\mathrm{TCV}}, n_{\mathrm{TA}}$ are the number of topologically protected core vertices and topologically protected adjacent vertices.

Proposition 4.1.8. The number of topologically protected states in a graph is given by $n_{\mathrm{TCV}} - n_{\mathrm{TA}}$.

Proof. If there is a block of zeros of the size $b \times (n_{\mathrm{TCV}} - b)$ in $Q^\dagger$ then there is an $n_{\mathrm{TA}} \times (n_{\mathrm{TCV}} - b)$ submatrix of $Q^\dagger$ with the same nullity as $Q^\dagger$. We can therefore localise every nullstate to this submatrix, which by proposition 4.1.5 is not possible, therefore no such block exists.

If no $b \times (n_{\mathrm{TCV}} - b)$ block of zeros exists then we can permute the columns of $Q^\dagger$ such that there is one non-zero term in its b, b-th entry. In this permutation there is a non-zero diagonal across the entries $Q^\dagger_{b,b}$ for every b. So by the Harary Sachs theorem every there is an $n_{\mathrm{TA}} \times n_{\mathrm{TA}}$ submatrix of $Q^\dagger$ that is almost always non-singular, so there are exactly $n_{\mathrm{TCV}} - n_{\mathrm{TA}}$ topologically protected states. □

Remark. The form of the TCV-TA-TR partition ensures that any structure with topological protection has a permutation of the sites with the form of (4.1.12) giving a direct connection between connectivity and topological protection. Furthermore this form means, for almost all hopping terms, topologically protected states are exactly localised to the set of TCV.

We now give the connection between the number of topologically protected states in a chiral graph, and the number of topologically protected states in any graph.

Proposition 4.1.9. For a graph G under the TCV-TA-TR partition the number of topologically protected states is given by the number of sites that cannot be included in a matching of the induced subgraph $\bar{G}$ of topological core vertices and topological adjacent vertices

$$\bar{G} = \begin{pmatrix} 0 & Q \\ Q^\dagger & A \end{pmatrix}. \tag{4.1.13}$$

Proof. From the above discussion the number of topologically protected states is given by $\mathcal{N}(Q^\dagger)$. Therefore, the largest non-singular submatrix of $Q^\dagger$ gives the rank of $Q^\dagger$, which corresponds to the largest non-zero diagonal of $Q^\dagger$. By the Harary Sachs theorem this defines the largest matching of $\bar{G}$. So by the rank nullity theorem the smallest number of sites which cannot be included in a matching of $\bar{G}$ is the number of topologically protected states. □

4.2 Conclusions and limitations

We have discussed how exact topological protection occurs in finite tight binding models. We have demonstrated that the number of topologically protected states in any graph may be related to the connectivity of that graph, relying on the adjacency matrix taking a TCV-TA-TR partition [101] with the form of

$$H = \begin{pmatrix} 0 & Q & 0 \\ Q^\dagger & A & C \\ 0 & C^\dagger & R \end{pmatrix}. \tag{4.2.14}$$

Using this form we have demonstrated that exactly topologically protected states in a finite tight binding model are almost always localised to an invariant subset TCV of sites.

It is relatively simple to design a graph that has a certain number of topologically protected stated using the TCV-TA-TR partition. However, this alone may not be enormously useful, and is a significant limitation of our above approach. For example, if you have a large structure it may not be viable to find a TCV-TA-TR partition numerically.

One approach to study such structures is to take a finite set of small regions with structural disorder and study these as isolated graphs. If you have a set of rules for how these may combine with the larger structure, and how the number and localisation of zero energy states is altered, it is possible to find the number of exactly protected states in the much larger structure. Our collaborator Prof. Barry T. Pickup [101] has derived a set of constructions that may be used for exactly this. The idea of the Pickup constructions are to maintain a TCV-TA-TR partition in the larger structure.

Another problem we have not touched on in this chapter is the possibility of introducing further zero energy states to a structure with topological protection. This will necessarily close a gap, and so if unavoidable under some continuous evolution of hopping terms, would be a topological phase transition. An infinite number of chiral and non-chiral examples of such graphs exist, although we do not detail the general approach to the classification of such graphs here. An example of a non-chiral graph with topological protection, and a $\mathbb{Z}_2$ classification is illustrated in Fig. 4.2.1.

Our approach also may not reveal topologically protected states that persist in chiral structures with interactions. In infinite interacting spin models defined on chiral structures the ground state degeneracy depends only on the difference in the number of sites in each partite set [102, 103] — a consequence of the Lieb-Schultz-Mattis theorem [104] — so, under our definition a number of supernumerary topologically protected states are lost. A finite analogue of this is Ovchinnikov's rule [105] which, based on a survey of a number

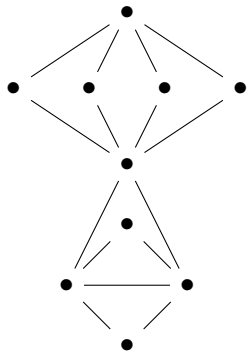

Figure 4.2.1: A graph with two topologically protected states, which is not chiral and has a topological classification of $\mathbb{Z}_2$.

of molecular systems by Alexandr Ovchinnikov, states that the degeneracy of the ground state also only depends on $|n_w - n_b|$ in chiral structures with the presence of interactions. While this rule has not been proven mathematically, it may indicate that some number of topologically protected states predicted with our methods are not robust to interactions in chiral structures.

For non-chiral structures, it is unknown (at least to the author) as to how our definition of topologically protected states may persist in the presence of interactions.

Chapter 5

Topology in finite chiral structures 2: zeroth step topology

There have been several approaches to classifying the topology of finite structures [20, 21, 106]. In most cases the approach is to calculate a bulk index and relate phenomena in the finite structure to a bulk index, or else to calculate a local realspace invariant which is indicative of a non-trivial bulk index (for instance, via the obstruction to atomic maximally localised Wannier functions [50, 51], or local markers that average to the correct bulk index [16, 17]). In structures with a clear periodicity, or low disorder, these are good approaches to predict the finite classification, and number of topologically robust states in a finite sample. However, when allowing arbitrary network topology (that is, an arbitrary graph) or strong disorder, changes in the bulk topology may not correspond to exact gap closures in the finite structure. In systems where this occurs, we say the structure has lost the bulk boundary correspondence. Furthermore, in such systems, properties associated with bulk invariants such as a number of boundary modes or protected transport can be lost even when the sample has a non-trivial bulk invariant.

To study finite topology while allowing the loss of a bulk boundary correspondence we take an approach using exact gap closures. In finite systems, where the bulk boundary correspondence is lost, the system may be represented by a real space tight binding Hamiltonian, H. The energy spectrum of H may still undergo exact gap closures, so we can define topological phase boundaries for a finite real Hamiltonian.

Loosely speaking, for this chapter we define the topological classification of H as the number of sets of Hamiltonians that are related under adiabatic evolution. That is, two Hamiltonians H_1 and H_2 are topologically equivalent if they are related by continuous evolution of their hopping terms, in such a way that preserves the underlying graph structure. Formally this defines equivalence classes of Hamiltonians. To allow arbitrary hopping disorder, we let each hopping term in H be algebraically independent.

Remark. In this chapter we study topology using gap closures that lead to two zero energy states. In Chapter 7 we will refer to this as zeroth step topology, however, for brevity in this chapter we refer to this as the topology of a structure.

Following our work in [90] we wish to derive a classification for arbitrary finite chiral

structures. To this end we define a tight binding Hamiltonian H on a graph G. Recall from section 2.1.4 to allow a Hamiltonian with arbitrary hopping disorder, H is defined on a bipartite graph G.

The classification itself is based on the possible factors of the determinant of the Hamiltonian, $|H| = -|Q||Q^\dagger|$ where Q is the (weighted) biadjacency matrix of H. For structures with an even number of sites, when $|Q| = 0$ there are two zero energy states in the Hamiltonian. Because $|Q|$ is itself a polynomial of the hopping terms of H it might be possible to factorise. Each irreducible factor may be possible to set to zero, and so we can associate topological phases to irreducible factors of $|Q|$. The idea is that by counting the number of irreducible factors of $|Q|$ that can be set to zero we can arrive at the topological classification of G.

We will demonstrate that the topological classification of a particular structure is related to the underlying network topology of the graph G. That is, the number of irreducible factors of $|Q|$ is a direct consequence of how different subgraphs of G connect to one another. This leads to some interesting consequences in the relationship between the average vertex degree of the graph, and the number of topological phases this graph will have. Some data based on the topological classification of 154131 non isomorphic graphs on 18 vertices or fewer is displayed in Fig. 5.0.1. Interestingly for when the mean vertex degree is much greater than 3, the graph is generally too connected to have many topological phases, and for a mean vertex degree less than 3 the graph generally has too many branches to have distinct topological phases. So there is evidence the most topologically interesting graphs tend to have a mean vertex degree of 3.

In section 5.1 we give more details on the type of structures we can classify, and give a qualitative description of our classification, and in sections 5.2 and 5.3 we give a description of our classification and how it relates to a structure's connectivity. Section 5.4 details an algorithm we have developed that classifies an arbitrary finite chiral structure. In section 5.5 we give our classification paper. We then proceed to give some results that are outside the scope of [90], including a proof of triangular transfer matrices for a structure in section 5.7 and we present a deep connection between nut graphs and a structures classification in section 5.6. Limitations and conclusions to our classification are given in section 5.8.

5.1 Finite chiral structures and topology — an overview

In most approaches to classification [15, 19, 56, 57, 107] a system is assumed to be large enough so that it may be approximated by an infinite system. Such an approach works well, as properties of the finite system converge exponentially fast to the infinite limit, even in the case where translation invariance has been lost [19]. However, convergence is only exact for systems of infinite size, meaning no matter the size of the sample, there is a finite disorder at which topologically robust properties of the boundary will likely be lost (this has been shown that it will be lost for quasi-1D and 1D systems [18] section 6). So if we are interested in developing an exact theory of topological phase transitions in finite structures, we need to consider exact properties of the real space Hamiltonian.

In finite systems, with an arbitrary underlying connectivity, it is not immediately clear

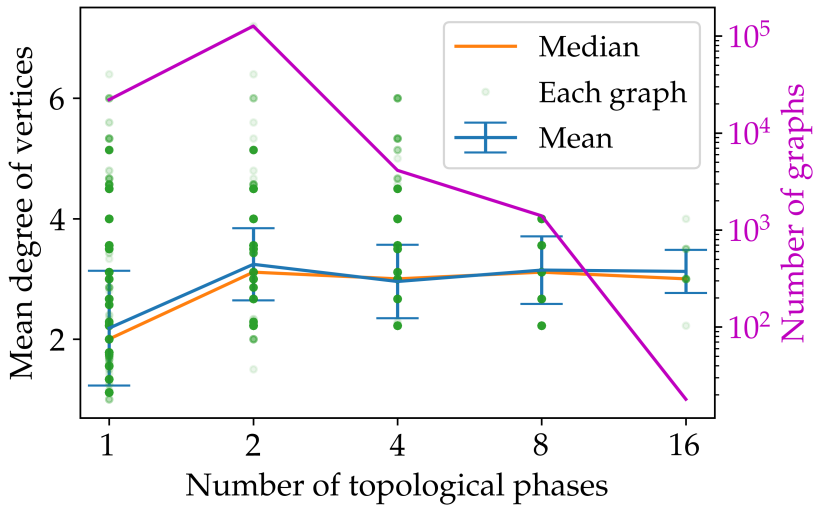

(a)

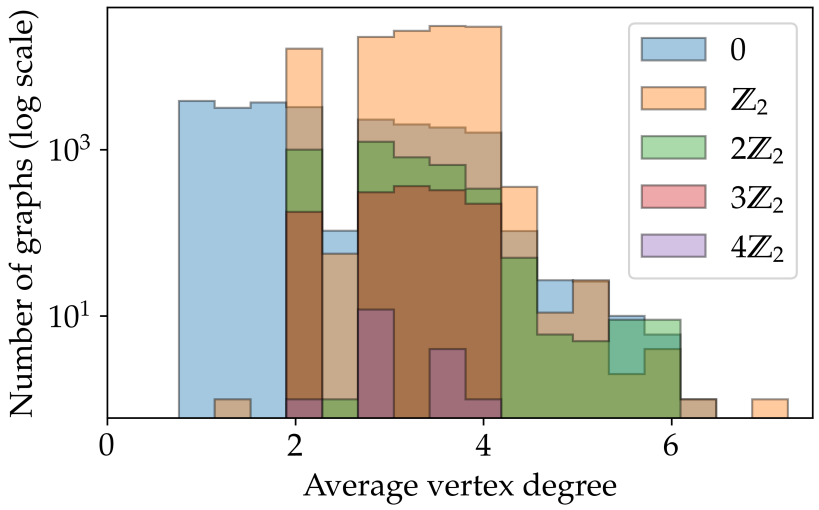

(b)

Figure 5.0.1: The distribution of graphs with a certain number of topological phases. (a) Displays a green point for every graph classified, with the mean and median degree of the graph plotted against the number of topological phases, and the total number of graphs for each number of topological phases given with a log scale plot. (b) Displays a histogram plotted with a log scale for each number of topological phases, showing the distribution of graphs for each case.

how to define a boundary or a bulk. As such, only zero momentum states may be exactly defined in such systems. Of course, it is possible to periodically repeat a finite structure. This will define a bulk Hamiltonian, but any unavoidable gap closures in the band structure away from zero momentum will not correspond to gap closures in the finite Hamiltonian. This further illustrates the loss of a bulk boundary correspondence. It should be noted that gap closures in the band structure can still be interesting in the finite Hamiltonian, for instance leading to extended states (an example of which is discussed in [76]), even if there is no gap closure in the finite system. But in order to study the exact topological properties of finite structures, we consider only the real space Hamiltonian.

We also impose some restrictions on the Hamiltonian. The first is that we wish to allow arbitrary hopping disorder. To do this we let each hopping term be algebraically independent. We also require that the Hamiltonian can undergo no discontinuous evolution, so non-zero hopping terms must remain non-zero and zero valued hopping terms must remain zero valued. Finally we assume that the system is itself connected.

For the hopping terms themselves we generally take them to be real, however they can be complex or taken over some other field. Some of the consequences of having complex hopping terms are discussed in section 5.7 and also discussed in section 7.4.1 of chapter 7.

5.2 Determinants and phase boundaries

In section 2.1.5 we introduced the parameter space that the Hamiltonian is in. In order to consider the topology of more general chiral structures, we recall the definition of the parameter space ξ.

Consider a Hamiltonian defined by,

$$H = \left(\sum_{i \geq j} h_{i,j} \left| i \right\rangle \left\langle j \right| \right) + H.c. \tag{5.2.2}$$

where $h_{i,j}$ are algebraically independent and are taken from some field $\mathbb{F}$. H.c. denotes the Hermitian conjugate. For this chapter we primarily consider the field to be the real, but other fields may also be chosen. H itself can be interpreted as a weighted graph defined on an unweighted graph G.

In order to consider the parameter space of H, we take the underlying graph G, and define H on G, where each non-zero hopping term in H is defined on an edge of G.

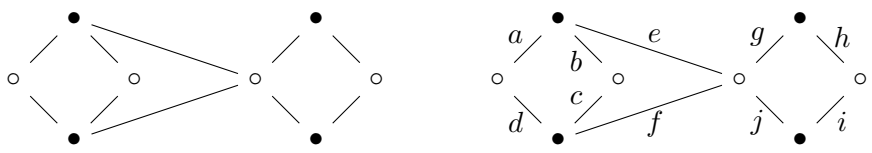

Figure 5.2.1: The graph on the left G has unlabelled hopping terms, as we are only interested in the connectivity of G. On the right is a Hamiltonian defined on G with the hopping terms labelled.

Definition 5.2.1. The parameter space ξ of G is an affine space given by the tuple of all non-zero hopping terms $(h_{i,j})$. Each point in ξ corresponds to a Hamiltonian H on G.

Remark. In ξ we can evolve each hopping term independently, meaning ξ is the space of all Hamiltonians that can be defined on G.

For a finite Hamiltonian, H, non-adiabatic evolution corresponds to a gap closure in the energy spectrum of H. Recall that a topological phase transition occurs when we continuously evolve hopping parameters to map $H_1 \mapsto H_2$ and no matter the path chosen in ξ we undergo non-adiabatic evolution. So for a finite structure a topological phase transition occurs when there is an unavoidable closure in the energy spectrum of H. An example of such evolution is given in Fig. 5.2.2.

For a chiral structure the topological phase boundaries are given by $|H| = 0$. This is because chiral symmetry ensures that if ε is an eigenvalue of H then so is $-\varepsilon$. If H has an even number of sites, then this symmetry is maintained only if there are a multiple of 2 zero energy states, ensuring $|H| = 0$ corresponds to a gap closure in the spectrum.

It follows from the Harary-Sachs theorem that non-zero gap closures in the energy spectrum of H are always avoidable with algebraically independent hopping terms. We can also see this from the characteristic equation of the Hamiltonian. Due to the chiral symmetry we can write

$$|H - \varepsilon I| = \prod_i (a_i - \varepsilon^2) \tag{5.2.4}$$

where a_i is some function of the hopping terms of H, and $\varepsilon = \pm\sqrt{a_i}$ define the eigenvalues of H. If we are looking to constrain the Hamiltonian to have a state at some energy δ then this occurs when

$$|H - (\varepsilon - \delta)I| = \prod_i (\sqrt{a_i} - \varepsilon + \delta)(\sqrt{a_i} + \varepsilon - \delta) = 0. \tag{5.2.5}$$

To get two states with the energy δ this requires two constraints on the hopping terms

$$\begin{aligned} \delta &= \pm\sqrt{a_i}, \\ \delta &= \pm\sqrt{a_j}. \end{aligned} \tag{5.2.6}$$

So if there are two Hamiltonians H_1 and H_2 which may be evolved to one another without going through $|H| = 0$, we can always avoid points where $a_i = a_j$. For $\delta = 0$ then there is only one constraint because $(\varepsilon + \sqrt{a_i}) = (\varepsilon - \sqrt{a_i})$ when $a_i = 0$.

The Hamiltonian is chiral, so we can write the real space basis of the Hamiltonian in an antidiagonal block form. This ensures the determinant

$$|H| = \det \begin{pmatrix} 0 & Q \\ Q^\dagger & 0 \end{pmatrix} = -|Q||Q^\dagger|. \tag{5.2.8}$$

When $|H| = 0$ then $|Q| = 0$ and $|Q^\dagger| = 0$. This ensures there are two zero energy states, one for each partite set, which closes a gap in the energy spectrum.

Each block Q contains algebraically independent hopping terms, therefore $|Q|$ defines

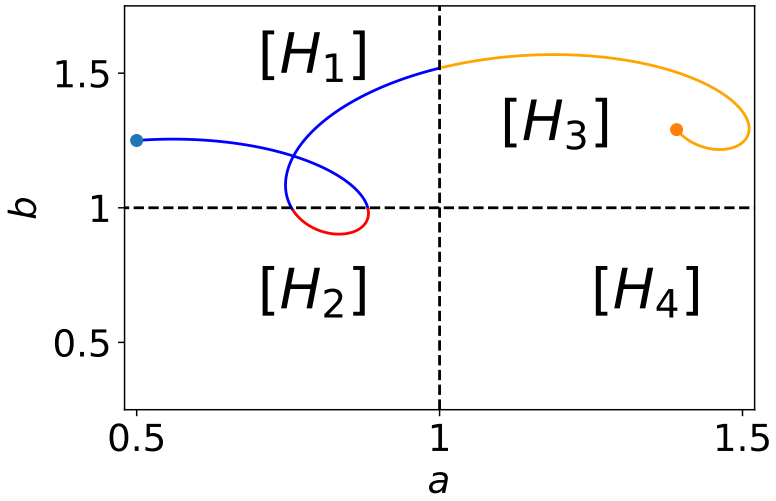

Figure 5.2.2: A slice of the parameter space for a $2\mathbb{Z}_2$ structure, where every hopping term but two (one for each section) are set to one. The dashed lines represent regions in the parameter space that correspond to a singular Hamiltonian, and therefore doubly degenerate zero energy modes. Each $[H_i]$ denotes a different equivalence class of adiabatically connected Hamiltonians, separated topological phase boundaries.

a polynomial that is linear in each hopping term in its expansion [1]. Because $|Q|$ depends continuously on the evolution of hopping terms, Sign($|Q|$) cannot be changed without going through $|Q| = 0$. This ensures that solutions to $|H| = 0$ define surfaces that splits ξ in to distinct regions. That is, the solutions to $|H| = 0$ give topological phase boundaries in ξ.

Remark. Recall that for the weighted graph H defined on G, the block Q corresponds to the *biadjacency matrix* of H.

The idea behind the classification is that, as a polynomial, $|Q|$ may be factorised. Because of the algebraic independence of hopping terms, each factor is also algebraically independent (we will give a sketch of the proof of this in section 5.3.1, with a full proof in the supplementary material of [90]). Algebraic independence of factors ensures solutions to each factor define a boundary to topologically distinct regions in ξ. Because of the linear nature of $|Q|$ each factor gives two distinct topological phases, so the factorisation of H is given by 2^N distinct topological phases. This is discussed in much more detail in [90].

Understanding phase boundaries in ξ allows us to take a geometric interpretation of the classification of a structure. Taking the parameter space, ξ, and removing the phase boundaries at $|H| = 0$ leaves a collection of disconnected regions. The number of disconnected regions is the number of distinct topological phases. This allows us to have a direct geometric interpretation of the classification of a structure. As will be seen in section 5.2.1, the number of topological phases corresponds to the zeroth homotopy group of a subspace of ξ.

[1] Note that some terms in Q do not feature in the expansion of $|Q|$, that is $|Q|$ is not linear in every hopping term in Q.

5.2.1 Constructing a physically motivated topology on a structures parameter space

Recall that the topological phase boundaries of G correspond to the solutions of $|Q| = 0$. In [90] we demonstrate that the factors of $|Q|$ correspond to the determinant of subgraphs of $|Q|$, and can provide more distinct phases to the structure. Suppose that we have the factorisation $|Q| = \prod |q_i|$, then whenever a factor $|q_i| = 0$ we have $|Q| = 0$. For a structure that is not on a phase boundary taking $|q_i| > 0$ to $|q_i| < 0$ drives a topological phase transition. Therefore, the sign of each factor $\text{Sign}(|q_i|)$ is a topological invariant. That is, by finding the maximum number of factors of $|Q|$ that can be set to zero we can arrive at the number of distinct topological phases of G.

To see this factorisation is well defined, we show that the irreducible factorisation of $|Q|$ is unique in the supplementary material of [90].

To understand our notion of distinct phases in a topological context, we wish to formally define a topology on the parameter space ξ. Recall that for a space X a topology τ on X gives a notion of continuous deformation in terms of open or closed subsets of that space. This allows us to calculate the number of equivalence classes of Hamiltonians $[H_i]$. In section 2.1.5.2 we discussed the usual topology on a space X. Here we will define the usual topology on a subspace of the parameter space ξ, where each distinct phase arising from a factor $|q_i|$ of $|Q|$ corresponds to a different equivalence class $[H_i]$.

Definition 5.2.2. Let T denote the subspace of ξ that contains every singular Hamiltonian $|H| = 0$ on G. Then let $E_0 = \xi \setminus T$ be the open the subspace of ξ with no singular Hamiltonians on G. The open subsets of E_0 are defined as an open n-ball around each point $H \in \xi$. The topology τ is given by any intersection or union of an open subset of E_0. Note that this is the *usual topology* on E_0.

We can now interpret the equivalence classes of $[H_i]$ in this setting. From the previous discussion E_0 is a collection of disconnected open subsets. The number of disconnected subspaces in E_0 is the number of distinct topological phases. This number is given by the zeroth homotopy group of E_0.

5.3 Network topology and a topological classification

In this section we discuss the relationship between the network topology of a graph G and the topological classification of a Hamiltonian H on G. In chapter 2.1.5.1 we discussed the Harary Sachs theorem, which relates perfect matchings on a bipartite graph to terms in the determinant of the adjacency matrix [63, 64]. As in section 2.1.5.1 and chapter 7 we will refer to a perfect matching on a graph G as a cover of G. The covers of a graph depend on the underlying network topology, so it is through the Harary Sachs theorem that we give a connection between network topology and the classification of a graph.

Remark. To avoid ambiguity, we will refer to a graphs network topology as the connectivity of that graph.

As we will argue in section 5.3.1 and prove in the supplementary material of [90], with algebraically independent hopping terms the determinant of the biadjacency matrix $|Q|$ defines a polynomial which has irreducible factors f_i where

$$|Q| = \prod_i f_i \tag{5.3.9}$$

if and only if there exists an ordering of the sites of H that gives an upper triangular block basis to Q. That is

$$Q = \begin{pmatrix} \ddots & \vdots & \vdots & \vdots & \\ & q_{i-2} & C_{i-2,i-1} & C_{i-2,i} & \cdots \\ & & q_{i-1} & C_{i-1,i} & \cdots \\ & & & q_i & \cdots \\ 0 & & & & \ddots \end{pmatrix}. \tag{5.3.10}$$

Furthermore, this demonstrates that each factor is given by the determinant of a block on the diagonal of Q, that is $f_i = |q_i|$.

As each factor $|q_i|$ can be associated to blocks on the diagonal of Q, we can interpret each q_i as the biadjacency of a subgraph of G. We denote such a subgraph as $g_i \in G$.

Definition 5.3.1. The subgraph $g_i \in G$ associated to an irreducible factor $|q_i|$ of $|Q|$ is a *section* of G.

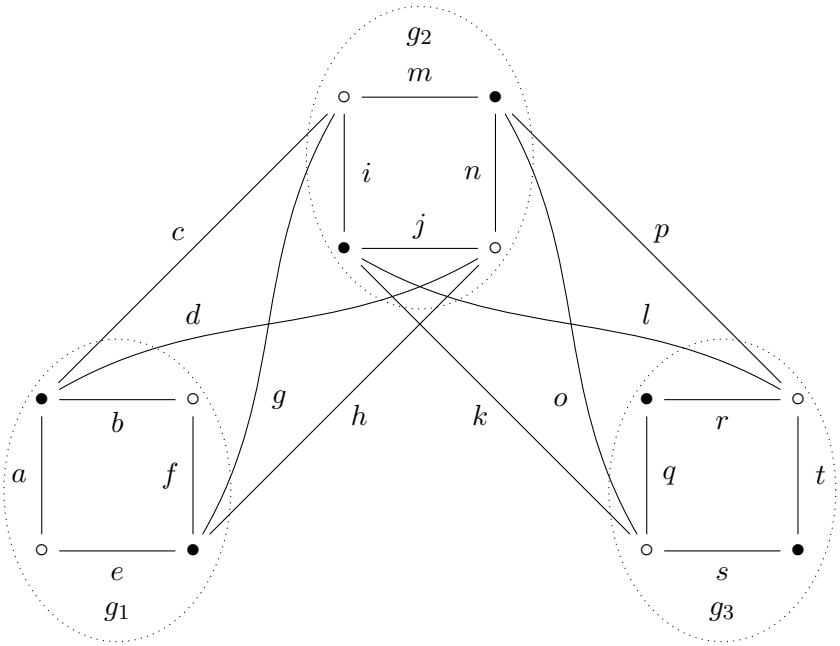

Figure 5.3.1: A structure with a zeroth step topology of $3\mathbb{Z}_2$. This structure has 3 sections g_1, g_2, and g_3. Each hopping term is labelled with a variable.

As discussed in [90] the physical consequences of our classification are revealed in the way zero energy states localise when a structure is on a topological phase boundary. In

particular how an individual section connects to other sections alter the localisation of nullstates originating from that section. To understand this localisation, we reproduce the definition of the partial ordering of sections here.

Definition 5.3.2. Assume Q is in an upper triangular block basis with diagonal blocks corresponding to the biadjacency matrices of sections. For every pair of sections $g_i, g_j \in G$ if the relative positions of q_i and q_j can be swapped while maintaining an upper triangular block basis of Q then $g_i = g_j$. Otherwise, if q_i is above q_j on the diagonal of Q, then we say $g_i > g_j$. That is

$$Q = \begin{pmatrix} \ddots & \vdots & \vdots & \vdots & \\ & q_i & \cdots & C_{i,j} & \cdots \\ & & \ddots & \vdots & \vdots \\ & & & q_j & \cdots \\ 0 & & & & \ddots \end{pmatrix}. \tag{5.3.12}$$

This defines a partial ordering on the sections g of G. If $g_i > g_j$ we say g_i is **above** g_j and g_j is **below** g_i[2].

5.3.1 A factorisation theorem

In this subsection we give a sketch the arguments that demonstrate the relationship between the underlying connectivity of a graph G and the topological classification of the Hamiltonians defined on that graph. The full proof is given in the supplementary material of [90].

There are two main elements to our proof. The first is to show that if Q has an upper triangular block basis, then $|Q|$ is factored by the determinants of the diagonal block. To show the converse we demonstrate that each section associated to an irreducible factor $|q_i|$ of $|Q|$ may only connect to other sections in a certain way, which leads naturally to an upper triangular block basis of Q. We sketch out the proof of the converse here, as the former assertion is not enormously complex, and may be generalised from the discussed in [90].

The main idea behind our proof of the converse is to show that if a structure has sections, then this implies the sections are connected in a certain way. The connectivity that leads to these sections gives a triangular block basis of Q with biadjacency matrices of each section on the diagonal. To do this we first show that, for almost all hopping terms, every first minor of a section is non-zero.

Remark. For almost all hopping terms, the intersection of a first minor of q and $|q| = 0$ are measure zero in $|q| = 0$. To see this, consider a section g with biadjacency matrix q, and a first minor $|q_m|$ of q. The polynomial $|q_m|$ is not factored by $|q|$ so $|q| = 0$ does not imply $|q_m| = 0$. If $|q_m| = 0$ is solvable, then the intersection of $|q_m| = 0$ and $|q| = 0$ defines a surface one dimension lower than $|q| = 0$ in ξ, and so the intersection of $|q_m| = 0$ and

[2]Note that if Q maps from the white sublattice to the black sublattice, then in [90] we use the term upper to denote an above section, and the term lower to denote a below section.

$|q| = 0$ are measure zero in $|q| = 0$. This is what we mean by every first minor of q being non-zero for almost all hopping terms, even when $|q| = 0$.

With the use of the Harary-Sachs theorem, each first minor being almost always non-zero ensures a subgraph of a section given by deleting one black site and one white site, has a cover. We can then use such covers to show that if sections are connected in a certain way, then this structure has a cover which is not given by the covers of the individual sections. By the Harary-Sachs theorem this shows there is a term in the determinant that is not factored by the determinant of the sections. This is contradictory to the definition of a section, proving the converse.

To see why every first minor of a section is almost always non-zero we delete a black site of a section. By the Harary-Sachs theorem a section (by definition) must have a cover, so there exists a matching of the remaining graph that does not include a white site which is a neighbour of the deleted black site. We then define a walk around the graph where we match and unmatch sites to change which white site is unmatched. We show that if some sites cannot be unmatched by this walk, then a section can be partitioned in to two sets, each with independent covers. This implies the sections determinant is reducible, which is a contradiction. Therefore, every first minor of a section is almost always non-zero. An example of such a walk is given in Fig. 5.3.2.

We next show that two sections can, pairwise, connect on only one sub lattice. This is because if two sections are connected on both sub lattices, we can construct a cover of the two sections which is not a cover of the individual sections. We can do this by seeing what happens if we delete two sites (a black and a white site) in each section (see Fig. 5.3.3 (a) for an example). As every first minor is almost always non-zero then the remaining graph is non-singular. So if we delete sites that connect between the two sections then by the Harary Sachs theorem we have found a perfect matching of the two sections. This cover is not related to the perfect matchings of the two individual sections. So two sections can only connect to one another on one sub lattice.

To show this leads to a triangular basis of Q, we prove that in an N section structure, at least one section may connect to all other sections on only one sub lattice.

Definition 5.3.3. An *edge section* is a section of G such that it may only connect to all other sections from one sublattice.

We can then start with an N section structure and delete the edge section, of what remains there must also be an edge section, and we can continue until only one section is left. This defines a triangular basis of Q giving us the factorisation theorem.

To show there is always at least one edge section we define a section cycle.

Definition 5.3.4. Consider a set of sections $\{g\}$ in G. If these sections have a *section cycle*, then there is a path through every section in $\{g\}$ such that the path starts on section $g_i \in \{g\}$ and ends on section g_i. The path goes through every section in $\{g\}$ exactly once, and enters each section on a white site, and leaves on a black site.

If no section cycles exist, then there must, by definition, be an edge section. To show no section cycles exist we assume that we do have a structure with section cycles. We then

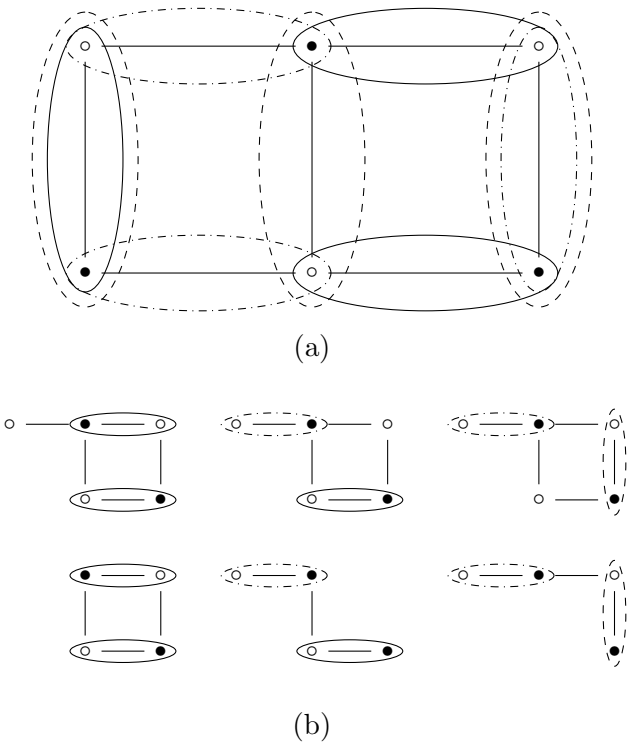

Figure 5.3.2: (a) 3 rung ladder graphene, which has the classification $\mathbb{Z}_2$, and all 3 covers of the structure denoted with a solid line, dashed line, and dash dot line. (b) Displays the structure having deleted one of the black vertices, and covering all but one white vertex. By swapping a single matching that neighbours the uncovered vertex at a time, it is possible to leave any of the white sites unmatched. Deleting the unmatched white vertex shows that for the deleted black vertex, deleting any of the white vertices leaves a cover.

delete a pair of sites from each section in the cycle (one black and one white) such that each site is connected between two sections (see Fig. 5.3.3 (b) for an example). Because every first minor of each section is almost always non-zero, then by the Harary-Sachs theorem what remains has a cover. Putting back in the deleted sites we now have a cover for the section cycle that is not given by the covers of the individual sections. This means the determinant of the section cycle is not factored by the determinant of the individual sections — a contradiction.

Putting all of this together, we then get the triangular basis of Q.

5.3.1.1 Localisation and topology

One of the important parts of proving the factorisation theorem is that every first minor of a section is almost always non-zero. We can use this to infer some properties about the nullstates of a Hamiltonian when $|H| = 0$, in particular, when only one section g_i has a singular biadjacency matrix $|q_i| = 0$.

In the supplementary material of [90] we give a proof that when a section q_i is critical

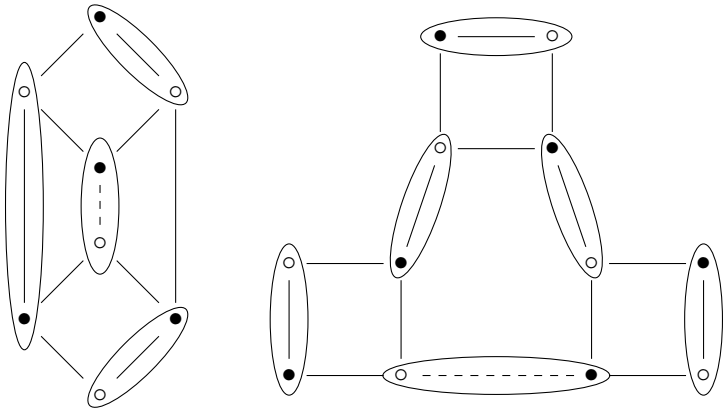

(a) (b)

Figure 5.3.3: Two structures with a $\mathbb{Z}_2$ classification. If the dashed edge were removed (a) would be a $2\mathbb{Z}_2$ structure, with two sections, however the drawn cover is not factorised by the determinant of each section, exemplifying that sections may only connect on one sublattice. If the dashed edge were removed from (b) it would be a $3\mathbb{Z}_2$ structure, however none of the determinants of sections in the structure with the deleted edge factorise the term in the determinant corresponding to the illustrated cover. a consequence of the non-existence of edge cycles.

($|q_i| = 0$) and all other sections are not critical, it almost always has support of the nullstates on every site of g_i. By almost always we mean that, if all but one hopping term of q_i are chosen randomly, and the final hopping term is chosen so that $|q_i| = 0$ then with probability 1 the nullstates have support on every site of g_i. This means a critical section is a weighted core graph [65].

Definition 5.3.5. A Hamiltonian H on a graph G with a nullity $\mathcal{N}(H) = \eta$ defines a weighted η-core graph if every vertex of G has non-zero support of the nullstates of H.

To see why a critical section is a weighted core graph we consider the first minors of q_i. By definition $|q_i|$ is an irreducible polynomial, and each first minor of q_i is the determinant of the biadjacency matrix of a subgraph of g_i obtained by deleting one black and one white site of g_i. Let $|q_m|$ denote such a minor. As $|q_i|$ is irreducible it is not factored by any $|q_m|$ so there are solutions to $|q_i| = 0$ that do not satisfy any $|q_m| = 0$. This ensures any subspace of ξ satisfying $|q_i| = 0$ and also $|q_m| = 0$ is at least one dimension lower than the subspace satisfying $|q_i| = 0$. That is $|q_m| \neq 0$ for almost all hopping terms. This means for almost all hopping terms that satisfy $|q_i| = 0$ every first minor $|q_m| \neq 0$.

We now consider what this means for the nullstates of q_i. To do this we wish to delete a column of q_i.

Definition 5.3.6. Let q_i^k denote the kth column of q_i, and let $q_i^{l\neq k}$ denote the submatrix of q_i where we have deleted the kth column.

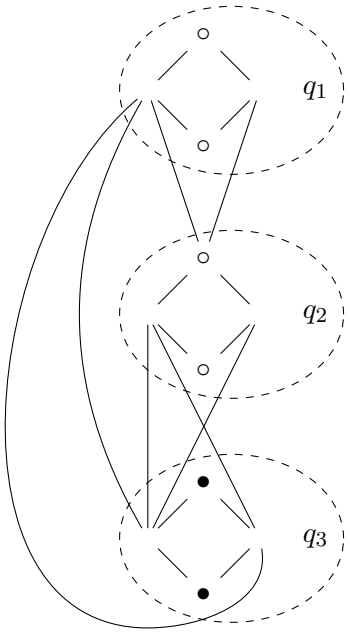

Figure 5.3.4: A structure with $|q_2| = 0$ and $|q_3| = 0$. For almost all hopping terms which satisfy the two constraints ($|q_2| = 0$ and $|q_3| = 0$) the only sites which may support zero energy states are those drawn (sites with no support of states are not drawn). If Q contains all the hopping terms from the black sites to the white sites then this structure has the partial ordering of sections $g_1 < g_2 < g_3$.

If we can localise a nullstate of q_i to have no support on at least one site of g_i then there must be a nullstate that satisfies

$$q_i^{l \neq k} \phi = 0. \tag{5.3.16}$$

But deleting any row of $q_i^{l \neq k}$ gives a non-singular submatrix, and so no ϕ with non-zero entries exists. Therefore, any null vector of q_i almost always has support on every site of g_i.

We also note that the partial ordering of section leads to consequences in how the nullstates of a topologically critical Hamiltonian localise. In [90] we discuss how the nullstates localise when only one section is critical. However, when two sections or more are critical there are some further consequences. To see this, consider a structure G with critical sections g_i and g_j where $g_i > g_j$. Let any section g_k such that $g_i > g_k > g_j$ be critical, or not, but otherwise assume any other section is not critical. Consider the biadjacency matrix

$$Q = \begin{pmatrix} \ddots & \vdots & \vdots & \vdots & \\ & q_i & \cdots & C_{i,j} & \cdots \\ & & \ddots & \vdots & \vdots \\ & & & q_j & \cdots \\ 0 & & & & \ddots \end{pmatrix}. \tag{5.3.17}$$

Because $|q_i| = 0$ there is some null vector ϕ_i^i that satisfies $q_j \phi_i^i = 0$. As no sections above

g_i are critical, we can define this null vector on the rest of Q which gives a nullstate for the Hamiltonian. However, the nullstate from g_j may also have support on g_i, and this needs to be, in some sense (as discussed in section 2.1.4) orthogonal to the nullstate from g_i. This requires further constraints on the hopping terms as will be discussed further in chapter 7. We also have the nullstate on $Q^\dagger$,

$$Q^\dagger = \begin{pmatrix} \ddots & & & & 0 \\ \cdots & q_i^\dagger & & & \\ \cdots & \vdots & \ddots & & \\ \cdots & C_{i,j}^\dagger & \cdots & q_j^\dagger & \\ \cdots & \vdots & \cdots & \cdots & \ddots \end{pmatrix}. \tag{5.3.18}$$

To get $Q^\dagger$ into an upper triangular diagonal basis, we can reverse the order of the sites that define the basis of H. Doing so reverses the partial ordering. Much like for Q this means only the nullstate of $q_j^\dagger$ remains in $Q^\dagger$. That is, for almost all hopping terms, the nullstates are split — on one sub lattice they have support on g_i and above sections only, and on the other sub lattice they have support on g_j and below sections only. An example is given in Fig. 5.3.4.

5.4 A classification algorithm

Full details of the classification algorithm are given in the supplementary material of [90]. This algorithm works by finding a permutation of Q which has the largest number of diagonal blocks. By the factorisation theorem, this finds all the sections of a structure.

Once all the sections are found, and the domain of each hopping term is specified, a second step calculates if each section has solutions within that domain or not. This gives the number of non-trivial sections of a structure, therefore giving its classification.

5.5 Classification paper

A Topological Classification of Finite Chiral Structures using Complete Matchings

Maxine M. McCarthy and D. M. Whittaker
University of Sheffield
(Dated: May 25, 2024)

We present the theory and experimental demonstration of a topological classification of finite tight binding Hamiltonians with chiral symmetry. Using the graph-theoretic notion of complete matchings, we show that many chiral tight binding structures can be divided into a number of sections, each of which has independent topological phases. Hence the overall classification is $N\mathbb{Z}_2$, corresponding to 2^N distinct phases, where N is the number of sections with a non-trivial $\mathbb{Z}_2$ classification. In our classification, distinct topological phases are separated by exact closures in the energy spectrum of the Hamiltonian, with degenerate pairs of zero energy states. We show that that these zero energy states have an unusual localisation across distinct regions of the structure, determined by the manner in which the sections are connected together. We use this localisation to provide an experimental demonstration of the validity of the classification, through radio frequency measurements on a coaxial cable network which maps onto a tight binding system. The structure we investigate is a cable analogue of an ideal graphene ribbon, which divides into four sections and has a $4\mathbb{Z}_2$ topological classification.

I. INTRODUCTION

Topology has become ubiquitous in modern physics, with many lattice structures and materials shown to have non-trivial topological attributes. A topological material is characterised by properties which remain unchanged during adiabatic evolution, making them robust in the presence of disorder. For instance, boundary states in one-dimensional topological lattices may have energies which are resistant to disorder [1], while in two-dimensions they may provide directional transport which is protected against backscattering [2–5]. In order to investigate these potentially useful properties, it is necessary to be able to classify the different topological phases of a given Hamiltonian.

Distinct topological phases are generally understood from two perspectives. The first is that two phases are distinct if, and only if, they cannot be related by (symmetry respecting) adiabatic evolution. The second is that a non-trivial topological phase has interesting boundary properties. The first perspective allows us to assign topological indices to distinct phases, and the second gives a physical significance to a classification. Both are connected by the famous bulk-boundary correspondence [6] which, since the discovery that the quantum Hall effect is topological [2, 7] has proven a powerful tool for the prediction of topological boundary phenomena. Most approaches to classification make use of the bulk-boundary correspondence in some way.

A ubiquitous topological classification is that of the 10-fold way [8], in which K-theoretic methods are used to classify each of the Altland-Zirnbauer (AZ) symmetry classes of momentum-space Hamiltonians [9]. Another approach is topological quantum chemistry [10, 11], where the classification is obtained by looking for topologically non-trivial states. In particular, the presence of states which cannot be adiabatically deformed to the atomic limit indicates a topologically non-trivial band in the bulk [12]. These methods provide a classification of stable and fragile topological phases in a huge number of systems [13].

A useful approach for strong disorder relies on defining a non-commutative Brillouin zone [14–16]. Using non-commutative geometry, the Brillouin zone is modified to allow for variations in each unit cell of the structure, by defining a configuration space for the set of distinct unit cells. Translational invariance is no longer required, giving a disordered bulk-boundary correspondence.

For finite structures, a spectral localiser [17, 18] can predict the presence of approximately zero energy boundary states (also by demonstrating states cannot be localised to an atomic limit), therefore classifying a structure via the converse of the bulk-boundary correspondence. Alternatively local realspace markers may be used [19, 20] whose average gives a topological index for the entire structure. While this averages to a quantised value in the thermodynamic limit, such local markers are not exactly quantised in finite structures.

It has been shown that finite size effects may cause a rich sequence of topological phase transitions, corresponding to gap closures separating *topological bubbles* [21] in inversion symmetric structures. The number of approximately zero energy boundary states in such a bubble takes an integer value corresponding to a $\mathbb{Z}$ classification in finite, inversion-symmetric Hamiltonians. These states are resistant to small amounts of disorder. Such an approach has also been extended to time-reversal symmetric systems [22]. Alternatively the finite structure may be repeated as a periodic supercell [23, 24] allowing the use of momentum-space methods to classify the topological phases.

These approaches leave open a problem: how may a structure be classified when we completely lose the bulk-boundary correspondence? That is, we no longer have any way to define a boundary or a bulk. This situation may occur in a small finite structure, particularly with strong disorder and/or no underlying lattice structure (for instance, a random finite network). Strongly disor-

dered finite systems may have a non-trivial topological classification [17, 25, 26] although the number of distinct topological phases is not always clear, motivating a general approach to topologically classify finite structures which have lost the bulk-boundary correspondence. In this paper, we propose a partial solution to this problem. Using graph-theoretic methods, we give a topological classification for finite chiral symmetric structures. We achieve this by considering equivalence classes of finite real space Hamiltonians with arbitrary values for the hopping terms.

In a finite structure at sufficient disorder, a bulk may not be possible to define, however non-adiabatic evolution may still be defined. For a finite system, a closing in the energy spectrum is analogous to a band gap closing in momentum space. In structures with chiral symmetry, and thus a symmetric energy spectrum, this corresponds to the appearance of pairs of zero energy states. Determining the conditions on the hopping terms which lead to the presence of these states allows us to define equivalence classes of Hamiltonians. A similar approach to defining topological phase boundaries has been used in [17, 25, 26].

Using this definition of equivalence classes we find that many structures have a rich classification resulting from the fact that they can be divided into a number of *sections*, each of which can be assigned an independent topological phase. These sections are identified as corresponding to factors of the determinant. Such factors may be determined by the hopping terms that appear in the expansion of the determinant of the Hamiltonian, and therefore play a role in defining the conditions for zero energy states. Any other hopping terms in the Hamiltonian can be removed without affecting the classification. This removal process results in the structure separating into disconnected pieces, each constituting a section. For each section we can determine an independent 0 or $\mathbb{Z}_2$ classification, using a sub-Hamiltonian defined on the section.

The existence of sections depends on the connectivity of the network representing the hopping terms in the Hamiltonian. They can occur in structures with some regularity, as in the graphene related examples which are considered in this work. However, they can also appear in more randomly connected structures. Checking 154131 non-isomorphic graphs which represent some of the connected chiral structures with 18 sites or fewer, and using randomised searches on larger finite chiral structures, we find that the classification of a structure is the most rich when each site has an average of three hopping terms. For an average of two the underlying connectivity is generally too sparse to provide a rich classification, and at four or greater, the structure is often too constrained by its connectivity to allow the division into many sections.

Of the 154131 graphs classified, for all positive and real hopping terms, 14% had no distinct topological phases, with the remaining being topologically non-trivial. 82% had two topological phases, and 4% had 4 to 16 distinct topological phases, with only 18 of the classified graphs having 16 phases. Including trivial and non-trivial sections 8% of structures has no sections, 68% had one section, and 24% had 2 to 9 sections (trivial sections can still affect physical properties, such as localisation).

The infinite and finite classification of the sub-Hamiltonian corresponding to a section may be different. Considering a section as a one-dimensional supercell of an infinite lattice a transfer matrix treatment leads to one trivial and one non-trivial topological phase, separated by a gap closure somewhere in the Brillouin zone. Hence, with this definition, every section has a $\mathbb{Z}_2$ classification. Furthermore, the classes AIII and BDI have a $\mathbb{Z}$ classification using the 10-fold way. In this infinite interpretation, a section having a non-trivial topological phase results in boundary localised topologically robust zero modes to one end of that section. This gives a connection to higher order topology arising through stacked chiral structures.

We seek to classify the actual finite structure, so we adopt the convention that only unavoidable gap closures which are observable (corresponding to closure at zero momentum) separate topological phases. This means that some sections will have a $\mathbb{Z}_2$ classification, while others will be topologically trivial. The complete structure behaves as a stack of sections, connected together in such a way that the topological phase of each section is independent. This gives a classification as the direct sum $\bigoplus_1^N \mathbb{Z}_2 \cong N\mathbb{Z}_2$ where N is the number of sections with a non-trivial classification, and depends on the underlying connectivity of the structure. For periodic materials, the stacking is not unlike that seen in [27]. Others have also shown that a rich classification can follow from the underlying connectivity of a structure [28, 29].

We also show that the localisation of the zero energy states that accompany a topological phase transition is determined by the connections between the sections. We define a partial ordering of the sections based on this connectivity, such that each of the zero energy states created by making one section topologically marginal spreads in only one direction through the remaining sections. This provides an experimentally accessible verification of the existence of the sections. We perform such an experiment using a coaxial cable network, which has been shown to map onto a tight-binding Hamiltonian [26, 30–32]. The structure we consider is a zigzag 'graphene' nanoribbon consisting of four rows of sites, each of which forms a separate section, leading to a $4\mathbb{Z}_2$ classification.

We begin by discussing the theory behind the classification in section II before discussing experimental results in a small graphene structure in section III, and concluding in IV. Supplementary material is provided with more mathematical and experimental details.

II. CLASSIFYING FINITE CHIRAL STRUCTURES

Chiral symmetry is one of the fundamental symmetries of the Altland-Zirnbeaur symmetry classes [9]. A chiral Hamiltonian H anticommutes with a unitary C, ensuring non-zero eigenvalues come in $\pm\varepsilon$ pairs. When allowing algebraically independent hopping terms (thereby letting the structure have arbitrary hopping disorder) a Hamiltonian with chiral symmetry necessarily has two sublattices of sites, which we label 'black' and 'white' (a consequence of the Harary-Sachs theorem [33, 34]). Each black site is only connected (through non-zero hopping terms) to white sites, and each white site is only connected to black sites. An example is shown in Fig. 1.

For a structure with n_B black sites and n_W white sites, there are are always at least $|n_B - n_W|$ zero energy states. Since these exist independently of the values of the hopping terms in H, they are described as topologically protected states. Such states can also occur in structures with $n_B = n_W$. If a structure has such protected states, the determinant of the Hamiltonian is necessarily zero for all values of the hopping terms, so a classification based on the conditions for $|H| = 0$ is not possible. In this work, we consider only structures with equal numbers of black and sites and no topologically protected states.

Two Hamiltonians H_1 and H_2, are considered to have a different topological phase if they cannot be related under adiabatic evolution. That is, there exists no continuous way to evolve between H_1 and H_2 without a gap closing in the spectrum. For a chiral Hamiltonian with an even number of sites, zero energy states necessarily occur in degenerate pairs. This degeneracy corresponds to a closed gap in the spectrum, indicating non-adiabatic evolution. Therefore finding the conditions for a singular Hamiltonian determines the topological phase boundaries in a finite structure.

To explore distinct topological phases on a finite chiral structure we consider a set of sites connected by non-zero hopping terms. Formally this defines a graph G. On G we define a tight binding (TB) Hamiltonian, H, where each hopping term may be continuously evolved, algebraically independently. To ensure changes to G only include continuous evolution we do not allow new connections to be introduced, or existing connections to be broken. In terms of H, this means non-zero hopping terms must remain non-zero, and hopping terms which are zero cannot be modified. Otherwise we allow complete freedom to continuously evolve hopping terms of H, giving access to strongly disordered Hamiltonians defined on G. We do, however, restrict the hopping terms to be real: any topological phase boundary in a finite structure can be avoided, by evolving the Hamiltonian through a path involving complex hopping terms. Although we can allow negative values, the requirement for non zero real hopping terms means that they cannot change sign as they evolve.

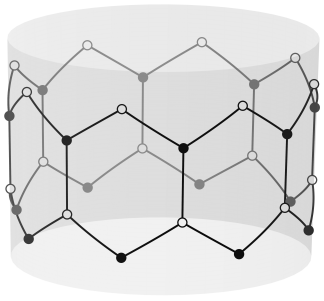

FIG. 1. A two row ribbon zigzag graphene, looped to form a cylinder. The structure has chiral symmetry, with the two sublattices indicated by the black and white sites. The topological classification of structures like this can be found using the methods we describe: this one is $2\mathbb{Z}_2$.

The tuple of algebraically independent hopping terms on G, defines an affine space, ξ. Each Hamiltonian H on G defines a point in ξ. Continuously evolving hopping terms in H corresponds to following a path in ξ. We refer to ξ as the *parameter space* of G. Topological phase boundaries in ξ correspond to boundary free surfaces one dimension lower than ξ. An example of a slice of a parameter space is given in Fig. 3.

The classification problem can be completely reduced to finding solutions to $|H| = 0$, which necessarily corresponds to degenerate zero energy states. Although degeneracies can occur at non-zero energies, in a system with algebraically independent hopping terms, such a gap closure requires at least two constraints on the hopping terms, a consequence of the Harary-Sachs theorem [33, 34]. Such constraints are described by surfaces which are at least two dimensions lower than ξ, and therefore cannot divide it: they are always avoidable gap closures. This ensures topological phase boundaries are only given by a collection of surfaces in ξ corresponding to $|H| = 0$.

The Hamiltonian for a chiral structure has an antidiagonal block basis corresponding to ordering the sites by sublattice,

$$H = \begin{pmatrix} 0 & Q \\ Q^\dagger & 0 \end{pmatrix} , \tag{1}$$

so the determinant $|H| = -|Q||Q^\dagger|$. For equal numbers of black and white sites, Q is a square matrix, so $|Q| = |Q^\dagger|$, and we can use either to determine the classification.

Every term in the expansion of Q is algebraically independent, so $|Q|$ is a multi linear form of the hopping terms. That is $|Q|$ varies linearly with respect to each hopping term in its expansion. For each hopping term in $|Q|$, solutions to $|Q| = 0$ follow from solving a linear equation, constraining exactly one hopping term. This ensures that every solution to $|Q| = 0$ corresponds to a surface in ξ which is both unbounded, and one dimension lower than that of the parameter space, splitting ξ in to distinct regions. This linear behaviour also ensures that $|Q|$ changes sign as we go over a phase boundary, meaning $\mathrm{Sign}\,[|Q|]$ is a topological invariant [17]. This is in

contrast to Sign $[|H|]$, which does not change at a phase boundary.

To classify a structure, we must understand how to set $|Q|$ to zero by continuously evolving hopping terms, which may be done by finding the irreducible factors of $|Q|$. If a factorisation of $|Q| = \prod |q_i|$ exists, and it is possible to solve $|q_i| = 0$, then the factor $|q_i|$ defines a pair of distinct phases, where Sign $[|q_i|]$ is a topological invariant. We say such a factor is *non-trivial*. The classification of the structure is then given by $\bigoplus^N \mathbb{Z}_2 \cong N\mathbb{Z}_2$ where N is the number of non-trivial factors.

The determinant $|Q|$ defines a polynomial in a unique factorisation domain (details are given in the supplementary material section A) ensuring the maximum number of non-trivial factors, N, of $|Q|$ is also a topological invariant, so the classification is well defined. It is only possible to change N by removing or introducing new hopping terms or sites, that is, under discontinuous evolution of H.

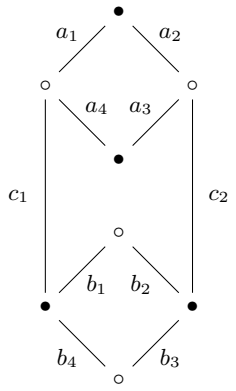

FIG. 2. A simple two row graphene zigzag structure with the hopping terms labelled as in Eq.(2). This structure has two sections and four distinct topological phases, corresponding to a $2\mathbb{Z}_2$ classification.

To show a simple example, we consider a 2 row zigzag graphene sructure, with 4 sites on each row, see Fig. 2. This is described by the matrix

$$Q = \begin{pmatrix} a_1 & a_4 & c_1 & 0 \\ a_2 & a_3 & 0 & c_2 \\ 0 & 0 & b_1 & b_2 \\ 0 & 0 & b_4 & b_3 \end{pmatrix} \tag{2}$$

giving the determinant,

$$|Q| = (a_1a_3 - a_2a_4)(b_1b_3 - b_2b_4) = |q_1||q_2|. \tag{3}$$

The condition $|Q| = 0$ can be satisfied by making either factor, $|q_1|$ or $|q_2|$, equal to zero. This gives four distinct topological phases corresponding to $(\text{Sign}[|q_1|], \text{Sign}[|q_1|]) = (+1,+1),(+1,-1),(-1,+1),(-1,-1)$. Therefore this structure has the classification $2\mathbb{Z}_2$.

It is also apparent from this simple calculation that some of the hopping terms – c_1 and c_2 – do not appear in the expansion of $|Q|$. This means that the topological classification will be the same as for a structure in which these hopping terms have been set to zero. Physically, removing these links creates two completely separate lattices, the top and bottom loops in Fig.2. We call these the two *sections* of the original structure.

The Hamiltonian, and thus Q, for a separated structure is block diagonal, so the determinant, $|Q|$, is simply a product of the two block determinants, as the expansion shows. The absence of the c terms from the expansion of $|Q|$ is a consequence of the block triangular form of Eq.(2). However, this pattern is only explicit if the sites are ordered correctly, which depends on finding the sections defining the blocks in the matrix. As we prove in the supplementary material section A.1, the determinant is factored if and only if there exists a block triangular form of Q, so finding an appropriate ordering of sites allows us to find the number of sections in a structure.

A graph-theoretic approach to this problem involves enumerating the *complete matchings* of a structure. A complete matching consists of a set of pairings of sites, or *matchings*, which are connected (by a non-zero hopping term), such that every site in the structure is included in exactly one pair. Examples of such complete matchings are shown in Fig. 4, for the four row graphene ribbon which we investigate experimentally in section III. A complete matching has an algebraic interpretation: if we index separately the black and white sites such that each each matched pair has the same index, the corresponding hopping terms appear along the diagonal of the matrix Q. The terms in the expansion of the determinant of a matrix correspond to the product of the diagonal elements for every possible permutation of the columns (or rows). Hence finding the set of complete matchings for a structure gives all the terms in the expansion (to get the signs, it is also necessary to keep track of the number of swaps required to go between matchings). This is the Harary-Sachs theorem [33, 34] for weighted bipartite graphs.

A consequence of the relationship between complete matchings and the expansion of $|Q|$ is that any connection which is not included in any matching does not appear in the expansion, so can be removed to reveal the sections. In the case of the structure in Fig. 4, all the connections between the rows can be removed, so the structure has four sections. For each section, there are two complete matchings, so each factor $|q_i|$ of $|Q|$ contains two terms. Since these have opposite signs, every factor can be made to pass through zero, so the structure has classification $4\mathbb{Z}_2$. Note that even small changes in connectivity can change this completely. If we add just one connection between the a white site of top row and a black site of the bottom row of the structure, we find that there are complete matchings which include every connection, so there are no sections and the classification is $\mathbb{Z}_2$.

The relationship between the number of sections of a structure and a block triangular form of Q in Eq.(2) can

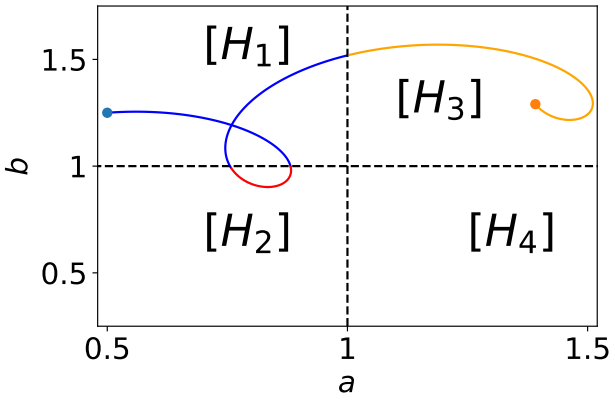

FIG. 3. A slice of the parameter space for 2 row ribbon zigzag graphene, which has the classification $2\mathbb{Z}_2$. This slice is defined by setting all the hopping terms equal to 1, apart from one in each row, a and b, which are allowed to evolve independently. $[H_x]$ denotes a set of topologically equivalent Hamiltonians, and the dashed lines denote phase boundaries. The path shown undergoes 3 phase transitions between the phases $[H_1]$, $[H_2]$, and $[H_3]$, where each phase transition is identified by the appearance of a pair of unavoidable degenerate zero energy states.

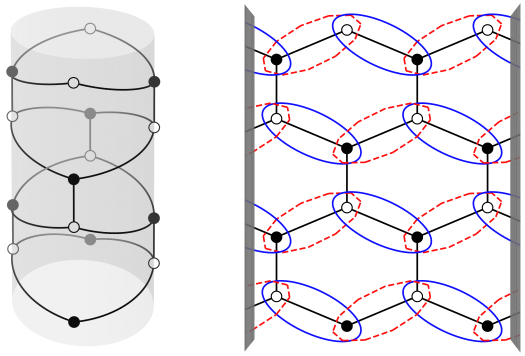

(a) (b)

FIG. 4. (a) The four row ribbon graphene structure looped to form a cylinder. (b) The complete matchings of this structure, flattened for clarity. A complete matching consists of a solid or dashed set of matchings from each row. The choice for each row is independent so there are 2^4 complete matchings. The connections between the rows do not appear in any of the matchings, so each row forms a separate section. the topological classification for this structure is $4\mathbb{Z}_2$.

be made rigorous. In the supplementary material section A.1, we prove that the factorisation of $|Q|$ according to sections, $|Q| = \prod_i |q_i|$, can be made if, and only if Q can be written in the block triangular form

$$Q = \begin{pmatrix} q_j & \cdots & c_{i+1,j} & c_{i,j} \\ & \ddots & \vdots & \vdots \\ & & q_{i+1} & c_{i,i+1} \\ 0 & & & q_i \end{pmatrix}, \tag{4}$$

where the q_i and c_{ij} are matrix blocks. Therefore by finding an appropriate order of the sites the number of sections will be revealed in a structure.

The diagonal blocks, q_i, in Eq.(4) define the sections of the structure. They include the hopping terms which connect the black and white sites within the section. The off diagonal blocks, $c_{i,j}$, contain the connections between the sections. The hopping terms in the off diagonal blocks do not appear in the expansion of $|Q|$. Note that the connecting terms only appear within superdiagonal blocks – the corresponding subdiagonal is necessarily zero. Thus the connections between sections are always between the sublattices. For instance if Q maps from the black to the white sublattice, then only the white sites of g_j may connect to the black sites of g_i. We will make use of this shortly to define a partial ordering of the sections.

The relationship between the block structure of a matrix and the topological classification of a chiral structure has allowed us to find an algorithm to classify a random chiral network. Details of this algorithm are given in the supplementary material section B. Of our classification algorithm, the most numerically expensive part is finding a basis with the largest number of triangular blocks. An alternative algorithm for this part of the classification is detailed in [35] although we have not compared the complexity of our algorithm to this alternative approach.

The factorisation and triangular form of Q tells us more than just the topological classification of the Hamiltonian. Physically the nature of localisation at criticality (that is, at a topological phase boundary) is affected, with nullstates exactly restricted to a particular subset of sections. We consider a structure represented by the graph G, with a section g_i corresponding to the factor q_i. For a topologically marginal chiral structure each nullstate can be localised to the black or white sub lattice. If only one section is singular, the black state may be non-zero only on a subset G_b of non-critical sections, and the white state may be non-zero on a subset G_w of non-critical sections. The sets G_w, G_b and the critical section g_c are disjoint, so that the only section with support of both the black and white states is g_c. This non-trivial localisation yields an experimental method to find the classification of a structure, discussed in section III.

To understand this localisation, we define a partial ordering of sections, $(g \in G, \leq)$, which provides the upper triangular form in Eq.(4). We say that $g_i < g_j$, or g_i is *lower* than g_j, if white sites of g_i connect to black sites of g_j, and $g_i > g_j$, or g_i is *higher* than g_j, if black sites of g_i connect to white sites of g_j. If the blocks q_i and

q_j can be permuted in Q to swap places on the diagonal in such a way that maintains an upper triangular block matrix Q, then $g_i = g_j$. Otherwise if g_i and g_j are not directly connected, we look to neighbouring sections to define the partial ordering. As the structure is connected, we may always iterate to neighbours of neighbours until we have the partial ordering relationship between any two sections.

In order to demonstrate how the localisation of nullstates in a critical section is altered by the partial ordering of sections, consider a 4 section structure where Q has the form

$$Q = \begin{pmatrix} q_1 & c_{12} & c_{13} & 0 \\ 0 & q_2 & 0 & c_{24} \\ 0 & 0 & q_3 & c_{34} \\ 0 & 0 & 0 & q_4 \end{pmatrix} \tag{5}$$

where q_i and $c_{i,j}$ are block matrices. The sections have the partial ordering $g_1 < g_2 = g_3 < g_4$. Suppose that section g_3 is marginal, so $|q_3| = 0$ and $|q_1|, |q_2|, |q_4| \neq 0$. Then there exists a null eigenvector $|\phi\rangle$ such that $q_3 |\phi\rangle = 0$. The solution over all of Q is then given by

$$\begin{pmatrix} q_1 & c_{12} & c_{13} & 0 \\ 0 & q_2 & 0 & c_{24} \\ 0 & 0 & q_3 & c_{34} \\ 0 & 0 & 0 & q_4 \end{pmatrix} \begin{pmatrix} -q_1^{-1} c_{13} |\phi\rangle \\ 0 \\ |\phi\rangle \\ 0 \end{pmatrix} = 0 \tag{6}$$

demonstrating the nullstate can have non-zero support on the black sites of g_1 and g_3 only. Similarly $|q_3^\dagger| = 0$ so we have a similar solution for $Q^\dagger$ where

$$\begin{pmatrix} q_1^\dagger & 0 & 0 & 0 \\ c_{12}^\dagger & q_2^\dagger & 0 & 0 \\ c_{13}^\dagger & 0 & q_3^\dagger & 0 \\ 0 & c_{24}^\dagger & c_{34}^\dagger & q_4^\dagger \end{pmatrix} \begin{pmatrix} 0 \\ 0 \\ |\psi\rangle \\ -(q_4^\dagger)^{-1} c_{34}^\dagger |\psi\rangle \end{pmatrix} = 0 \tag{7}$$

and $q_3^\dagger |\psi\rangle = 0$. Hence this nullstate has non-zero support on the white sites of g_3 and g_4 only. The localisation of the support by sublattices is a direct consequence of the partial ordering, in this example $g_1 < g_2 = g_3 < g_4$. These rules generalise in a straightforward way when there are more sections: the black zero energy state is localised on the marginal section and those lower in the partial ordering, while the white state is confined to the marginal section and those which are higher.

It should be noted that within the critical section itself, for a randomly selected distribution of hopping terms that satisfy the condition for a section to be critical, the zero energy states have, with probability one, support on every site of the section. Proofs of this, and of the general relationship between the factorisation and localisation, are given in the supplementary material section A.1.

It is natural to ask what happens when a structure has more than one critical section. In some instances it is possible to have more than two zero energy states. However, for most structures, for almost all sets of hopping terms, there remain only two zero energy states when there are multiple critical sections. This is because the null states originating from each critical section must be orthogonal to each other, which imposes additional constraints on the hopping terms, including those which connect the sections. The conditions for such higher nullity will be explored in future work.

III. EXPERIMENTAL DEMONSTRATION OF CLASSIFICATION

To demonstrate the topological classification defined in Section III, we have performed experiments on a coaxial cable network which represents the 4 row ribbon graphene structure of Fig. 4. A network where all coaxial cables have the same transmission time, τ, maps on to a tight binding model [26, 30] where the sites are the junctions in the network. The 'energy', ε, is given by $\varepsilon = \cos \omega\tau$ where ω is the driving frequency. This yields a Schrödinger type eigenvalue equation $H\psi = \varepsilon\psi$. Entries in ψ correspond to scaled voltages at the junctions. Up to this scaling factor, individual hopping terms are given by the reciprocal of the impedance of a cable connecting the sites. Swapping between cables of different impedances thus allows us to traverse a structure's parameter space ξ.

Experimental measurements are made with a vector network analyser (VNA) and takes two forms. From on-site reflectance measurements, we determine the structure's impedance, the real part of which is proportional to the local density of states (LDOS) at that site [26]. We use this to demonstrate the localisation of the null states. Transmittance measurement give the relationship between the magnitude of a state on two sites. This gives a direct experimental determination of the block triangular form of Q, Eq.(2), and thus the classification of the structure.

1. *Measuring the Local Density of States*

Measuring the local density of states on every site allows us to characterise the localisation properties of the zero energy states in a marginal structure with multiple sections, of which only one is critical. Fig. 5 displays the LDOS measurements of the disordered looped 4 row ribbon zigzag graphene in Fig. 4. According to the classification of Sec. II, this structure has four non-trivials sections, corresponding to the horizontal rows, so its topological classification is $4\mathbb{Z}_2$. Individual cables are chosen randomly from a binary distribution of 50Ω and 93Ω cables (see more details in supplementary material section C). One section is critical, the second row in the figure, while the other three are not. The localisation of the nullstates is clear: the white state only has significant strength on the top two rows, while the black state appears only on the lower three. This is in agreement

with the predicted localisation, given the ordering of the rows $g_1 > g_2 > g_3 > g_4$.

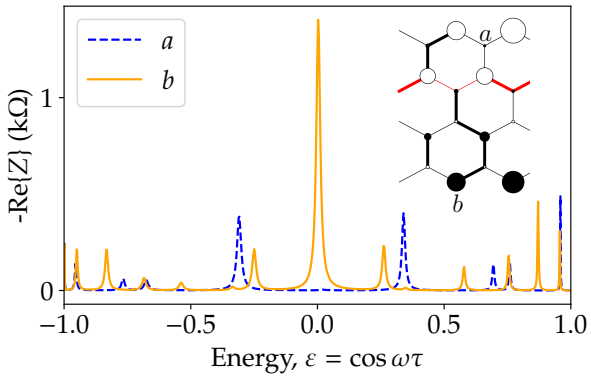

FIG. 5. Experimental measurement of the impedance spectra in a topologically marginal 4 row ribbon graphene structure. The strucure has four sections, correponding to the rows of the structure. Spectra are shown for two sites on the black sublattice, labelled a and b in the structure diagram in the inset. In the plot of the structure the diameter of the circle representing each site is proportional the amplitude of the zero energy state at that point, which is derived from the strength of the corresponding impedance peak. The widths of the lines showing the connections indicates the impedance of the corresponding cable, with wide lines being 93Ω and narrow lines 50Ω cables. The red lines pick out the second row which is the critical section. The localisation of the zero energy eigenstates onto distinct sublattices on the upper and lower sections relative to the critical row agrees with our theoretical prediction. Note that the structure has cylindrical boundary conditions as displayed in Fig. 4 (b), with the hanging connections at either side linked together.

2. *Topological Classification through Transmittance*

Measurements of the transmittance can be used to verify the triangular form of Q, Eq.(2), and thus the division of the structure into sections. We describe here an experiment where we make a cut in each section of the structure, by disconnecting one end of a cable, and measure transmittance between various cuts. We show that transmittance at zero energy ($\cos\omega\tau = 0$) only occurs when the measurement is within one section: the transmittance between sections is zero.

In order to describe the transmittance of the coaxial cable network, we use a transfer matrix formalism to relate the voltages and currents at the output sites to those at the input sites. If we cut a site on every section (creating an input and output site on each section), the transfer matrix will have dimensions $2\tilde{N} \times 2\tilde{N}$, corresponding to the voltage and current variables for each of the $\tilde{N}$ sections. Here we use $\tilde{N}$ for the total number of sections,

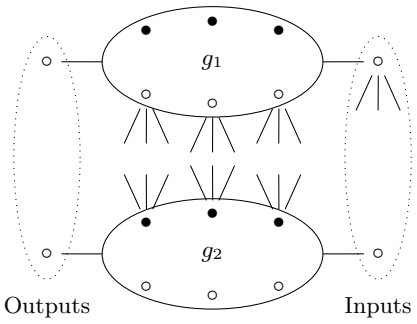

FIG. 6. A structure with two sections, g_1 and g_2, with the partial ordering of $g_1 < g_2$ since white sites in g_1 connect to black sites in g_2. The sections correspond to the ellipses, and contain arbitrary numbers of sites, which are not shown individually. The hopping terms connecting the two sections are denoted schematically by bunches of three lines, but they may join any white sites of g_1 to any black sites of g_2. Each section has been cut to create input and output sites for transmittance measurements.

to distinguish from N, the number of topologically nontrivial sections from earlier.

For a chiral structure at zero energy, all the variables can be coloured black or white, according to the two sublattices, in such a way that the matrix consists of two $\tilde{N} \times \tilde{N}$ diagonal blocks. At zero energy the voltage at a given site is determined entirely by the currents flowing out of the neighbouring sites. The neighbours in a chiral structure are on the other sublattice, so, if we assign the voltage the same colour as its site, and the currents flowing into and out of a site the opposite colour to the site, the variables of the two colours are completely independent, giving the two blocks.

To see how the form of the transfer matrix for the cut structure is related to the sections, consider making a cut within a section, forming an input and output site. The cut adds a site to the structure, unbalancing the black and white sublattices in the section, and thus creating a new zero energy state. For instance cutting on a white site creates one extra white site, resulting in a zero energy state that only has support on the white sites of that section and of any higher sections in the partial ordering. This means that the block triangular form of the matrix Q in Eq.(2) translates to a triangular form of each block of the transfer matrix. This triangular form persists regardless of the site at which the cut is made in each section; it can shown to exits if, and only if, the uncut structure has at least $\tilde{N}$ sections.

As a simple example, consider a structure with just two sections, g_1 and g_2, as shown in Fig. 6. The white sites in g_1 connect to the black sites in g_2, so in the partial ordering, $g_1 < g_2$. Each section is cut at a white site, so the white block of the transfer matrix relates the input and output voltages, while the black block connects the

currents. The transfer matrix is thus

$$\begin{pmatrix} I_{\text{out}}^{g_1} \\ I_{\text{out}}^{g_2} \\ V_{\text{out}}^{g_1} \\ V_{\text{out}}^{g_2} \end{pmatrix} = \begin{pmatrix} \gamma & \delta & 0 & 0 \\ 0 & \beta & 0 & 0 \\ 0 & 0 & \alpha & 0 \\ 0 & 0 & \nu & \mu \end{pmatrix} \begin{pmatrix} I_{\text{in}}^{g_1} \\ I_{\text{in}}^{g_2} \\ V_{\text{in}}^{g_1} \\ V_{\text{in}}^{g_2} \end{pmatrix}, \tag{8}$$

where the non-zero matrix entries represented by Greek letters are functions of the hopping amplitudes in the Hamiltonian, and depend on the details of the actual structure.

It is not possible to measure directly the form of such a transfer matrix using a two-port VNA, which can only give the transmittance between one input and one output site. The voltages and currents at the other input and output sites cannot simply be made zero: we can either leave them open circuit, in which case there can be a voltage on the site, but no current flowing in or out, or they can be shorted, giving a current but no voltage. In our experiment, the output site is always open circuit, and the choice of whether to short or leave open the input site is made according to the partial ordering.

To see how this works, consider the case where the input and output are connected to section g_1 and the input to g_2 is open circuit. Then $I_{\text{in}}^{g_2} = 0$ and $I_{\text{out}}^{g_2} = 0$. From Eq.(8), we get $I_{\text{out}}^{g_1} = \gamma I_{\text{in}}^{g_1}$ and $V_{\text{out}}^{g_1} = \alpha V_{\text{in}}^{g_1}$, so non-zero transmittance occurs. However, if the input to g_2 is shorted, the boundary conditions instead become $V_{\text{in}}^{g_2} = 0$ and $I_{\text{out}}^{g_2} = 0$. This gives $I_{\text{out}}^{g_1} = 0$ and $V_{\text{out}}^{g_1} = \alpha V_{\text{in}}^{g_1}$, so no transmittance can be seen, because this requires both the output voltage and current to be non-zero. Hence, for our classification experiment to work, with intra-section transmittance non-zero, we need the g_2 input site to be open circuit.

Proceeding in the same way, we find that if the input port is connected to the input site of g_1 and the output port to the output site of g_2, we get non-zero transmittance if the input to g_2 is shorted, but not if it is open circuit. Thus, to see no transmittance between sections, we again need g_2 to be open circuit.

If we do these experiments with input port connected to the input site of g_2, the requirement is reversed: the g_1 input site has to be shorted to get non-zero transmittance within the section g_2, and no transmittance between sections g_1 and g_2. The reason for this difference is the partial ordering of the sections $g_1 < g_2$. However, these rules only work because we have cut the sections on the white sites. Going through the different cases, we find that the requirement for shorting or leaving open the unused input sites depends on the sublattice of the site and the position of the section in the partial ordering relative to the input site connected to the VNA. These requirements are summarised in Table I. When these rules are satisfied, there is non-zero transmittance between the input and output sites when they are on the same section, but not when they are on different sections. This pattern is a direct consequence of the triangular blocks in the transfer matrix, and does not occur otherwise. For example, in a structure without sections but with two cuts on white sites, shorting one of the input sites results in no transmittance for either output site.

Input site	Higher	Lower	Equal
Black	Short	Open	Open/Short
White	Open	Short	Open/Short

TABLE I. Conditions for shorting or leaving open circuit the inputs to the sections where the input site is not connected to the VNA. The requirements depend on the sublattice which the input belongs to, black or white, and its position in the partial ordering, higher or lower than the connected section. With these choices, non-zero transmittance occurs only when the output site is in the same section as the input.

Having established these rules, we use transmittance measurements to verify the presence of the sections in the looped four row zigzag graphene ribbon shown in Fig. 4 (which has been used as an example elsewhere in this paper). Recall that this structure has four sections, corresponding to the four rows of sites. Where the subscript of each row is sequentially labelled, the partial ordering of the sections is $g_1 > g_2 > g_3 > g_4$. A cut is made in each row, so the looped structure is transformed into a sheet, shown in Fig. 7 (a), creating an extra site on each row. Note, however, that the sections we find correspond to the uncut loop rather than the sheet. In two of the sections, the cut is on a white site, while in the other two the site is black. We perform transmittance measurements going through the four output sites, and measuring a spectrum for every input sites in each case. The rules in Table I determine whether the unconnected input sites are left open circuit or shorted. For example, when the VNA is connected to the input site on the second row, the first row, which is higher in the ordering and has a white input site, is left open, while the third and fourth rows are, respectively, shorted and open circuit. Using the transfer matrix for the clean structure, where all the cables have impedance $Z_0 = 50\Omega$, this input gives

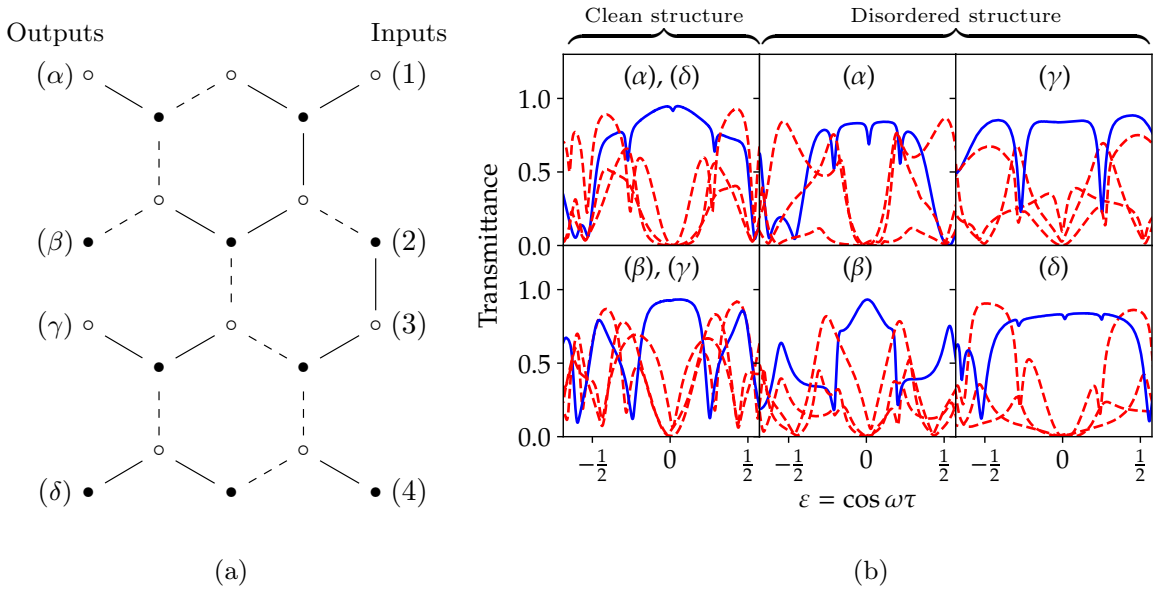

(a) (b)

FIG. 7. (a) The looped four row zigzag ribbon structure cut so it forms a flat sheet. The looped structure is predicted to consist of four sections, corresponding to the four rows of sites. Input sites for the transmittance measurements are labelled on the right hand side, and outputs on the left hand side. For the disordered structure, dashed lines indicate 93Ω RG62 cables, while solid lines indicate 50Ω RG58 cables. The clean structure had only 50Ω RG58 cables. (b) Experimental transmittance data. Each subplot corresponds to a different output site according to the labels in (a), with spectra shown for all four inputs in each case. The blue spectrum is for the case where the input and output site are on the same section, with the dashed red spectra corresponding to transmittance between sections. The transmittance at zero energy is expected to be zero if the input and output sites are in different sections, but non-zero when they are in the same section. The experiment thus confirms that each row is a separate section.

$$\begin{pmatrix} V^{g_1}_{\text{out}} \\ \boldsymbol{I^{g_2}_{\text{out}}} \\ V^{g_3}_{\text{out}} \\ I^{g_4}_{\text{out}} \\ I^{g_1}_{\text{out}} \\ \boldsymbol{V^{g_2}_{\text{out}}} \\ I^{g_3}_{\text{out}} \\ V^{g_4}_{\text{out}} \end{pmatrix} = \begin{pmatrix} 1 & Z_0 i & -1 & -Z_0 i & & & & \\ 0 & 1 & \frac{1}{Z_0} i & -1 & & & & \\ 0 & 0 & 1 & Z_0 i & & & & \\ 0 & 0 & 0 & 1 & & & & \\ & & & & 1 & 0 & 0 & 0 \\ & & & & Z_0 i & 1 & 0 & 0 \\ & & & & -1 & \frac{1}{Z_0} i & 1 & 0 \\ & & & & -Z_0 i & -1 & Z_0 i & 1 \end{pmatrix} \begin{pmatrix} V^{g_1} \\ \boldsymbol{I^{g_2}_{\text{in}}} \\ 0 \\ 0 \\ 0 \\ \boldsymbol{V^{g_2}_{\text{in}}} \\ I^{g_3} \\ V^{g_4} \end{pmatrix} = \begin{pmatrix} V^{g_1} + Z_0 i I^{g_2}_{\text{in}} \\ \boldsymbol{I^{g_2}_{\text{in}}} \\ 0 \\ 0 \\ 0 \\ \boldsymbol{V^{g_2}_{\text{in}}} \\ I^{g_3} + \frac{1}{Z_0} i V^{g_2}_{\text{in}} \\ V^{g_4} + Z_0 i I^{g_3} - V^{g_2}_{\text{in}} \end{pmatrix}. \tag{9}$$

For the disordered structure, the blocks of the matrix are still triangular, but the expression for the elements are more complicated. The numerical value for this matrix if given in the supplementary material section C.

If the other port of the VNA is not attached to the output site on the second row, it is left open circuit, that is $I^{g_2}_{\text{out}} = 0$. However, this forces $I^{g_2}_{\text{in}}$ also to be zero, so no current enters the structure, and no transmittance occurs. However, for the output on the same row, $I^{g_2}_{\text{out}} = I^{g_2}_{\text{in}}$ and $V^{g_2}_{\text{out}} = V^{g_2}_{\text{in}}$, so, in the absence of absorption, there is a perfect transmittance of 1.

The transmittance experiment was carried out twice, first using a 'clean' structure with all 50Ω (RG58) cables, and then for a disordered structure where hopping terms were randomly selected from a binary distribution of 50Ω (RG58) and 93Ω (RG62) cables, identical to the one in Sec. III 1. The clean structure has reflection symmetry about a line between the second and third rows, so we need only need to use two outputs, α and β (labelled in Fig.7 (a)), but in each case we measure transmittance for all four input sites. In the disordered structure this symmetry is broken, requiring measurements for every input and output site in order to complete the experiment.

The measured transmittance spectra are shown in Fig. 7 (b). Each panel shows data for a particular output site, with the four spectra corresponding to the different input sites. As predicted, in both the clean and disordered structures, the transmittance at $\varepsilon = \cos\omega\tau = 0$ is non-zero only when the output site is on the same section as the input (blue curves). This confirms that the structure has 4 sections, experimentally verifying the $4\mathbb{Z}_2$ classification of this structure. The actual value of the

zero-energy transmittance between the sites within the section is determined by how close the section is to being topologically marginal. For a marginal section, the ideal transmittance, in the absence of losses, would be expected to have a value of unity [26]. Although the differences are not great, it can be seen that the transmittance is highest in the clean structure, where all the sections are marginal, and for the second row section of the disordered structure (output (b)), which is also marginal.

As the structure has chiral symmetry, we expect a symmetry in the transmittance spectra around zero energy. The slight asymmetry in the data is mainly a result of losses in the cables, which have more effect at higher frequencies, but there is also some chiral symmetry breaking due to imperfections in the structure. These necessarily occur because the mapping of the coaxial cable structure to the tight binding model requires the sections of cable between the sites to be of uniform impedance. However, the SMA connectors which form the junctions between the cables are 50Ω components, so for the connections with 93Ω cables this uniformity is necessarily unachievable. As a result, the symmetry breaking is generally greater for the disordered structure than the clean one, where minor variations in the cable lengths are the likely cause.

IV. CONCLUSION

We have described an approach to determining exact topological phases in finite chiral structures, identifying the phase boundaries by the appearance of degenerate pairs of zero energy states. This has been shown, in many cases, to lead to a rich topological classification, obtained by finding a division into sections which correspond to irreducible factors of the determinant of the Hamiltonian. The topological classification is then $N\mathbb{Z}_2$, where N is the number of topologically non-trivial sections or factors. The sections can be identified using the complete matchings of the underlying structure, relating the topological classification to the structures underlying connectivity. Each complete matching is related to a term in the expansion of the determinant, so a hopping term which does not appear in any matching can be omitted without changing the determinant. The sections correspond to parts of the structure which become separated when these connections are removed. We also give, in section B of the supplementary material, a simple computational algorithm for finding the sections of a structure.

We have defined a partial ordering of the sections in a structure which gives rise to an unusual localisation of the zero energy states which are present when one of the sections is topologically marginal. The zero energy states can be separated so they each have support on a single sublattice. With our definition, the white state is confined to the marginal section and those which are higher in the ordering, while the black state appears on the marginal section and lower sections. This localisation can be seen as a property of finite structures which has some equivalence to the bulk boundary correspondence in infinite structures.

This localisation provides a way in which the sections, and corresponding topological classification can be demonstrated experimentally. We have performed such experiments on simple coaxial cable networks which map directly onto chiral tight binding models. When we make one section marginal, we can use impedance measurements to map out the local density of states on each site. This provides a direct demonstration of the predicted localisation related to the partial ordering. Even without a marginal section, we can use transmittance measurements to show that the structure separates into the expected sections. We have used this method to confirm the $4\mathbb{Z}_2$ classification which our theory predicts for a four row ribbon graphene structure.

ACKNOWLEDGEMENTS

We are enormously grateful for help in the experimental work from Qingqing Duan, Ben Kinvig, and Elena Callus, and also to Belle Darling and Phillip Graham for huge help in finding space to run the experiments. Many thanks also to Patrick Fowler, Barry Pickup, Qingqing Duan, Ben Kinvig, and Elena Callus for many illuminating and insightful discussions while completing this work.

[1] B.-H. Chen and D.-W. Chiou, An elementary rigorous proof of bulk-boundary correspondence in the generalized Su-Schrieffer-Heeger model, Physics Letters A **384**, 126168 (2020).

[2] D. J. Thouless, M. Kohmoto, M. P. Nightingale, and M. den Nijs, Quantized Hall Conductance in a Two-Dimensional Periodic Potential, Phys. Rev. Lett. **49**, 405 (1982).

[3] F. D. M. Haldane, Model for a Quantum Hall Effect without Landau Levels: Condensed-Matter Realization of the "Parity Anomaly", Phys. Rev. Lett. **61**, 2015 (1988).

[4] M. Büttiker, Absence of backscattering in the quantum Hall effect in multiprobe conductors, Phys. Rev. B **38**, 9375 (1988).

[5] Z. Wang, Y. Chong, Y. Chong, J. D. Joannopoulos, and M. Soljačić, Observation of unidirectional backscattering-immune topological electromagnetic states, Nature **461**, 772 (2009).

[6] E. Prodan, Bulk and Boundary Invariants for Complex Topological Insulators: From K-Theory to Physics (Springer International Publishing, 2016).

[7] B. Simon, Holonomy, the Quantum Adiabatic Theorem, and Berry's Phase, Phys. Rev. Lett. **51**, 2167 (1983).

[8] A. Kitaev, Periodic table for topological insulators and superconductors, AIP Conference Proceedings **1134**, 22 (2009), https://pubs.aip.org/aip/acp/article-pdf/1134/1/22/11584243/22_1_online.pdf.

[9] A. Altland and M. R. Zirnbauer, Nonstandard symmetry classes in mesoscopic normal-superconducting hybrid structures, Phys. Rev. B **55**, 1142 (1997).

[10] J. Cano, B. Bradlyn, Z. Wang, L. Elcoro, M. G. Vergniory, C. Felser, M. I. Aroyo, and B. A. Bernevig, Building blocks of topological quantum chemistry: Elementary band representations, Phys. Rev. B **97**, 035139 (2018).

[11] B. Bradlyn, L. Elcoro, J. Cano, M. G. Vergniory, Z. Wang, C. Felser, M. I. Aroyo, and B. A. Bernevig, Topological quantum chemistry, Nature **547**, 298 (2017).

[12] C. Brouder, G. Panati, M. Calandra, C. Mourougane, and N. Marzari, Exponential Localization of Wannier Functions in Insulators, Phys. Rev. Lett. **98**, 046402 (2007).

[13] M. G. Vergniory, L. Elcoro, C. Felser, N. Regnault, B. A. Bernevig, and Z. Wang, A complete catalogue of high-quality topological materials, Nature **566**, 480 (2019).

[14] E. Prodan, Disordered topological insulators: a non-commutative geometry perspective, Journal of Physics A: Mathematical and Theoretical **44**, 113001 (2011).

[15] E. Prodan, Non-commutative Brillouin Torus, in *A Computational Non-commutative Geometry Program for Disordered Topological Insulators* (Springer International Publishing, Cham, 2017) pp. 25–48.

[16] I. Mondragon-Shem, T. L. Hughes, J. Song, and E. Prodan, Topological Criticality in the Chiral-Symmetric AIII Class at Strong Disorder, Phys. Rev. Lett. **113**, 046802 (2014).

[17] T. A. Loring, K-theory and pseudospectra for topological insulators, Annals of Physics **356**, 383 (2015).

[18] A. Cerjan and T. A. Loring, Local invariants identify topology in metals and gapless systems, Phys. Rev. B **106**, 064109 (2022).

[19] R. Bianco and R. Resta, Mapping topological order in coordinate space, Phys. Rev. B **84**, 241106 (2011).

[20] U. Gebert, B. Irsigler, and W. Hofstetter, Local Chern marker of smoothly confined Hofstadter fermions, Phys. Rev. A **101**, 063606 (2020).

[21] A. M. Cook and A. E. B. Nielsen, Finite-size topology, Phys. Rev. B **108**, 045144 (2023).

[22] R. Flores-Calderon, R. Moessner, and A. M. Cook, Time-reversal invariant finite-size topology, Phys. Rev. B **108**, 125410 (2023).

[23] N. Marzari, A. A. Mostofi, J. R. Yates, I. Souza, and D. Vanderbilt, Maximally localized Wannier functions: Theory and applications, Rev. Mod. Phys. **84**, 1419 (2012).

[24] N. Marzari and D. Vanderbilt, Maximally localized generalized Wannier functions for composite energy bands, Phys. Rev. B **56**, 12847 (1997).

[25] H. Zhang and A. Kamenev, Anatomy of topological anderson transitions, Phys. Rev. B **108**, 224201 (2023).

[26] D. M. Whittaker, M. M. McCarthy, and Q. Duan, Observation of a Topological Phase Transition in Random Coaxial Cable Structures with Chiral Symmetry (2023), arXiv:2311.11040 [cond-mat.dis-nn].

[27] S.-J. Choi and B. Trauzettel, Stacking-induced symmetry-protected topological phase transitions, Phys. Rev. B **107**, 245409 (2023).

[28] A. García-Fuente, D. Carrascal, G. Ross, and J. Ferrer, Full analytical solution of finite-length armchair/zigzag nanoribbons, Phys. Rev. B **107**, 115403 (2023).

[29] R. K. Malakar and A. K. Ghosh, Engineering topological phases of any winding and Chern numbers in extended Su–Schrieffer–Heeger models, J. Phys.: Condens. Matter **35**, 335401 (2023).

[30] D. M. Whittaker and R. Ellis, Topological Protection in Disordered Photonic Multilayers and Transmission Lines (2021), arXiv:2102.03641 [physics.optics].

[31] T. Jiang, M. Xiao, W. Chen, L. Yang, Y. Fang, W. Y. Tam, and C. T. Chan, Experimental demonstration of angular momentum-dependent topological transport using a transmission line network, Nat Commun **10**, 10.1038/s41467-018-08281-9 (2019).

[32] C. Oliver, D. Nabari, H. M. Price, L. Ricci, and I. Carusotto, Photonic lattices of coaxial cables: flat bands and artificial magnetic fields (2023), arXiv:2310.18325 [physics.optics].

[33] F. Harary, The Determinant of the Adjacency Matrix of a Graph, SIAM Review **4**, 202 (1962).

[34] H. Sachs, Beziehungen zwischen den in einem Graphen enthaltenen Kreisen und seinem charakteristischen Polynom., Publ. Math. Debrecen **11**, 119 (1964).

[35] I. S. Duff and B. Uçar, On the Block Triangular Form of Symmetric Matrices, SIAM Review **52, no. 3**, 455–470 (2010).

Supplementary Materials: A Topological Classification of Finite Chiral Structures using Complete Matchings

A. FACTORISATION THEOREM

In this section we prove a theorem relating the triangular block form of Q to the factorisation of $|Q|$. Consider a real or complex matrix Q, where Q is a chiral block of a Hamiltonian

$$H = \begin{pmatrix} 0 & Q \\ Q^\dagger & 0 \end{pmatrix}. \tag{S1}$$

Below we show that, for algebraically independent hopping terms, then $|Q|$ is reducible if and only if there exists a way of ordering the sites such that Q is upper block triangular. We refer to the resultant form of Q as the maximal triangular block basis, or triangular block basis of Q, but it should be emphasised that this basis specifically corresponds to a permutation of H. We will use this in section B to define an algorithm that classifies a particular structure.

Note that often in the following arguments we will refer to a property that occurs *almost always*. By this we mean that if hopping terms were selected randomly from a continuous distribution (possibly one that satisfies a certain constraint) then this property occurs with probability 1.

We proceed by showing that the factorisation is well defined, before proving that a square weighted matrix has a factored determinant (for all matrix entries) if and only if it is block triangular. In proving this relationship we will show that when a section is singular, for almost all hopping terms a section has non-zero support of an eigenstate on all sites.

In order to interpret determinants of a matrix as a polynomial, we consider a polynomial ring that contains them. Formally this ring is larger then the set of polynomials corresponding to determinants, but this is unimportant for our discussion. In particular we are interested in determinants of matrices, so we consider an $N \times N$ matrix,

$$Q_{i,j} = X_{i,j} \tag{S2}$$

where $X_{i,j}$ is an indeterminate over some field, or else fixed at 0, and all non-zero $X_{i,j}$ are algebraically independent. Generically we take this to be $\mathbb{R}$ or $\mathbb{C}$, but more arbitrary fields are perfectly reasonable to consider. We then take the polynomial ring $P[X_{i,j}]$ over the indeterminates $X_{i,j}$. The determinants $|Q|$ are polynomials in this ring which are linear for each hopping term in $|Q|$. To consider the matrices that may only represent tight binding models undergoing continuous evolution, then we need to restrict the domain for each indeterminate to be $\mathbb{R}^{\pm}$ or $\mathbb{C} \setminus \{0\}$ or else fixed at 0. Non-zero indeterminates are then in a semiring.

Formally when we classify a structure we are interested in the subspace E_0 of ξ which has no (exactly) zero energy states. We then wish to calculate the number of ways we can map a Hamiltonian to this subspace, which corresponds to calculating the zeroth homotopy group of E_0 under the usual topology. The zeroth homotopy group of a space counts the number of disconnected components of that space. The irreducible factorisation of $|Q|$ tells us the number of path connected components in E_0.

Definition A.1. Let X be the subspace of ξ corresponding to a solution to $|Q| = 0$. Then $E_0 := \xi \setminus X$.

In order for our classification to be well defined, we need there to exist a factorisation of $|Q|$ that is irreducible and unique, that is we need the polynomial ring to be prime. This follows directly from the fact that the indeterminates are taken over a field. In other words P is a unique factorisation domain. For a less abstract argument, consider the following:

Proposition A.2. If for some hopping terms $|Q| \neq 0$ then $|Q|$ has a unique irreducible factorisation in P.

Proof. Suppose $|Q| = \prod a_i$ and $|Q| = \prod b_i$ such that a_i, b_i are irreducible. Assume that for the irreducible factor a_j there is no irreducible factor b_k such that $a_j = mb_k$ for some non zero constant m, then

$$\prod_{i \neq j} a_i \neq \frac{\prod_{i \neq k} b_i}{m}. \tag{S3}$$

multiplying by $a_j = mb_k$ we see

$$a_j \prod_{i \neq j} a_i \neq b_k \prod_{i \neq k} b_i \tag{S4}$$

which is a contradiction. Hence for every j there is a k such that $a_j = mb_k$ for some constant m, showing a factorisation of $|Q|$ is unique and irreducible. □

Given that the irreducible factorisation of $|Q|$ is well defined, we now give a proof that $|Q| = \prod |q_i|$ if and only if there exists a block triangular structure of Q with q_i as diagonal blocks.

A.1.

Here we aim to prove that a determinant of Q is factored if and only if there exists a block triangular basis of Q. A corollary of one of the propositions is that a critical section almost always has non-zero support of the nullstates on every site. To prove this we first show that two sections, pairwise, may only connect on one sublattice. Then we show that for a structure with N sections there must always be at least one section that may only connect to any other section on one sublattice. As this is true for any number of sections N this implies that if $|Q|$ is factored, then there exists a triangular block structure of Q.

More specifically, given a section g_i, if every first minor of q_i is almost always non-zero then deleting a black and a white site from g_i will result in a structure with a complete matching, because the determinant of the remaining structure is almost always non-zero. Therefore if we have two sections, g_i and g_j and they connect to one another on both sub lattices, then we can delete a black and a white site from both sections (each) that are connected to one another. The remaining structure has a complete matching because the associated minor is factored by a first minor of q_i and a first minor of q_j. Consequently g_i and g_j can connect to one another on only one sublattice.

Our proof relies on knowing when hopping terms are in a complete matching of some graph or not. For this we need to define a type of matching.

Definition A.3. A **valid matching** is a matching between two sites on some graph g such that the matching is part of a complete matching of g.

We then show that there cannot exist a particular type of cycle of sections (see Definition A.8). This ensures at least one section can only connect to other sections from one sublattice. This is true for an arbitrary number of sections, giving the triangular structure to Q.

For consistency if two sections g_i and g_j connect from a black site in g_i to a white site in g_j we say g_i connects to g_j on the black sub lattice.

Proposition A.4. Given a section g_i with tight binding model $h_i = \begin{bmatrix} 0 & q_i \\ q_i^\dagger & 0 \end{bmatrix}$ such that $|q_i|$ is irreducible, then every first minor of q_i is almost always nonzero.

Proof. Given that h_i is chiral, a non-zero term in $|q_i|$ corresponds to a complete matching of g_i. Any first order minor of q_i can be accessed by deleting a white and a black site from g_i, with the first order minors corresponding to determinants of the $(N-1) \times (N-1)$ sub matrices of q_i. So if there exists a complete matching of every structure where we delete a black and a white site from g_i then for almost all hopping terms the minor is non-zero.

Suppose that we have a section with the set of complete matchings $\mathscr{C} = \{C_i\}$ and delete a black site b_1. Match all the remaining sites possible from the complete matching C_i, leaving a single unmatched white site w_1. If an individual site is in only one valid matching, as every complete matching must include a matching on every site, this would factorise the determinant. So every site is in at least two distinct valid matchings contained in the set of complete matchings $\mathscr{C}$. So w_1 may be matched to a black site b_2 with a matching in C_j. Removing the original matching containing b_2 which is in the complete matching C_i leaves a second white site w_2 unmatched. This process has changed which site is the unmatched white site, see Fig. S1 for an example. Iterating this step defines a walk over the structure. If we delete the unmatched white site, we automatically get a complete matching of the remaining structure, showing the associated minor is almost always non-zero.

We now demonstrate any white site in a section may be unmatched by such a walk. Assume there are a set $\mathscr{W}_m$ of white sites that cannot be unmatched by iterating this walk, and a set $\bar{\mathscr{W}}_u$ of white sites that can be unmatched by iterating this walk. In C_i all $\mathscr{W}_m$ white sites are matched to a black site. If there exists a valid matching from a black site b_1 to a white site in $\mathscr{W}_m$ and a valid matching from b_1 to a white site in $\bar{\mathscr{W}}_u$, then the site in $\mathscr{W}_m$ is unmatchable. So the black neighbours of $\mathscr{W}_m$ sites do not have a valid matching to any white site in $\bar{\mathscr{W}}_u$. If a white site has a valid matching to b_1 it is possible to unmatch, so no white site $w_m \in \mathscr{W}_m$ has a valid matching to b_1. This partitions the sites of G in to two sets: one with white sites that can be unmatched U, and one with white sites that cannot be unmatched M, with valid matchings. The valid matchings over M are therefore independent of the valid matchings over U, giving a factorisation of $|q_i|$. By contradiction all white sites in a section are possible to unmatch via such a walk. As the choice of b_1 was arbitrary, this proves the existence of a complete matching of a section when deleting one white and one black site, that is, every first minor of $|q_i|$ is non-zero. □

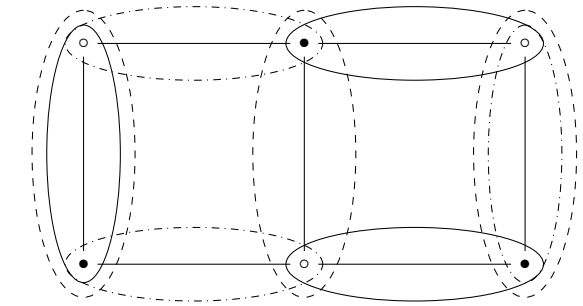

(a)

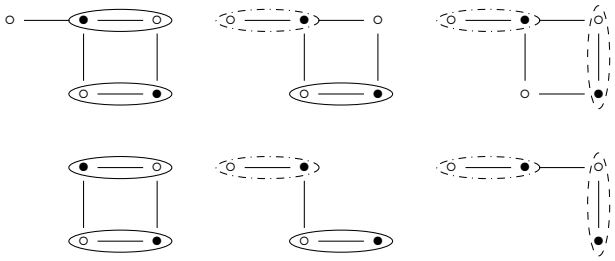

(b)

FIG. S1. (a) 3 rung ladder graphene, which has the classification $\mathbb{Z}_2$, and all 3 complete matchings of the structure denoted with a solid line, dashed line, and dash dot line. (b) Displays the structure having deleted one of the black vertices, and matching all but one white vertex. By swapping a single matching that neighbours the unmatched vertex at a time, it is possible to leave any of the white sites unmatched. Deleting the unmatched white vertex shows that for the deleted black vertex, deleting any of the white vertices leaves a structure with a complete matching.

Corollary A.5. Suppose a section is singular, then $q_i |\psi\rangle = 0$ for some non-zero $|\psi\rangle$, and for almost all hopping terms $|\psi_j\rangle$ indexed over the j sites of g_i is non-zero for every j.

Proof. By Prop. A.4 every first minor of q_i is almost always non-zero. Therefore any submatrix $\bar{q}_i$ resulting from deleting a white and black site of g_i is almost always non-singular. Projecting the eigenstate $q_i |\psi\rangle = 0$ on to the submatrix gives

$$\bar{q}_i \left|\bar{\psi}\right\rangle \neq 0 \tag{S5}$$

for all $\bar{q}_i$. Therefore given any submatrix of $\begin{bmatrix}\bar{q}_i & \alpha\end{bmatrix}$ of q_i such that

$$\begin{aligned} q_i &= \begin{bmatrix} \bar{q}_i & \alpha \\ A & \end{bmatrix} \\ \text{and} \quad |\psi\rangle &= \begin{bmatrix} \left|\bar{\psi}\right\rangle \\ |\psi_\alpha\rangle \end{bmatrix} \quad \text{for} \quad q_i |\psi\rangle = 0 \end{aligned} \tag{S6}$$

we see

$$\bar{q}_i \left|\bar{\psi}\right\rangle = -\alpha |\psi_\alpha\rangle . \tag{S7}$$

As every first minor is non-zero then for almost all hopping term values $|\psi\rangle$ has non-zero support on every site of g_i. □

We now wish to show that, given a pair of sections g_i, g_j then they may only connect on one sublattice.

Proposition A.6. Given two section g_i, g_j then non-zero hopping terms may only be between black sites on g_i to white sites on g_j.

Proof. Given two sections g_i, g_j assume they connect to one another on both sublattices. Delete four sites, a black and a white site in g_i and a white and a black site in g_j that connect to the original white and black site g_i. By Prop. A.4 the resulting structure has a complete matching. Therefore if we put back in the four deleted sites, and match them via their associated hopping terms, then there exists a complete matching of g_i and g_j that is not factored by $|q_i|$ and $|q_j|$. So by contradiction g_i and g_j connect on only one sublattice. □

To show that given N sections there exists a section which can only connect to any other section from one sub lattice, we first define an edge section.

Definition A.7. An **edge section** is a section that may only connect to all other sections from one sub lattice.

To prove there always exists an edge section we consider a cycle of sections.

Definition A.8. A **section cycle** is a path through a subset of sections in G such that it starts and ends on the same section following hopping terms in g_i and leaves each section on a different sub lattice to the one it entered on.

We now show there cannot exist a section cycle.

Proposition A.9. A section cycle cannot exist in any structure.

Proof. Suppose every section is in a cycle, then every section connects to a distinct section on both sub lattices. For each distinct section cycle we can delete a pair of sites, one black and one white, from each section in the cycle such that the black and white sites connect to different sections in the cycle. By Prop. A.4 the resulting structure has a complete matching. Putting back in the deleted sites and hopping terms, we can now construct a complete matching that is not factored by any of the sections in that cycle. Therefore by contradiction there exist no section cycles. □

Corollary A.10. In a structure with N sections there exists at least one edge section.

Proof. Suppose every section g_i connects to at least one other section g_j on the white sub lattice and one different section g_k on the black sub lattice. Given such a requirement, then if no edge section exists there must be at least $N + 1$ sections. Therefore by the pigeonhole principle, if every section connects on both sub lattices a section cycle exists, which is not possible by Prop. A.8 giving a contradiction. □

We now wish to show that the existence of an edge section gives the triangular basis to Q.

Theorem A.11. *If $|Q| = \prod |q_i|$ for $|Q|, |q_i| \in P[X_{i,j}]$ then there exists a permutation of H that gives a triangular block basis for Q.*

Proof. Given a structure with N sections then by corollary A.10 there is at least one section, g_1, which only connects to all others from one sub lattice. Taking G and deleting g_1 yields a new structure, $\bar{G}$, with $N - 1$ sections. By corollary A.10 this structure also has an edge section g_2. This may be iterated until only one section remains. This gives the partial ordering of the structure and therefore defines a triangular block basis of Q. □

B. A CLASSIFICATION ALGORITHM

We present an algorithm to find the classification of a structure based on Theorem A.11. That is, we take some input structure, with a chiral Hamiltonian and find an ordering of the sites where Q is block triangular, and every diagonal block corresponds to a section of the structure. We refer to the corresponding basis as the **maximal triangular block basis** of Q. Then, given the domain of each hopping term and numerical bounds on the determinant, we check if a section is trivial or not. We anticipate that this algorithm can be significantly optimised, but currently we are able to analyse up to random networks with around 50 sites. Of course, given a more consistent underlying lattice structure it often makes sense to classify a large (say many thousand sites or more) system by proving some simple results about the complete matchings of that lattice, coupled with some boundary conditions.

There are two main parts of the algorithm: to find a triangular block basis of Q with all sections on the diagonal, and then to classify each section. The former is more technically challenging. The first part uses the fact that to get a triangular block structure to and $N \times N$ size Q there needs to be a $j \times (N - j)$ block of zeros, so by taking the complement of Q (with all unit hopping terms) then we can find overlaps in zeros by taking dot products between column vectors, or a generalised product over several column vectors. The generalised product is defined as follows.

Definition B.1. The generalised product of N column vectors $\{c^i\}$ is given by

$$p = \sum_j \prod_i c^i_j \tag{S8}$$

where j denotes the jth entry of the column vector c^i.

Given $N-j$ columns, if $p \geq j$ then there is a $j \times (N-j)$ block of zeros in Q. The algorithm then follows the following general outline

1. Compute Q° where $Q^\circ_{i,j} = 1$ if $Q_{i,j} = 0$, otherwise $Q^\circ_{i,j} = 0$
2. Check for $1 \times (N-1)$ blocks of zeros by checking $\sum_i Q^\circ_{i,j}$ for every j. Take indices of all blocks of this size.
3. Find pairwise overlap matrix, A, of two column vectors of $Q^\circ_{i,j} = 1$,

$$A_{i,j} = \sum_k Q^\circ_{k,i} Q^\circ_{k,j} \tag{S9}$$

4. If any $A_{i,j} \geq N-2$ there is a $2 \times (N-2)$ block of zeros. Take indices of all blocks of this size.
5. For $j \geq 2$ take all columns that have overlap greater than $N-j$. If number of columns with such an overlap $\geq N-j$ set Check $= 1$.

   If Check==1:

   For all combinations of $N-j$ columns with pairwise overlap $\geq N-j$ compute p.

   If $p \geq N-j$ return indices of $j \times (N-j)$ block of zeros.

A simple way to optimise this algorithm slightly is to project on to a sub matrix of Q that excludes any individual section, whenever a relevant $j \times (N-j)$ block of zeros is found. Then the combinations of column vectors that need to be checked to find more blocks of zeros is significantly smaller. Furthermore the complexity of the search scales with the number of potential column vectors to check. So if the search for zero blocks can be done up until $j \leq \frac{N}{2}$ for the column vectors, and then switched to do a search over the remaining row vectors the algorithm may be faster.

The second part of the algorithm is much simpler, and only applies when hopping terms are restricted to being real. By the fundamental theorem of algebra if all hopping terms are complex then a solution to $|q_i| = 0$ always exists for at least a 2×2 size block q_i corresponding to a section. For hopping terms restricted to $\mathbb{R}^\pm$ we require some more computation. The first part of the algorithm computes the number of sections of Q, and by indexing blocks of zeros finds a maximal triangular block basis for Q. So we now need to see if each factor can be set to 0. This works by considering bounds for the largest value of $|q_i|$ for all $|u| \in (0.5, 1]$ hopping terms, where the sign of u set by the domain of that individual hopping term (i.e. if $u \in \mathbb{R}^+$ then $u > 0.5$ and if $u \in \mathbb{R}^-$ then $u < -0.5$). All hopping terms are then selected as a random float in $\pm(0.5, 1]$, and it is checked if this gives a singular section, if not we proceed, otherwise we reselect randomly reselect hopping terms. Suppose all hopping terms in q_i are non-zero, then by Prop. A.4 every hopping term appears in the expansion of $|q_i|$. The maximum number of non-zero terms in the determinant of an $N \times N$ matrix is $N!$ and so $|q_i| \leq N!$. Therefore if a particular hopping term, a, is left free to vary then $|q_i| = aA + B$. If solutions to $|q_i| = 0$ exist for some a then for $|a| \times (0.5)^{N-1} > (N-1)!$ and $|q_i|$ has one sign, and for $a = 0$ then $|q_i| = B$ and has a different sign. This is then repeated for every hopping term until a solution is shown to exist, or it is shown to not exist for all sections. That is

1. Randomly select all hopping terms u so that $|u| \in (0.5, 1]$ and the sign corresponds to the domain of that hopping term. If $|q_i| \neq 0$ proceed, otherwise randomly reselect all hopping terms until $|q_i| \neq 0$.
2. Keeping the hopping terms as in the first step set $a = \pm 2^N (N-1)!$ where the sign is specific to the domain of a. Calculate Sign($|q_i|$).
3. Keeping the hopping terms as in the first step set $a = 0$ where the sign is specific to the domain of a. Calculate Sign($|q_i|$).
4. If a change of sign is found:

   Return section non-trivial

5. Else:

   If all hopping terms checked:

   Return section trivial

   Else:

   Set a to its value from step 1 and repeat from step 2 for a different hopping term b

This part of the algorithm can be optimised by finding a set of sites connected on a loop within the section that is itself non-trivial, then only one hopping term would need to be varied (one from this ring) for q_i to be non-trivial.

C. EXPERIMENTAL DETAILS

Experimental data were collected with a NanoVNA V2 Plus 4 and NanoVNA V2 Plus 4 pro. Two measurements were considered: two port measurements for transmittance and a single port measurement for reflectance. To operate the VNA, the software NanoVNA-Saver was used. In making a structure, cables were taken from a binary distribution of 50Ω RG58 SMA cables, and 93Ω RG62 SMA cables. SMA connecters are generically available at only 50Ω impedances and so for the clean structure all cables were chosen to be 50Ω. The exact cables used in the disordered structures are displayed in Fig. S2.

Data were collected between $1 - 240$MHz with $\approx 114MHz$ being the frequency at which $\varepsilon = \cos\omega\tau = 0$.

For transmittance data, the four input states described in Table I were measured in both the clean and disordered structure, and transmittance data taken in separate experiments on each of the four output sites.

Input site	Input 1	Input 2	Input 3	Input 4
g_1	(I, V)	Open	Open	Open
g_2	Open	(I, V)	Short	Short
g_3	Short	Short	(I, V)	Open
g_4	Open	Open	Open	(I, V)

TABLE I. The input states for the classification experiments in the graphene CCN. An entry of (I, V) denotes that this is the site where the input port of the VNA is attached to the CCN.

At zero energy, the transfer matrix for the disordered 4 row ribbon graphene is given by the following

$$\begin{pmatrix} \frac{50}{93} & 100i & -\frac{143}{93} & -\frac{2500}{804357}i & & & & \\ 0 & 1 & \frac{143}{2500}i & -\frac{8649}{2500} & & & & \\ 0 & 0 & \frac{93}{50} & \frac{557450}{8649}i & & & & \\ 0 & 0 & 0 & \frac{50}{93} & & & & \\ & & & & \frac{93}{50} & 0 & 0 & 0 \\ & & & & \frac{557450}{8649}i & \frac{50}{93} & 0 & 0 \\ & & & & -\frac{1161857}{804357} & \frac{143}{8649}i & 1 & 0 \\ & & & & -\frac{125000}{8649}i & -\frac{50}{93} & 186i & \frac{93}{50} \end{pmatrix} \tag{S10}$$

where numerical values are a consequence of the 50 Ω and 93 Ω coaxial cables. By applying the four input states of Table I to equation (S10) shows the transmittance is only non-zero for sites in the same section.

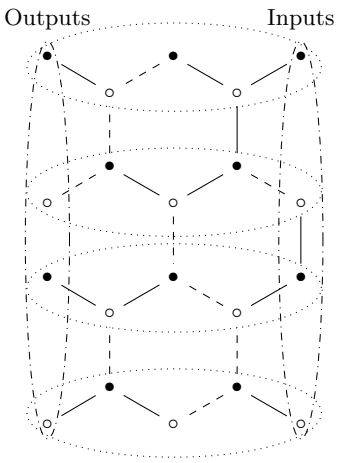

FIG. S2. The disordered structure the transmittance experiment was performed on, as discussed in section III 2 of the paper, with sites in each section already cut for measurements. The dashed lines denote the 93Ω RG62 cables, and the solid lines denote 50Ω RG58 cables. The same structure with all 50Ω RG58 cables is the clean structure used for the transmittance experiments. The dash-doted ellipses denote the input and output sites. The same structure with uncut sites was used for the localisation experiment in section III 1 of the paper. This structure has 4 sections and a $4\mathbb{Z}_2$ classification.

5.6 An aside on nut graphs

Recall from chapter 2.1.5.1 that in the graph theory literature a core graph of nullity 1 is known as a nut graph [66, 67]. That is

Definition 5.6.1. A nut graph is an unweighted graph γ with nullity 1 such that a nullstate has support on every site of γ.

We can use the result of section 5.3.1.1 to provide an algebraic definition of a weighted nut graph. In order to do this we need to give an algebraic interpretation of our classification. We do this by considering a polynomial ring that contains $|Q|$. Take an $N \times N$ matrix

$$A = a_{ij} \tag{5.6.19}$$

where a_{ij} is an indeterminate in the field $\mathbb{F}$. Then $P[a_{ij}]$ is the polynomial ring over the indeterminates $a_{i,j}$ for all $N \times N$ sized matrices. For every possible G the polynomial $|Q| \in P$.

Remark. Note that the unique irreducible factorisation of the determinant also follows from the fact that P is a ring over a field, and therefore all irreducible polynomials in P are unique. That is P is a prime ring.

As we will see below, we can then define weighted nut graphs as being associated to prime polynomials of P.

In general, a critical section g_i is almost always a weighted 2-core graph. However, a large number of sections also satisfy the following symmetry (up to a graph automorphism)

$$q_i = q_i^\dagger. \tag{5.6.20}$$

In such instances we can interpret q_i as the weighted adjacency matrix of its own graph. This leads to a natural definition of a weighted nut graph.

Definition 5.6.2. A weighted nut graph with adjacency matrix γ_w is a graph such that when edge weights satisfy $|\gamma_w| = 0$ then γ_w is almost always a 1-core graph.

Furthermore, from our discussion in section 5.3.1.1 and from the definition of a section then every weighted nut graph γ_w has an irreducible determinant $|\gamma_w|$. From the definition of the ring P we can associate every section to a prime polynomial in this ring. Formally this means we can consider weighted nut graphs as being, in some sense, prime.

Definition 5.6.3. A weighted nut graph with adjacency matrix γ_w is a graph such that if $|\gamma| \neq 0$ then $|\gamma|$ is a prime polynomial in P.

Finally, we note two properties of a weighted nut graph. The first is that, by the factorisation theorem, adding any edges to a weighted nut graph does not stop it being a weighted nut graph. This means we can define a minimal weighed nut.

Definition 5.6.4. A minimal weighted nut graph is a weighted nut graph such that the graph remaining upon the removal of any edge is no longer a weighted nut graph.

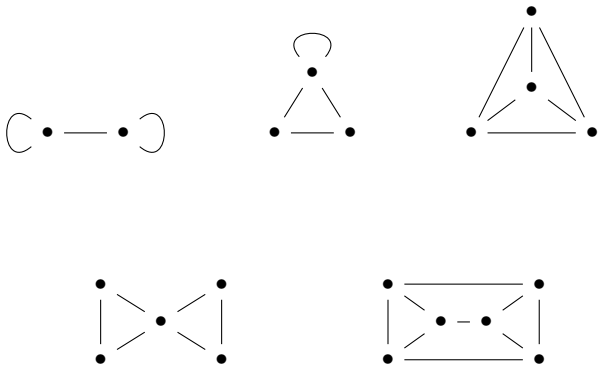

Figure 5.6.1: A selection of small weighted nut graphs.

It is unknown currently if a minimal weighted nut is unique (up to a graph isomorphism), however I currently believe it is likely not. Secondly from the factorisation theorem for every number of vertices there exist sections, and so there are an infinite number of weighted nut graphs. We give a selection of some small weighted nuts in Fig. 5.6.1. We go into some more details of unweighted nut graphs in Chapter 6.

5.7 A classification experiment

As discussed in [90] and in sections 5.3.1 a structures classification is directly related to the existence of an upper triangle basis of a Hamiltonian H on a graph G. That is the classification follows from finding a way to order the sites of G that give a block upper triangular basis to H. As discussed in section 5.3 this gives a connection between the connectivity of G and its topological classification.

The connection between a graphs connectivity and its topological classification may be observed in the localisation of null states of the Hamiltonian, as discussed in [90]. Furthermore, this gives a connection between the form of the transfer matrix, and the topological classification of a structure. This is discussed in the context of an experiment to verify the classification of ribbon graphene in [90], but here we give a general proof that a triangular transfer matrix is a consequence of the topological classification of a particular structure.

In order to prepare a structure for the classification experiment, the structure is cut once on each section, on a hopping term connecting a site to that section, as illustrated in a Fig. 5 of [90]. The cut site now becomes two sites, one may be labelled an input site, and the other an output site, one of each for every section.

Definition 5.7.1. Let i label the section, so that $(V_i^{\text{in}}, I_i^{\text{in}})$ is the voltage and current on an input site of the ith section, and $(V_i^{\text{out}}, I_i^{\text{out}})$ is the voltage and current on an output site of the same section. For an input (output) site, let an input (output) current or voltage be called an input (output) variable.

Definition 5.7.2. A transfer matrix $M(\varepsilon)$ maps the voltages and currents of the input

sites to those of the output sites, at energy $\varepsilon = \cos\omega\tau$. That is

$$M(\varepsilon)\begin{pmatrix} \vdots \\ V_i^{\text{in}} \\ I_i^{\text{in}} \\ \vdots \end{pmatrix} = \begin{pmatrix} \vdots \\ V_i^{\text{out}} \\ I_i^{\text{out}} \\ \vdots \end{pmatrix}. \tag{5.7.22}$$

For brevity, we denote the transfer matrix at zero energy with $M = M(\varepsilon = 0)$.

To demonstrate that there exists a permutation of M that is upper triangular, we use the connectivity of G to show that for each output site, one output variable may be written as a linear combination of the input variables of that section and above sections, and the other output variable may be written as a linear combination of the input variables of that section and below sections. This defines a permutation of M that is upper triangular.

We first notice that due to chiral symmetry, the voltage on one sublattice does not affect the voltage on the other. As we discuss in [90] this demonstrates that for a white (black) input site i the input current I_i^{in} affects voltage on the black (white) sub lattice only, and the input voltage V_i^{in} affects voltage on the white (black) sub lattice only. We also recall that at zero energy, the transfer matrix for an individual coaxial cable is given by

$$\begin{pmatrix} 0 & \frac{i}{Z} \\ iZ & 0 \end{pmatrix}. \tag{5.7.23}$$

Proposition 5.7.3. The current output I_i^{out} on a white site on section g_i depends only on the voltages of the black sites of g_i and above sections.

Proof. By Kirchhoff's rules, the voltage on a site must be equal in every cable terminating on the site, so we can write

$$V = iI_jZ_j \tag{5.7.24}$$

for every nearest neighbour j. This means we can always write the voltage on a black (white) site in terms of the current output of a neighbouring white (black) site within the same section. So it is only through the current on sites in which an output variable picks up dependence on the input variables of different sections.

Furthermore, by Kirchhoff's rules, the current on a single site must sum to zero. So we can write the current output as

$$I_i^{\text{out}} = \sum_j i\frac{V_j}{Z_j} \tag{5.7.25}$$

where we sum over all nearest neighbours j. For a white site the current output depends on the voltage of all neighbouring black sites. By the partial ordering, all neighbouring black sites are either in g_i or above sections. Therefore, we can write I_i^{out} as a linear combination of the input current on g_i and the voltage of black sites of above sections.

In turn, the voltage on a section $g_k > g_i$ depends only on one input variable of g_k and the voltage of black sites of sections above g_k. So we may write the current output on a white site I_i^{out} as a linear combination of the current input I_i^{in} of g_i and one input variable of each above section. □

Corollary 5.7.4. The output voltage V_i^{out} on a white site is given by a linear combination of the input voltage on g_i and one input variable of each below section.

Proof. Due to chiral symmetry V_i^{out} depends on the current outputs of white sites. By the partial ordering white sites may only connect to the same section and below sections. □

To show that this leads to a triangular basis for M, we now demonstrate that for any section $g_j < g_i$ the output variable of g_j that depends on the input variable of g_i depends on the same input variable. Furthermore, we also show that for any section $g_k > g_i$ the output variable of g_k that depends on the input variable of g_i depends on the other input variable of g_i.

Proposition 5.7.5. For all sections $g_j < g_i$ the output variable of g_j that depends on an input variable of g_i all depend on the same input variable of g_i.

Proof. By proposition 5.7.3 the only output variable of section g_j below g_i that depends on an input variable of g_i depends on the voltages of the black sites of g_i. Therefore, the only input variable of g_i that affects an output variable of g_j is the input current I_i^{in} of the white input site of g_i. □

Corollary 5.7.6. For all sections $g_k > g_i$ the output variable of g_j that depends on the input variables of g_k depend on the same input variable of g_i.

Proof. By symmetry, the only input variable of g_i that affects an output variable of g_k is the voltage on white sites of g_i which, by the partial ordering, only affect the current output of black sites of g_k and voltage output of white sites on g_k. □

So we now know that the output variables must depend on the same set of input variables from above sections, and from below sections. Along with the fact that on each output site, one output variable depends on input variables of the same section and above sections, and the second output variable depends on the other input variable of the same section and below sections this defines a permutation of M that is triangular.

Remark. Because the triangular basis of M follows from the connectivity of G, the permutation of sections that gives the triangular basis of M is given by the partial ordering of the sections. More precisely M has two diagonal triangular blocks, one block follows exactly the partial ordering of Q, and the second block follows the reverse partial ordering of Q.

5.7.1 A note on complex Hamiltonians

Recall from the discussion in section 2.2.2.1 that topological phase transitions can be observed in the transfer matrix. When M has a pair of eigenvalues given by 1 (which come as pairs due to the chiral symmetry) then the transfer matrix defines two zero energy states which satisfy the boundary conditions of the uncut Hamiltonian. When cut once on each section the triangular structure of M ensures that for a real Hamiltonian its eigenvalues are real, so taking any eigenvalue of M from greater than one to less than one corresponds to a topological phase transition.

This notion can be extended to complex Hamiltonians, and gives a way to connect our classification to the infinite case. Suppose the Hamiltonian has complex hopping terms. This means that topological phase boundaries are not well defined, as the determinant $|H| = 0$ now imposes two constraints on an individual hopping term u, given by

$$u = a + bi \tag{5.7.26}$$

for some $a, b \in \mathbb{R}$. This is discussed a little further in section 7.4.1. However, we can use the transfer matrix to make an observation about the topology of periodic structures.

Suppose u is a hopping term associated to the section $g \in G$, and we cut g on one site and repeat it periodically, then when $|u| = |a + bi|$ an eigenvalue of the transfer matrix is given by $e^{i\theta}$, so for some θ there is a zero energy state of the Hamiltonian. This ensures there is a closed gap somewhere in the Brillouin zone, defining a topological phase boundary.

Furthermore, this is independent of the number of sections that are cut and made infinitely periodic. It is possible to associate each side of such a topological phase boundary to a winding number, although this winding number changes depending on how unit cells are defined for each period.

5.8 Conclusions and limitations

We have proposed a rigorous method for the topological classification of finite chiral structures. By relating topological properties of a Hamiltonian to the polynomial associated to a determinant we have given a classification that allows for arbitrary hopping disorder. Using irreducible factors of the determinant, we have demonstrated all non-singular finite chiral structures have 2^N topological phases associated to an $N\mathbb{Z}_2$ topological classification.

We have shown a connection between the irreducible factors of the determinant, and subgraphs we call sections g of the structure G. By considering properties of sections, we have given a definition for weighted nut graphs and shown a deep connection between weighted nut graphs and the topological classification of a particular structure.

The localisation properties of a Hamiltonian on a topological phase boundary are associated with the partial ordering of sections. This gives experimentally observable properties to a finite chiral Hamiltonian undergoing a topological phase transition. We have demonstrated that for coaxial cable networks this gives a transfer matrix with an upper triangular form. Using a kind of transfer matrix tomography (as discussed more in [90]) we can probe this form giving an experimentally viable method to confirm the topological classification of a particular structure.

As we have not made any assumptions about the underlying connectivity of the structure our methods could perhaps give a rigorous way to see how finite structural defects may affect the classification of a much larger structure. We believe this may be done by separating the defect and studying the topology of the structure and the defect separately.

The topological classification we have discussed here is limited to chiral symmetry in a non-interacting system. It is possible to use some of the methods described in this chapter to classify an interacting system, however as the size of the Hilbert space grows so

rapidly when allowing interactions, this becomes computationally non-viable for all but the smallest of systems. Beyond this we have not considered how interactions may affect our classification.

Experimentally we have given a general approach to verify a structures classification, however this may not be so simple to implement in atomic structures especially for structures that do not have exact chiral symmetry. How exactly the validity of our classification is altered when allowing disorder that breaks chiral symmetry, is a question entirely unexplored by our work. I suspect if the breaking of chiral symmetry is adiabatic, then our classification remains valid, however this may alter the localisation of null states at topological criticality. Such chiral breaking disorder would be interesting to study.

The connection between our notion of topology in finite systems is also not enormously easy to relate to the classification of infinitely periodic systems. For instance, if allowing each section to become infinitely periodic, both phases can have a non-trivial Berry phase, or a trivial Berry phase depending on which sites are chosen to be in a unit cell. Furthermore, because the connectivity of G allows for each section to be infinitely extended independently, it is not clear how to interpret the number of dimensions in an infinite $N\mathbb{Z}_2$ structure. This makes it difficult to see how our classification relates the 10 fold way. We discuss a little on infinitely periodic structures later in section 7.4.1.

We have also presented an algorithm to classify an arbitrary graph, G. Our algorithm uses permutations of the columns of submatrices of the Hamiltonian. Without further optimisation, this limits our classification of structures with arbitrary connectivity to those with around 50 sites or less. I am reasonably confident further optimisation will improve this limit, but for now this is a considerable constraint. Although for structures with a highly consistent connectivity, it is possible to prove a structure has a particular classification (for instance finite graphene ribbons with different boundary conditions), but this is not an easily generalisable approach.

Chapter 6

Nut graphs: an experimental realisation in coaxial cable networks

As discussed in section 2.1.5.1 a nut graph is an unweighted graph with one null vector such that every vertex of the graph has support of the null vector. They were first described by Irene Sciriha [66, 67] in 1998. Nut graphs have all real edge weights, so their nullstates are real. We display a selection of nut graphs — the Sciriha graphs — each on 7 vertices, and the smallest chemical nut graph in Fig. 6.0.1.

In chemical graph theory nut graphs have been of particular importance [68], due to the fact there is only one nullstate and it is delocalised [69, 70]. This delocalisation leads to significant consequences in the ballistic transport properties of a chemical graph representing a tight binding system, resulting in the phenomena of omni-conduction [71] at zero energy. At zero energy the ballistic transport is related to the transmission properties of coaxial cable networks, so predictions of omni-conduction can be explored experimentally with this platform.

An omni-conductor is a chemical graph, such that attaching two microscopic leads to sites, will result in non-zero ballistic transport between the two leads. If, when connecting the leads to the same site, conduction is non-zero for every site the structure is an ipso omni-conductor, and if connecting between any pair of distinct sites the conduction is non-zero the graph is said to be a distinct omni-conductor. A graph that is both is a strong omni-conductor [71].

Let A be the adjacency matrix of a graph. It has been shown (Theorem 4.2 of [71]) that a graph of nullity one conducts between two sites i and j if the minor of the entry $A_{i,j}$ is non-zero. In a nut graph, the delocalised nature of the null state is a consequence of the first minors all being non-zero (Theorem 6.1 [66]) so this is exactly the requirement for a strong omni-conductor. Note that this means all weighted nut graphs are strong omni-conductors for almost all edge weights that satisfy the graph being singular (that is $|H| = 0$).

Nut graphs themselves are difficult to make in a molecular setting. Especially nut

graphs whose nullstate is near the Fermi level. In this chapter we present some results that experimentally confirm some properties of nut graphs in a coaxial cable network. In particular we demonstrate support of a single null state on every site of a nut graph for a selection of small nut graphs. Using the two site transmission of a graph we experimentally verify that a particular nut graph is omni-conducting [71]. Finally, we give an experimental demonstration of one of the constructions for chemical nut graphs, in particular the addition of two vertices on a bridge maintains graph being a nut [66, 68].

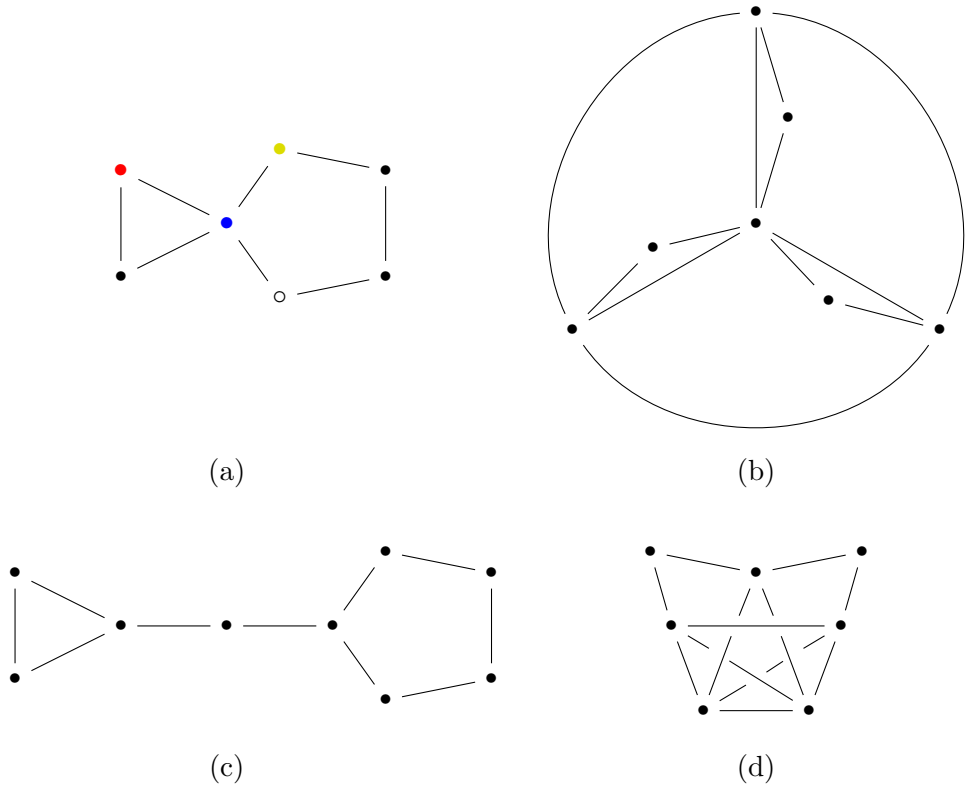

Figure 6.0.1: The Sciriha graphs (a), (b) and (d) — the smallest nut graphs each on 7 vertices. Four of the sites of (a) have been coloured to indicate the input and output sites for some measurements displayed in Fig. 6.1.1 and Fig. 6.1.3. (c) Displays the smallest chemical nut graph.

6.1 Measuring eigenstates

As discussed in section 2.2.2 we can make two main measurements on a coaxial cable network. The first is of the local density of states (LDOS) which is proportional to the real part of the local impedance. Using this measurement, we can go site by site and experimentally verify if a particular coaxial cable network does have support of a null state on every vertex, confirming if it is a nut graph.

The second measurement we make is of the transmission (that is the s_{21} parameter

of the scattering matrix) which (at zero energy) gives the (complex) phase relationship between the support of the nullstate on two sites. We may use this to get the sign of the nullstate on every site, giving us experimental access to the entire nullspace of a coaxial cable network. Throughout the rest of this thesis, we make use of the transmittance, however this loses the phase information of a two site measurement. The use of transmission does leave some experimental problems, however.

The first issue is that VNA has finite size ports. This means that transmission and reflectance measurement are not taken directly on a site. A special measurement cable was made to account for the length of the VNA port, but the slightly off site measurement does result in a small shift in the measured LDOS between sites. Furthermore, to allow sites with a large degree, connectors were made with a combination of T-connectors. This also results in a slight frequency shift in the data. This shift was sufficiently small so that calculating the LDOS and the relative sign of the nullstate around the graph from the data, the shifts were not accounted for. Despite this our data agree well with the theory.

Secondly on the VNA itself the input and output ports are calibrated to have 50Ω losses which sometimes leads to a phase shift in the measured transmission, as displayed in Fig. 6.1.1. This phase shift is a consequence of the non-infinite impedance of the output and input port of the VNA. However, because the nullstates of a nut graph are real, the phase shift is never enough to change the sign of the real part of the transmission.

To see this, recall that (with the application of the Woodbury matrix identity, as discussed in sections 2.2.2 and 3, and also in [76]) when connecting the VNA to two sites a, b the Greens functions between the two sites is given by

$$G_{a,b} = \frac{g_{a,b}}{1 + \Gamma_{\text{in}}\Gamma_{\text{out}}(1-\varepsilon^2)(g_{a,b}g_{b,a} - g_{a,a}g_{b,b}) + i(1-\varepsilon^2)^{\frac{1}{2}}(\Gamma_{\text{in}}g_{a,a} + \Gamma_{\text{out}}g_{b,b})} \tag{6.1.2}$$

where $g_{i,j}$ is the Greens function of the Hamiltonian when not connected to the VNA between two sites i, j, and $\Gamma \sim Z_0^{-1}$ is the scaled loss term of the VNA ports for the port impedance Z_0.

The Greens functions relate the voltage on one site, relative to a reference input voltage. Because the nut graph has real eigenvectors, in the limit of zero energy each term $g_{i,j}$ is real. Furthermore because there is only one null state at zero energy $g_{a,a}g_{b,b} - g_{a,b}g_{b,a} = \frac{V_a}{V_a^{\text{in}}}\frac{V_b}{V_b^{\text{in}}} - \frac{V_a}{V_b^{\text{in}}}\frac{V_b}{V_a^{\text{in}}} = 0$ so we may rewrite the denominator as

$$1 + \alpha i \tag{6.1.3}$$

where $\alpha = (1-\varepsilon^2)^{\frac{1}{2}}(\Gamma_{\text{in}}g_{a,a} + \Gamma_{\text{out}}g_{b,b})$ and is real. This results in a phase shift in $(-\frac{\pi}{2}, \frac{\pi}{2})$ of the transmission. So we can use the real part of the transmission to experimentally verify the relative sign of the nullstate on one site, to that of the nullstate on another.

One further issue with the measurements is that the measured voltages are scaled in order to realise the map between a coaxial cable network and a tight binding model, as discussed in section 2.2.1. Recall that we may interpret such a scaling on the hopping terms of the tight binding model itself, given by

$$H_{\text{CCN}} = p^{-\frac{1}{2}}Ap^{-\frac{1}{2}} \tag{6.1.4}$$

where $p^{-\frac{1}{2}}$ is a non-singular diagonal matrix, and A is the adjacency matrix of the nut graph. Because a nut graph has all unit edge weights, every cable used in a nut graph has the same impedance Z_0. Because $p^{-\frac{1}{2}}$ is a non-singular diagonal matrix support of the nullstate on every site is still maintained in H_{CCN}, but this does mean the eigenstates of H_{CCN} are scaled relative to the eigenstates of A.

Recall from section 2.2.1 the scaling matrix $p^{-\frac{1}{2}}$ is given by

$$p_{i,i}^{-\frac{1}{2}} = \left[\left(\sum_{i>j} Z_{i,j} \right) + \left(\sum_{i>j} Z_{j,i} \right) \right]^{-\frac{1}{2}}. \tag{6.1.5}$$

Because every cable has the same impedance this means

$$p_{i,i}^{-\frac{1}{2}} = (Z_0 d_i)^{-\frac{1}{2}} \tag{6.1.6}$$

where d_i is the degree of the vertex i. This scales the eigenstate on each site i by $(Z_0 d_i)^{-\frac{1}{2}}$.

To measure the nullstates of A this scaling does not need to be accounted for in data analysis, however. Recall from section 2.2.1 that for an eigenstate of H_{CCN} with support $\bar{v}_i$ on site i the measured voltages correspond to $p_{i,i}^{\frac{1}{2}} \bar{v}_i$. This is exactly the scaling between eigenstates of A and H_{CCN}, and so the measured voltages correspond to the eigenstates of the nut graph itself. In all cases our measured data agrees quite well with the eigenstates of A.

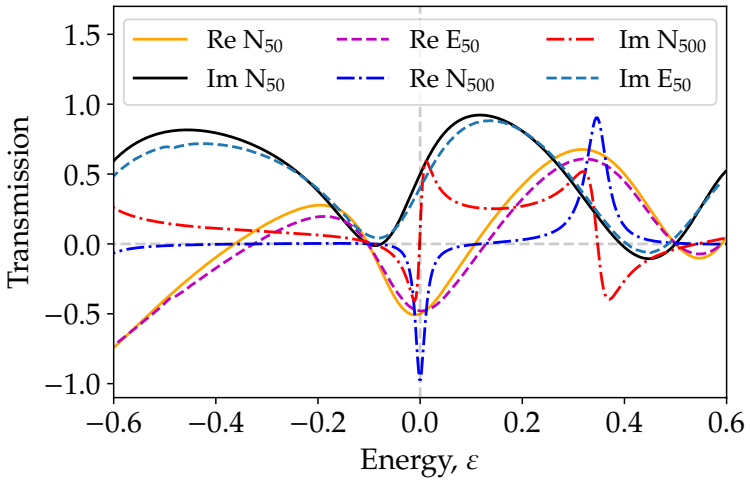

Figure 6.1.1: A plot of transmission measured experimentally (denoted E in the legend) and calculated numerically (denote N in the legend) using the Greens functions between the yellow and white sites of the Sciriha graph in Fig. 6.0.1 (a). The subscript in the legend denotes the impedance of the input and output port, demonstrating that changing loss can give a phase shift to the transmission. The experimental data were included to demonstrate the measured phase shift is a consequence of the losses.

One fascinating property of nut graphs is that they display omni-conductance [71, 108]. In a molecular setting this means that if connecting any two vertices to a microscopic lead,

the ballistic conduction is non-zero. At zero energy the ballistic transport properties of a molecular system and the transmission properties of a coaxial cable network are related to the same transmission coefficients. So a prediction of omni-conduction in a molecular system is also a prediction of omni-conduction in a coaxial cable system.

It has been shown that the requirements for omni-conduction can be related entirely to graph theoretic properties of a structure [71, 108]. In particular for graphs of nullity 1 if the minor associated to the entry of the Hamiltonian $H_{i,j}$ is non-zero then transmission is non-zero between site i and j. Strong omni-conduction occurs when every minor is non-zero, which is exactly the case for nut graphs.

In section 6.1.1 we present results experimentally demonstrating omni-conductance for one of the Sciriha graphs.

As a final experiment we also demonstrate that the addition of two vertices to a bridge of a nut graph constructs a new nut graph. We do this with the smallest chemical nut graph as displayed in Fig. 6.1.2. We can imagine this construction as adding two additional equal impedance cables to it, which (at zero energy) has the transfer matrix of

$$\begin{pmatrix} -1 & 0 \\ 0 & -1 \end{pmatrix}. \tag{6.1.8}$$

Because this is true for any two vertices of the bridge this maintains a single nullstate of the graph with support on every site. However, the sign of the transfer matrix switches the relative sign of the nullstate on one side of the two added vertices, compared to the original graph.

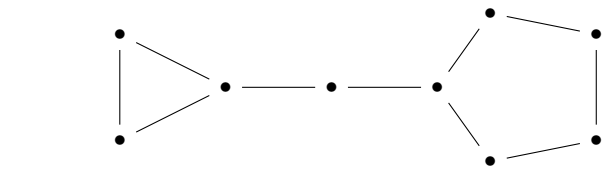

(a)

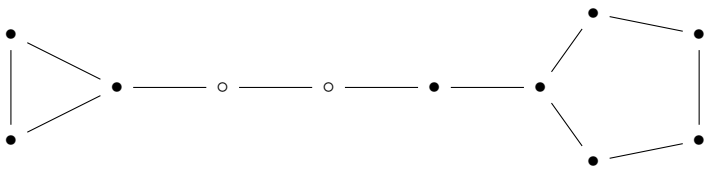

(b)

Figure 6.1.2: (a) The smallest chemical nut graph, and (b) a chemical nut graph constructed with the addition of 2 vertices on the bridge (for example the two vertices in white).

6.1.1 Experimental results

In Fig. 6.1.3 we give an example plot of the transmission and LDOS data for a single site of the nut graph in Fig. 6.0.1 (a). LDOS data were collected for each site in each graph, while transmission data are collected from one site in each graph to every other site. This gives us the relative sign of the eigenvector on each site, allowing us to reconstruct the nullspace experimentally.

In order to compare the experimentally measured nullstate, and that of the original nut graph, we need to find an appropriate normalisation of the graphs nullstate. To do this we scaled the experimentally measured nullstate and normalised by the largest voltage. To normalise the predicted nullstate of the nut graph we multiplied it by some scalar k which minimises the standard deviation. This minimum is found for

$$k = \frac{\sum_i a_i^{\text{graph}} V_i^{\text{exp}}}{\sum_i \left(a_i^{\text{graph}\,2} \right)} \tag{6.1.10}$$

where a_i^{graph} is the nullstate on site i calculated directly from the adjacency matrix of the nut graph, and V_i^{exp} is the experimentally measured support of a nullstate on site i (using the transmission for the sign and the square root of the LDOS for the amplitude). The resultant standard deviation for each structure is indicated in each figure caption.

Normalising the eigenstates of the nut graph, and the measured nullstate so that they each have an inner product of 1 we then calculated the fidelity. In each case the fidelity was above 97% with a maximum of 99.9% demonstrating how precisely we are able to create a tight binding structure with a coaxial cable network. The fidelity for each experiment is indicated in each figure caption.

In Fig. 6.1.4 we present the experimentally measured nullstates for the three Sciriha graphs. The colour of a vertex corresponds to the relative sign of the nullstate, as measured by the real part of the transmission. The diameter of each vertex is proportional to the LDOS on that site, measured as an integral of the experimental LDOS between 104-119 MHz. For each graph the point of zero energy is slightly shifted, due to the addition of multiple T-connectors to create high degree sites, as such this frequency range corresponds to the energy windows of $\varepsilon = -0.12$ to $\varepsilon = 0.09$ for the graphs (b) and (d) of Fig. 6.0.1 and $\varepsilon = -0.04$ to $\varepsilon = 0.17$ for (a) of Fig. 6.0.1. The convention was chosen to integrate the LDOS over the same frequency range instead of over the same energy window, due to a possible ambiguity arising in how to define zero energy when different sites have significantly different degrees, as is the case for the Sciriha graphs. The diameter on each vertex agrees well with the scaling from the adjacency matrix of the underlying nut graph and the Hamiltonian of the coaxial cable network.

In Fig. 6.1.5 we present the same experiment but for the smallest chemical nut, and another chemical nut constructed by the addition of two vertices to the bridge, experimentally corroborating this construction maintains a nut graph. These LDOS measurements were integrated over a 109-119MHz range (to account for the lower average degree in both of these graphs compared to the Sciriha graphs) or equivalently $\varepsilon = -0.04$ to $\varepsilon = 0.09$. Our data agrees well with the scaled voltages, and we experimentally confirm this construction

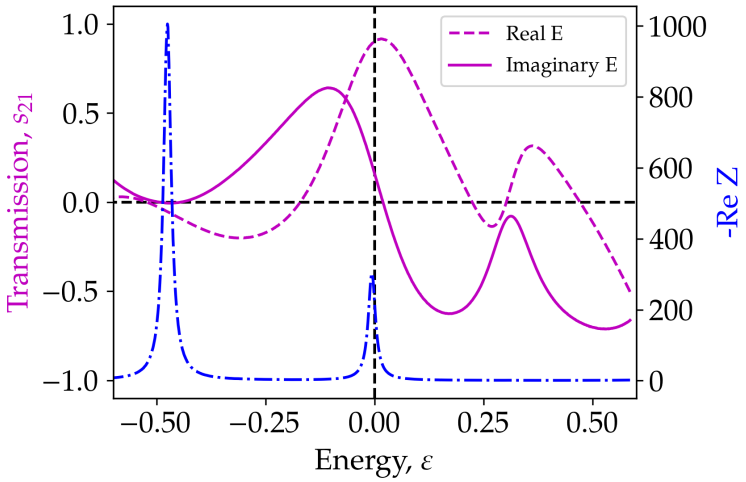

Figure 6.1.3: Experimentally measured transmission (with real and imaginary components represented as the magenta solid and dashed lines respectively) and LDOS (blue dashed dotted line) of the Sciriha graph in Fig. 6.0.1 (a). The transmission data were measured between the blue and yellow site of Fig. 6.0.1 (a) and the LDOS data were measured on the red site.

has produced a new nut graph from the other.

In Fig. 6.1.6 and Fig. 6.1.7 we give the transmittance data for Sciriha graph in Fig. 6.0.1 (b). There are three distinct orbits of vertices in this graph, as indicated by the different colour vertices in Fig. 6.1.6 (a). To verify the graph is an omni-conductor we need only put an input on one vertex of each orbit, reducing the number of required experiments. In Fig. 6.1.6 (b-d) we demonstrate that for each pair of input and output sites the transmittance is non-zero, where transmittance is indicated by the opacity of the output site vertex. We plot the transmittance for every pair of input and output vertices in Fig. 6.1.7. Our data experimentally confirm this nut graph is a distinct omni-conductor. Furthermore, the peaks in the LDOS occur only when the reflectance is near unity, so the fact that the LDOS is non-zero on every site demonstrate nut graphs are ipso-omni-conductors. Our experimental data therefore confirm this graph is a strong omni-conductor.

6.2 Conclusions and limitations

We have detailed an experimental platform for the realisation of nut graphs using coaxial cable networks. Using the fact that the nullstate of a nut graph is real, we have demonstrated a complete experimental measurement of the null space of a selection of nut graphs. Using a combination of transmission and reflectance measurements we have experimentally confirmed 5 coaxial cable networks of graphs — the Sciriha graphs, and two chemical graphs — are nut graphs. Furthermore, we have given the first experimental demonstration of strong omni-conduction in one of the Sciriha nut graphs.

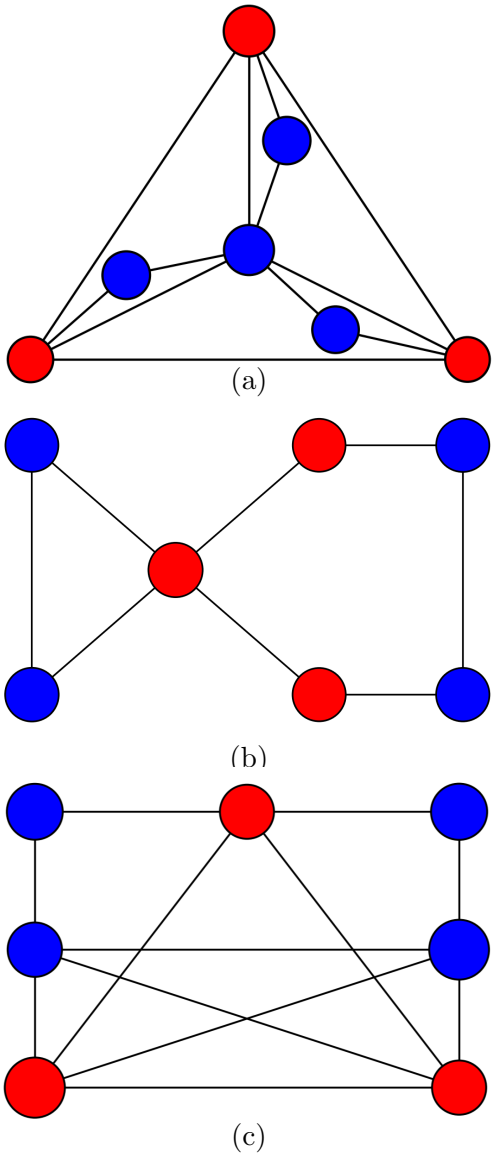

Figure 6.1.4: Support of a nullvector on each site where the diameter is proportional to the square root of the experimentally measured integrated local density of states for each of the nullvectors of the three Sciriha graphs. The relative sign is indicated by the colour of the vertex and found experimentally with the transmission. Normalising the experimentally measured eigenstate by the site with the largest support, the measured eigenstates had a standard deviation of 0.08, 0.03, and 0.08, and each measurement was within $\pm 0.12, \pm 0.03, \pm 0.12$ with a fidelity of 99.3%, 99.9%, and 99.3% of the graph theoretic prediction for (a), (b), and (c) respectively.

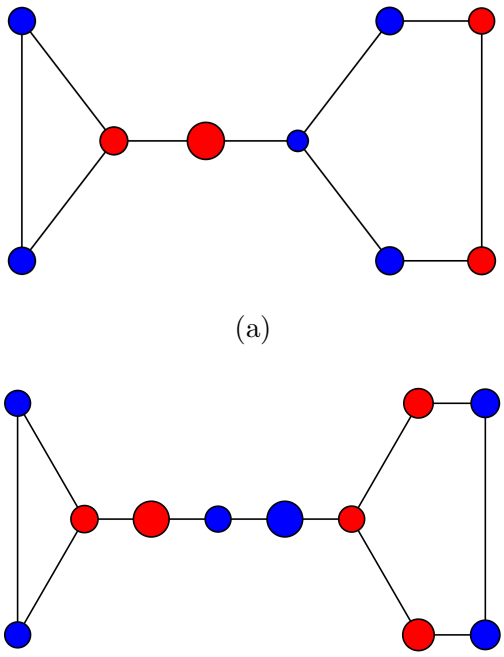

(a)

(b)

Figure 6.1.5: The support of a nullstate on each site, calculated from the square root of the experimentally measured integrated local density of states for (a) the smallest chemical nut graph, and (b) a chemical nut graph constructed with the addition of two vertices on a bridge. The relative sign is indicated by the colour of the vertex, and the diameter is proportional to the support of the nullstate on that vertex. Notice that the sign of the nullstate on the pentagon are opposite on the two nut graphs. Normalising the experimentally measured eigenstate by the site with the largest support, the measured eigenstates had a standard deviation of 0.07 and 0.1 and all measurements were within ± 0.18 and ± 0.22, with a fidelity of 98.6% and 97.9% of (a) and (b) respectively.

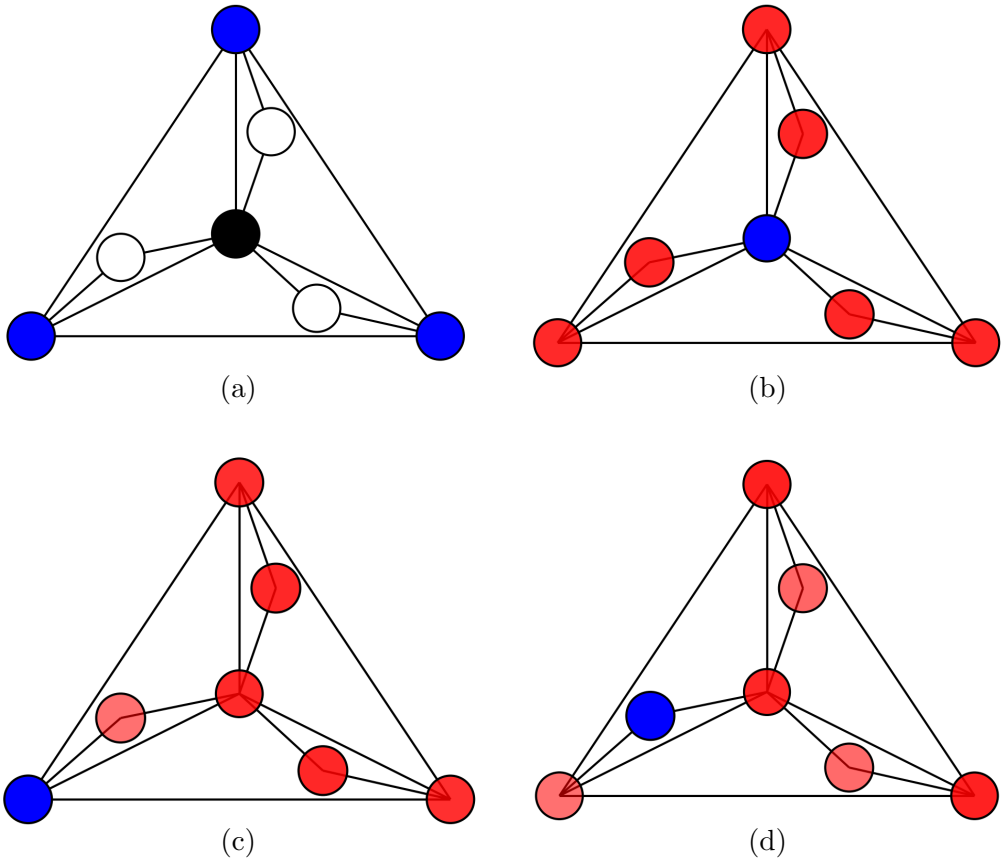

Figure 6.1.6: (a) Displays the three vertex orbits of this nut graph: a black orbit, a white orbit, and a blue orbit. We only need to attach the input to one vertex of each orbit in order to verify omni-conduction. (b-d) Display the transmittance on every site but the input site (denoted in blue). The opacity of the red is proportional to the transmittance measured on that site at zero energy, with complete transparency corresponding to no transmittance.

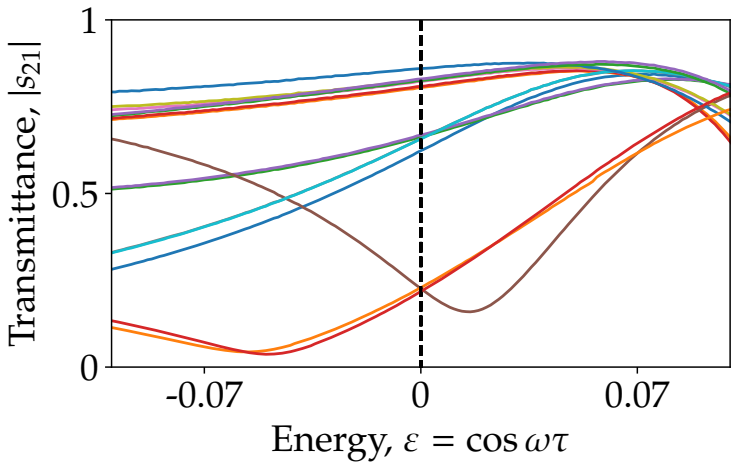

Figure 6.1.7: The transmittance for every pair of input and output sites. Observe that at zero energy the transmittance is non-zero for every pair. These data confirm this graph is a distinct omni-conductor.

As discussed in section 5.6 there is a deep connection between nut graphs and a critical section. This is a consequence of every minor of a biadjacency matrix being almost always non-zero. In fact, core graphs in general are closely related to the finite classification we discuss in this thesis, as we will detail more in chapter 7.

Despite the good agreement of our data with both simulation of the measurements, and graph theoretic prediction of networks behaviour, there are some complications relating to the measurements on a structure. These are a consequence of the fact that on site measurements are not possible with SMA connectors — the connectors themselves have a finite length. We have accounted for this with making a measurement cable (as discussed in section 2.2.2.4) which is slightly shorter to account for the extra length of introduced to the system when connecting the VNA. This does result in a small shift in energy of the LDOS however.

A second issue results from some sites having a large number of neighbours. To allow such a large number of connections T connectors were combined to one another, this resulted in some quite bulky sites that also result in an energy shift in the LDOS data. We anticipate that both this and the issue with measuring slightly off a site can be improved with the design of custom connectors for this purpose.

Chapter 7

Topology in finite chiral structures 3: sequential topology — iterative topological phase transitions

In chapter 5 we studied exact and unavoidable gap closures of 2 zero energy states between non-singular Hamiltonians with different hopping terms. This allowed us to give a well defined notion of finite topologically distinct Hamiltonians at strong disorder. In this chapter, we extend this approach to study unavoidable gap closures with $2n$ exactly zero energy states, separating equivalence classes of Hamiltonians with $2n-2$ zero energy states.

In order to find such topological phase transitions, we put constraints on the hopping terms. For example, if an almost always non-singular chiral structure with the Hamiltonian H satisfies the constraint $|H| = 0$, then the structure has 2 zero energy states. Given the set of all Hamiltonians that satisfy $|H| = 0$, is there a topological phase boundary corresponding to 4 zero energy states? To answer this question, we apply sequences of constraints to the hopping terms of H, and study the topological properties of the surfaces that satisfy this sequence of constraints. We call this sequential topology, and the associated topological classification, a sequential classification. Our application of constraints results in a rich sequence of iterative topological phase transitions.

In sequential topology, we study lower dimensional topological features of a Hamiltonian's parameter space, and so there is a significant analogy with higher order topology. We proceed with a brief discussion of higher order topology.

In first order topological materials, for a topologically non-trivial phase a d dimensional system has robust $d-1$ dimensional boundary states, a direct consequence of the bulk-boundary correspondence. Higher order topology studies $d-n-1$ dimensional boundary states in a d dimensional system [109–112]. To explain such phenomena, theory for a higher order bulk-boundary correspondence has been developed [113, 114] as well as theory for systems with bulk and crystalline symmetries [60, 110, 112, 115, 116]. Due to the difficulty of relating lower dimensional boundary states to the bulk a complete picture of the bulk boundary correspondence for higher order topological insulators has not yet been developed.

The theory of higher order topological materials has made a large number of predictions in the behaviour of topological boundary states. For instance, localisation of corner and hinge states in 2 and 3 dimensional topological insulators, respectively [60, 109–113, 115, 116].

In chiral symmetric systems, N stacked $1d$ topological insulators have been predicted to have non-trivial higher order phases [110]. Theory of such systems demonstrates the presence of a certain number of corner states in each $1d$ topological insulator. As discussed in Chapter 5, in finite structures the network topology of stacking topological insulators have significant impact on the number of topological phases. In section 7.4.1 we demonstrate the classification we discussed in Chapter 5 can be thought of as a finite analogue of the higher order topology of stacked $1d$ topological insulators.

In section 7.6 we will show that the localisation of zero energy states to certain sections is a physical consequence of a structures sequential classification. Much like the number of $d-n-1$ dimensional boundary states is related to higher order bulk invariants in higher order topology, localisation in sequential topology corresponds to the number of zero energy states on each section. Such localisation gives a further analogy between our sequential topology and higher order topology. We then experimentally verify such properties in section 7.7, demonstrating the physical validity of our sequential topological classification.

Recall that ξ is the parameter space of a structure G with a tight binding Hamiltonian H defined on it. The main work of this chapter will be studying unavoidable gap closures with $2n$ exactly zero energy states, separating Hamiltonians with $2n-2$ zero energy states. In further analogy to higher order topology, we demonstrate such gap closures may be predicted with lower dimensional topological features in ξ. In sections 7.2, 7.3 and 7.4 we will demonstrate that this is exactly the same classification problem as in chapter 5 but translated to such lower dimensional subspaces. As such, a considerable part of this chapter is devoted to how we find and translate this problem to these subspaces of ξ.

Remark. Note that sequential topology does not fit cleanly with higher order topology. This is because sequential topology is the simplest to study when considering multiple sections. Depending on how the dimension of a section is interpreted, this means sequential topology may be best interpreted as *increasing* the dimension of relevant zero energy states. However, as such states only exist at topological criticality, in the absence of a bulk it is not clear how best to interpret the dimension of our sequential classification. The interpretation of dimension is even more complex when considering sequential topology for an individual section.

To summarise the differences between higher order topology, and sequential topology for finite chiral structures, we refer to Table 7.0.0.1.

An alternative way of understanding sequential topology of a structure is to flip the question around. Take a Hamiltonian H with $2n$ zero energy states. What is maximum amount of allowable disorder while maintaining $2n$ zero energy states? Here we interpret the maximum amount of disorder to mean the minimum number of hopping terms that need to be constrained or the maximum number of degrees of freedom. From this perspective we are interested in the largest dimensional subspaces X_i of ξ that correspond to $2n$ or

Table 7.0.0.1: A summary of differences between higher order topology, and sequential topology in finite chiral structures

Property	Higher order topology	Sequential topology
Physical states	Number of $d-n$ boundary states	Number of zero energy states at phase boundary
Topological invariants	Lower dimensional features of momentum space	Lower dimensional features of ξ
Localisation	Localisation of robust boundary states	Localisation of zero energy states at phase boundary

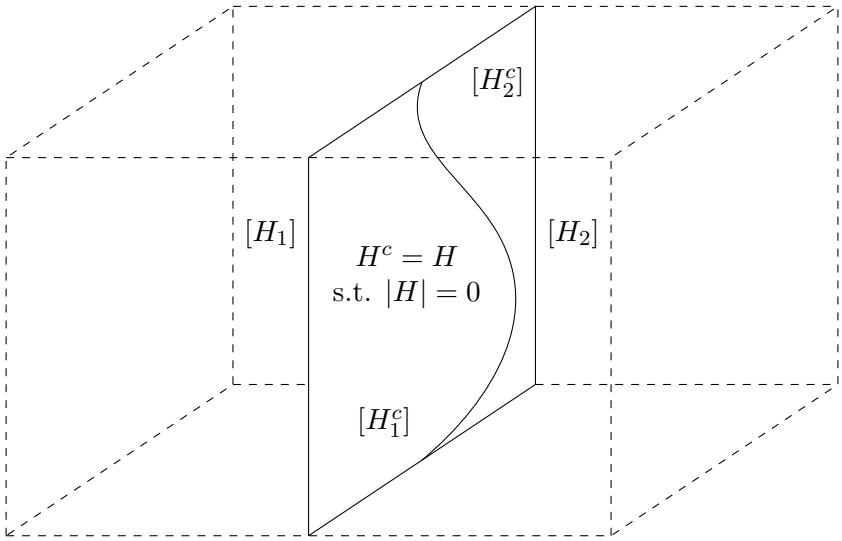

Figure 7.0.1: A slice of the parameter space ξ of a structure where H^c denotes the subspace corresponding to $|H| = 0$. H^c defines a phase boundary separating the two equivalence classes of Hamiltonians $[H_1], [H_2]$. For this structure a subspace corresponding to four zero energy states exists within the subspace H^c and splits H^c in to two topologically distinct regions corresponding to the equivalence classes $[H_1^c], [H_2^c]$.

more zero energy states. To get the subspaces X_i we derive a set of algebraic constraints on hopping terms of H. Relaxing one of these constraints can lead to a subspace X_{i-1} to which X_i defines a topological phase boundary.

Consider the parameter space ξ of a balanced structure (that is, the same number of black and white sites) G without topological protection. The Hamiltonian H on G has phase boundaries given by $|H| = -|Q||Q^\dagger| = 0$. To understand the constraints on H to get a particular number of zero energy states, we can look to the secular equation

$$|H - \lambda I| = \sum_{n=0} a_n \lambda^n \tag{7.0.2}$$

where $a_0 = |H|$. The set of constraints which satisfy $a_1 = a_2 = 0$ while maintaining $|H| = 0$ defines the subspace of ξ with four zero energy states. Each individual constraint

is defined by the solution to a polynomial, so satisfying one more constraint gives a surface one dimension lower than the previous constraints. Therefore, each satisfiable constraint defines a new subspace. We can go further, setting $a_0 = a_1 = a_2 = a_3 = a_4 = 0$ gives six zero energy states. Setting each term $a_n = 0$ gives a set of constraints on the hopping terms of H, which defines a sequence of subspaces in ξ. So the question of sequential topology, is the question of classifying this sequence of subspaces.

Remark. For clarity we call the topological classification of a Hamiltonian satisfying n constraints, the nth step topology. That is, the classification we discuss in chapter 5 is the 0th step or zeroth step topology of a structure.

As will be shown in section 7.2.1, constraints themselves are given by the determinants of sub Hamiltonians h_i of H (which correspond to minors of H). So there is a very natural way to understand the relevant subspaces in ξ as the zeroth step topology of subgraphs of G.

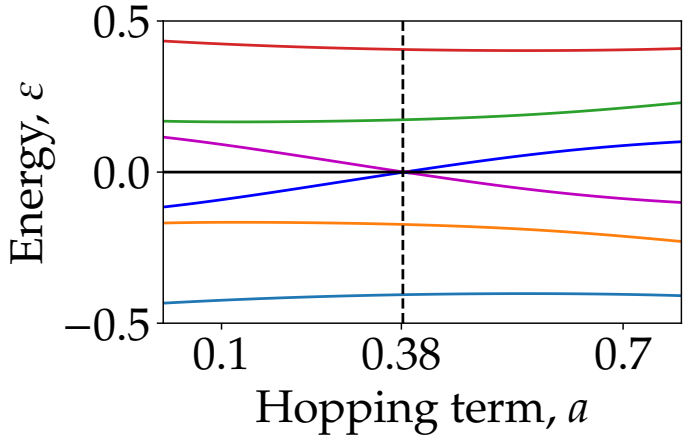

Figure 7.0.2: The energy spectrum of a structure as it undergoes a 1st step (sequential) topological phase transition, going from 2 to 4 to 2 zero energy states.

To give an intuitive understanding of the sequence of subspaces we look at the structure in Fig. 7.0.3. This structure has three sections, and a 0th step classification of $3\mathbb{Z}_2$. For this structure each section is not capable of hosting more than two zero energy states (as we will prove in section 7.5.3). But a higher nullity can be realised by ensuring that zero energy states from distinct sections are mutually orthogonal on each section. We can use this to derive *sequential constraints* on a particular structures' hopping terms. To begin we can set $|q_1| = 0$ which corresponds to the surface $af - be = 0$, and gives two zero energy states.

To get four zero energy states in this structure, there are two further additional constraints. The first is to set another section to be singular. This is because g_1 can only host two zero energy states, so we get the constraint $|q_2| = 0$ or $|q_3| = 0$. For the purposes of this example, we take $|q_2| = 0$. Recall from chapter 5 that nullstates of a section

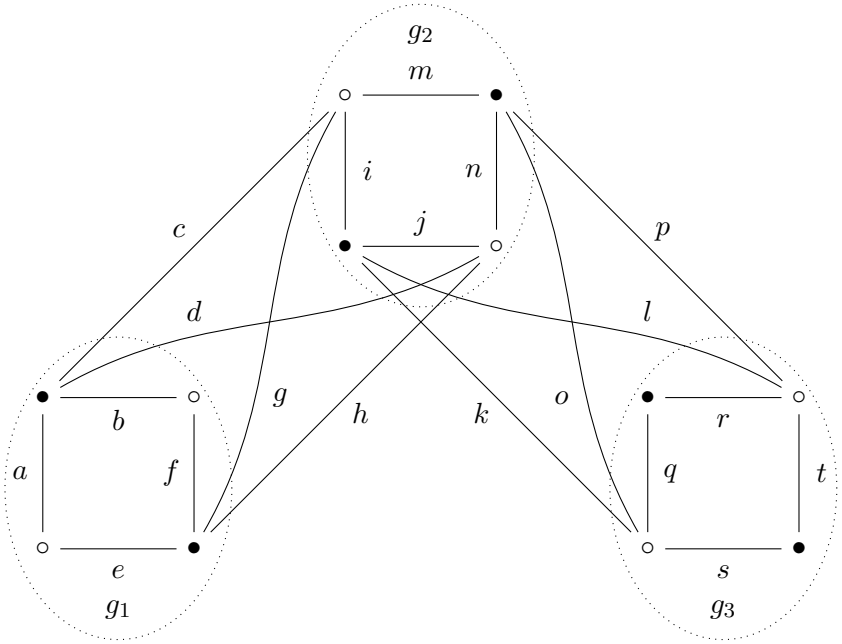

Figure 7.0.3: A structure with a zeroth step topology of $3\mathbb{Z}_2$. This structure has 3 sections g_1, g_2, g_3. Each hopping term is labelled with a variable.

g spread throughout the structure in a very particular way. With two singular sections, $|q_1| = 0, |q_2| = 0$ for all the nullstates of both sections to satisfy the Hamiltonian, all four nullstates must also spread out throughout G. These states need to be well defined on all of G to satisfy H. This requires that the null states are orthogonal on each singular section. For this we get our third constraint

$$dfm - bhm + bgn - cfn = 0 \tag{7.0.5}$$

which gives a structure with four zero energy states. Suppose that $|q_1| = 0$ and one of these constraints is satisfied, while the other is not. The remaining constraint splits the relevant subspace in to two distinct regions separated by a necessary gap closure. That is, the subspace with all but one constraint satisfied has a $\mathbb{Z}_2$ classification. Under a phase transition in this subspace, the spectrum of H undergoes a gap closure illustrated in Fig. 7.0.2.

Finally, we consider the constraints needed to get 6 zero energy states. Like before we cannot use an individual section in this structure for extra zero energy states, so our first constraint is from $|q_3| = 0$. We then need the zero energy states from g_1, g_2 and g_3 to be well defined on each section g_1, g_2, g_3. For this we get two more constraints,

$$\begin{aligned} lns - jps + jot - knt &= 0 \\ df - bh &= 0. \end{aligned} \tag{7.0.6}$$

The first constraint ensures the null states for g_2 are defined on g_3 and for g_3 are defined on g_2. This requires the nullstates to be mutually orthogonal as discussed in section 2.1.4. The

second ensures nullstates from g_1 and g_3 are mutually orthogonal in this sense. Once again, if all but one of these constraints is satisfied, the structure lies on a subspace in ξ with four zero energy states. The final constraint splits this subspace in to two topologically distinct regions, giving the classification $\mathbb{Z}_2$. Similar arguments will be generalised in sections 7.3 and 7.4 to classify the sequential topology of arbitrary finite chiral structures.

Suppose the above 6 constraints are satisfied, then H has 6 zero energy states. In this structure each section can only have a nullity of at most 2 (as we will prove in section 7.3) so with 3 sections for this structure we have reached a maximum number of zero energy states. So we now have the complete sequential topological classification for this structure and the relevant constraints to construct a sequence of subspaces, X_i. We illustrate this sequence in the below diagram.

$$\begin{array}{ccccccccc} (\xi =)\, X_0 & \xrightarrow{af-be=0} & X_1 & \xrightarrow{in-mj=0} & X_2 & \xrightarrow{dfm-bhm+bgn-cfn=0} & X_3 & & \\ & & & & & & \Big\downarrow{\scriptstyle qr-ps=0} & & \\ & & & & & & X_4 & & \\ & & X_6 & \xleftarrow[df-bh=0]{} & X_5 & \xleftarrow[lns-jps+jot-knt=0]{} & & & \end{array}$$

This sequence of subspaces defines a sequence of zeroth homotopy groups which give the sequential classification of this structure

$$3\mathbb{Z}_2 \to 0 \to \mathbb{Z}_2 \to 0 \to 0 \to \mathbb{Z}_2 \to 0. \tag{7.0.7}$$

Each arrow corresponds to a single constraint defining a subspace in ξ. We will show in section 7.3 that this sequence of subspaces corresponds to a minimum number of constraints to get a certain number of zero energy states. For each subspace we will also calculate the topological classification in an analagous way to the zeroth step topology of chapter 5.

In this chapter, we prove that (up to some consideration in the partial ordering of sections discussed in chapter 5, and how nullstates localise in the structure) the sequential topological classification of finite chiral structures is given by a sequence of zeroth homotopy groups

$$N\mathbb{Z}_2 \to 0 \to \mathbb{Z}_2 \to 0 \to 0 \to M\mathbb{Z}_2 \to 0 \to 0 \to 0 \to P\mathbb{Z}_2 \to \cdots \tag{7.0.8}$$

for Hamiltonians with real hopping terms, and where M, P are natural numbers. And

$$0 \to N\mathbb{Z}_2 \to 0 \to 0 \to 0 \to \mathbb{Z}_2 \to 0 \to 0 \to 0 \to 0 \to 0 \to M\mathbb{Z}_2 \to \cdots \tag{7.0.9}$$

for Hamiltonians with complex hopping terms. As in the above example, each arrow is a map that takes a subspace $X_i \mapsto X_{i+1}$ where X_{i+1} is one dimension lower than X_i, that is, each arrow adds one constraint to the hopping terms. In both the complex and real cases N comes directly from the classification discussed in chapter 5.

This chapter is split roughly in to two main components. The first is focussed on the topology of the space ξ itself, and the second details physical consequences of this topology, allowing us to connect our theory to experiments, and test these out in a coaxial cable network.

In section 7.2 we discuss how the subspaces of interest are defined, before describing their topological properties for real Hamiltonians in section 7.3. We then describe an extension to this for complex Hamiltonians, and give a brief discussion of how this relates to infinite structures in section 7.4. The last section that focusses on topological properties of ξ is section 7.5 which deals with the case when sections may have more than two nullstates, and the limit of sequential topology. In section 7.1 we give a higher level overview of the main results of these sections.

In section 7.6 we discuss how a Hamiltonian lying on a sequential phase boundary has unusual properties in the localisation of eigenstates, much like that seen in chapter 5. Using these localisation properties we show how transmittance is altered when a structure is on a higher steps' phase boundary. In section 7.7 we give a case study of a structure fully classified with the methods developed in section 7.3. Furthermore, using the experimental signatures discussed in section 7.6 we experimentally verify the sequence of zeroth homotopy groups of this structure, corroborating the validity of our sequential classification.

7.1 An overview of sequential topology

In this section we give a higher level description of sequential topology in finite chiral structures. The claims we make here are made more rigorous in sections 7.2, 7.3, and 7.4. There are some more physically relevant details discussed in the more rigorous sections, however these are not discussed in sections 7.6 and 7.7 and so are not enormously consequential in understanding the main physical discussion of this chapter. Specifically, these details are discussed in sections 7.4.1 and 7.5. In section 7.4.1 we discuss an extension to sequential topology for infinitely periodic materials and draw some parallels between sequential topology and higher order topology. In section 7.5 we discuss sequential topology in individual sections, however our results for individual sections are only for an approximate sequence of non-trivial subspaces of ξ.

In section 7.2 we also give a different interpretation of the sequential topology of a structure. In this second interpretation we are interested in asking what is the maximum amount of disorder (that is, the minimum number of constraints) a system can have while maintaining $2n$ zero energy states? This can be understood by considering the subspaces of ξ with a certain number of zero energy states, and in section 7.2 we study how such subspaces are related. This interpretation is not explored in this section, but the maps between subspaces with different numbers of zero energy states can be defined with compositions of constraints on a Hamiltonian (which are discussed in this section).

In section 7.1.1 we discuss some the geometric properties of sequential topology, and how this relates to constraints on the Hamiltonian. And in section 7.1.2 we give a description of the most significant proofs we present in later sections.

7.1.1 A triangular number of constraints

In the introduction to this chapter, we described how a Hamiltonian may be constrained to lower dimensional subspaces in ξ. Under certain conditions this subspace may be topo-

logically non-trivial, with distinct regions separated by an unavoidable gap closure in the energy spectrum. In section 7.2 we discuss in detail a geometric understanding of these subspaces. The main idea is that when a Hamiltonian is constrained to have $2n-2$ zero energy states, further constraints may be imposed that give $2n$ zero energy states. Relaxing a single one of these further constraints defines a subspace with $2n-2$ zero energy states, with a topological phase boundary corresponding to a gap closure with $2n$ zero energy states. Such a subspace is topologically non-trivial.

As discussed above, we may use the secular equation to classify subspaces of ξ. For a chiral Hamiltonian the energy spectrum is symmetric about zero energy. We can therefore write $|H-\lambda I| = \lambda^p \prod_i (\lambda^2 - \varepsilon_i^2)$ where p is the number of topologically protected states. Expanding this equation ensures (when no topological protection is present) that only even order terms are non-zero (for more details see proposition 7.2.3). So we can write

$$|H-\lambda I| = \sum a_{2n}\lambda^{2n}. \tag{7.1.10}$$

When $a_{2m} = 0$ for all $m < n-1$ then H has $2n-2$ zero energy states. To find the constraints on H that give $2n$ zero energy states therefore comes from solving $a_{2(n-1)} = 0$.

In general, solving each term ($a_{2n} = 0$) of the secular equation requires more than one constraint on the hopping terms of H. This is because a_{2n} is given by a sum of $2n$th order principal minors of H, as will be shown in proposition 7.2.4. This means we may interpret higher step constraints as relating to the determinants of subgraphs of G. That is, sequential topology directly relates to the zeroth step topology of subgraphs as explored in section 7.2.1.

Satisfying each constraint defines a subspace in ξ, as in definition 7.3.13. We denote by $X_i \subset \xi$ a subspace of ξ which satisfies some set of constraints. To find these subspaces we can use a composition of maps acting on the hopping terms of H. Each map takes a space satisfying some set of constraints, to a space satisfying one more constraint. We call a map that takes one subspace to another $b : X_i \to X_j$ such that X_j satisfies one more constraint than X_i a *constraint map*. So by applying a composition of constraint maps we now have a subspace within ξ that may or may not be topologically interesting.

There are two problems with this approach alone to find if each subspace X_i is topologically non-trivial. The first is how to choose constraint maps. The second is how to tell apart topologically distinct Hamiltonians on a subspace X_i.

The first problem arises because we may be required to solve a reducible polynomial (as each polynomial is defined from the determinant of a subgraph). This means there may be more than one choice for each constraint map. The simplest example of why this is a problem is for a structure G with at least two sections $g \in G$. For a Hamiltonian H on G the constraints to set $|H| = 0$ are given by a reducible polynomial, and so we may choose $|H| = 0$, or any number of the irreducible factors to define a constraint map.

Ambiguity in the choice of constraint map can result in missing a topologically non-trivial subspace of ξ with our sequential classification. The simplest example of this is for a 3 section structure, with two equal sections (by the partial ordering). In this structure there are a minimum of 2 constraints required to be satisfied to get 4 zero energy states, defining an unbounded subspace two dimensions lower than ξ and one dimension lower

than $|H| = 0$. It stands to reason that this splits $|H| = 0$ in to two topologically distinct regions. However, using the unequal section (by the partial ordering) it is possible to find a path between these two regions that does not increase the nullity of the Hamiltonian, thus avoiding the 1st steps' phase boundary. Details of this path are given in proposition 7.3.8. The existence of such paths indicate that the notion of sequential topology is not well motivated. However to follow such a path requires (in places) exact control of 2 hopping terms, so if we assume only 1 hopping term may be exactly controlled, then such paths are almost always avoided. This allows us to recover a notion of topologically distinct 1st step Hamiltonians, which we may achieve with our definition of a constraint map.

To prevent our classification depending on paths such as those previously described, we define constraint maps using irreducible polynomials associated to setting $a_{2n} = 0$ (this approach is detailed much more in section 7.3.2). This allows us to use the dimension of a subspace corresponding to a certain number of zero energy states to study the sequential topology of a structure.

Definition 7.1.1. Let $X_j \subset X_i \subset \xi$ be subspaces of the parameter space where a Hamiltonian constrained to X_i has $2n-2$ zero energy states. A constraint map $b : X_i \to X_j$ is the set of all points in $x \in X_i$ that satisfy an irreducible polynomial $p(x)$ given by a constraint map needed to solve $a_{2(n-1)} = 0$ under the above convention. That is

$$bX_i := X_j = \{x \in X_i | p(x) = 0\} \tag{7.1.11}$$

where $p(x)$ is defined from the set of constraints that are needed to be satisfied to solve $a_{2(n-1)} = 0$.

We now need to find an approach for choosing the order in which we apply constraint maps. This is because for any particular subspace $X_i \subset \xi$ applying the composition of constraint maps define the same subspace, regardless of the order in which we apply the constraint maps. This is because the solutions to an irreducible polynomial define a connected subspace of ξ, and so any composition of the same constraint maps define the same subspace[1].

There is a way to group constraint maps that ensures we can know which subspaces are topologically non-trivial just from the number of constraint maps we have applied to the Hamiltonian. To do this we define a convention for the order we apply constraint maps. The idea is that we choose a non-singular section, and then derive the set of constraint maps that will make this section singular, and increase the nullity of H without increasing the nullity of any other individual section. More details of this convention are given in the discussion around definition 7.2.1 in section 7.2, and it is important for the proofs in sections 7.3.2 and 7.3.3.1.

This now brings rise to the second problem. We are interested in the zeroth homotopy group of the subspace X_i, as this counts the number of equivelance classes of topologically

[1] A consequence of the fact an irreducible polynomial cannot be decomposed as the union of two disconnected algebraic sets, which satisfies the topological definition of connectivity: the surface that corresponds to the solution to an irreducible polynomial cannot be decomposed in to disjoint irreducible open subsets, so is connected.

distinct Hamiltonians in X_i. But, from the definition of constraint maps, each X_i is defined with a set of irreducible constraints and so X_i is connected. To solve this problem, we do not classify the subspace X_i directly, but instead we calculate the zeroth homotopy group of the space $X_i \setminus T$ where we remove any higher steps' topological phase boundaries T. Let this zeroth homotopy group be denoted by $\mathcal{P}(X_i) = \pi(X_i \setminus T)$. This is in direct analogy to the zeroth homotopy groups calculated in Chapter 5 but is now translated to a lower dimensional subspace of ξ. More details of the geometric picture of these subspaces are discussed in section 7.2.

Under the aforementioned convention (with two exceptions) a subspace is topologically non-trivial only when one less than a triangular number of constraint maps are applied to the Hamiltonian. To see this, we consider an example of a Hamiltonian H with zeroth step classification $3\mathbb{Z}_2$ and biadjacency matrix Q. From Chapter 5 we know if H on G has N sections $g \in G$, then there exists a permutation of the ordering of sites on G that gives Q an upper triangular block form. For our $3\mathbb{Z}_2$ example this gives

$$Q = \begin{pmatrix} q_1 & C_{1,2} & C_{1,3} \\ 0 & q_2 & C_{2,3} \\ 0 & 0 & q_3 \end{pmatrix}. \tag{7.1.12}$$

Suppose that $|q_1| = 0$ then there is a nullvector of Q given by

$$\begin{pmatrix} q_1 & C_{1,2} & C_{1,3} \\ 0 & q_2 & C_{2,3} \\ 0 & 0 & q_3 \end{pmatrix} \begin{pmatrix} \psi_1^1 \\ 0 \\ 0 \end{pmatrix}. \tag{7.1.13}$$

where ψ_j^i denotes a null vector on a section q_j which has originated from the section q_i. If $|q_2| = 0$ then $q_2\phi_2^2 = 0$, but as $C_{1,2}$ is a non-zero matrix then if a nullvector of Q has support on q_2 we need to solve the equation

$$\begin{pmatrix} q_1 & C_{1,2} & C_{1,3} \\ 0 & q_2 & C_{2,3} \\ 0 & 0 & q_3 \end{pmatrix} \begin{pmatrix} \phi_1^2 \\ \phi_2^2 \\ 0 \end{pmatrix} = \begin{pmatrix} q_1\phi_1^2 + C_{1,2}\phi_2^2 \\ 0 \\ 0 \end{pmatrix} = 0. \tag{7.1.14}$$

This is solved when $q_1\phi_1^2 = -C_{1,2}\phi_2^2$. If solutions to this equation exist, then we must be able to write $C_{1,2}\phi_2^2$ as a linear combination of the column vectors of q_1, which requires $C_{1,2}\phi_2^2$ to be orthogonal to the column nullspace of q_1.

Remark. When this condition is satisfied, there are two linearly independent null vectors satisfying Q. This gives 4 zero energy states to the Hamiltonian. For a more detailed discussion on this see lemma 7.3.1 and corollary 7.3.2 in section 7.3.1.

We can check when $C_{1,2}\phi_2^2$ is orthogonal to the column nullspace of q_1 by deleting a column of q_1 and replacing it with the vector $C_{1,2}\phi_2^2$. Denote by $q_1^{l\neq k}$ the matrix with a deleted column of q_1^l. Replacing the vector deleted column with $C_{1,2}\phi_2^2$ then gives the matrix

$$\kappa = \begin{pmatrix} q_1^{l\neq k} & C_{1,2}\phi_2^2 \end{pmatrix}. \tag{7.1.15}$$

If $C_{1,2}\phi_2^2$ is a linear combination of the remaining columns of q_1 then the determinant of this resulting matrix is zero. This gives three total constraints to get 4 zero energy states: $|q_1| = 0, |q_2| = 0, |\kappa| = 0$. So we have one constraint for 2 zero energy states, and three for 4 zero energy states.

We can go further and ask about getting 6 zero energy states. A similar process gives 6 total constraints with three from before, $|q_1| = 0, |q_2| = 0, |\kappa| = 0$. An additional constraint is from $|q_3| = 0$, another to allow the nullvector from q_3 to be orthogonal to the column nullspace of q_2, and a final one to allow the nullvector from q_3 to be orthogonal to the column nullspace of q_1. This gives 6 total constraints.

The number of constraints are a direct results of the triangular form of Q, so if we iterate this process to get 8 zero energy states (say if there was a fourth section) then there are now 4 additional constraints, giving 10 in total. More generally (up to some simple considerations, and the convention to group constraint maps) there is a minimum of a triangular number of constraints to get a certain number of zero energy states. A general proof is given in section 7.3.17.

Let $X_i \subset \xi$ denote a subspace of ξ satisfying i constraints. Let $\mathcal{P}(X_i)$ denote the topological classification of that space. As discussed above, only if all but one constraint is satisfied, we get a topologically non-trivial subspace. Up to some simple considerations this gives the sequence of zeroth homotopy groups

$$N\mathbb{Z}_2 \to 0 \to \mathcal{P}(X_2) \to 0 \to 0 \to \mathcal{P}(X_5) \to 0 \to 0 \to 0 \to \mathcal{P}(X_9) \to \cdots \tag{7.1.16}$$

where an arrow denotes the application of a constraint map, and $\mathcal{P}(X_i) = 0$ if i is not one less than a triangular number.

In proposition 7.3.7 we use the dependence of hopping terms of subgraphs two demonstrate that, for two unequal sections $g_i < g_j$ with biadjacency matrices q_i, q_j then there are exactly three constraints to get 4 zero energy states. In doing so we demonstrate the equivalence of all first minors of a particular submatrix of Q. As such we can write the third constraint $|\kappa| = 0$ as an irreducible polynomial so $\mathcal{P}(X_2) = \mathbb{Z}_2$.

More generally $\mathcal{P}(X_i) = M\mathbb{Z}_2$. Much like in the zeroth step topology of chapter 5 M comes from the number of irreducible factors of the final polynomial that needs to solved to give 2 more zero energy states. Choosing one of these irreducible factors defines the final constraint map. This is discussed in more detail in section 7.3.2.

There are exceptions to the number of constraints giving a certain number of zero energy states is triangular. This occurs when $C_{i,j}\phi_j^i = 0$ already. This localises a nullstate to specific sections and can happen in two instances. The first is when two sections are equal by the partial ordering, and so $C_{i,j}$ has all zero entries ensuring $C_{i,j}\phi_j^i = 0$. The second case is when a constraint itself is satisfied by $C_{i,j}\phi_j^i = 0$. In both cases the minimum number of constraints to increase the number of zero energy states is reduced. This is explored in more detail in section 7.3.17.

We can extend the sequential topological classification to complex Hamiltonians quite simply. To do this we note that each constraint map is satisfied when, for some hopping term $h \in \mathbb{C}$

$$h = a + bi. \tag{7.1.17}$$

To satisfy this equation, $\mathrm{Re}(h) = a$ and $\mathrm{Im}(h) = b$. This means we need to modify each constraint map to act as the composition of two constraint maps. One that satisfies $\mathrm{Re}(h) = a$ and one for $\mathrm{Im}(h) = b$. For an example of such constraint maps see definition 7.4.2 in section 7.4. This doubles the number of constraint maps required to get a certain number of zero energy states, that is $\mathcal{P}(X_i)$ is non-trivial when $i = 2t - 1$ where t is a triangular number, so for complex Hamiltonians the sequence of zeroth homotopy groups is

$$0 \to N\mathbb{Z}_2 \to 0 \to 0 \to 0 \to \mathbb{Z}_2 \to 0 \to 0 \to 0 \to 0 \to 0 \to \mathcal{P}(X_{11}) \to \cdots \tag{7.1.18}$$

7.1.2 Overview of main arguments

There are three main results in sections 7.2, 7.3, 7.4, and 7.6. The first is a no go theorem which states that under the least restricted definition for a constraint map, no finite chiral Hamiltonian can have non-trivial 1st step topology. The second is the sequences of zeroth homotopy groups for real or complex chiral Hamiltonians. The final results are some experimental signatures discussed in section 7.6. Of these results the most technical proofs are for finding sequences of zeroth homotopy groups. We give an outline of the main idea behind the proof of the sequence of zeroth homotopy groups below. Throughout sections 7.2, 7.3, 7.4, and 7.6 we make use of the Harary-Sachs theorem, especially to relate terms in the secular equation to subgraphs of G.

To get the sequence of zeroth homotopy groups, we first define a subspace that we calculate the zeroth homotopy group for. As previously discussed, this subspace is given by $X_i \setminus T$, which is detailed more in section 7.3.3.

We then assume the support of nullstates from a singular section on above sections. This assumption is violated only by the two exceptions described in section 7.1.1. Then we use the triangular block structure of Q to show there are at least $\frac{n(n-1)}{2}$ constraints to get $2n$ zero energy states under the convention described above, and will be defined in definition 7.2.1. This follows a very similar argument to the example described in section 7.1.1 and uses the algebraic independence of sections to demonstrate these constraints are also algebraically independent.

In order to satisfy the set of constraints requires orthogonality of a nullstate of the section g_n and the column null spaces of all above sections g_i. Using a minimum number of constraints, we define a protocol to increase the nullity of the Hamiltonian and we show this satisfies the minimum number of constraints. With this assumption we therefore know the sequence of which zeroth homotopy groups are non-trivial.

7.2 Sequential topology and the parameter space

We are essentially interested in the same classification problem as Chapter 5, however, now we wish to extend it to lower dimensional subspaces of ξ. In order to do this, we need to understand how to derive the constraint maps to define such subspaces, and how to define a topology on these subspaces.

As discussed in section 7.1.1 in this thesis we take the convention that, given a structure H with $2n$ zero energy states, and choosing a section q_i which is non-singular. Then we satisfy (in some order) the set of constraints with the minimum number of constraints such that the nullity of H becomes $2n+2$ and (other than q_i) all non-singular sections q_j remain non-singular. We make this convention explicit in the following definition.

Definition 7.2.1. The sequence of constraints are chosen iteratively. Let H be a non-singular Hamiltonian defined on a structure G. To find a set of constraints, we choose a non-singular section. The first constraint is chosen from a section $g_i \in G$ with the biadjacency matrix q_i. The first constraint is $|q_i| = 0$. Later constraints are chosen as follows:

1. Choose a non-singular section $g_j \in G$.

2. Maintaining all the previously applied constraint maps on H, find the set of constraint maps $c_j = \{b_1, b_2, \cdots\}$ with the smallest cardinality such that nullstates are supported on both sub lattices of g_j (ensuring $|q_j| = 0$) and no other non-singular sections are made singular.

3. Apply a composition of constraint maps from c_j in any order you choose.

Repeat this step to get new sets of constraints.

There are sequences of constraint maps that do not follow this convention. However, under our convention we have a way to understand the largest dimensional subspaces in ξ that have a certain number of zero energy states, while controlling the localisation of these states. In other words, what the allowable amount of disorder in a structure is to achieve a certain number of zero energy states, and a certain localisation. Thus giving a physical motivation to our convention.

We can interpret a set of constraint maps in definition 7.2.1 as a kind of boundary operator. Definition 7.2.1 is a set of constraint maps that increase the number of zero energy states by 2. Now consider the subspace $E_{2n} \subset \xi$ of Hamiltonians with exactly $2n$ zero energy states. If all but one constraint map of c_i^{2n} are fulfilled, then we are in this subspace. Fulfilling the final constraint map gives $2n + 2$ zero energy states, however any infinitesimal change of the final constraint gives a structure with $2n$ zero energy states. Therefore, satisfying the set of constraints defines a boundary of E_{2n} with $2n + 2$ zero energy states (this boundary may be several dimensions lower then E_{2n}).

Note that there may be multiple constraints that define subspaces with $2n$ zero energy states, so we need to distinguish between these subspaces. To do this we associate a space X_i to satisfying some composition of constraints. So for each subspace E_{2n} we often need to specify a space given by the intersection of $E_{2n} \cap X_i$ which satisfies a certain number of constraints.

We can iterate this process, giving us a sequence of subspaces with a certain number of zero energy states, a set of constraints that give a boundary operator, and a set of sections that support zero energy states on both of their sub lattices.

$$E_0 \xrightarrow{c_0^0} E_2 \cap X_i \xrightarrow{c_i^2} E_4 \cap X_j \xrightarrow{c_j^4} E_6 \cap X_k \xrightarrow{c_k^6} \cdots$$

The order in which we choose sections does change this sequence, as it alters the choice of constraints. Therefore, for each structure there is a family of such sequences. So, loosely speaking, we are only studying a part of the subspace of $2n$ zero energy states when considering one sequence of boundary operators, that consist of choosing a set of sections to make singular.

We currently have two ways to understand the sequence of subspaces in ξ of interest. The first is to have one map for each constraint, as discussed in the previous section. The second is to restrict only to subspaces with a certain number of zero energy states. We can relate these by looking at the boundary operator between two such subspaces. Consider the boundary operator from E_{2n} to E_{2n+2} given by

$$E_{2n} \cap X_i \xrightarrow{c_i^{2n}} E_{2n+2} \cap X_{i+f}.$$

The boundary operator $c_i^{2n} \sim b_1 \circ b_2 \circ \cdots \circ b_f$ is really the composition of a set of constraint maps on the Hamiltonian, such that no extra constraint maps are satisfied. Each constraint map lowers the dimension of the subspace by one dimension, so we can expand this in to a diagram of constraint maps and boundary operators

$$\begin{array}{ccccccccc} E_{2n} \cap X_i & & \xrightarrow{\qquad\qquad c_i^{2n} \qquad\qquad} & & & & & & E_{2n+2} \cap X_{i+f} \\ \downarrow & & & & & & & & \downarrow \\ X_i & \xrightarrow{b_1} & X_{i+1} & \xrightarrow{b_2} & X_{i+2} & \xrightarrow{b_3} & \cdots & \xrightarrow{b_f} & X_{i+f}. \end{array}$$

The vertical arrows denote inclusion maps. This is because $X_i \subset \xi$ is the subspace which satisfies a certain set of constraints, and so can have more then $2n$ zero energy states. But $E_{2n} \cap X_i$ is the intersection of these constraints and the subspace of exactly $2n$ zero energy states. So X_i may also have a subspace with more zero energy states. The horizontal arrows denote either the boundary operators (between subspaces of a particular nullity) or maps adding individual constraints (between subspaces X_i). The maps between X_i are restrictions.

Each row of the above diagram provides a different way to imagine the subspaces of ξ. But using both pictures helps give a well defined way to study the topology of a structure. That is, a subspace $X_i \subset \xi$ is topologically non-trivial, when $X_i \setminus \left(\bigcup_j E_{2m+2j}\right)$ for some m has a non-trivial zeroth homotopy group. We now recall the definition of the usual topology on the subspace $X_i \setminus \left(\bigcup_j E_{2m+2j}\right)$.

Definition 7.2.2. Let X_i be a subspace defined by some sequence of constraints, with $2n$ zero energy states. Let $X_i \setminus \left(\bigcup_{j=1} E_{2m+2j}\right)$ be the open subspace of X_i with exactly $2n$ zero energy states. The open subsets of $X_i \setminus \left(\bigcup_{j=1} E_{2m+2j}\right)$ are defined as an open n-ball around each point where n is the dimension of X_i. Let the empty set $\emptyset$ and $X_i \setminus \left(\bigcup_{j=1} E_{2m+2j}\right)$ be in the topology τ, along with any intersection or union of an open subset of $X_i \setminus \left(\bigcup_{j=1} E_{2m+2j}\right)$.

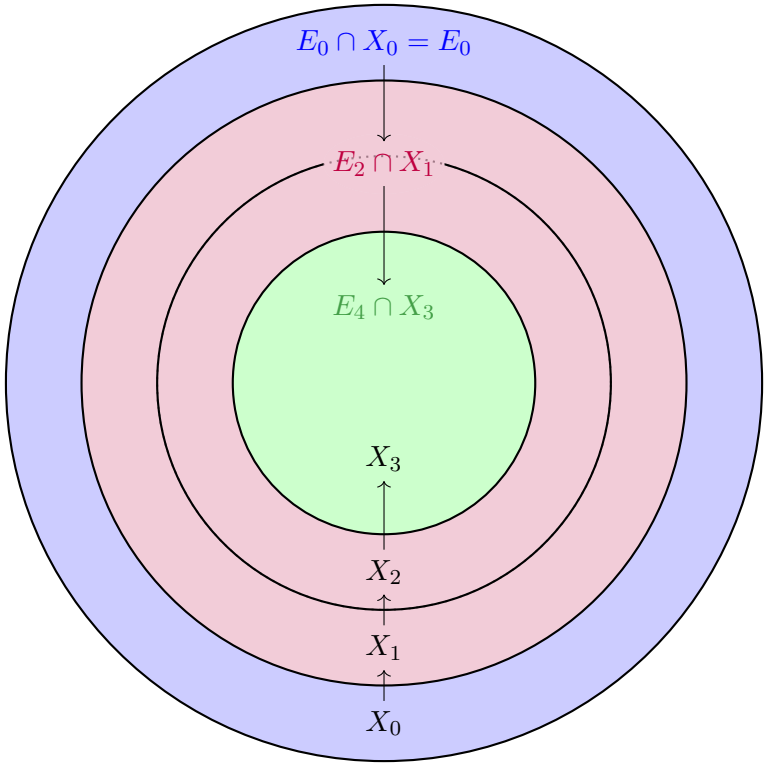

Figure 7.2.1: The relationship between the subspaces $E_{2n} \cap X_i$, X_i. The maps between each $E_{2n} \cap X_i$ are given by a boundary operator, and for maps between each X_i are given by a constraint map. Note that each black circle denotes a difference of one dimension of each respective subspace.

So far our discussion has got more abstract than in chapter 5 but this is effectively still the same problem, just for a subspace of ξ rather than all of ξ. In the previous discussion we have demonstrated how to translate our approach to zeroth step topology to the same problem in subspaces of ξ.

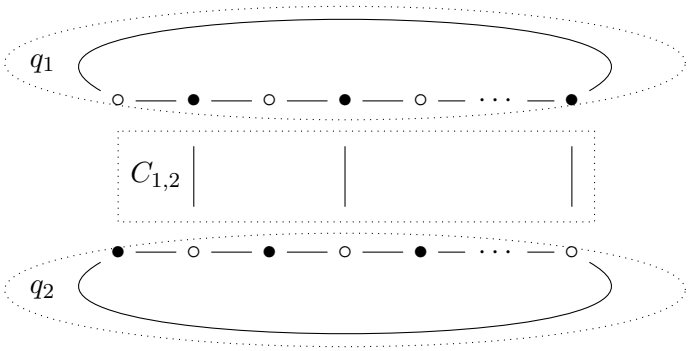

Figure 7.2.2: Finite 2 row ribbon graphene, with a multiple of 4 sites in each section, and algebraically independent hopping terms. This structure has a $2\mathbb{Z}_2$ zeroth step classification and requires 3 constraints on the hopping terms to get 4 zero energy states.

For example, consider 2 row ribbon graphene illustrated in Fig. 7.2.2 with a zeroth step classification of $2\mathbb{Z}_2$. The first terms of the secular equation are given by

$$|H - \lambda I| = -|q_1||q_2||q_1^\dagger||q_2^\dagger| + \left(\alpha|q_1|\alpha^*|q_1^\dagger| + \beta|q_2|\beta^*|q_2^\dagger| + \gamma\gamma^*\right)\lambda^2 + \cdots \tag{7.2.21}$$

where α, β, γ are polynomials of hopping terms. To get 2 zero energy states, there are two solutions. One for $|q_1| = 0$ and the second for $|q_2| = 0$. To set $a_2 = 0$ and get 4 zero energy states there are three total constraints

$$|q_1| = |q_2| = \gamma = 0. \tag{7.2.22}$$

Note that γ is actually given by the first order minor of the biadjacency matrix Q of the structure G. More details are given in section 7.3.

Remark. Use the shorthand of $c_i^j = \{\gamma_1 = 0, \gamma_2 = 0, \cdots\}$ to denote the map

$$\begin{aligned} c_i^j(E_{2n} \cap X_i) :&= E_{2n+2} \cap X_{i+f} \\ &= \{x \in E_{2n+2} \cap X_{i+f} | \gamma_1 = 0, \gamma_2 = 0, \cdots \text{ and } \mathcal{N}(H) = 2n+2\}. \end{aligned} \tag{7.2.23}$$

This gives us the following boundary operators $c_1^0 = \{|q_1| = 0\}$, $c_2^0 = \{|q_2| = 0\}$, $c_1^1 = \{|q_1| = 0, \gamma = 0\}$, $c_2^1 = \{|q_2| = 0, \gamma = 0\}$. Setting $|q_1| = 0$ first, then $|q_2| = 0$ gives us the following sequence of subspaces

$$\begin{array}{ccccccc} E_0 & \xrightarrow{c_1^0=\{|q_1|=0\}} & E_2 \cap X_1 & & \xrightarrow{c_2^1=\{|q_2|=0,\gamma=0\}} & & E_4 \cap X_3 \\ \downarrow & & \downarrow & & & & \downarrow \\ \xi & \xrightarrow{|q_1|=0} & X_1 & \xrightarrow{|q_2|=0} & X_2 & \xrightarrow{\gamma=0} & X_3. \end{array}$$

The important features of the above sequence of subspaces are sufficiently low dimensional to be able to visualise. This is because we are applying 3 constraints, which we can associated to three dimensions, with E_4 and X_3 denoted as a point. A suitable slice of the parameter space of two row ribbon graphene to illustrate this sequence of subspaces is given in Fig. 7.2.3, with the relationship of the subspaces for this example illustrated in Fig. 7.2.1.

Remark. When the maximum number of zero energy states is reached, then the subspace $E_{2n} \cap X_m$ is exactly the subspace X_m. This is because there are no subspaces of X_m with more than $2n$ zero energy states so the inclusion between $E_{2n} \cap X_m$ and X_m is just the identity map. Furthermore, in the 2 row graphene example $E_4 = E_4 \cap X_3$. We conjecture that for any Hamiltonian H defined on the structure G, when maximum nullity is reached then $E_{2n} \cap X_m = E_{2n}$. That is there is exactly one set of constraints that define the subspace E_{2n}.

Now we have a geometric picture for the maps between certain subspaces of ξ, we turn to defining the exact boundary operators for each E_{2n} corresponding to constraints in the subspaces X_i. The simplest way to do this is to use the terms in the secular equation, a_i, as a boundary operator. However, as we argued in section 7.1 and will prove with a no go theorem in section 7.3.1, this is not always a sensible choice. As mentioned (an proven in section 7.2.1) we give a way to interpret such boundary operators from subgraphs of the structure, and give a complete definition for a boundary operator for real Hamiltonians in section 7.3.2 and for complex Hamiltonians in section 7.4.

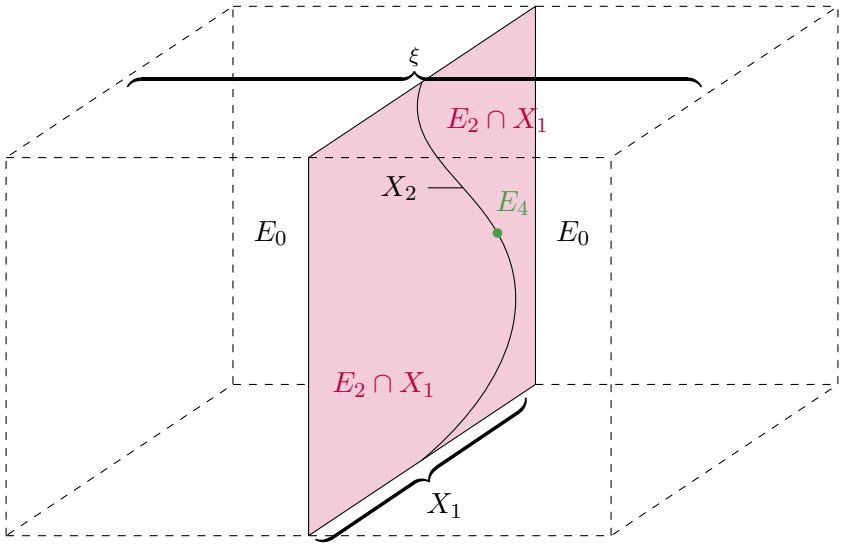

Figure 7.2.3: A slice of the parameter space of 2 row ribbon graphene. In this structure there is one constraint map to get at least 2 zero energy states, and three constraint maps to get 4 zero energy states. Each subspace satisfying a certain number of constraints is denoted X_i where i is the number of satisfied constraint maps. This structure cannot host more than 4 zero energy states, so E_4 is uniquely defined.

7.2.1 A connection between subgraphs and sequential topology

As discussed in sections 7.1 and 7.2 to define a topology on each subspace, the secular equation is particularly important. In this subsection we wish to give a way of interpreting the terms of the secular equation as subgraphs on the Hamiltonian. By doing so, we demonstrate each constraint is given by the determinant of a sub-Hamiltonian — an example of a subgraph corresponding to such a sub-Hamiltonian is given in Fig. 7.2.4. To do this we first show we are only interested in even order terms of the secular equation, and that each of these terms can be understood as a sum of principal minors of H.

Proposition 7.2.3. For a balanced chiral structure, the secular equation is given by $|H - \lambda I| = \sum a_{2n}\lambda^{2n}$.

Proof. As the Hamiltonian is chiral, the solutions to the secular equation come in $\lambda = \pm\varepsilon$ pairs. Therefore we can write

$$|H - \lambda I| = \lambda^p \prod_i (\lambda^2 - \varepsilon_i^2) \tag{7.2.25}$$

where p is the number of topologically protected states. For $p = 0$ then expanding equation 7.2.3 gives a polynomial with only even powers of λ. Therefore

$$|H - \lambda I| = \sum a_{2n}\lambda^{2n} \tag{7.2.26}$$

□

Remark. From proposition 7.2.3 we know the Hamiltonian has $2m + 2$ zero energy states when $a_{2n} = 0$ for all $n \leq m$.

We now show that a_{2n} can be interpreted as the sum of determinants of chiral subgraphs of G. This is an application of the Harary-Sachs theorem [63, 64] for the secular equation of weighted bipartite graphs. To do this we interpret

$$H - \lambda I \tag{7.2.27}$$

as a structure with on site energies $-\lambda$.

Proposition 7.2.4. Any term $|q_m|$ in the sum $a_{2n} = \pm \sum |q_m||q_m^\dagger|$ is the determinant of a subgraph of G.

Proof. By the Harary-Sachs theorem any term in the secular equation that multiplies λ^{2n} multiplies a $2n$th principal minor of H. A principal minor of H defines a chiral Hamiltonian on a subgraph g of G.

From chapter 4 we know that any structure with a different number of black and white sites is singular, therefore the only terms that persist in the secular equation are from deleting n black and n white sites of H. So we can write

$$a_{2n} = (-1)^n \sum_m |q_m||q_m^\dagger| \tag{7.2.28}$$

where $(-1)^n$ comes from the negative $-\lambda$ term in $H - \lambda I$ and q_m is the biadjacency matrix of a subgraph of G. □

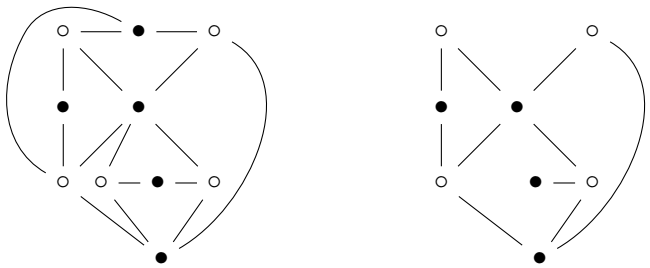

(a) (b)

Figure 7.2.4: (a) Example of a chiral structure with a zeroth step classification of $\mathbb{Z}_2$. (b) A subgraph obtained by deleting a black and a white site. The determinant of this subgraph is a polynomial with two irreducible factors, one trivial polynomial from the matching on the branch, and a non-trivial factor from the matchings of the complementary subgraph.

The constraints to set $a_{2n} = 0$ are not immediately clear from the secular equation alone. This is because it is generally not possible to solve $a_{2n} = 0$ with only one constraint.

Proposition 7.2.5. The minimum (under the convention in definition 7.2.1) number of constraints for $a_{2n} = 0$ is bounded above by the number of non-zero minors that a_{2n} sums over.

Proof. Each subgraph is Hermitian so $|q_m||q_m^\dagger| \geq 0$. Therefore $a_{2n} = 0$ only when $|q_m| = 0$ for each m. □

In proposition 7.2.5 we demonstrate $a_{2n} = 0$ is not generally solvable with only one constraint and get a simple upper bound on the number of constraints as the number of non-zero principal minors. In sections 7.3 and 7.4 we discuss how an exact number of constraints can be found.

7.3 Sequential topology in real finite chiral structures

In this section we give a detailed overview of how to get boundary operators from the secular equation and infer the number of constraints to get a certain number of zero energy states in a real Hamiltonian. We begin by illustrating a no go theorem for non-trivial sequential topology in section 7.3.1 which can be overcome with a subtlety in the definition of the boundary operator detailed in 7.3.2.

In section 7.3.3 we derive the sequence of zeroth homotopy groups given in the diagram (7.0.8) and show it is (up to some simple considerations) independent of the underlying structure. Later in section 7.5 we go on to show how this sequence is altered when we allow individual sections to have a nullity greater than 2.

7.3.1 A no go theorem for real Hamiltonians

In this section we will demonstrate that even for 1st step topology, the simplest choice of boundary operator does not give well defined topological phases. That is a boundary operator corresponding to $a_{2n} = 0$. This is true for any case where the zeroth step classification is $N\mathbb{Z}_2$ for $N \geq 2$. Using the arguments developed in this section we will motivate a more general choice of boundary operator which works for defining a sequence of subspaces.

The fact that $|H| = 0$ does not define a good boundary operator stems from the fact it can be factorised. Using these distinct factors, we will show that the subspace $|H| = 0$ is connected under a topology with closed sets of $a_2 = 0$. That is, there is no non-trivial 1st step topology for this choice of boundary operator. As we will argue in section 7.3.2 we can get non-trivial 1st step topology by using constraints directly from the factors of $|H|$.

To show that using $|H| = 0$ as a boundary operator never gives non-trivial 1st step topology, we first demonstrate that an individual section requires at least four constraints to satisfy $|H| = a_2 = 0$. We then show for any structure with all non equal sections (by the partial ordering of sections given in chapter 5) at least three constraints are required to get $|H| = a_2 = 0$. These two cases illustrate that the subspace of 4 zero energy states does not divide the subspace of $|H| = 0$ in to distinct regions for a structure with all equal sections (by the partial ordering of chapter 5).

Finally, we consider the case where there are two or more equal sections (by the partial ordering of sections) then there can be two constraints to satisfy $|H| = a_2 = 0$. However using the map we discussed in section 7.1.1 we describe a path around this pair of constraints that remains on $|H| = 0$. The existence of this path is what necessitates the different

definition of a boundary operator given in section 7.3.2, and ensures it is the number of constraints that define a topological phase boundary.

Consider a Hamiltonian H with the zeroth step classification $N\mathbb{Z}_2$. We proceed by considering a single section g_i in the structure G that H is defined on, with the corresponding sub Hamiltonian

$$h_i = \begin{pmatrix} 0 & q_i \\ q_i^\dagger & 0 \end{pmatrix}. \tag{7.3.30}$$

Recall that for a matrix A we use $\mathcal{N}(A)$ to denote the nullity of A.

Lemma 7.3.1. If $\mathcal{N}(h_j) = 4$ and all other sections are non-singular then $\mathcal{N}(H) = 4$.

Proof. If $\mathcal{N}(h_j) = 4$ then $\mathcal{N}(q_j) = 2$, so there are two orthogonal nullstates $|\phi\rangle, |\psi\rangle$ such that

$$q_j |\phi\rangle = 0, \qquad q_j |\psi\rangle = 0. \tag{7.3.31}$$

Suppose

$$Q = \begin{pmatrix} \ddots & \vdots & \vdots & \vdots & \\ & q_{j-2} & C_{j-2,j-1} & C_{j-2,j} & \cdots \\ & & q_{j-1} & C_{j-1,j} & \cdots \\ & & & q_j & \cdots \\ 0 & & & & \ddots \end{pmatrix} \tag{7.3.32}$$

then

$$Q \begin{pmatrix} \vdots \\ q_{j-2}^{-1}\left(C_{j-2,j-1}q_{j-1}^{-1}C_{j-1,j} - C_{j-2,j}\right)|\psi\rangle \\ -q_{j-1}^{-1}C_{j-1,j}|\psi\rangle \\ |\psi\rangle \\ 0 \\ \vdots \\ 0 \end{pmatrix} = Q|\Psi\rangle = 0. \tag{7.3.33}$$

Similarly for $|\phi\rangle$,

$$Q \begin{pmatrix} \vdots \\ q_{j-2}^{-1}\left(C_{j-2,j-1}q_{j-1}^{-1}C_{j-1,j} - C_{j-2,j}\right)|\phi\rangle \\ -q_{j-1}^{-1}C_{j-1,j}|\phi\rangle \\ |\phi\rangle \\ 0 \\ \vdots \\ 0 \end{pmatrix} = Q|\Phi\rangle = 0. \tag{7.3.34}$$

Because h_i is Hermitian, its eigenvectors are orthogonal so $|\psi\rangle$ and $|\phi\rangle$ are linearly independent. Therefore $|\Psi\rangle$ and $|\Phi\rangle$ are in the nullspace of Q and are linearly independent.

By symmetry we can define two linearly independent nullstates for $Q^\dagger$ giving a dimension 4 nullspace to H, hence $\mathcal{N}(h_i) = 4 \Rightarrow \mathcal{N}(H) = 4$. □

Corollary 7.3.2. If a connected subgraph $\bar{G} \in G$ of sections $\{g_i\}$ with associated submatrix $\bar{h}$ has $\mathcal{N}(h) = 2n$ and the minor of G when deleting $\bar{G}$ is non-singular, then $\mathcal{N}(H) = 2n$.

Proof. There are $2n$ linearly independent null states on h. As the minor when deleting $\bar{G}$ from G is non-singular, we can define each null state on the remaining graph, giving $2n$ linearly independent null states on H. □

Remark. Suppose a section $|q_i| = 0$ with nullity $\mathcal{N}(q_i) = 1$ and that g_i is a subgraph of G and G has the biadjacency matrix Q of equation (7.3.32). If $q_i\psi_i^i = 0$ then index by i the eigenstate over the section g_i of G, so that

$$Q\left|\Psi\right\rangle = Q\begin{pmatrix}\psi_1^i\\ \vdots\\ \psi_i^i\\ \vdots\end{pmatrix} = 0 \tag{7.3.35}$$

then the term ψ_{i-n}^i is given by

$$\begin{aligned}\psi_{i-n}^i &= q_{i-n}^{-1}\left(-C_{i-n,i} + C_{i-n,i-1}q_{i-1}^{-1}C_{i-1,i} - C_{i-n,i-2}q_{i-2}^{-1}C_{i-2,i}\right.\\ &\qquad \left. + C_{i-n,i-2}q_{i-2}^{-1}C_{i-2,i-1}q_{i-1}^{-1}C_{i-1,i} + \cdots\right)\psi_i^i\\ &= \sum_{s\in S}\prod_{(m,p)\in s}\left(-q_{i-m}C_{i-m,i-p}\right)\psi_i^i\\ &=: -q_{i-n}^{-1}\mathscr{C}_{i,j}\psi_i^i.\end{aligned} \tag{7.3.36}$$

Where ψ_j^i denotes the support of the nullstate originating from section i on section j and s is a sequence of integer pairs (m,p) such that $m < p \leq i$ and m starts with $m = i - n$. The next m is given by the previous p and so on. That is

$$m_{j+1} = p_j, \qquad m_{j+1} < p_{j+1} < i. \tag{7.3.37}$$

S is then the set of all such sequences of s between $i - n$ and i.

The matrix $\mathscr{C}$ allows us to study a smaller effective structure when considering sequential topology.

Definition 7.3.3. Let $\mathscr{C}_{i,j}$ be the matrix given between two sections biadjacency matrices in the previous remark. Then the *effective subgraph* or *effective sub-Hamiltonian* is given by the adjacency matrix

$$\begin{pmatrix} & & q_i & \mathscr{C}_{i,j}\\ & & 0 & q_j\\ q_i^\dagger & 0 & & \\ \mathscr{C}_{i,j}^\dagger & q_j^\dagger & & \end{pmatrix}. \tag{7.3.38}$$

Let $\{g_c\}$ be the set of singular sections of G. Then $\mathscr{C}_{i,j}$ is no longer well defined for any two sections in $\{g_c\}$. But we can define the contribution to $\mathscr{C}_{i,j}$ which does not multiply the

inverse of a singular biadjacency matrix. Let $\bar{\mathscr{C}}_{i,j}$ denote this contribution. The effective subgraph of the $\{g_c\}$ singular sections is defined by the biadjacency matrix

$$\begin{pmatrix} q_{c_1} & \bar{\mathscr{C}}_{c_1,c_2} & \cdots & \bar{\mathscr{C}}_{c_1,c_n} \\ 0 & q_{c_1} & \cdots & \bar{\mathscr{C}}_{c_2,c_n} \\ \vdots & \vdots & \ddots & \vdots \\ 0 & 0 & \cdots & q_{c_n} \end{pmatrix}. \tag{7.3.39}$$

The effective subgraph can also be generalised to find the constraints for $2n$ zero energy states between n sections.

Proposition 7.3.4. At least four constraints are required to set $\mathcal{N}(h_i) = 4$.

Proof. Take a section g_i with the biadjacency matrix q_i. Assume this section can be constrained to have a nullity of 4.

If $\mathcal{N}(h_i) = 4$ then each first minor of q_i is zero. By proposition 7.2.4 this defines a set of subgraphs of g_i which have one deleted black site, and one deleted white site.

Assume every first minor of q_i is factored by a solvable polynomial α. From the factorisation theorem in chapter 5 we know α is associated to a subgraph g_α of g. So now take a minor of g that deletes a black site from g_α, and a white site from somewhere else in the section. From Chapter 5 we know this subgraph has a minor that is almost always non-zero, because g is a section. Furthermore, we know this minor is solvable, because we have assumed g can have a nullity of 4. Therefore, we now have a minor that is not factored by α, giving at least two constraints.

Let this minor be given by the product of polynomials $\prod \beta_i$ with each factor associated to the subgraph g_{β_i} of g.

Now take a minor for each factor β_i with a white site deleted from g_α and a black site deleted from g_{β_i}. As every first minor of q_i is almost always non-zero this defines a set of non-zero minors. The sum of these minors not factored by α or any factor of $\prod \beta_i$. Therefore, there is at least one more constraint necessary to solve $a_2 = 0$.

Finally, we also require $|q_i| = 0$, giving at least four total constraints. □

Corollary 7.3.5. For an individual section g_i at least four constraints are required to set $a_2 = 0$.

Proof. By proposition 7.3.1 if the section g_i has four nullstates, and all other sections are non-singular, then H has four nullstates. By proposition 7.3.4 this requires at least four constraints. □

Remark. We will show in section 7.5 that it is exactly 4 constraints to get an individual section with 4 zero energy states. Only upper bounds are known for higher nullity of an individual section, as also detailed later on.

We have now demonstrated that using $|H| = 0$ to define a boundary operator gives no non-trivial 1st step topology for an individual section. But with $|H| = 0$ as a boundary operator is it possible that there is non-trivial topology when setting two sections to be

individually critical? To show it is not, we will use two arguments, the first only works for two unequal sections (by the partial ordering), but we proceed with this argument as it illuminates certain properties of a structure when it is on a higher steps' phase boundary. The second is a stronger argument which uses the fact that the subspace E_2 is path connected, therefore demonstrating any two sections (even equal ones, by the partial ordering) must have at least three constraints to have non-trivial 1st step topology.

Proposition 7.3.6. For two sections which are not equal by the partial ordering of sections, at least three total constraints are required to set $a_2 = 0$.

Proof. Consider the biadjacency matrix of the effective subgraphs of two sections $g_i > g_j$ such that

$$Q = \begin{pmatrix} q_i & \mathscr{C}_{i,j} \\ 0 & q_j \end{pmatrix}. \tag{7.3.40}$$

From corollary 7.3.2 we know that if $\mathcal{N}(Q) = 2$ and all other sections are singular than $\mathcal{N}(H) = 4$. Therefore, we can restrict questions about the nullity of H to the nullity of Q.

We have assumed extra constraints on the Hamiltonian are coming from two sections, each being singular, so the first two constraints are defined by

$$|q_i| = 0, \qquad \text{and} \qquad |q_j| = 0. \tag{7.3.41}$$

Let $q_i\phi_i^i = 0$ and $q_j\psi_j^j = 0$, where ψ_i^j is the support of the nullstate originating from q_j on q_i. Therefore Q has nullity 2 when

$$q_i\psi_i^j = -\mathscr{C}_{i,j}\psi_j^j. \tag{7.3.42}$$

We now show $\mathscr{C}_{i,j}$ is non-zero, so this defines at least one more constraint on the hopping terms.

By the definition of the partial ordering of sections, for $g_i > g_j$ then there must exist at least one sequence of sections that are connected such that $g_i > g_\alpha > g_\beta > \cdots > g_\gamma > g_j$. From the definition of $\mathscr{C}_{i,j}$ this defines a sequence of integer pairs that denote sections as defined in equation 7.3.37. Each section in this sequence, apart from g_i and g_j is assumed to be non-singular, therefore this defines a non-zero contribution to $\mathscr{C}_{i,j}$. As each hopping term is algebraically independent this ensures $\mathscr{C}_{i,j}$ is non-zero for almost all hopping terms. Hence there are at least 3 constraints to get $\mathcal{N}(H) = 4$ with two unequal sections, each of nullity 2. □

We now have that there are at least 3 constraints to get $\mathcal{N}(H) = 4$ with two unequal sections when we only allow each section to have nullity 2. We now give a proof that there are exactly 3 constraints to get $\mathcal{N}(H) = 4$ with two unequal sections.

Proposition 7.3.7. For two unequal sections $g_i > g_j$ and each section limited to a nullity less than or equal to 2, there are three constraints to get $\mathcal{N}(H) = 4$ when all other sections are not singular.

Proof. From chapter 5 we know each section is almost always a core graph when singular. Therefore, for each singular section g_i we can write each row (column) of q_i as a linear combination of every other row (column) of q_i. Label each column of q_i as q_i^l. Take q_i and delete a column. Denote the matrix where the column q_i^k has been deleted as

$$\left(q_i^{l\neq k}\right). \tag{7.3.43}$$

When q_i is singular each column is almost always a linear combination of every other column (a consequence of a section being a weighted 2-core graph), so there exists some invertible matrix $A_{k,m}$ for every deleted row k and deleted row m such that we can write

$$\left(q_i^{l\neq k}\right) = \left(q_i^{l\neq m}\right) A_{k,m}. \tag{7.3.44}$$

By symmetry we can do this for the rows of q_i. To avoid ambiguity, we denote a row of q_i as q_l^i. Let the sub matrix of q_i with the row q_k^i deleted be denoted by $\left(q_{l\neq k}^i\right)$. Then for some invertible matrix $B_{k,m}$ for every row k, m

$$\left(q_{l\neq k}^i\right) = B_{k,m}\left(q_{l\neq m}^i\right). \tag{7.3.45}$$

We can therefore write for a submatrix where we have deleted a column of q_i and a row of q_j

$$P_1 q_m P_2 = \begin{pmatrix} I & 0 \\ 0 & B_{o,k} \end{pmatrix} \begin{pmatrix} q_{l\neq k}^i & \mathscr{C}_{i,j} \\ 0 & q_j^{m\neq n} \end{pmatrix} \begin{pmatrix} A_{p,n} & 0 \\ 0 & I \end{pmatrix} = \begin{pmatrix} q_{l\neq o}^i & \mathscr{C}_{i,j} \\ 0 & q_j^{m\neq p} \end{pmatrix}. \tag{7.3.46}$$

Let $h_{k,o}$ be the adjacency matrix of the effective subgraph of g_i and g_j where we have deleted the kth column of q_i and nth row of q_j. Then

$$\det h_{k,n} = \det\left[\begin{pmatrix} P_1 & 0 \\ 0 & P_2^{-1} \end{pmatrix} h_{k,n} \begin{pmatrix} P_1^{-1} & 0 \\ 0 & P_2 \end{pmatrix}\right] = \det h_{o,p}. \tag{7.3.47}$$

From proposition 7.2.4 we know $\det h_{k,n}$ is the square of an irreducible polynomial, so $\det h_{o,p}$ is as well. Furthermore, from the above argument this irreducible polynomial is given by

$$\det \begin{pmatrix} q_i^{l\neq o} & \mathscr{C}_{i,j} \\ 0 & q_{m\neq p}^j \end{pmatrix} \tag{7.3.48}$$

therefore $\det h_{k,n} = \det h_{o,p}$ for any k, n, o, p.

Finally, if we delete two sites from g_i (g_j) this keeps q_i (q_j) on the diagonal, so all such minors are zero. If we take a minor from a term in $\mathscr{C}_{i,j}$ then the block of zeros is sufficiently large to make all such minors zero. So the only non-zero minors are of the form $\det h_{o,p}$. This ensures all such minors define the same constraint, giving exactly three total constraints. □

Remark. We will give another proof in section 7.3.3.1 that it is exactly three constraints needed to set $|H| = 0$ and $a_2 = 0$. The argument used later more easily generalises to higher than 1st step topology.

Proposition 7.3.8. For two equal sections exactly two constraints are required to get $a_2 = 0$. However, this boundary is not a topological boundary for the subspace corresponding to $|H| = 0$.

Proof. Take two sections g_i and g_j which are equal by the partial ordering. The effective subgraph for two such sections has the biadjacency matrix

$$\begin{pmatrix} q_i & 0 \\ 0 & q_j \end{pmatrix}. \tag{7.3.49}$$

Therefore, to get $\mathcal{N}(H) = 4$ requires satisfying two constraints given by $|q_i| = 0$ and $|q_j| = 0$.

However, we know G is connected, so there must be a subgraph of G which is connected in some way to the two equal sections. Because $g_i = g_j$ by the partial ordering any section g_k which is above (or below) g_i is also above (or below) g_j. For the following argument assume $g_k < g_i = g_j$ but the argument works the same for $g_k > g_i = g_j$.

Take the effective subgraph of g_k, g_i, g_j with the biadjacency matrix

$$\begin{pmatrix} q_k & \mathscr{C}_{k,i} & \mathscr{C}_{k,j} \\ 0 & q_i & 0 \\ 0 & 0 & q_j \end{pmatrix}. \tag{7.3.50}$$

Because $g_k < g_i$ and $g_k < g_j$ the submatrices $\mathscr{C}_{k,i}$ and $\mathscr{C}_{k,j}$ are non-zero. Consider a map that continuously connects the following points.

$$H(t) = \begin{cases} |q_i| = 0, |q_k| > 0, |q_j| > 0 \,\text{for}\, t = 0 \\ |q_i| = 0, |q_k| = 0, |q_j| > 0 \,\text{at}\, t = \frac{1}{5} \\ |q_i| > 0, |q_k| = 0, |q_j| = 0 \,\text{at}\, t = \frac{2}{5} \\ |q_i| > 0, |q_k| = 0, |q_j| < 0 \,\text{at}\, t = \frac{3}{5} \\ |q_i| = 0, |q_k| = 0, |q_j| < 0 \,\text{at}\, t = \frac{4}{5} \\ |q_i| = 0, |q_k| > 0, |q_j| < 0 \,\text{at}\, t = 1 \end{cases} \tag{7.3.51}$$

It is possible to continuously evolve the hopping terms of each section independently, so there exists such a map where $|q_i| = 0$ and $|q_j| = 0$ are not satisfied at the same time. Furthermore, from proposition 7.3.6 we know when $|q_i| = 0$ and $|q_k| = 0$ there are only two nullstates without satisfying further constraints, so such a map exists that maintains a nullity of 2. □

This is the same map we first discussed in section 7.1.1. To make the argument in Prop. 7.3.8 clearer, we give display an example of this map in Fig. 7.3.1.

Corollary 7.3.9. The boundary operator corresponding to $|H| = 0$ gives all trivial 1st step topology.

Proof. There are two main ways we can increase the nullity of H by constraining hopping terms. The first is to increase the nullity of an individual section. The only other alternative

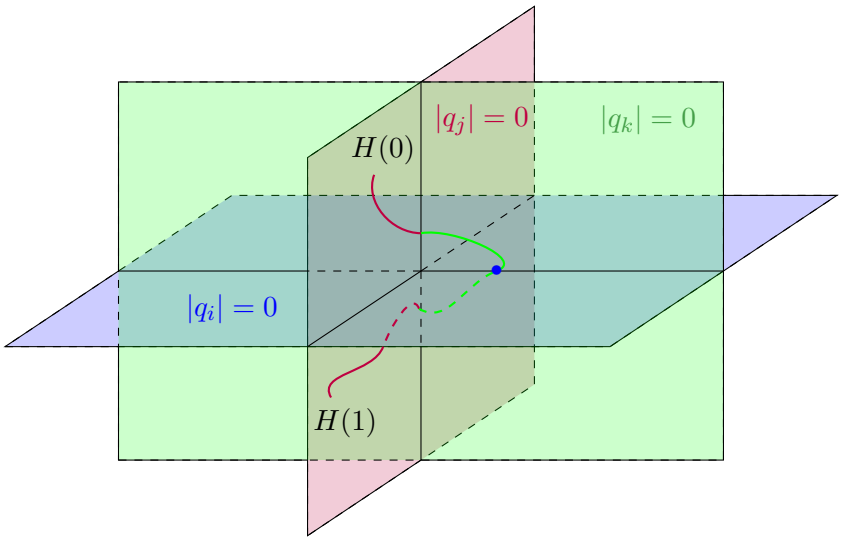

Figure 7.3.1: A slice of the parameter space ξ for some structure with three sections related by the partial ordering $g_k > g_i = g_j$. The evolution between $H(0)$ and $H(1)$ maintains 2 zero energy states throughout this path, because when $|q_j| = |q_k| = 0$ the nullity is 2 unless a further constraint map is satisfied. When the map is red, green, or blue, it is passing through the subspace corresponding to the solution to one of the factors being zero.

is to increase the nullity of multiple sections. We know that every section is either equal, or not equal, by the partial ordering. Therefore propositions 7.3.5, 7.3.6 and 7.3.8 show every way to increase nullity of a Hamiltonian to get 4 zero energy states, has at least 3 constraints. Therefore using $|H| = 0$ as a boundary operator gives no non-trivial 1st step topology. □

We now have an argument against using the terms a_{2n} directly to define a boundary operator. So how should we define such boundary operators? We will argue in section 7.3.2 that the most sensible definition is from using irreducible polynomials for each constraint map, and their composition for boundary operators.

7.3.2 A modified boundary operator

In section 7.3.1 we demonstrated that the subspace corresponding to $|H| = 0$ has no non-trivial 1st step topology. This is because we can get around a boundary corresponding to $a_2 = 0$ while maintaining $|H| = 0$ using the intersection of constraints from two sections $|q_i| = 0$ and $|q_j| = 0$. Mathematically we may wish to have a topological classification that can 'detect' features such as the dimension of a subspace with a certain number of zero energy states.

We can also understand a physical motivation for rejecting $|H| = 0$ as the relevant zeroth step boundary operator. Suppose we turn the sequential classification problem around and start with a subspace of hopping terms that give a Hamiltonian with $2n$ zero

energy states. Then it would be convenient to know exactly how many hopping terms may be unconstrained, yet we retain $2n$ zero energy states. That is, what is the minimum number of constraints necessary for a certain number of zero energy states? So it is useful to have a topological classification where the number of constraints is given by a topological phase boundary of some subspace.

The map (in Fig. 7.3.1) which prevents $|H| = 0$ giving any non-trivial 1st step topology can be understood as requiring more control of the system then a particular boundary operator. This is because the map constructed in proposition 7.3.8 requires (at points) exact control of two hopping terms to avoid a boundary (to set $|q_k| = 0$ and $|q_j| = 0$. The boundary itself divides a surface in ξ with a constraint on only one hopping term. So for almost all Hamiltonians satisfying $|H| = 0$ we can assign a sequential topological phase if we allow only one hopping term to be controlled. This larger allowance for disorder is our physical motivation for a different boundary operator.

From chapter 5 we know the factorisation of $|Q| = \prod |q_i|$ tells us the zeroth step classification of H. So we can use a boundary operator using the factors of $|Q|$.

Definition 7.3.10. A zeroth step constraint map $b_i^0 : X_0 \to X_1$ is defined from the set of factors $\{|q_i| = 0 || Q| = \prod |q_i|\}$ so that

$$b_i^0 X_0 = X_1 := \{x \in X_1 | x \in \xi \,\text{solves}\, |q_i| = 0\}. \tag{7.3.53}$$

Definition 7.3.11. A zeroth step boundary operator $c_i^0 : E_0 \to E_2 \cap X_1$ is defined from the constraint map of definition 7.3.10 and the intersection of the subspace with exactly two zero energy states. That is

$$c_i^0 E_0 = E_2 \cap X_1. \tag{7.3.54}$$

The reason maps such as that used in proposition 7.3.1 exist is that the subspace associated to $|H| = 0$ defines a connected subspace of ξ. That is, each factor $|q_i|$ of $|Q|$ defines a $\dim \xi - 1$ surface in ξ. As $|q_i|, |q_j|$ are polynomials over distinct hopping terms any set of factors can be solved simultaneously. Therefore, these surfaces all intersect. In the case that a_{2n} is irreducible such a map no longer exists, so it is only when a_{2n} is reducible that this issue arises. This requirement that a constraint map is irreducible will also be used in the more general definition of a constraint map.

As mentioned in sections 7.1.1 and 7.2 we can apply constraint maps in different orders. So we allow, up to the convention in definition 7.2.1, each sequence of spaces to be a valid choice. Under this convention we can choose any subset of sections, and have each singular section provide two nullstates to the Hamiltonian. This allows us to detect the largest dimensional features of a particular subspace of $2n$ zero energy states that intersect with our sequence of constraints. We now give the definition for a general boundary operator and constraint maps for a real chiral Hamiltonian.

Definition 7.3.12. The boundary operator c_i^{2n} maps $E_{2n} \cap X_i \mapsto E_{2n+2} \cap X_j$ such that c_i^{2n} satisfies the composition of each constraint map given in the convention described in definition 7.2.1.

Definition 7.3.13. Take a Hamiltonian with $2n$ zero energy states, so that H is in the subspace $E_{2n} \cap X_i$. The constraint map $b_i : X_i \to X_{i+1}$ defines a subspace in ξ that ensures H satisfies one irreducible polynomial necessary to set $a_{2n} = 0$ under the convention in definition 7.2.1.

For example, consider the structure in Fig. 7.0.3. To take $\mathcal{N}(H) = 2$ to $\mathcal{N}(H) = 4$ defines two constraint maps. In that example the constraint maps are satisfied when

$$\begin{aligned} b_i^1 X_i :&= X_{i+1} = \{H \in X_i | in - mj = 0\} \\ b_i^2 X_i :&= X_{i+1} = \{H \in X_i | dfm - bhm + bgn - cfn = 0\}, \end{aligned} \tag{7.3.55}$$

while maintaining the previous constraints. There are three further constraint maps to get 6 zero energy states, so the subspace $E_4 \cap X_3$ is given when the above constraint maps are satisfied, but not all of the three further constraint maps. This defines a boundary operator $c_i^2 : X_1 \cap E_2 \to X_3 \cap E_4$ by

$$\begin{aligned} c_i^2 X_1 \cap E_2 :=& X_3 \cap E_4 \\ =& \{H \in X_1 \cap E_2 | in - mj = 0, dfm - bhm + bgn - cfn = 0, \\ & qt - rs + df - bh + lns - jps + jot - knt \neq 0\}. \end{aligned} \tag{7.3.56}$$

Boundary operators and constraint maps can be derived analogously once the constraining polynomials are known. Note that the way we have defined boundary operators endures that $c_i^{2n+2} \circ c_j^{2n} E_{2n} \cap X_i = 0$ because the image of $c_j^{2n} E_{2n} \cap X_i$ is in the kernel of $c_i^{2n+2} E_{2n+2} \cap X_i$.

As in the zeroth step case for $|H| = 0$ for each sequence of subspaces defined using these boundary operators, we can often map between each sequence while maintaining a nullity of at least $2n < 2N$ (where the number of non-trivial sections of H is N) such that each section has $\mathcal{N}(q_i) \leq 1$. This is because, under certain circumstances, there exists a path between each subspace $E_{2n} \cap X_i$ to $E_{2n} \cap X_j$ that maintains at least $2n$ zero energy states. To prove this, we demonstrate below that we can change which sections provide (at most 2) nullstates to the structure without changing nullity.

In the following, let X^α denote a subspace of ξ with $2n$ zero energy states, with a set of n singular sections (including the section g_α) such that each singular section has $\mathcal{N}(q_i) = 1$ and all the remaining sections are non-singular. Let $X^{\alpha,\beta} \subset X^\alpha$ be a subspace of X^α with $2n + 2$ zero energy states, where an additional section g_β has $\mathcal{N}(q_\beta) = 1$. And let X^β denote a subspace of ξ with $2n$ zero energy states with a set of n singular sections, such that g_α is non-singular, but g_β is.

Proposition 7.3.14. If $X^{\alpha,\beta}$ exists then X^α and X^β are connected.

Proof. If $X^{\alpha,\beta}$ exists, then there are constraint maps such that

$$\begin{aligned} X^\alpha &\to X^{\alpha,\beta}, \\ X^\beta &\to X^{\alpha,\beta} \end{aligned} \tag{7.3.57}$$

so we can define a map $X^\alpha \to X^{\alpha,\beta} \to X^\beta$. Because $X^{\alpha,\beta} \subset X^\alpha$ and $X^{\alpha,\beta} \subset X^\beta$ then this map does not reduce nullity. □

Remark. The intersection of $X^\alpha \cap X^\beta$ is often larger dimensional than $X^{\alpha,\beta}$. As such there is, in many cases, a map $X^\alpha \to X^\beta$ which maintains exactly $2n$ zero energy states. Furthermore in the case that $X^{\alpha,\beta}$ does not exist, there are still many cases where $X^\alpha \cap X^\beta$ does. For this reason, we conjecture that $\bigcup_i E_{2n} \cap X_i$ is a connected subspace

Corollary 7.3.15. Consider two Hamiltonians H_1 and H_2 with a different set of singular sections, where each singular section has $\mathcal{N}(q_i) = 1$ and $\mathcal{N}(H_1) = \mathcal{N}(H_2)$. Consider a set of pairwise substitutions for which set of singular sections the Hamiltonian changes (like in Prop. 7.3.14) such that $H_1 \to H_2$. If there exists a space $X^{\alpha,\beta}$ for any pair of substituted sections g_α, g_β along such an evolution, then there exists a map $H_1 \to H_2$ which maintains at least $2n$ zero energy states.

Proof. By Prop 7.3.14 we can always change one section being singular at a time without decreasing nullity. Therefore, we can define a sequence of section substitutions that take us from $H_1 \to H_2$ without decreasing nullity. □

Corollary 7.3.16. If, for an N section structure, there exists a subspace $E_{2N} \subset \xi$ with each section having $\mathcal{N}(q_i) = 1$ then every subspace X_i with at least $2N - 2b$ zero energy states for $b > 1$ is connected.

Proof. In such a case then $X^{\alpha,\beta}$ exists for every pair of sections g_α, g_β so such maps exist. □

Remark. We conjecture that E_{2n} itself is path connected for any nullity n. However, we have no proof of this more general statement.

By corollary 7.3.15 whenever we are on a higher steps' phase boundary, we can often map between different sequences of subspaces without decreasing the nullity of the Hamiltonian. In the below diagram, each horizontal arrow corresponds to a constraint map, and vertical arrows indicate a map between subspaces where $a_{2n} = 0$. The starting and ending subspace in the diagram does not depend on the choice of path, and so this diagram is commutative. As we will see in section 7.3.17 following the convention we defined in section 7.2 for most real finite chiral structures, this is the general structure for such a diagram where we only allow for individual sections to have at most a nullity of 2. For complex Hamiltonians this structure is very similar, as discussed in section 7.4.2.

$$\begin{array}{ccccccc}
X_0 & \xrightarrow{|q_1|=0} & X_1^1 & \longrightarrow & X_2^1 & \longrightarrow & X_3^1 \longrightarrow \cdots \\
 & & \downarrow & & & & \downarrow \\
X_0 & \xrightarrow{|q_2|=0} & X_1^2 & \longrightarrow & X_2^2 & \longrightarrow & X_3^2 \longrightarrow \cdots \\
 & & \downarrow & & & & \downarrow \\
X_0 & \xrightarrow{|q_3|=0} & X_1^3 & \longrightarrow & X_2^3 & \longrightarrow & X_3^3 \longrightarrow \cdots \\
 & & \downarrow & & & & \downarrow \\
X_0 & \xrightarrow{|q_4|=0} & X_1^4 & \longrightarrow & X_2^4 & \longrightarrow & X_3^4 \longrightarrow \cdots \\
 & & \downarrow & & & & \downarrow \\
 & & \vdots & & & & \vdots
\end{array}$$

Here X_f^g denotes a subspace defined by f constraint maps, and g denotes the choice of zeroth step boundary operator.

7.3.3 Multiple critical sections: a zeroth homotopy theory

In this subsection we will discuss the sequential topology of a structure when only allowing individual sections to have a nullity of at most $\mathcal{N}(q_i) = 1$. In particular we will show how to derive constraint maps for a particular structure, and associated boundary operators. We will then show these boundary operators follow the convention given in definition 7.2.1. Finally, we will show that (up to some simple considerations) these boundary operators and constraint maps give the sequence of zeroth homotopy groups given in the diagram 7.0.8, and how to alter the sequence to account for these considerations.

Before we discuss maps on the parameter space, we first recall how the zeroth homotopy group gives a physical number of sequential topological phases. Recall that we are interested in how many ways a Hamiltonian H_1 can be continuously mapped in some subspace $X_i \setminus \left(\bigcup_j E_{2n+2j}\right) \subset \xi$ to a Hamiltonian H_2. This is exactly the question of whether a continuous map (confined to the subspace) exists between the two Hamiltonians. As each individual Hamiltonian defines a point in ξ this corresponds to the number of path connected regions of the subspace, which is exactly what the zeroth homotopy group detects.

In section 7.2 we make the claim that the zeroth homotopy group, $\pi\left(X_i \setminus \left[\bigcup_j E_{2n+2j}\right]\right)$, is non-trivial (that is, there are two or more topologically distinct phases) when we satisfy all but one constraint in a boundary map. We formalise this notion here.

Definition 7.3.17. Let X_i be a subspace of ξ, defined by a set of constraint maps. Suppose these constraint maps ensure any point in X_i has at least $2n-2$ zero energy states. The number of topological phases of X_i is given by

$$\mathcal{P}(X_i) := \pi\left(X_i \setminus \left[\bigcup_{j=0} E_{2n+2j}\right]\right). \tag{7.3.58}$$

We now show that the constraint maps can be used to find $\mathcal{P}(X_i)$.

Proposition 7.3.18. The zeroth homotopy group $\mathcal{P}(X_i)$ can be deduced from the constraint maps.

Proof. By proposition 7.2.5 we know each constraint can be associated to the determinant of a subgraph of the structure G, and that each subgraph is chiral. So each constraint map defines a subspace in ξ that satisfies

$$|q_m||q_m^\dagger| = 0 \tag{7.3.59}$$

for some biadjacency matrix q_m. Fixing all hopping terms in q_m apart from a single hopping term h and multiplying through by any denominator of $|q_m|$ and $|q_m|^\dagger$ gives a pair of polynomials $f(h), f^*(h)$ respectively. Expanding out we have

$$f(h) = \sum_{n=0} \alpha_n h^n \tag{7.3.60}$$

which is defined for all $h \in \mathbb{R}$. If $f(h) = 0$ has solutions, we can divide f in to three regions where $f = 0$, $f > 0$ and $f < 0$. Therefore, if f has solutions then f with the solutions removed, that is $f(h) \setminus \{h|f(h) = 0\}$, is disconnected.

The choice of hopping term h is arbitrary, and the choice of how we fixed the remaining hopping terms in $f(h)$ is also arbitrary, so by continuity, if we can satisfy the constraint map $c_i : X_i \to X_{i+1}$ then $X_i \setminus X_{i+1}$ is disconnected.

Suppose that $X_i \setminus X_{i+1}$ has $2n$ zero energy states, and X_{i+1} has at least $2n + 2$ zero energy states. Then by definition 7.3.12 of the boundary operator $X_{i+1} \subset \left[\bigcup_{j=1} E_{2n+2j}\right]$. Furthermore, the union of all irreducible constraint maps (where we reference the constraint map by the superscript a that defines a subspace of $X_{i+1}^a \subset \bigcup_{j=1} E_{2n+2j}$) gives every subspace of X_i with $2n + 2$ or more zero energy states. Therefore, the zeroth homotopy group is given by

$$\mathcal{P}(X) = \pi\left(X_i \setminus \left[\bigcup_{j=1} E_{2n+2j}\right]\right) = \pi\left(X_i \setminus \left[\bigcup_{a} X_{i+1}^a\right]\right) \tag{7.3.61}$$

so can be deduced from the constraint maps. □

It is important to note that the above argument works only when we use the constraint maps which are defined with irreducible polynomials. This is because our definition for constraint maps ensures each solvable constraint map $c_i : X_i \mapsto X_{i+1}$ takes a subspace of dimension d_i to a subspace of dimension $d_i - 1$, so no maps like those given in Fig. 7.3.1 exist.

Now we have a way to distinguish topological phases on a subspace X_i we need to find the classification of X_i. Later we will show that when $\mathcal{P}(X_i)$ is non-trivial, then $\mathcal{P}(X) = M\mathbb{Z}_2$ where M is the number of irreducible factors that can define a final constraint map. Note that this means the classification is altered by the order of applying constraint maps, but the dimension of the subspace is not altered by the order of applying constraint maps.

7.3.3.1 A sequence of constraints

In section 7.3.2 we gave a proof that there are exactly 3 required constraint maps to get $\mathcal{N}(H) = 4$ when we require all sections have at most a nullity of 2. We give an alternative proof here, which only relies on the zero energy states being mutually orthogonal. While this treatment makes the constraints themselves a little opaque, it is more convenient to generalise to cases with a larger number of zero energy states.

Our argument here uses the effective subgraph between the two sections we wish to be critical, and the biadjacency matrix

$$\begin{pmatrix} q_i & \mathscr{C}_{i,j} \\ 0 & q_j \end{pmatrix}. \tag{7.3.62}$$

We assume the two sections are not equal via their partial ordering, hence $\mathscr{C}_{i,j}$ is non-zero.

Proposition 7.3.19. For two unequal sections via their partial ordering, and the convention in definition 7.2.1, exactly three constraints are required to get $\mathcal{N}(H) = 4$.

Proof. By the convention in definition 7.2.1 the first two constraints are given by $|q_i| = 0$ and $|q_j| = 0$. Assume these constraints are satisfied, so that $q_i\psi_i^i = 0$ and $q_j\phi_j^j = 0$.

If all other sections are non-singular, then recall that we can define an eigenvector over the complete Hamiltonian for $|\psi\rangle$ given by

$$\begin{aligned} \psi_{i-n}^i &= q_{i-n}^{-1}\left(-C_{i-n,i} + C_{i-n,i-1}q_{i-1}^{-1}C_{i-1,i} - C_{i-n,i-2}q_{i-2}^{-1}C_{i-2,i}\right. \\ &\qquad \left. + C_{i-n,i-2}q_{i-2}^{-1}C_{i-2,i-1}q_{i-1}^{-1}C_{i-1,i} + \cdots\right)\psi_i^i \\ &= \sum_{s\in S}\prod_{(m,p)\in s}\left(-q_{i-m}C_{i-m,i-p}\right)\psi_i^i \\ &= q_{i-n}^{-1}\mathscr{C}_{i,j}\psi_i^i. \end{aligned} \tag{7.3.63}$$

as defined in equation 7.3.36. We can almost do the same with ϕ_j^j up to the section q_i where we need to find a solution to

$$\begin{pmatrix} q_i & \mathscr{C}_{i,j} \\ 0 & q_j \end{pmatrix}\begin{pmatrix} \phi_i^j \\ \phi_j^j \end{pmatrix} = 0. \tag{7.3.64}$$

That is,

$$q_i\phi_i^j = -\mathscr{C}_{i,j}\phi_j^j = \bar{\phi}. \tag{7.3.65}$$

If we can solve equation 7.3.65 then we must be able to write $\bar{\phi}$ as a linear sum of the columns of q_i. We can do this when $\bar{\phi}$ is orthogonal to the left null space of q_i. That is $\psi_{i_L}^i\bar{\phi} = 0$ where we have the left null vector of q_i satisfying $\psi_{i_L}^i q_i = 0$.

Because a section is almost always a core graph when singular, labelling each column with a superscript j then we can write when $\psi_{i_L}^i q_i = 0$

$$q_i^j = \sum_{k\neq j}\alpha_k q_i^k \tag{7.3.66}$$

where α_k is non-zero for all q_i^k. So deleting a single column of q_i does not alter the left null vector $\psi^i_{i_L}$. Now take any column q_i^k of q_i and replacing it with $\bar{\phi}$ to define a new matrix κ

$$\kappa = \begin{pmatrix} q_i^{l\neq k} & \bar{\phi} \end{pmatrix}. \tag{7.3.67}$$

While maintaining $|q_i| = 0$ when $|\kappa| = 0$ then we have a solution to $\psi^i_{i_L}\bar{\phi} = 0$ and to $q_i\,|\psi\rangle = 0$, giving two linearly independent null states to Q, ensuring $\mathcal{N}(H) = 4$.

When solutions to $|\kappa| = 0$ exist, it constrains exactly one hopping term. Giving three constraints total. □

We now have the following sequence of constraints

$$\begin{array}{ccccccc} E_0 & \longrightarrow & E_2 \cap X_1 & & \longrightarrow & & E_4 \cap X_3 \\ \downarrow & & \downarrow & & & & \downarrow \\ (\xi =) X_0 & \xrightarrow{|q_1|=0} & X_1 & \xrightarrow{|q_2|=0} & X_2 & \xrightarrow{|\kappa|=0} & X_3. \end{array}$$

Assuming each constraint has solutions, then we are interested in classifying the following sequence of zeroth homotopy groups

$$\mathcal{P}X_0 \xrightarrow{|q_1|=0} \mathcal{P}X_1 \xrightarrow{|q_2|=0} \mathcal{P}X_2 \xrightarrow{|\kappa|=0} \mathcal{P}X_3$$

where we have dropped the brackets for convenience.

From proposition 7.3.19 we know $|\kappa|$ is just a determinant. So we can put the constraint for $|\kappa| = 0$ on a previously unconstrained hopping term in q_i or $\mathscr{C}_{i,j}$ or q_j. For another perspective, we also know from the previous way we proved there are three constraints in proposition 7.3.7 that this is a linear constraint, and so there are two topologically distinct regions to $\mathcal{P}X_2$. Finally, we know from section 7.3.1 $\mathcal{P}X_1$ is trivial as it is path connected. This leads to the following sequence of zeroth homotopy groups

$$N\mathbb{Z}_2 \to 0 \to 0 \to \mathbb{Z}_2 \to \mathcal{P}X_3 \to \cdots. \tag{7.3.68}$$

In proposition 7.3.6 we know there must be at least three constraints to satisfy $\mathcal{N}(H) = 4$. In proposition 7.3.19 we have given a construction requiring exactly three constraints on the hopping terms of H. Therefore, this construction follows the convention given in definition 7.2.1.

We now generalise this argument to get a longer sequence for the sequential topology of a finite chiral structure. Once again, we limit ourselves to considering structures where $\mathcal{N}(q_i) \leq 1$, and there are no equal sections by the partial ordering of chapter 5. For the higher steps' constraints, we also now assume that no constraint gives $\mathscr{C}_{i,j}\phi^j_j = 0$. We will consider the case where a constraint gives $\mathscr{C}_{i,j}\phi^j_j = 0$ later on.

To deal with the general sequential case, under the assumption that each constraint has solutions we first give a minimum number of constraints given the convention of definition 7.2.1. We then show that if we satisfy, pairwise, the condition for mutual orthogonality of null states from any set of sections, then this gives a higher nullity.

Definition 7.3.20. For the following proofs we require making an assumption about the support of nullstates. We will go beyond this assumption later on. For each pair of sections q_i, q_j (with the partial relation $g_i > g_j$) then if $|q_j| = 0$ and q_i has non-zero support of the nullstate from q_j, then we can write the nullstate of the biadjacency matrix Q as

$$\left|\Psi^j\right\rangle = \begin{pmatrix} A_1\psi_1^j \\ A_2\psi_2^j \\ \vdots \\ A_{j-1}\psi_{j-1}^j \\ \psi_j^j \\ 0 \\ \vdots \\ 0 \end{pmatrix}. \tag{7.3.69}$$

Where A_j is some non zero matrix, and ψ_j^j is the nullstate of q_j. Let this be known as the *assumption of support*.

Proposition 7.3.21. Consider a finite chiral structure with $\mathcal{N}(q_i) \leq 1$ for all sections i, $2n-2$ zero energy states, and with the assumption of support. By the convention in definition 7.2.1 there are at least n further constraints to get $2n$ zero energy states.

Proof. Suppose Q has $n-1$ null vectors, giving $2n-2$ zero energy states. Index each nullvector by $\left|\Psi^j\right\rangle$ and left null vector by $\left\langle \Psi_L^j\right|$ when the section j is the origin of this (left) null vector. For a new null vector from a section g_n with the biadjacency matrix q_n and null vector $|\Psi^n\rangle$ to satisfy Q we need $\left\langle \Psi_L^j\middle|\Psi^n\right\rangle = 0$ for all left null vectors $\left\langle \Psi_L^j\right|$ defining a set of $n-1$ equations.

Under the assumption of support for each pair of sections q_i, q_j with the partial relation $g_i > g_j$ then each q_i has non-zero support of the nullstate from q_j given by $A_i\left|\psi_i^j\right\rangle$. Therefore, every constraint to ensure the mutual orthogonality of the original $n-1$ null vectors of Q depend individually on each $\left|\psi^j\right\rangle$. Each $\left|\psi^j\right\rangle$ is only changed by each section's biadjacency matrix q_j so we can alter each constraint independently, by changing hopping terms in each q_j. That is the mutual orthogonality condition for each left null vector and the new null vector is independent,

$$\left\langle \Psi_L^j\middle|\Psi^n\right\rangle = 0 \not\Rightarrow \left\langle \Psi_L^i\middle|\Psi^n\right\rangle = 0. \tag{7.3.70}$$

So under the assumption of support there are at least $n-1$ independent equations of this form, and one from $|q_n| = 0$ giving at least n algebraically independent constraint maps that need to be satisfied to increase the nullity of H.

Iterating this bound on the number of constraints, we see there are at least $\sum_1^n m = n(n+1)/2$ total constraints to get a nullity of $2n$ following our convention. □

Now we have a minimum number of constraints to get a certain nullity in our $N\mathbb{Z}_2$ structure, when the conditions in definition 7.3.20 is fulfilled, follows the triangular numbers. We will now give a construction for the constraint maps that exactly satisfy this lower bound.

Proposition 7.3.22. For a structure with a nullity of $2n-2$, then for a Hamiltonian satisfying the conditions in definition 7.3.20 there are exactly n further constraints required to get $\mathcal{N}(H) = 2n$.

Proof. Take a Hamiltonian H of a graph G with the biadjacency matrix Q. Let g_n be the section that will be made singular (under the convention in definition 7.2.1). For each singular section g_i with biadjacency matrix q_i, let $\left|\Phi^i\right\rangle$ denote the nullstate of Q with an origin from the section g_i. Let ϕ^i_j denote the support of the nullstate $\left|\Phi^i\right\rangle$ on the section g_j.

By the conditions in definition 7.3.20 the nullstate $\left|\Phi^i\right\rangle$ has support on each q_j where $g_j > g_i$ by the partial ordering. Take the singular sections and partition them to two sets: m below sections $g_i < g_n$ and $n-m-1$ above sections $g_i > g_n$ by the partial ordering.

The first constraint is to set $|q_n| = 0$. Let this define a potential nullstate $|\Psi_n\rangle$ of Q with support on each section above $g_i > g_n$ of ψ^i_n.

We now take the m below sections. By the condition in definition 7.3.20 each nullstate from a below section has support on q_n. For each nullstate to be defined on Q we need to be able to write ϕ^i_n as a linear sum of the columns of q_i — the *orthogonality condition* — for each below section. Letting ϕ^i_n denote the support on q_n from the nullstate originating from q_i then we can define a nullstate $\left|\Phi^i\right\rangle$ on Q when

$$\det\begin{pmatrix} q_n^{l\neq k} & \phi^i_n \end{pmatrix} = 0. \tag{7.3.71}$$

From proposition 7.3.21 we know for each nullstate this constraint is independent, defining m constraints on the hopping terms of H.

We now consider the $n-m-1$ above singular sections. For $|\Psi_n\rangle$ to be defined on Q we need to be able to write, for each above section with the biadjacency matrix q_i, the support of nullstate ψ^n_i on q_i as a linear combination of the columns of q_i. This is satisfied when, for each q_i

$$\det\begin{pmatrix} q_i^{l\neq k} & \psi^n_i \end{pmatrix} = 0. \tag{7.3.72}$$

Under the conditions in definition 7.3.20 this needs to be satisfied for each above section biadjacency matrix q_i giving $n-m-1$ further constraints.

Satisfying all of these constraints allows n linearly independent null vectors to be defined on Q, therefore $\mathcal{N}(Q) = n$ and $\mathcal{N}(H) = 2n$. In total this corresponds to $1+m+n-m-1 = n$ constraints on the hopping terms. □

Remark. The boundary operator $c^{2n-2}_{i+n} : E_{2n-2} \cap X_i \to E_{2n} \cap X_{i+n}$ is defined with the composition of the n constraint maps defined in proposition 7.3.20, such that the Hamiltonian does not have $2n+2$ zero energy states.

Remark. We now have n further constraints to satisfy a Hamiltonian with $2n-2$ zero energy states. Iterating for each n this gives a total of $\frac{n(n+1)}{2}$ constraints on the Hamiltonian. So if we relax one constraint, then the Hamiltonian has, for almost all hopping terms, $2n-2$ zero energy states. It is the subspace defined by $\frac{n(n+1)}{2} - 1$ constraints that is topologically non-trivial.

We now know that (under our convention from definition 7.2.1) a zeroth homotopy group is non trivial when it is over a subspace defined by one less than a triangular number of constraints. So we have the following sequence of subspaces

$$N\mathbb{Z}_2 \to 0 \to \mathbb{Z}_2 \to 0 \to 0 \to \mathcal{P}X_5 \to \cdots \tag{7.3.73}$$

where the zeroth homotopy group (under our convention for constraints) is non-trivial when the index i of $\mathcal{P}X_i$ is one less than a triangular number. Furthermore we know from proposition 7.2.4 that each constraint map corresponds to solving the determinant of a subgraph of G, so this sequence becomes

$$N\mathbb{Z}_2 \to 0 \to \mathbb{Z}_2 \to 0 \to 0 \to M\mathbb{Z}_2 \to \cdots \tag{7.3.74}$$

where M is the number of irreducible factors of the final constraint map.

Now we have the number of constraints that define a boundary operator $c^{2n}_{i+n} : X_i \cap E_{2n-2} \to X_{i+n} \cap E_{2n}$. However, there are some instances this number of constraints is reduced. This happens exactly when the assumption of support is not satisfied. That is, the conditions in definition 7.3.20 are not met as now $A_{j-n}\psi^j_{j-n} = 0$ for some A_{j-n}. There are two possible ways this can happen, under the convention defined in 7.2.1.

The first case is when two (or more) sections are equal by the partial ordering. Consider two sections g_i and g_j which are equal by the partial ordering ($g_i = g_j$) then the effective subgraph of these two sections has the biadjacency matrix

$$\begin{pmatrix} q_i & 0 \\ 0 & q_j \end{pmatrix}. \tag{7.3.75}$$

Therefore, any nullstate from g_j (g_i) has no support on g_i (g_j). For each equal section (by the partial ordering) to the section being made singular (by a boundary operator) this reduces the number of constraint maps in the boundary operator by one.

The second way the assumption of support is broken is when a constraint map sets $A_{j-n}\psi^j_{j-n} = 0$ for some n. For each n that $A_{j-n}\psi^j_{j-n} = 0$ this reduces the number of constraint maps by one. Individually a constraint that sets $A_{j-n}\psi_j = 0$ can ensure the nullstate is not supported on sections which are further from the new critical section (by the partial ordering), so it is important constraints are calculated via the partial ordering. Because this is accounted for when computing constraints, then our approach still captures the sequential topology of a structure under the convention in definition 7.2.1.

To tie all of the above together, we now outline the procedure to compute the sequential topological classification of a particular structure. To do this we consider a Hamiltonian H with $2n-2$ zero energy states, a set of $n-1$ singular sections $\{g_j\}$ which originate the null states, and a section g_n which we wish to make singular. Let g_j provide the null vector that satisfies $Q\left|\Phi^j\right\rangle$ which has support on the section q_i with ϕ^j_i. This procedure requires partitioning the set of singular sections into m sections below g_n and $n-m-1$ sections above g_n.

We denote by $C_{j,i}$ the matrix connecting the jth section to the ith section in Q, and ϕ^j_i is the support of the null vector originating from the jth section on the ith section.

For g_n specifically ψ_i^n is the support of the nullvector from g_n on the ith section. For a biadjacency matrix q_i then $q_i^{l\neq k}$ is q_i with the kth column deleted.

The procedure is as follows:

1. Require q_n to be non-singular (for now). Let $\bar{q}_n$ be the biadjacency matrix of g_n where $|\bar{q}_n| = 0$.
2. Compute the set of null vectors that satisfy Q.
3. Start with the section g_j most below g_n.
   (a) Compute
   $$\bar{\phi}_n^j = \sum_{g_i<g_n} C_{n,i}\phi_i^j. \tag{7.3.76}$$
   (b) Delete a column $\bar{q}_n^k$ of $\bar{q}_n$, replacing it with $\bar{\phi}_n^j$. Compute
   $$\det\begin{pmatrix} \bar{q}_n^{l\neq k} & \bar{\phi}_n^j \end{pmatrix}. \tag{7.3.77}$$
   (c) Choose an irreducible factor of this equation, this defines a constraint map. Satisfy this on the Hamiltonian.
   (d) Repeat, increasing the sections via the partial ordering, until the constraint maps are satisfied for all the below singular sections of g_n.

Now we turn to the sections above g_n.

1. We now require $|q_n| = 0$, so set $q_n = \bar{q_n}$.
2. Begin the the section g_j that is the least above g_n.
   (a) Compute
   $$\bar{\psi}_i^n = \sum_{g_n<g_i<g_j} C_{j,i}\psi_i^n. \tag{7.3.78}$$
   (b) Delete a column q_j^k of q_j, replacing it with $\bar{\psi}_i^n$. Compute
   $$\det\begin{pmatrix} \bar{q}_j^{l\neq k} & \bar{\psi}_i^n \end{pmatrix} \tag{7.3.79}$$
   (c) Choose an irreducible factor of this equation, this defines a constraint map. Satisfy this constraint on the Hamiltonian.
   (d) Repeat, increasing in the partial ordering of the sections.

This procedure defines a set of constraint maps for the boundary operator $c_{i+n}^{2n} : E_{2n-2} \cap X_i \to E_{2n} \cap X_{i+m}$. Even though this procedure defines an order to satisfy constraint maps, now we have the constraint maps we can apply them in any order to satisfy the boundary operator.

7.4 An extension for sequential topology in complex finite chiral structures

As discussed in section 5.7.1 the zeroth topology of a finite complex chiral Hamiltonian is trivial, but such structures can have a non-trivial sequential topology. To understand this consider closing a gap by solving

$$|H| = -\prod |q_i||q_i^\dagger| = 0. \tag{7.4.80}$$

As in the real case, $|q_i|$ is linear for each hopping term in its expansion, but it is now over complex terms. Solving equation (7.4.80) thus imposes 2 constraints on an individual hopping term, one on the absolute value and one on the phase (or equivalently one on the real part and another on the imaginary part). That is to satisfy an irreducible polynomial which defines constraints for a hopping term $u \in \mathbb{C}$ then

$$u = a + bi. \tag{7.4.81}$$

As in section 7.3.2 we can define constraint maps to satisfy $|H| = 0$. Satisfying these two constraints indicates a complex finite Hamiltonian can have a non-trivial sequential topology.

The sequences of zeroth homotopy groups of a real Hamiltonian, defined on some structure G, and those of a complex Hamiltonian defined on the same structure G are very related. For each constraint map of a real structure, there are two constraint maps of a complex structure. This means that the number of constraint maps is doubled for each boundary operator. This allows a simple extension of the theory of sequential topology on real structures to be extended to complex structures.

There are two further consequences to the classification of a complex structure. The first is that the fundamental theorem of algebra ensures each polynomial that defines a pair of constraint maps always has a solution. As a result, the upper bound (we will discuss in section 7.5.1) on the nullity of a structure is tight. The second is that each pair of constraint maps becomes a single constraint when we make the structure infinitely periodic. This is a natural extension of the topology discussed in chapter 5.

We begin by proving the correspondence between the sequence of homotopy groups for real structures. Because each polynomial that defines constraints now defines two constraint maps, we then define a pair of constraint maps to satisfy this polynomial.

Proposition 7.4.1. Under the convention in definition 7.2.1 each polynomial defining a constraint map in a real Hamiltonian $H_\mathbb{R}$ defined on a structure G gives two constraint maps for a complex Hamiltonian $H_\mathbb{C}$ defined on G.

Proof. From proposition 7.2.4 we know that each term in the secular equation can be written as a sum of the determinants of subgraphs of the structure,

$$a_{2n} = \pm \sum |q_m||q_m^\dagger|. \tag{7.4.82}$$

So constraint maps are defined as the sum of polynomials $|q_m| = p_m$. Writing $p_m = (\alpha_m + \beta_m h)$ for some hopping term h we see

$$p_m p_m^* = |\alpha_m|^2 |h|^2 + \alpha_m \beta_m^* h + \alpha_m^* \beta_m h^* + |\beta_m|^2 \tag{7.4.83}$$

which is a non-negative equation with all real terms. So the polynomials $p_m p_m^*$ and $p_{m'} p_{m'}^*$ in the sum in equation 7.4.82 can only be combined if they share a common factor. This is exactly the origin of the polynomials that define constraint maps under the convention in definition 7.2.1, so the boundary operators are defined by the same polynomials, but now over the complex numbers.

Finally, for each polynomial that defines constraint maps, in a complex structure this defines two constraint maps. □

We now have a simple way to extend the classification of the sequential topology of real structures to that of complex ones. The boundary operators have double the number of constraint maps that define them, otherwise the classification is largely the same. For structures that satisfy the condition in definition 7.3.20 this means a subspace is non-trivial exactly when it is indexed by 2 times a triangular number minus one. Otherwise, the boundary operators are defined in exactly the same way, ensuring each such subspace has the classification $\mathbb{Z}_2$. Thus giving the general classification (when each section is constrained by $\mathcal{N}(q_i) \leq 1$)

$$0 \to N\mathbb{Z}_2 \to 0 \to 0 \to 0 \to \mathbb{Z}_2 \to 0 \to 0 \to 0 \to 0 \to 0 \to 0 \to M\mathbb{Z}_2 \to \cdots \tag{7.4.84}$$

To make this extension to complex Hamiltonians explicit, we define the pair of constraint maps for each polynomial that defines a boundary operator. We note that there are many equivalent ways we these constraint maps may be defined.

Definition 7.4.2. For each polynomial p defining constraints on the Hamiltonian, the constraint maps come in pairs. Let p have solutions when $h = \rho e^{i\theta}$. The first constraint map acts on the absolute value of h,

$$b_i^{\text{abs}}(X_i) := \{X_{i+1} \,||h| = \rho\}\,. \tag{7.4.85}$$

The second constraint map takes $\arg(h) \mapsto \theta$, where

$$b_i^{\text{arg}}(X_i) := \{X_i | \arg(h) = \theta\}. \tag{7.4.86}$$

Just as in the case for the constraint maps on a real Hamiltonian, the constraint maps that define a boundary operator on a complex Hamiltonian may be applied in any order.

7.4.1 A note on sequential topology and infinitely periodic structures

In chapter 5 we demonstrated that a structure with an $N\mathbb{Z}_2$ zeroth step classification necessarily has a $2N \times 2N$ upper triangular transfer matrix when cutting the structure for one input and one output site on each section. Using the triangular transfer matrix we demonstrated that for complex Hamiltonians, the zeroth step topology becomes non-trivial

when extending each section to be infinitely periodic. We now give an extension to this to understand how our notion of sequential topology extends to infinite structures with complex Hamiltonians.

In the introduction, we remarked how our zeroth step topology can be used to predict the higher order topology of an infinitely periodic system, where we periodically repeat each section. To see this, consider infinitely repeating each section of the Hamiltonian giving a structure with N stacked $1d$ topological insulators. For each section we may define a $1d$ winding number around Brillouin zone, which may have a trivial or non-trivial Berry phase. The Berry phase associated to each section relates to the finite topological invariant of each section, as discussed in chapter 5. As such, the zeroth step classification does, in a sense, predict the higher order topology of chiral structures. If we truncate our system to be semi-infinite for each section, a section in a non-trivial phase will have topologically robust zero energy states localised to the boundary of that section.

We now wish to understand how sequential topology is extended to an infinitely periodic system. That is, when a section is topologically marginal, what number of constraints on the hopping terms are needed to give a second gap closure in the spectrum? For this discussion we assume that such a system is infinitely periodic in each section, and all hopping terms are complex unless otherwise specified.

To avoid confusion, we refer to higher order topology of a Hamiltonian as $T(H)$ and sequential topology as $\tau(H)$.

Definition 7.4.3. For a Hamiltonian H on G which is infinitely periodic in each section g of G, then $\tau(H)$ is the topological classification of a subspace of ξ corresponding to a (higher steps') topological phase boundary.

To understand gap closures in an infinitely periodic system, we will use the transfer matrix formalism, where we infinitely and periodically repeat each individual section and so we have a triangular transfer matrix (as discussed in section 5.7) with two entries on the diagonal corresponding to each section. Consider a real Hamiltonian with the transfer matrix M and eigenvalue λ_i corresponding to the section g_i. If we evolve hopping terms of H such that

$$\lambda_i > 1 \to \lambda_i < 1 \tag{7.4.87}$$

then if $\lambda_j \neq 1$ for all $j \neq i$ this system undergoes a topological phase transition. The reason sequential topology $\tau(H)$ is trivial for many subspaces of ξ is that if $\lambda_j = 1$ as $\lambda_i > 1 \to \lambda_i < 1$ then M becomes defective. In other words, M does not have linearly independent null states. The problem of $\tau(H)$ in finite systems studies the constraint maps on H that make it not defective, in other words this is the problem we discuss in section 7.3. This problem changes for complex infinite Hamiltonians.

For a complex infinite Hamiltonian, the problem of defective eigenvalues of M is reduced. This is because a triangular matrix M is almost always defective when M has degenerate eigenvalues, but if all eigenvalues of M are distinct, then M is not defective. For a complex Hamiltonian the eigenvalues of M have a phase. This ensures eigenvalues of the same magnitude are almost always non-defective.

In a complex Hamiltonian then H undergoes a spectral gap closure somewhere in the Brillouin zone when

$$|\lambda_i| > 1 \to |\lambda_i| < 1 \tag{7.4.88}$$

if λ_i is not defective when $|\lambda_i| = 1$. That is, if $\text{Arg}(\lambda_i) \neq \text{Arg}(\lambda_j)$ for all j such that $|\lambda_j| = 1$ during this transition then there is an unavoidable gap closure in the Brillouin zone. So if we maintain all $|\lambda_j| = 1$ eigenvalues of M having distinct phases, then we get a non-trivial sequential topology $\tau(H)$. This requirement defines a constraint map on the hopping terms.

Definition 7.4.4. Let $\{\lambda_i\}$ be the set of eigenvalues of M such that $|\lambda_i| = 1$. Let $\lambda_j(t)$ be an eigenvalue of M that is being continuously evolved such that

$$|\lambda_j(0)| > 1 \to |\lambda_j(t)| < 1. \tag{7.4.89}$$

Let $b : \mathbb{C} \times \mathbb{R} \to \mathbb{C}$ act on λ_j such that

$$b(\lambda_j, t) := \lambda_j e^{2\pi i \theta t} \tag{7.4.90}$$

where $\text{Arg}\left(\lambda_j e^{2\pi i \theta t}\right) \neq \text{Arg}(\lambda_i)$ when $|\lambda_j| = 1$ for all $i \neq j$.

There are two ways we can interpret this constraint map. The first assumes we have complete control of the phases of hopping terms in the Hamiltonian. In such a case the constraint map is fundamentally important to ensure $\tau(H)$ is non-trivial, so

$$\mathcal{P}X_i \tag{7.4.91}$$

is non-trivial only for even i. However, this constraint map is different from the constraint maps defined in our previous discussion. This is because the constraint map gives a subset of spaces all the same dimension as the subspace the constraint map operates, as displayed in Fig. 7.4.1. This gives rise to a second, perhaps more physically relevant interpretation of $\tau(H)$.

The second interpretation of $\tau(H)$ is to assume we do not have exact control of the (complex) phases of hopping terms, this makes every higher steps' subspace of ξ topologically non-trivial. This is because the complement of the constraint map defines a subspace of ξ is one dimension lower than the subspace b is operating on, so is measure zero on the phase boundary. As such, if we do not have exact control of the phases of hopping terms with probability 1 the map

$$|\lambda_i| > 1 \to |\lambda_i| < 1 \tag{7.4.93}$$

defines a $\tau(H)$ sequential topological phase transition.

Given these two pictures, we now have which subspaces of ξ (for $\tau(H)$) of an infinitely periodic complex Hamiltonian are topologically non-trivial.

We now show each non-trivial subspace has a $\mathbb{Z}_2$ classification. The constraint map for each subspace is given by solutions to

$$|\lambda_i| = 1. \tag{7.4.94}$$

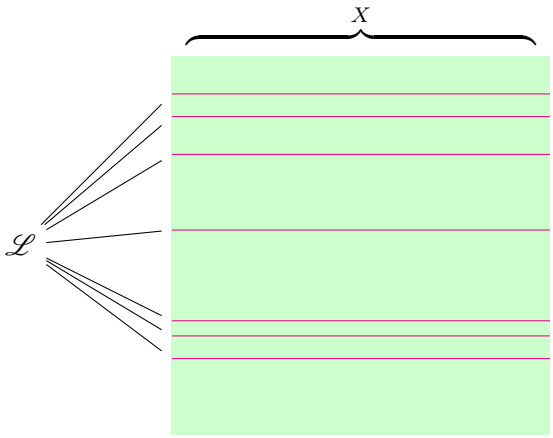

Figure 7.4.1: A 2D plane representing a slice X of a parameter space ξ. The collection of lines $\mathscr{L}$ denote the set of phases that give defective eigenvalues in the transfer matrix. The lines are of zero width so have zero measure in X.

Let h be a hopping term in the section g_i. Then for each section we get the irreducible polynomial

$$|q_i| = ah + b \tag{7.4.95}$$

where a, b are polynomials of the hopping terms in g_i. When

$$|h| = \left|\frac{-b}{a}\right| \Rightarrow |\lambda_i| = 1. \tag{7.4.96}$$

Because $|q_i|$ is an irreducible polynomial there are two disconnected regions separated by $|\lambda_i| = 1$, so we get a $\mathbb{Z}_2$ classification of each non-trivial subspace.

This gives two sequences for $\tau(H)$ for infinitely periodic complex Hamiltonians, one for each interpretation on the necessity of the constraint map in definition 7.4.4.

$$\begin{aligned} &N\mathbb{Z}_2 \to 0 \to \mathbb{Z}_2 \to 0 \to \mathbb{Z}_2 \to 0 \to \mathbb{Z}_2 \to 0 \to \mathbb{Z}_2 \to \cdots \\ &N\mathbb{Z}_2 \to \mathbb{Z}_2 \to \mathbb{Z}_2 \to \mathbb{Z}_2 \to \mathbb{Z}_2 \to \mathbb{Z}_2 \to \mathbb{Z}_2 \to \mathbb{Z}_2 \to \cdots . \end{aligned} \tag{7.4.97}$$

7.5 Approximate homotopy for individual sections

So far, we have considered only allowing each section to provide at most 2 zero energy states to the structure. But in many structures, it is possible to have a section that provides more than 2 zero energy states. To distinguish from multiple critical sections (as discussed previously) we refer to a section with a nullity greater than 2 as a hyper-critical section.

Definition 7.5.1. Consider a structure G with a section g having the biadjacency matrix q. If $\mathcal{N}(q) \geq 2$ we say g is *hyper-critical* or has *hypercriticality*.

If a section can become hyper-critical then the sequence of subspaces, and therefore our zeroth homotopy theory, is altered. This is because we can no longer rely on the localisation of nullstates to be related to the partial ordering of sections. This ensures the number of

constraint maps that define a boundary operator are no longer given by a triangular number. As we will demonstrate, if hyper-criticality is possible on an individual section, then hyper-criticality requires at most a square number of constraints. We conjecture that under a similar convention to that in definition 7.2.1 this is an optimal number of constraints, however, we have no proof of this.

The sequence of subspaces is altered in a second way. In section 7.5.2 we will show the number of constraints required to satisfy hyper-criticality and multiple critical sections simultaneously, alters the number of constraint maps that define a boundary operator. Furthermore, we give an upper bound to the number of constraints required for each boundary map under the convention in definition 7.2.1 in the presence of hyper-critical sections. This change is not dependent on the number of constraints to get a hyper-critical section.

7.5.1 An upper bound

To understand how an individual section g can host hyper-criticality, we first look at the constraints on q to get $\mathcal{N}(q) = 1$ from a non-singular q. Consider the $M \times M$ biadjacency matrix q with rows q^i, that is

$$q = \begin{pmatrix} \cdots & q^1 & \cdots \\ \cdots & q^2 & \cdots \\ & \vdots & \\ \cdots & q^i & \cdots \\ & \vdots & \end{pmatrix}. \tag{7.5.98}$$

If we delete a row of q we have an $(M-1) \times M$ matrix. As demonstrated in chapter 5 every first minor of q is almost always non-singular, so the submatrix of q with one deleted row has maximum row rank of $M-1$. The sub-matrix when we delete the first row has a null vector ψ. That is,

$$q_1\psi = \begin{pmatrix} \cdots & q^2 & \cdots \\ & \vdots & \\ \cdots & q^i & \cdots \\ & \vdots & \end{pmatrix} \psi = 0. \tag{7.5.99}$$

When the row q^1 is orthogonal to ψ then $\mathcal{N}(q)$ is 1. This requires one constraint on q^1. To generalise this argument, we consider the case to get $\mathcal{N}(q) \geq 2$. We then demonstrate, by induction, that the number of constraints grows by a maximum of n^2 where n is the desired nullity.

Proposition 7.5.2. The number of constraints on a section g with biadjacency matrix q to get $\mathcal{N}(q) = 2$ is exactly 4 constraints.

Proof. By proposition 7.3.4 we know there are at least 4 constraints to set a section with $\mathcal{N}(q) = 2$. So here we give a construction that only requires four constraints.

Consider the biadjacency matrix q with the first two rows deleted, that is

$$q_2 = \begin{pmatrix} \cdots & q^3 & \cdots \\ & \vdots & \\ \cdots & q^i & \cdots \\ & \vdots & \end{pmatrix}. \tag{7.5.100}$$

This submatrix is $(M-2)\times M$ so has at least 2 linearly independent null vectors. Suppose we initially have $|q| \neq 0$ then there is an $(M-2)\times(M-2)$ submatrix of q_2 that contains all but 2 terms of a complete matching of g. Because q is non-singular, this matrix is almost always non-singular, therefore q_2 has (almost always) maximum rank. The maximum rank of q_2 is $M-2$ giving two linearly independent null vectors ψ_1 and ψ_2.

To get $\mathcal{N}(q) = 2$ we must satisfy the equation

$$\begin{pmatrix} q^1 \\ q^2 \end{pmatrix} \begin{pmatrix} \psi_1 & \psi_2 \end{pmatrix} = 0_2 \tag{7.5.101}$$

where 0_2 is the 2×2 zero matrix. Because each null vector is linearly independent, the constraint to satisfy $q^1\psi_1 = 0$ does not satisfy $q^1\psi_2 = 0$. Similarly, because q^1 and q^2 are initially linearly independent, this defines four total constraints, two for each row to satisfy orthogonality to each nullvector. □

Remark. For each null vector ψ_i and non-orthogonal row q^j there is one constraint for on the row q^j which is not already orthogonal to ψ_i. This is because each constraint map $q^j\psi_i = 0$ is satisfied by the solutions to a polynomial of hopping terms in H.

We now prove that there are at most n^2 constraints on q to get $\mathcal{N}(q) = n$.

Proposition 7.5.3. The number of constraints to get a $\mathcal{N}(q) = n$ is less than or equal to n^2.

Proof. Take the $(M-n)\times M$ sub matrix q_n of q where we have deleted the first n rows of q, and we initially have $|q| \neq 0$. Each complete matching of q must contain $M-n$ terms from q_n so q_n almost always has the rank $M-n$. Because $|q| \neq 0$ each row q^i is initially linearly independent.

Index the n linearly independent null vectors ψ_i of q_n by the subscript i. Let 0_n denote the $n\times n$ zero matrix. When

$$\begin{pmatrix} q^1 \\ \vdots \\ q^n \end{pmatrix} \begin{pmatrix} \psi_1 & \cdots & \psi_n \end{pmatrix} = 0_n \tag{7.5.102}$$

is satisfied then $\mathcal{N}(q) = n$. As in the $\mathcal{N}(q) = 2$ case, satisfying

$$\begin{pmatrix} q^1 \end{pmatrix} \begin{pmatrix} \psi_1 & \cdots & \psi_n \end{pmatrix} \tag{7.5.103}$$

defines n constraints. Because each row q^i of q is initially linearly independent, we must satisfy (independently) this for every row q^i with $i \leq n$. Thus giving n^2 total constraints on the hopping terms of q. □

Unfortunately, we do not have a proof that this sequence is optimal, under a convention like that in definition 7.2.1 for multiple critical sections. However, we conjecture that under a similar convention, this does give an optimal sequence of constraints.

7.5.2 Hyper-critical sections and multiple critical sections

We now have a picture for the sequential topology for multiple sections, as well as an upper bound for the number of constraint maps that define boundary operators for hyper-criticality in an individual section. We now turn to how the number of constraint maps for a boundary operator is altered when we allow both hyper-critical sections, and multiple critical sections.

Definition 7.5.4. A structure G where we allow both individual sections with hyper-criticality, and multiple critical sections is referred to as a structure with *mixed criticality* or is *mixed critical*.

Much like in the case for hyper-criticality, we will give bounds on the number of constraint maps that define a boundary operator for a mixed critical structure. To find an upper bound we assume a hyper-critical section g defines a core subgraph of G. Assuming g is core when hyper-critical ensures that each nullstate can be localised over the structure in a certain way, giving us an upper bound on the number of constraint maps. This requires writing each nullstate as a core vector of the biadjacency matrix. We can then use the boundary operators for multiple sections to get the number of constraint maps for a boundary operator.

Proposition 7.5.5. Let g_i be a section with a biadjacency matrix q_i having nullity $n_i - 1$. Let a boundary operator take $n_i - 1 \mapsto n_i$ so that the nullity of H increases by 2. Let all other singular sections g_j of H have a biadjacency matrix q_j with nullity n_j. The number of constraint maps to increase nullity by 2 for a mixed criticality structures is bounded above by $n_i^2 + \sum_{j \neq i} n_j$.

Proof. We wish to find the constraint maps that allow each nullstate from a section to be defined on the remaining critical sections of the structure. Take the effective subgraph of the critical sections of G. Let ζ_j^i denote the support of the i-th critical sections biadjacency matrix q_i's nullstates on the j-th critical sections biadjacency matrix q_j, where each column of ζ_i^i a null vector. Let ν^j denote the left null vectors of q_j.

When

$$q_j \zeta_j^i = A \zeta_i^i \tag{7.5.104}$$

has solutions for some matrix A (defined from how g_i and g_i are connected in the Hamiltonian), and every pair of sections $g_i < g_j$, then every nullstate from a critical section is defined on G. If equation 7.5.104 is satisfied, then we can write each column of ζ_j^i as a linear combination of the columns of q_j. That is every left null vector of q_j is linearly independent of every null vector of q_i so

$$\nu^j A \zeta_i^i = 0. \tag{7.5.105}$$

Because the nullity of q_i is increasing by one, only one column of ζ_i^i is not already orthogonal to each row of ν^j. This defines n_j constraint maps. This is true pairwise, for each critical section.

Including the upper bound of constraint maps from the hypercritical section in proposition 7.5.3 this gives an upper bound of $n_{g_i}^2 + \sum_{j \neq i} n_{g_j}$ constraint maps to define a boundary operator in a structure with mixed criticality. □

Remark. The constraint maps given above are defined for real Hamiltonians. To extend this to complex Hamiltonians, we can use the same argument as in section 7.4. This doubles the number of constraint maps (two for each constraint map in the real case) for complex mixed critical structures.

7.5.3 A limit on non-trivial sequential topology

Using the relationship between the subgraphs of a structure G and the terms of the secular equation, we can give a simple upper bound to the number of zero energy states that a structure may host. This is because the largest rank submatrix of H defines the rank of H. We know that any triangular matrix has only one cover, therefore the largest triangular submatrix h of H gives a minimum bound on the rank of H. Let h be $n \times n$ and H be $m \times m$, then by the rank nullity theorem $\mathcal{N}(H) \leq m - n$.

We can use this bound to find a limit of nullity for certain structures. For example, ladder graphene and an SSH chain can have at most a nullity of 2. Furthermore, recall from proposition 7.3.4 there are four constraints for an individual section to have 4 zero energy states. This ensures there are at least three cycles in each section. So this is a necessary condition for an individual section to be able to have a nullity greater than 2.

As an example, we show that a looped SSH chain can have a nullity of at most 2.

Proposition 7.5.6. For a looped SSH chain $\mathcal{N}(H) \leq 2$.

Proof. Delete any neighbouring sites in the SSH chain. The remaining structure is a connected open chain with an even number of sites. Therefore, this structure has exactly one cover so $a_2 = 0$ has no solutions. □

This is useful because there are many structures which naturally have sections given by SSH chains (for example, graphene ribbons). We give an experimental case study of a structure with sections that are analogous to looped SSH chains in section 7.7.

7.6 Experimental signatures

Physically a system on a higher steps' phase boundary has a lot of similar properties to those discussed for the zeroth step topology in chapter 5. These consequences fall in to two main categories. The first relates to the localisation of null states in a structure, and the second (a consequence of this localisation) relates to the transmittance between two sites of a cut structure. We begin by discussing some properties of the localisation of null states of a structure on a higher steps' phase boundary. We then discuss how transmittance is

affected in such a structure.

For the purposes of this section, we say a structure is on a higher steps' phase boundary when only the minimum number of constraints are satisfied for the structure to be on that boundary (under the convention in definition 7.2.1). This is because the localisation of nullstates is altered when further constraint maps are satisfied, as discussed below. Furthermore, because we only have an upper bound on the number of constraint maps for individual sections, unless otherwise stated, we consider multiple critical sections only.

We begin by considering a structure G with a subset of n singular sections $\{g_s\} \in G$, such that the minimum number of constraint maps are satisfied to ensure $\mathcal{N}(H) = 2n$ with $\mathcal{N}(q_s) = 1$.

Proposition 7.6.1. For such a structure on a higher steps' phase boundary with critical sections g_s of G, then each critical section has support for a nullstate on both sub lattices.

Proof. When we satisfy a boundary operator for all the g_s sections, then each section, a priori, provides two nullstates to G. That is each critical sections' biadjacency matrix q originates a state on one partite set, and $q^\dagger$ on the complementary partite set. Therefore, each critical section, when the Hamiltonian is on a higher steps' phase boundary, hosts a state on both partite sets. □

We can give a much stronger consequence when no first minor of a section can be set to zero. This is a feature in a large number of structures, such as those with SSH like sections.

Proposition 7.6.2. Consider a structure such that no first minor of a section can be set to zero. For such a structure on a higher steps' phase boundary with $2n$ zero energy states, and n critical sections $\{g_s\}$ of G, then for the set of critical sections $\{g_s\}$ has a $2n$-core effective subgraph.

Proof. On each section, no first minor of a section can be set to zero. Therefore, for each critical section g_s is a 2-core graph. So the effective subgraph of the g_s critical sections is $2n$-core. □

Remark. We conjecture that, for any structure which is on a higher steps' phase boundary, the effective subgraph of all the singular sections is a core graph. This is something we have found numerically for all investigated structures, but we do not have a proof.

We now consider how the partial ordering affects support of nullstates on non-critical sections. For a non-singular section g there are three possibilities: g is below all singular sections, g is above all singular sections, and g has both above and below singular sections.

In the first two cases, the localisation of nullstates is identical to that of a single section as discussed in section 5.3.1.1. This is because nullstates on g are restricted to only one sublattice for each nullstate from a singular section.

The final case is different, because a structure may now have at least one singular section $g_i < g$ and at least one singular section $g_j > g$ that provide nullstates to H.

Proposition 7.6.3. If a non-singular section g is below some singular sections, and above others, g may have support of nullstates on both sub lattices.

Proof. We can partition the singular sections in to two sets, those below g and those above g. From Chapter 5 we know every singular section below g may provide nullstate to G with support on one sublattice of g. Furthermore, we know there are nullstates for a section above g defined over G. This may provide support to nullstates on the other sub lattice of g. Therefore, g may support nullstates on both sub lattices. □

Corollary 7.6.4. If $\mathcal{G}$ is a core graph, then any non-singular section $g \in G$ which is not equal to at least one singular section (by the partial ordering) has support of nullstates on at least one site of each sublattice of g which may support nullstates.

Proof. Take a non-singular section g_i. Let $\mathcal{G}_a$ denote the effective subgraph of above singular sections and $\mathcal{G}_b$ denote below singular sections. Take the effective subgraph of $g, \mathcal{G}_a, \mathcal{G}_b$ with the biadjacency matrix

$$\begin{pmatrix} Q_a & \mathscr{C}_{a,i} & \mathscr{C}_{a,b} \\ 0 & q_i & \mathscr{C}_{i,b} \\ 0 & 0 & Q_b \end{pmatrix}. \tag{7.6.106}$$

Because q_i is not equal to any section in $\mathcal{G}_a, \mathcal{G}_b$ then $\mathscr{C}_{a,i}$ and $\mathscr{C}_{i,b}$ are non-zero. Furthermore, $\mathcal{G}$ is core so every site in the effective subgraph of $\mathcal{G}_a$ and $\mathcal{G}_b$ has non-zero support of a nullstate. Therefore, g_i supports a nullstate on at least one site of each sub lattice of q_i that may support a nullstate. □

We now turn to a consequence in the transmittance of a structure on a higher steps' phase boundary. Suppose we have two sections g_i and g_j and by the partial ordering $g_i > g_j$. Assume $|q_i| = 0$ and $|q_j| = 0$. Cut a site on g_i that connects to a below section g_k such that $g_k \geq g_j$. Assume for all l the sections $g_i < g_l < g_j$ are non-singular. An example of this kind of cut is given in Fig. 7.6.1. We will show that unit transmittance occurs on a cut structure with a core effective subgraph only if the structure is on a higher steps' phase boundary.

Proposition 7.6.5. Inter section transmittance for a structure cut as in Fig. 7.6.1 is value 1 between sections with a core effective subgraph only when on a higher steps' phase boundary.

Proof. Take the subgaph $\bar{G}$ of g for every section $g_i \geq g_k \geq g_j$ by the partial ordering. Cut the site on g_i as described in Fig. 7.6.1. This gives the corresponding biadjacency matrix for the cut structure of

$$\bar{q}_{\text{cut}} = \begin{pmatrix} q_i & C_{i,i+1} & \cdots & C_{i,j} & a \\ 0 & q_{i+1} & \cdots & C_{i+1,j} & 0 \\ \vdots & \vdots & \ddots & \vdots & \vdots \\ 0 & 0 & \cdots & q_j & 0 \end{pmatrix}. \tag{7.6.107}$$

Let $\bar{q}$ denote the biadjacency matrix for the corresponding uncut structure. Then if G is on a higher steps' phase boundary, and the effective subgraph is core then there is a null

state of the uncut structures biadjacency matrix $\bar{q}$ such that

$$\bar{q}\Psi^j = \bar{q}\begin{pmatrix} \psi_i^j \\ \psi_{i+1}^j \\ \vdots \\ \psi_j^j \end{pmatrix} = 0 \tag{7.6.108}$$

where ψ_i^j has support on the site of q_i that we cut. Summing over all nullstates of critical sections $g_j < g_i$ we get the nullstate

$$\Psi = \sum_{g_j < g_i} \Psi^j \tag{7.6.109}$$

where Ψ^j is a nullstate originating from the section g_j. We now partition the support of Ψ over the cut and uncut sites of g_i to get

$$\Psi_i = \begin{pmatrix} \phi_1 \\ \alpha \\ \phi_2 \end{pmatrix} \tag{7.6.110}$$

where α is the support of the sum of nullstates on the cut site, ϕ_2 is support on below sections $g_j < g_i$ and ϕ_1 is support on the uncut sites of g_i, equal sections and above sections $g_k \geq g_i$.

Because we are looking for a higher steps phase transition, we already have some nullstates in the uncut structure so we can define a nullstate of the biadjacency matrix of the uncut structure $\bar{q}$ (related to the biadjacency matrix in equation (7.6.107)) given by

$$\begin{pmatrix} \Psi \\ \alpha \end{pmatrix}. \tag{7.6.111}$$

where α is the voltage on the site that will be cut. Because cutting the structure introduces one extra site then we always have

$$\bar{q}_{\text{cut}} \begin{pmatrix} \Psi \\ \beta \end{pmatrix} = 0 \tag{7.6.112}$$

If $\beta = \alpha$ satisfies this equation, then

$$\bar{q}\Psi = 0 \tag{7.6.113}$$

which occurs only when on a higher steps' phase boundary. This ensures the input and output voltage is the same.

We now consider the transfer matrix for the structure on the cut site only. At zero energy this is a 2×2 transfer matrix M where

$$\begin{pmatrix} V_{\text{out}} \\ I_{\text{out}} \end{pmatrix} = \begin{pmatrix} a & 0 \\ 0 & b \end{pmatrix} \begin{pmatrix} V_{\text{in}} \\ I_{\text{in}} \end{pmatrix} \tag{7.6.114}$$

Where a, b are rational functions of the hopping terms of H. We know from the above argument that $V_{\text{out}} = V_{\text{in}}$, so assuming no losses $|M| = 1$ so $b = 1$ too, so at a higher steps' phase boundary the current input equals the current output.

Finally, we have assumed that the uncut subgraph corresponding to $\bar{q}$ is core when on a higher steps' phase boundary. This ensures that every white site in $\bar{q}$ has non-zero support of null states, meaning the voltage output and the current output are both non-zero, giving perfect transmittance. □

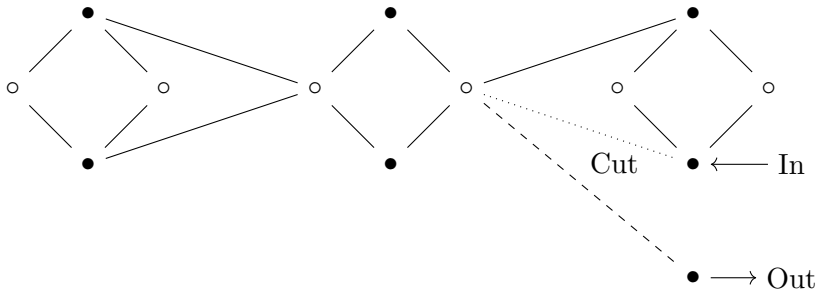

Figure 7.6.1: A structure with three non-trivial sections corresponding to a $3\mathbb{Z}_2$ structure. One site is cut on a hopping term that connects the two different sections (represented by a dotted line). This creates a new site connected on the dashed line, and the dotted connection between the two sections is removed. This allows the transmittance experiment described above to be undertaken.

7.7 A theoretical and experimental case study

In this section, we will give a case study where we use the techniques developed in section 7.3 to classify the sequential topology of a particular structure. We will then predict physical attributes of sequential phase transitions in this specific structure following the predictions in section 7.6. Finally, we experimentally verify these predictions in a coaxial cable network of the structure displayed in Fig. 7.7.1.

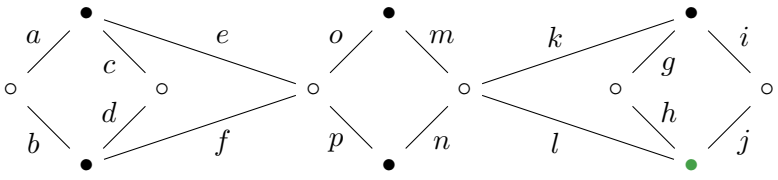

Figure 7.7.1: The structure we will carry out an experimental and theoretical case study on. Each labelled hopping term is real and algebraically independent. The green solid site denotes the site which was experimentally measured to confirm properties of the localisation throughout different sequences of sequential phase transitions.

For a case study, we consider the structure illustrated in Fig. 7.7.1 with all real hopping terms. We initially assume algebraically independent hopping terms before applying

constraint maps. This structure has a $3\mathbb{Z}_2$ zeroth step classification, and the following biadjacency matrix

$$Q = \begin{pmatrix} q_3 & C_{3,2} & C_{3,1} \\ 0 & q_2 & 0 \\ 0 & 0 & q_1 \end{pmatrix} = \begin{pmatrix} m & n & k & l & 0 & 0 \\ o & p & 0 & 0 & e & f \\ 0 & 0 & g & h & 0 & 0 \\ 0 & 0 & i & j & 0 & 0 \\ 0 & 0 & 0 & 0 & a & b \\ 0 & 0 & 0 & 0 & c & d \end{pmatrix}. \tag{7.7.117}$$

This structure has SSH like sections so by proposition 7.5.6 each section can have, at most, a nullity of 2. So for each sequence of zeroth homotopy groups, using the convention for defining constraint maps in definition 7.2.1, there is one boundary operator for each section.

There are 6 distinct sequences of homotopy groups for this structure. This is because, as we will demonstrate, each constraint map for this structure is irreducible. So with 3 sections there are $3! = 6$ distinct sequences of subspaces. We now give the full derivation for the boundary operators for one of these sequences, and then state the boundary operators for the remaining sequences.

We consider the sequence of boundary operators associated to setting g_1 then g_2 then g_3 to be singular. The first boundary operator is defined with the constraint map which is satisfied when

$$|q_1| = ad - bc = 0. \tag{7.7.118}$$

For this example, to apply this constraint map we set $c = \frac{ad}{b}$.

For the second boundary operator we can use the partial ordering $g_2 = g_1$. That is, there are no singular sections above or below g_2 so the second boundary operator is defined with the constraint map which is satisfied when

$$|q_2| = gj - ih = 0. \tag{7.7.119}$$

This is irreducible, so the 1st steps' subspace has a classification of $\mathbb{Z}_2$. For the purpose of this example, we apply this constraint map by setting $i = \frac{gj}{h}$.

Finally, we have the section $g_1 = g_2 < g_3$. So with 2 singular sections above g_3 by the protocol outlined in the list 7.3.3.1 the first constraint map comes from setting g_3 to being singular. So the first constraint map is given with

$$|q_3| = mp - on = 0. \tag{7.7.120}$$

As the two remaining sections are equal by the partial ordering, we can choose to find the remaining constraint maps in either order. We first consider g_2. By proposition 7.3.22 to find this constraint map we need to find the null vector of q_2. Letting $i = \frac{gj}{h}$ this gives a null vector

$$\psi_2^2 = \begin{pmatrix} h \\ -g \end{pmatrix}. \tag{7.7.121}$$

We now need to find a set of hopping terms for which the equation

$$q_3\psi_3^2 = -C_{3,2}\begin{pmatrix} h \\ -g \end{pmatrix} \tag{7.7.122}$$

has solutions. By proposition 7.3.20 this is satisfied when

$$|\kappa_1| = \det\begin{pmatrix} n & 0 \\ p & kh - lg \end{pmatrix} = m(kh - lg) = 0 \tag{7.7.123}$$

defining the second constraint map for this boundary operator. For this example, we solve equation (7.7.123) with $k = \frac{lg}{h}$.

We now consider g_1. Because $g_1 = g_2$ by the partial ordering, the final constraint map is satisfied when

$$q_3\psi_3^1 = -C_{3,1}\begin{pmatrix} b \\ -a \end{pmatrix} \tag{7.7.124}$$

has solutions. So we now need to solve

$$|\kappa_2| = \det\begin{pmatrix} n & 0 \\ p & eb - fa \end{pmatrix} = n(eb - fa) = 0. \tag{7.7.125}$$

This gives the three constraint maps for the final boundary operator, which are defined by

$$\begin{aligned} mp - on &= 0 \\ kh - lg &= 0 \\ eb - fa &= 0 \end{aligned} \tag{7.7.126}$$

each of which is irreducible, so relaxing a single constraint map gives a subspace with the classification of $\mathbb{Z}_2$.

To illustrate one of the 6 sequences of subspaces, and zeroth homotopy groups (for setting g_1 then g_2 then g_3 as singular) we choose to apply the constraint maps for the final boundary operator in the order derived above. This gives the following diagram

$$\begin{array}{ccccccccccc}
E_0 & \xrightarrow{c_1^0} & E_2 \cap X_1 & \xrightarrow{c_2^4} & E_4 \cap X_2 & & \xrightarrow{\qquad\qquad c_5^6 \qquad\qquad} & & & & E_6 \cap X_5 \\
\downarrow & & \downarrow & & \downarrow & & & & & & \downarrow \\
(\xi =)X_0 & \xrightarrow{|q_1|=0} & X_1 & \xrightarrow{|q_2|=0} & X_2 & \xrightarrow{|q_3|=0} & X_3 & \xrightarrow{|\kappa_1|=0} & X_4 & \xrightarrow{|\kappa_2|=0} & X_5 \\
\downarrow & & \downarrow & & \downarrow & & \downarrow & & \downarrow & & \downarrow \\
3\mathbb{Z}_2 & \longrightarrow & \mathbb{Z}_2 & \longrightarrow & 0 & \longrightarrow & 0 & \longrightarrow & \mathbb{Z}_2 & \longrightarrow & 0
\end{array}$$

There are 5 remaining topologically distinct sequences of subspaces. To classify these sequences we only need to consider the order we define boundary operators. This is because the constraint maps for each sequence are the same, but they are grouped together differently for each boundary operator, a consequence of the commutativity of constraint maps. To see this, consider a pair of unequal (by the partial ordering) sections $g_i < g_j$, setting g_i then g_j to being singular defines three constraint maps. The first is from solving $|q_i| = 0$

the second is from solving $|q_j| = 0$ and the third from satisfying the solutions of q_i on q_j. Applying these constraint maps in any order defines the same subspace.

Under these considerations, we have the following diagram of subspaces, where we use the superscript to denote the order in which sections are being set to being singular.

$$\begin{array}{ccccccccccc}
X_0 & \xrightarrow{|q_1|=0} & X_1^1 & \xrightarrow{|q_2|=0} & X_2^{1,2} & \xrightarrow{|q_3|=0} & X_3^{1,2,3} & \xrightarrow{kh-lg=0} & X_4^{1,2,3} & \xrightarrow{eb-fa=0} & X_5^{1,2,3} \\
\downarrow & & \downarrow & & \downarrow & & & & & & \downarrow \\
X_0 & \xrightarrow{|q_2|=0} & X_1^2 & \xrightarrow{|q_1|=0} & X_2^{2,1} & \xrightarrow{|q_3|=0} & X_3^{2,1,3} & \xrightarrow{kh-lg=0} & X_4^{2,1,3} & \xrightarrow{eb-fa=0} & X_5^{2,1,3} \\
\downarrow & & \downarrow & & & \searrow & & & & & \downarrow \\
X_0 & \xrightarrow{|q_1|=0} & X_1^1 & \xrightarrow{|q_3|=0} & X_2^{1,3} & \xrightarrow{eb-fa=0} & X_3^{1,3} & \xrightarrow{|q_2|=0} & X_4^{1,3,2} & \xrightarrow{kh-lg=0} & X_5^{1,3,2} \\
\downarrow & & \downarrow & & & & \downarrow & & & & \downarrow \\
X_0 & \xrightarrow{|q_2|=0} & X_1^2 & \xrightarrow{|q_3|=0} & X_2^{2,3} & \xrightarrow{kh-lg=0} & X_3^{2,3} & \xrightarrow{|q_1|=0} & X_4^{2,3,1} & \xrightarrow{eb-fa=0} & X_5^{2,3,1} \\
\downarrow & & \downarrow & & & & \downarrow & & & & \downarrow \\
X_0 & \xrightarrow{|q_3|=0} & X_1^3 & \xrightarrow{|q_1|=0} & X_2^{3,1} & \xrightarrow{eb-fa=0} & X_3^{3,1} & \xrightarrow{|q_2|=0} & X_4^{3,1,2} & \xrightarrow{kh-lg=0} & X_5^{3,1,2} \\
\downarrow & & \downarrow & & & & \downarrow & & & & \downarrow \\
X_0 & \xrightarrow{|q_3|=0} & X_1^3 & \xrightarrow{|q_2|=0} & X_2^{3,2} & \xrightarrow{kh-lg=0} & X_3^{3,2} & \xrightarrow{|q_1|=0} & X_4^{3,2,1} & \xrightarrow{eb-fa=0} & X_5^{3,2,1}
\end{array}$$

Because each constraint map is defined from an irreducible polynomial, each topologically non-trivial subspace has a $\mathbb{Z}_2$ classification. This gives two distinct sequences of zeroth homotopy groups connected by paths in the E_{2n} subspaces of ξ.

$$\begin{array}{ccccccccccc}
3\mathbb{Z}_2 & \longrightarrow & \mathbb{Z}_2 & \longrightarrow & 0 & \longrightarrow & 0 & \longrightarrow & \mathbb{Z}_2 & \longrightarrow & 0 \\
\downarrow & & \downarrow & & & \searrow & & & & & \downarrow \\
3\mathbb{Z}_2 & \longrightarrow & 0 & \longrightarrow & \mathbb{Z}_2 & \longrightarrow & 0 & \longrightarrow & \mathbb{Z}_2 & \longrightarrow & 0
\end{array} \tag{7.7.127}$$

From the perspective of zero energy subspaces E_0, E_2, E_4, E_6 of ξ we have the following diagram.

$$\begin{array}{ccccc}
E_0 & \longrightarrow & E_2 \cap X_1^1 & \longrightarrow & E_4 \cap X_2^{1,2} & \longrightarrow & E_6 \cap X_5^{1,2,3} \\
\downarrow & & \downarrow & & \downarrow & & \downarrow \\
E_0 & \longrightarrow & E_2 \cap X_1^2 & \longrightarrow & E_4 \cap X_2^{2,1} & \longrightarrow & E_6 \cap X_5^{2,1,3} \\
\downarrow & & \downarrow & & \downarrow & & \downarrow \\
E_0 & \longrightarrow & E_2 \cap X_1^1 & \longrightarrow & E_4 \cap X_2^{1,3} & \longrightarrow & E_6 \cap X_5^{1,3,2} \\
\downarrow & & \downarrow & & \downarrow & & \downarrow \\
E_0 & \longrightarrow & E_2 \cap X_1^2 & \longrightarrow & E_4 \cap X_2^{2,3} & \longrightarrow & E_6 \cap X_5^{2,3,1} \\
\downarrow & & \downarrow & & \downarrow & & \downarrow \\
E_0 & \longrightarrow & E_2 \cap X_1^3 & \longrightarrow & E_4 \cap X_2^{3,1} & \longrightarrow & E_6 \cap X_5^{3,1,2} \\
\downarrow & & \downarrow & & \downarrow & & \downarrow \\
E_0 & \longrightarrow & E_2 \cap X_1^3 & \longrightarrow & E_4 \cap X_2^{3,2} & \longrightarrow & E_6 \cap X_5^{3,2,1}
\end{array}$$

Using the commutativity of constraint maps, this reduces to the following diagram of distinct subspaces.

$$\begin{array}{ccccccc}
 & & E_2 \cap X_1^1 & \longrightarrow & E_4 \cap X_2^{1,2} & & \\
 & \nearrow & \downarrow & \searrow\ \nearrow & \downarrow & \searrow & \\
E_0 & \longrightarrow & E_2 \cap X_1^2 & & E_4 \cap X_3^{1,3} & \longrightarrow & E_6 \cap X_5^{1,2,3} \\
 & \searrow & \downarrow & \nearrow\ \searrow & \downarrow & \nearrow & \\
 & & E_2 \cap X_1^3 & \longrightarrow & E_4 \cap X_3^{2,3} & &
\end{array} \tag{7.7.128}$$

We use a coaxial cable network to experimentally verify the homotopic structure for G. First we randomly assign hopping terms for G from a binary distribution such that none of the constraint maps are initially satisfied. This allows us to make G from RG58 (50Ω) and RG62 (93Ω) coaxial cables. Then we choose a path through the homotopic structure of G. To satisfy each constraint, we use a random number generator to indicate which hopping term may be changed to satisfy a constraint map of the relevant boundary operator. Then, as we add each constraint map, we take measurements on the structure to verify predictions in the localisation, and transmittance of eigenstates in the structure. Details of the exact distribution of hopping terms for each structure measured are given in Appendix A.

As each homotopic sequence falls in to two types (illustrated in the diagram (7.7.127)) so we consider two paths through the homotopic structure, one path for each type. The first path uses boundary operators for g_2 then g_1 then g_3. The constraint maps were satisfied

in the following order:

$$\begin{aligned} |q_2| &= 0 \\ |q_1| &= 0 \\ |\kappa_2| &= 0 \\ |\kappa_1| &= 0 \\ |q_3| &= 0. \end{aligned} \tag{7.7.129}$$

The second path uses boundary operators for g_3 then g_1 then g_2. Boundary maps were taken in the following order:

$$\begin{aligned} |q_3| &= 0 \\ |q_2| &= 0 \\ |\kappa_2| &= 0 \\ |q_1| &= 0 \\ |\kappa_1| &= 0. \end{aligned} \tag{7.7.130}$$

We can make quite broad predictions about the localisation of nullstates at each point in the diagram 7.7.127. As discussed in section 7.6 the first is when a structure is on a higher steps' topological phase boundary, but no extra constraint maps are satisfied. At this point in a homotopic sequence, the effective subgraph for the singular sections is a core graph (as each section is SSH like). The second relates to how states localise when extra constraints are satisfied. This follows from the partial ordering of sections and is a sequential analogue of the localisation discussed in chapter 5.

To demonstrate the core properties of a subgraph of G when on a higher steps' phase boundary, we plot the experimentally measured LDOS for a particular structure on every site (at $\varepsilon = \cos\omega\tau = 0$). These results are given in Fig. 7.7.2. These confirm our prediction of a core effective subgraph for a structure on a higher steps' phase boundary.

We now turn to how localisation throughout a structure is altered when following a homotopic sequence. To illustrate these results, we consider a single site of our structure, in each point of both sequences given in the diagrams (7.7.129) and (7.7.130). The LDOS are displayed in Fig. 7.7.3. We have also experimentally measured the LDOS for 2 sites in each section through both sequences of subspaces. We have attached these data plotted in a similar way to these results in Appendix A, corroborating our predictions of section specific localisation.

Finally, as discussed in section 7.6 in a coaxial cable network the transmittance between two sections, when a structure is cut as described above, is non-zero only when a structure is on a higher steps' phase boundary. For this experiment we cut the structure as displayed in Fig. 7.7.4 (b). Measuring transmittance on a higher steps' phase boundary, and away from a higher steps' phase boundary we confirm our prediction of unit transmittance only on the higher steps' phase boundary, as displayed in Fig. 7.7.4 (a).

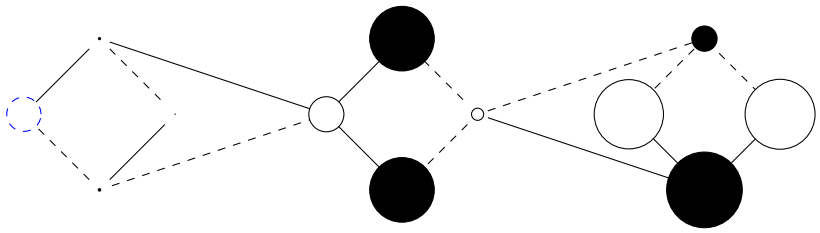

(a)

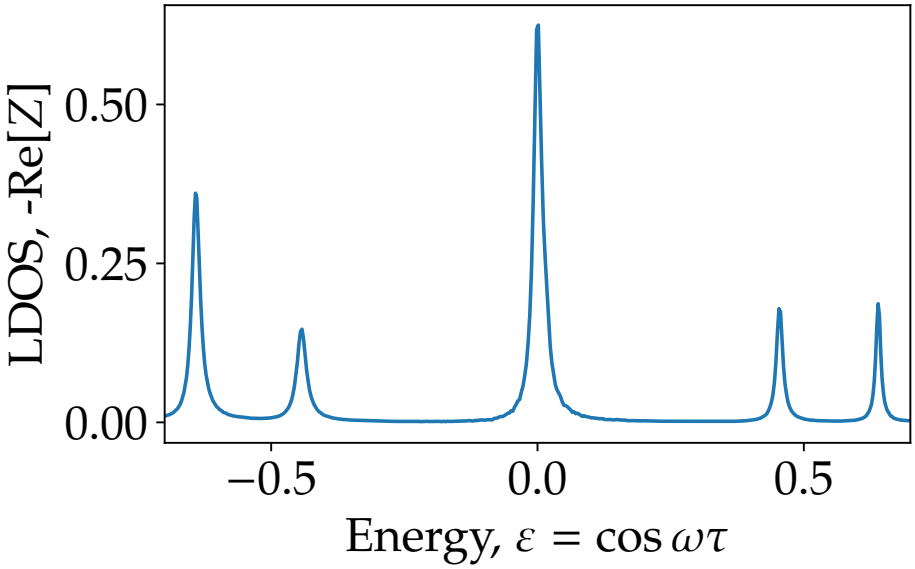

(b)

Figure 7.7.2: (a) The structure on a higher steps' phase boundary. RG58 cables are indicated with a dashed line, and RG62 cables with a solid line. The vertex diameter is proportional to the experimentally measured local density of states when this structure is on a higher steps' phase boundary. Observe that the two sections on the right hand site have a core subgraph, as predicted in section 7.6. The local density of states was taken as an integral over the impedance on that site between 100 MHz and 126 MHz. (b) Displays the local density of states for the white site with a blue and dashed boundary.

7.8 Conclusions and limitations

We have defined and studied sequential topology for finite chiral structures in terms of highly degenerate spectral gap closures in a Hamiltonian H defined on a graph G. Under our convention, we have shown that the number of zero energy states in G, localised to certain subgraphs of G, can be understood from the topology of lower dimensional subspaces within the parameter space ξ. Furthermore, we have demonstrated to what extent a Hamiltonian H on G can exhibit disorder in hopping terms (that is the largest degree of freedom of hopping terms) yet retain a certain number of zero energy states localised to a

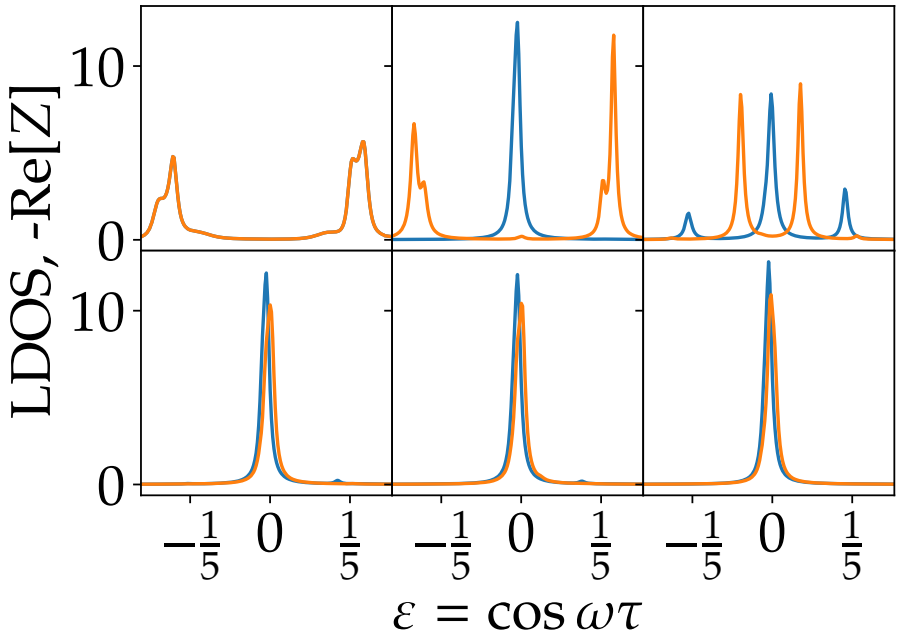

Figure 7.7.3: The orange plots denote the LDOS of the site C0 for the first sequence setting the constraints in equation (7.7.129). The blue plots denote the site C0 for the second sequence setting the constraints in equation (7.7.130). The top left sub plot satisfies no constraint maps, and the bottom left subplot satisfied 3 constraint maps. Each subplot satisfies one more constraint map then its left neighbour.

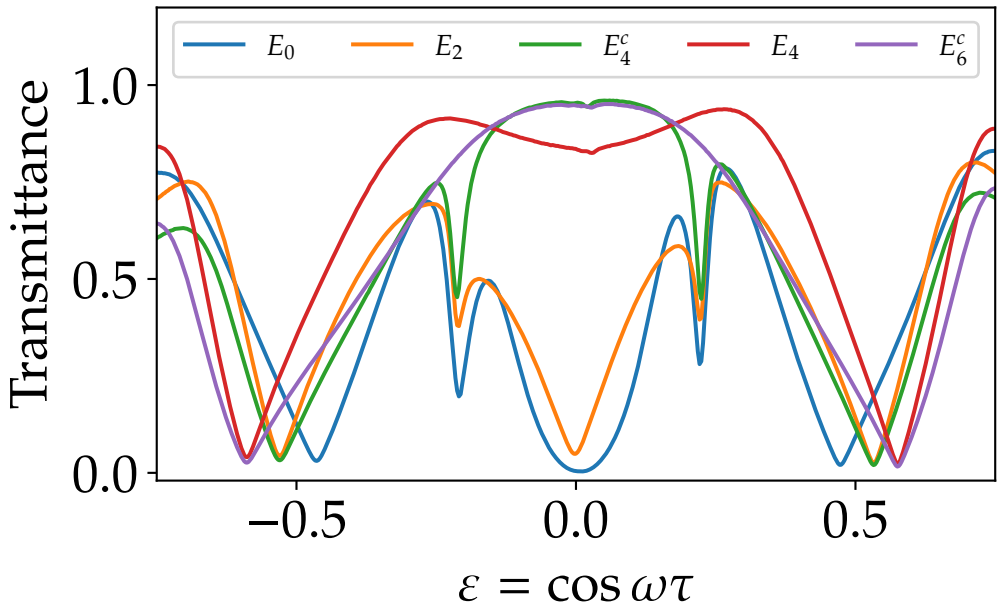

(a)

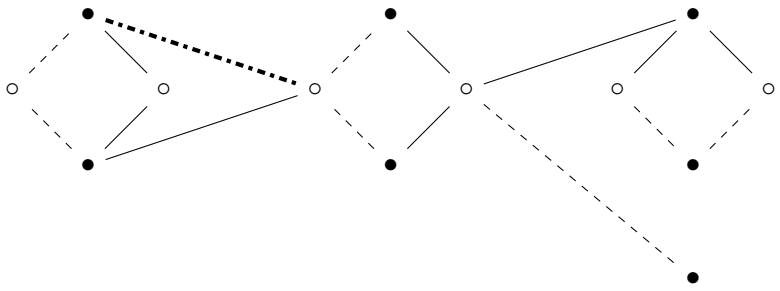

(b)

Figure 7.7.4: (a) Transmittance between the site when taking the structure through a sequence of sequential phase transitions. E_{2n} denotes if the structure lies on the $2n$ zero energy subspace of ξ, the superscript c indicates if the structure is on a higher (i.e. beyond zeroth) steps' phase boundary. (b) A picture of the structure with the cut hopping term, as it is taken to from 4 zero energy states (but not on a phase boundary) to 6 zero energy phase boundary, this corresponds to the E_4 and E_6^c data in (a). The solid lines are RG62 cables, and the dashed lines are RG58 cables. The dash dot line is changed from an RG58 to an RG62 cable.

certain region of G.

Higher order topology, where zero energy states localise to certain dimensional boundaries of a structure, loses meaning when the bulk boundary correspondence is lost. We believe our sequential topology has, in some sense, well defined parallels to a notion of higher order topology in finite chiral structures. We do note, however, that there are many different ways to define a topology on the parameter space ξ. We have focussed solely on spectral gap closures around zero energy, but non-zero energy gap closures may also give a physically significant way to define a sequential topology on ξ, or even something not involving gap closures. Such alternative approaches will likely calculate different invariants and give different physical predictions from topological properties of a system, properties we have neglected here.

Under our approach, we have demonstrated that (up to some simple considerations) a sequence of which subspaces of ξ are topologically non-trivial is universal for a real or complex finite chiral structure. We have also given a method to calculate the classification of each non-trivial subspace. Under our choice of topology, this gives a well defined classification of the zeroth homotopy groups a structure. Using the techniques we have developed, we can calculate such sequences exactly for an arbitrary chiral structure.

Using properties in the localisation of null states in a Hamiltonian H on G, we have demonstrated a set of physical consequences of sequential topological phase transitions. Furthermore, we have verified predictions in the localisation and transmittance of states experimentally in a coaxial cable network. Such properties may be useful in the design of quantum networks.

Our approach does have limitations, however. Topological phenomena are very likely highly non-trivial outside the limited scope we have explored. Furthermore, there are large computational limits to our approach.

One significant limit relates to the convention we use for multiple critical sections. The question of how sequential topology is altered when we do not follow our convention for defining constraint maps and boundary operators has been left unexplored. There may be large amounts of topological phenomena using different conventions, or having no convention at all.

We have not given a computationally efficient method for sequential classification. This is because our classification protocol requires directly calculating determinants and nullspaces of individual sections and subgraphs of G. As such, our results currently may only be applied in full generality to very small structures with an order of 10s of sites. However, for structures exhibiting large symmetry in their network topology, our results can be generalised quite efficiently through analytical observations. This does give a significant computational limit to our approach, however. We anticipate significant optimisation is possible.

We also have many unanswered conjectures about sequential topology for finite chiral structures even under our convention. These include questions on defining a convention for constraint maps in mixed and hyper-critical sections, and whether our upper bound on constraint maps in such cases are in any way optimal. We also have unanswered questions in the localisation of null states, for example is an effective subgraph on a higher steps'

phase boundary almost always core? Or on the path connectivity of $2n$ zero energy state subspaces E_{2n} of ξ.

Questions about how our sequential topology relates to structures with a bulk boundary correspondence are also not fully answered. For instance, which subgraph of G, when periodically repeated, exhibits robust zero energy states when a structure is on one side of a higher steps' phase boundary? How should a structure be cut to find such a bulk boundary correspondence?

We also anticipate many unexplored physical consequences of our sequential classification, or how it is altered when we have hopping terms over fields other than real or complex numbers. The question of whether a similar approach can be defined for systems with different symmetries, such as negative time reversal symmetry, or particle hole symmetry is also a direction where many interesting questions remain unexplored.

Mathematically we have formalised finite sequential topology in terms of minors of a Hamiltonian, to define subspaces. Formally these subspace correspond to determinantal varieties. However, there are many results from algebraic geometry on determinantal varieties that we have not explored in our work. We believe the connections between our work and algebraic geometry may lead to many fruitful results to some of the above questions, and more.

Chapter 8

Conclusion and outlook

We have presented a description of a few topological phenomena in finite and strongly disordered chiral structures. In particular we have proposed a definition of exact topological protection and studied a selection of topological phase transitions in finite media. Throughout this work we have demonstrated some of our theoretical predictions experimentally and have also shown the promise and flexibility of using coaxial cable networks for topological physics experiments.

We began by demonstrating an exact topological phase transition for the SSH model in a coaxial cable network and experimentally found a very precise topologically protected state in chapter 3. These results showed the flexibility and promise of coaxial cable networks for topological physics experiments, and also experimentally confirmed the map between coaxial cable networks and tight binding models. Our results verified our predicted experimental signatures of topological phenomena in coaxial cable networks.

In chapter 4 we proposed a definition for topological protection where the bulk does not protect any states. We found a deep connection between a structure's connectivity and numbers of topologically protected states. Using this connection, we demonstrated that topologically protected states are, almost always, exactly localised to a subset of sites and also provided a simple probabilistic protocol to find numbers of topologically protected states in finite structures with any symmetry. We also experimentally found such topologically protected states in both an SSH chain and graphene with a vacancy.

We then studied topological phase transitions in finite chiral structures in chapter 5 and uncovered a rich $N\mathbb{Z}_2$ classification of many finite chiral structures by finding a connection between topological phases and structural connectivity, thereby giving a basis for designing topologically interesting structures for experiments and applications. By surveying a large number of small bipartite graphs, we also demonstrated that the proportion of topologically non-trivial finite chiral structures is significant. Furthermore, we derived some physical consequences of our finite classification regarding the nature of localisation at a topological phase boundary. In doing so we demonstrated a deep connection between nut graphs and a structures topological classification. We experimentally confirmed physical consequences of our classification in a graphene sample and gave a simple algorithm for the classification of finite chiral structures.

In chapter 6 we made use of coaxial cable networks to experimentally verify some properties of nut graphs. We experimentally showed that 5 different nut graphs: the three Sciriha graphs, and two small chemical nut graphs have support of nullstates on every vertex, and using transmission were able to map the nullstates of these structures. We then gave an experimental confirmation of omni-conduction in one of the Sciriha graphs, but a general property of all nut graphs. With the two smallest chemical nut graphs, we also verified one of the constructions of nut graphs, by extending a bridge with two vertices. Our experimental data agreed well with theory.

Finally in chapter 7 we studied topology as we begin to allow constraints on hopping terms — sequential topology. This allowed us to study phase transitions in topologically critical structures. We demonstrated that under the least restricted definition for a topological phase boundary, first step topological phase transitions do not exist in finite chiral structures. By carefully choosing a more restricted definition for a topological phase boundary we uncovered (up to some simple considerations) a universal homotopic sequence for real finite chiral Hamiltonians, and a corresponding sequence for complex Hamiltonians. We gave a protocol for finding the distributions of hopping terms necessary for a structure to undergo a series of sequential phase transitions, allowing for a theoretical case study. We then demonstrated that for a large class of structures, their sequential phase transitions are deeply connected to core graphs, where support of zero energy states occurs on every sight of a particular subgraph of the structure. Using this localisation, we experimentally observed a complete sequence of topological phase transitions in an experimental component of our case study.

We hope this work has given a small survey of some of the basic topological properties of finite media and that we have demonstrated that topology, even in the smallest of samples, and those with a complex connectivity, is an interesting area of study. We hope that some of our work will perhaps go on to inspire a greater use of graph theoretic approaches in condensed matter physics, especially in finite structures.

8.1 Outlook

We have demonstrated that even in very small structures, there can be interesting topological properties. But there remain many unanswered questions. Beyond the conjectures we leave open in this work, from a convention for sequential topology in mixed and hypercritical structures to the exact nature of localisation on higher steps' phase boundaries, there are a number of directions which I believe would be interesting to study.

One of the more open questions left unanswered in our work is the interplay of our classifications compared to infinite classifications. It would be interesting to see exactly how the bulk-boundary correspondence scales with system size, and at what point only a finite treatment remains valid. The converse would also help give some interpretation to our classification in finite media: for instance, what is the dimension of an infinite structure with N sections? It would also be interesting to see how our finite sequential topology is altered when we take the limit to infinite structures, would we be able to interpret our sequential classification in the context of the 10 fold way? What does a bulk boundary

correspondence look like in this case? We anticipate new phases in larger systems may be uncovered when constraining hopping terms, such as non-crystalline higher order topological insulators.

Beyond this it would be interesting to know how topology in finite structures with different symmetries behave. Can a graph theoretic approach also be applied to such systems? What does topological phenomena look like in such systems where the bulk boundary correspondence has been completely lost?

Our approach allows us to study finite structures with strong disorder. But what is the limit of disorder for which our zeroth step and higher step classification still, in some sense, holds? That is, if we have a Hamiltonian H and provide disorder in the form of $H + W$ where W is some matrix, what properties of W do we require so that the topological properties of $H + W$ are the same as H?

We also believe that the effects of structural disorder on topological protection and topological classification may also be possible to study analytically, by considering structural disorder as a set of finite graphs and seeing how they combine to a larger otherwise perfect structure. It would be interesting to study how such structural disorder alters topological classification.

It would also be interesting to see what parts of topological protection, and our classification are maintained in systems with interactions. It is possible to model interacting Hamiltonians with a much larger effective 1 particle Hamiltonian [117] so can some of our results directly apply to such structures? Or will understanding topology in interacting finite structures require a whole new approach? What does topology look like in finite T-J models or Heisenberg models? It may even be possible to explore these questions experimentally using electronics to create on site non-linearities in a coaxial cable network or using gain.

It would also be interesting to study some of our theoretical work in other experimental systems. For instance, micropillar polariton devices can have dynamically changed hopping terms [28, 82], could some of our predicted phenomena be observed in such systems? It would be interesting to explore what experimental signatures of finite topology might be present in such systems. Another possible platform is in integrated photonic devices to create some structures designed to have highly non-trivial topological properties, perhaps from a macroscopic pcb down to much smaller integrated chips. What experimental signatures of finite topology may look like in different systems, such as spin chains, will also be interesting to find.

There are also some applications of the coaxial cable network platform that would be interesting to study experimentally. For instance, a recently discovered renormalisation group treatment for random graphs [118, 119] would be possible to experimentally study in a coaxial cable network. Or experimental tests of the different equivalence classes of diffusion scales [120] experimentally implemented in coaxial cable networks. It would also be interesting to study non-Euclidean devices in coaxial cable networks.

Finally, there may be a number of technological applications worth exploring. For instance, can phase transitions be used in nanographene for controlling the localisation of zero energy states? Could this open the door for controlled braiding in possible Majorana

devices? Some of our results also broadly apply to networks in general, and so may aid in the design of robust quantum networks, or a topological basis for radio frequency encryption or in designing topological filters or antennas. It would be interesting to see in what ways our results relating spectral gaps or topological protection might be useful in designing such structures.

Appendix A

Sequential topology — further experimental details

Here we detail all of the structures used for the sequential topology experiments of section 7.7. In particular we confirm the homotopic structure of the structure in Fig. A.0.1. That is the diagram of zeroth homotopy groups

$$\begin{array}{ccccccccc} 3\mathbb{Z}_2^{\alpha} & \longrightarrow & \mathbb{Z}_2^{\beta} & \longrightarrow & 0^{\gamma} & \longrightarrow & 0^{\delta} & \longrightarrow & \mathbb{Z}_2^{\varepsilon} & \longrightarrow & 0^{\mu} \\ \downarrow & & \downarrow & & & \searrow & & & & & \downarrow \\ 3\mathbb{Z}_2^{\alpha} & \longrightarrow & 0^{\nu} & \longrightarrow & \mathbb{Z}_2^{\theta} & \longrightarrow & 0^{\zeta} & \longrightarrow & \mathbb{Z}_2^{\kappa} & \longrightarrow & 0^{\sigma} \end{array}$$

where the superscript denotes the specific structure, which is labelled in the data presented in Fig.'s A.0.3 to A.0.13. To confirm this homotopic structure experimentally we measure the LDOS on two sites on each section. This works because of the localisation nullstates as we drive a structure through sequential phase transitions.

Recall from section 5.3.1.1 that for a structure with two zero energy states a non-singular section may host zero energy states on at most one sublattice. For a structure with more than two zero energy states, then a non-singular section g_i may host nullstates on both sub lattices only if nullstates originate from at least one above section $g_j > g_i$ and one below section $g_k < g_i$ as by proposition 7.6.3, otherwise a non-singular section will host nullstates on at most one sub lattice. The structure we experimentally study has two equal sections $g_1 = g_2$ and one section $g_3 < g_2 = g_1$ so a non-singular section will only host nullstates on at most one sublattice.

The structure we experimentally study has all SSH like sections, so by proposition 7.6.2 a structure on a higher steps' phase boundary has a core effective subgraph. Therefore, if we measure the LDOS on two sites of every section, for a structure at each point in the above homotopic diagram, we will have verified the number of zero energy states at each point, as well as which section zero energy states originate.

To illustrate these sequences of sequential phase transitions we give the data below for the LDOS on two sites for each section, where the diameter is proportional to the LDOS on that site calculated as an integral between 110.9 MHz and 125.9 MHz. This is roughly

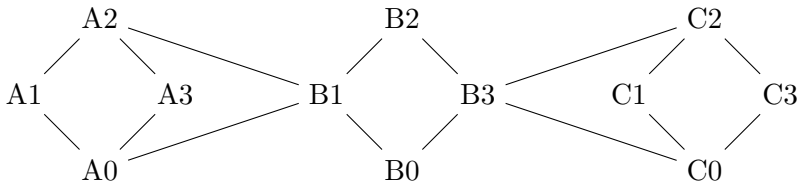

Figure A.0.1: The structure we use for a case study in section 7.7. The sites are labelled for easier reference to the LDOS data. We experimentally confirm the homotopic structure of this graph.

from $\varepsilon = -0.146$ to $\varepsilon = 0.058$, the reason the integral was not exactly around zero energy is that the inclusion of a large number of T-connectors shifted the zero energy point of the structure which was not accounted for in the calculation. The distribution of hopping terms is indicated on each structure. These data are given in Fig.'s A.0.3 to A.0.13. The LDOS measurements are normalised relative to the largest LDOS measured for the entire sequence of structures. And an $\times$ on a site indicates the site was not measured.

We also reproduce the transmittance data below while taking a structure through the sequential phase transitions in Fig. A.0.2. The structures for each measurement is made by cutting the site C0 on the hopping term between B3 and C0, where the plots $E_0, E_2, E_4^c, E_4, E_6^c$ correspond to the structures $\alpha, \nu, \theta, \kappa, \sigma$ in the above sequence of homotopy groups.

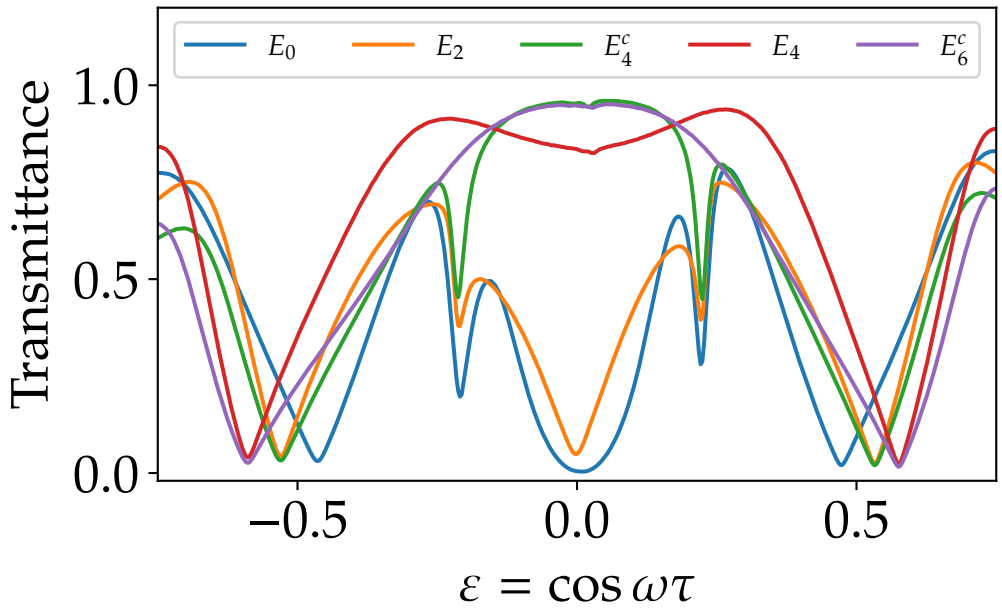

Figure A.0.2: Transmittance between the cut site C0 when taking the structure through a sequence of sequential phase transitions. E_{2n} denotes if the structure lies on the $2n$ zero energy subspace of ξ, the superscript c indicates if the structure is on a steps' phase boundary. The plots $E_0, E_2, E_4^c, E_4, E_6^c$ correspond to the structures $\alpha, \nu, \theta, \kappa, \sigma$ in the above sequence of homotopy groups.

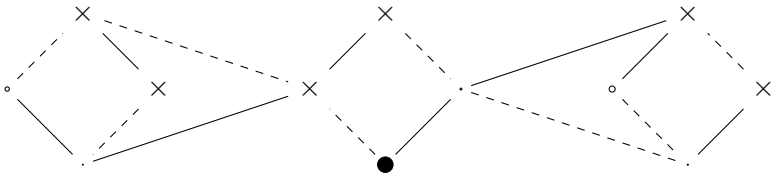

(a)

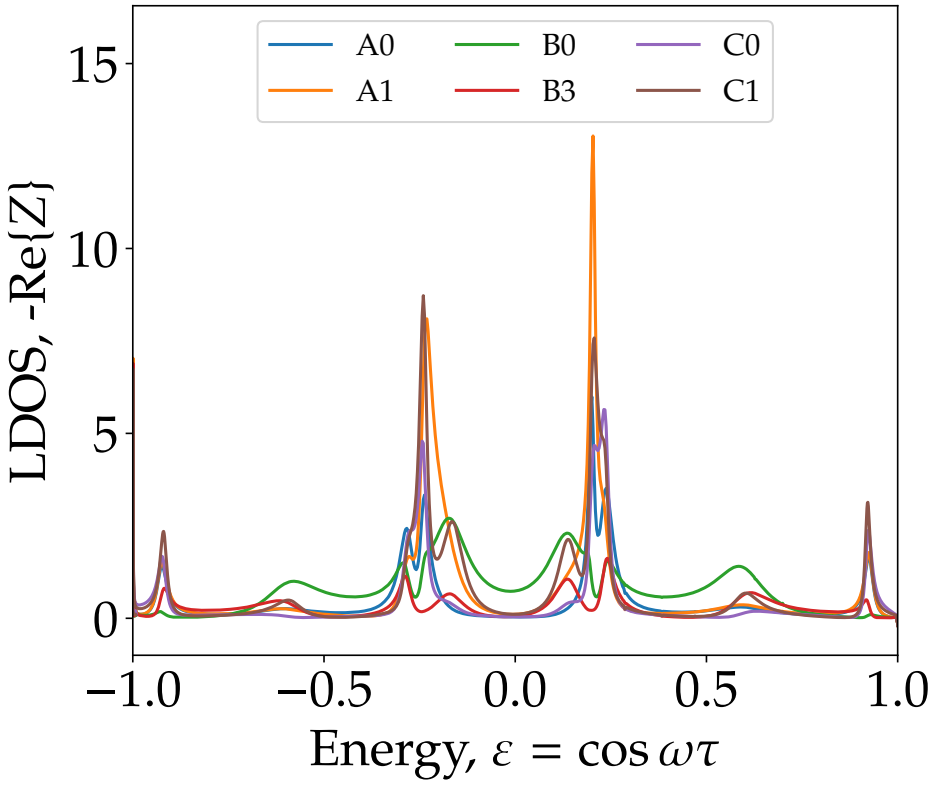

(b)

Figure A.0.3: This is the structure α in the sequence of zeroth homotopy groups. This structure has no zero energy states, although the data for the site B0 has a non-zero LDOS at zero energy. We believe this is a consequence of a highly broadened LDOS for this measurement, perhaps as a result of a faulty connection. Despite this, zero energy occurs at a minima in the LDOS, so we infer that there are no zero energy states in this structure. We anticipate remeasuring B0 will give better data. A site with an $\times$ indicates the site was not measured. RG58 cables are indicated with a dashed line, and RG62 cables with a solid line.

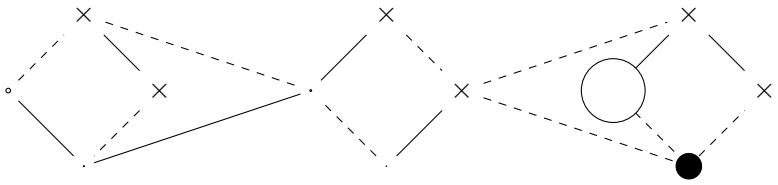

(a)

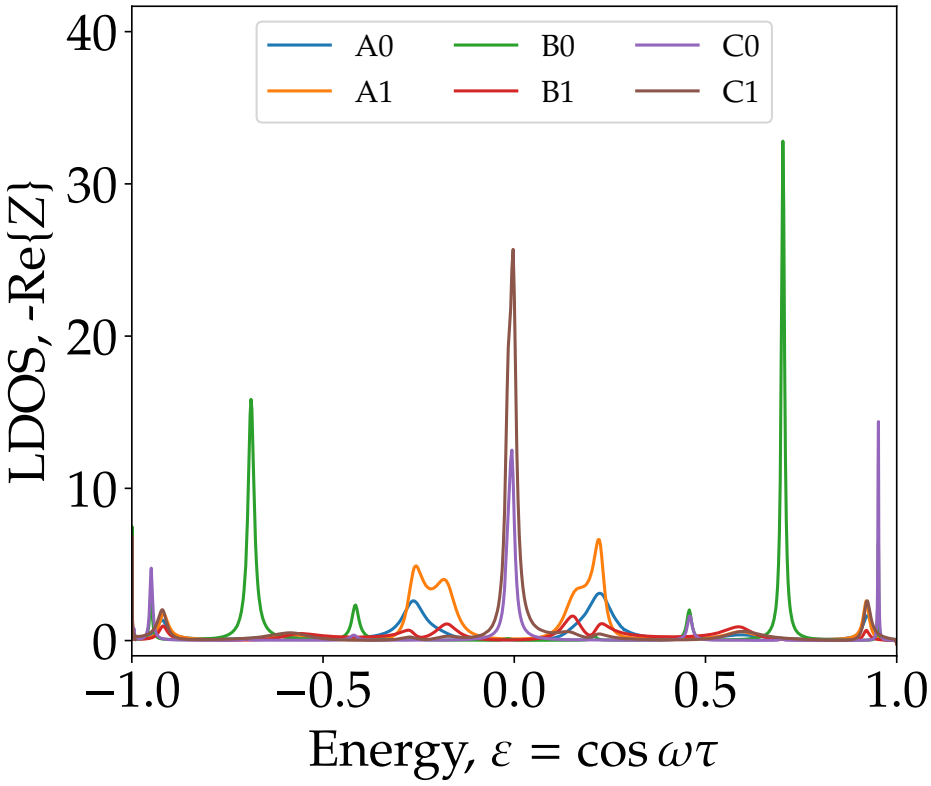

(b)

Figure A.0.4: This is the structure β in the sequence of zeroth homotopy groups. Only one section is critical, resulting in two zero energy states. This is confirmed with support of nullstates only on both sublattices of one section. RG58 cables are indicated with a dashed line, and RG62 cables with a solid line.

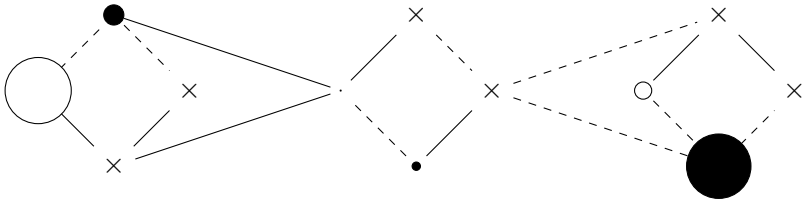

(a)

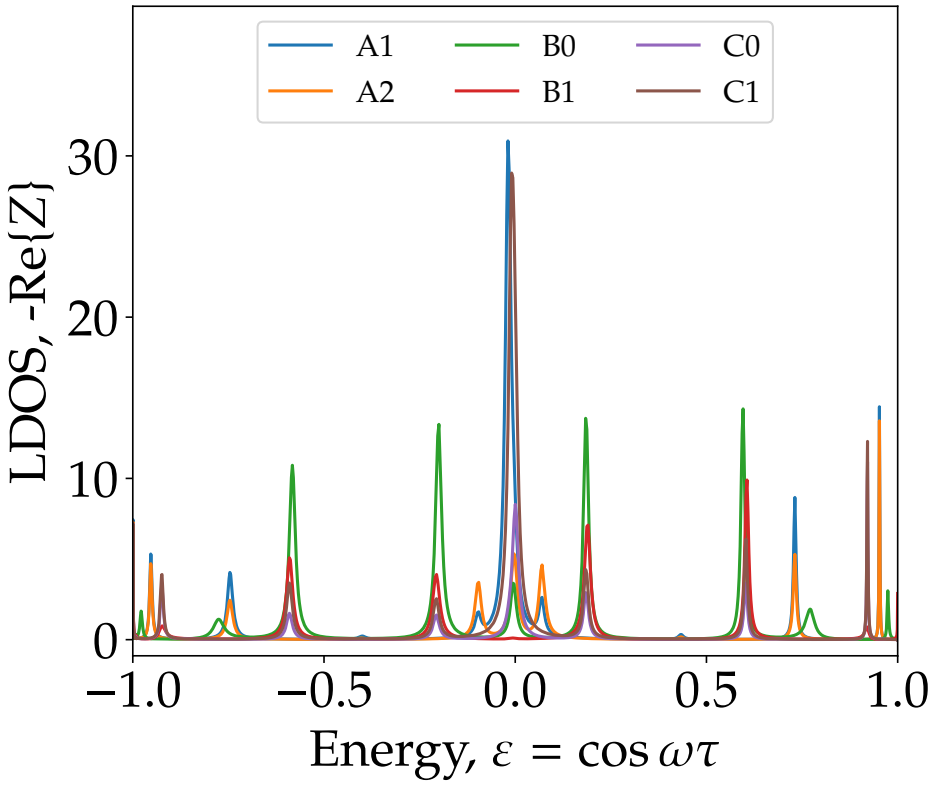

(b)

Figure A.0.5: This is the structure γ in the sequence of zeroth homotopy groups. With two critical sections, being the equal sections (by the partial ordering) results in four zero energy states. This is confirmed with support of nullstates on both sublattices of each equal section. RG58 cables are indicated with a dashed line, and RG62 cables with a solid line.

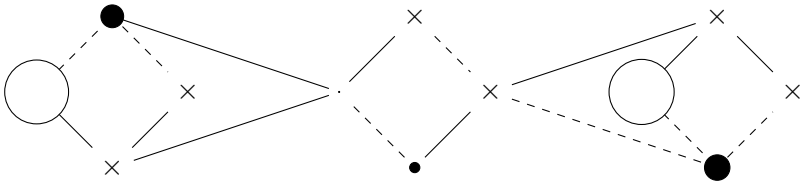

(a)

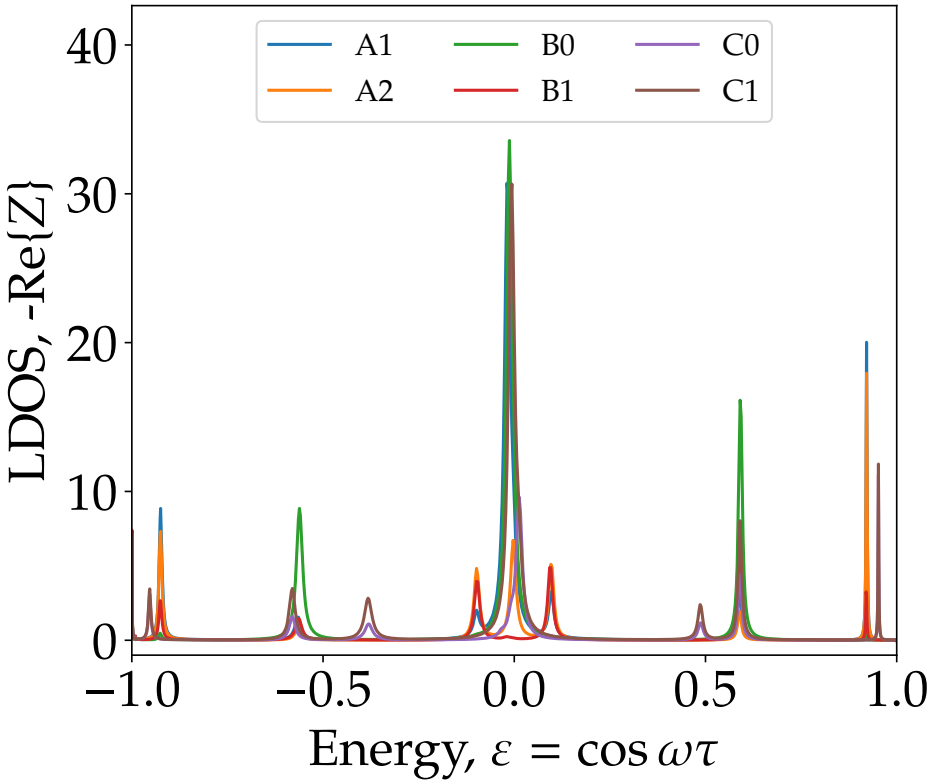

(b)

Figure A.0.6: This is the structure δ in the sequence of zeroth homotopy groups. With two critical sections and a further constraint map being satisfied, this structure has four zero energy states, confirmed in the support of nullstates on both sublattices of each singular section. There is also support on the non-singular section on one sublattice — a consequence of the partial ordering. Notice that support on the nullstates of g_2 have changed compared to the structure γ, this is a result of the change in hopping term between B3 and C2. RG58 cables are indicated with a dashed line, and RG62 cables with a solid line.

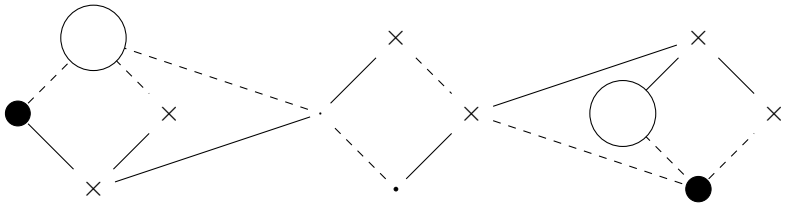

(a)

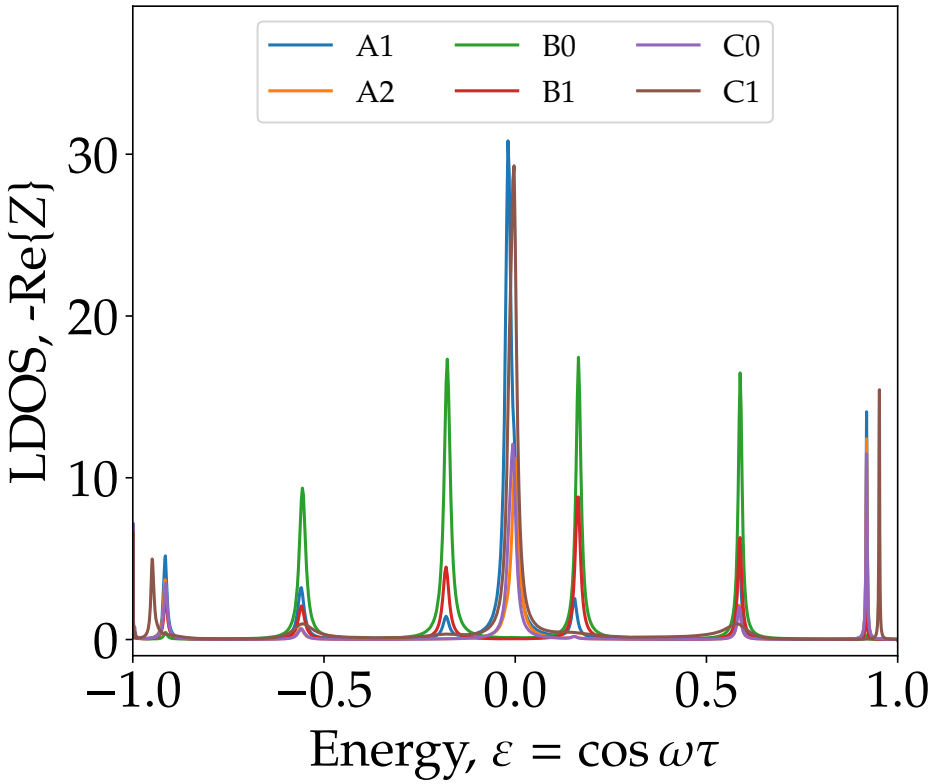

(b)

Figure A.0.7: This is the structure ϵ in the sequence of zeroth homotopy groups. This structure satisfies all but one constraint for 6 zero energy states. For this structure this is satisfied when the nullstates have no support on the unequal section, as confirmed in (a). RG58 cables are indicated with a dashed line, and RG62 cables with a solid line.

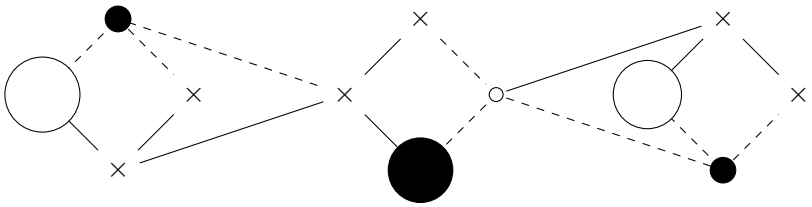

(a)

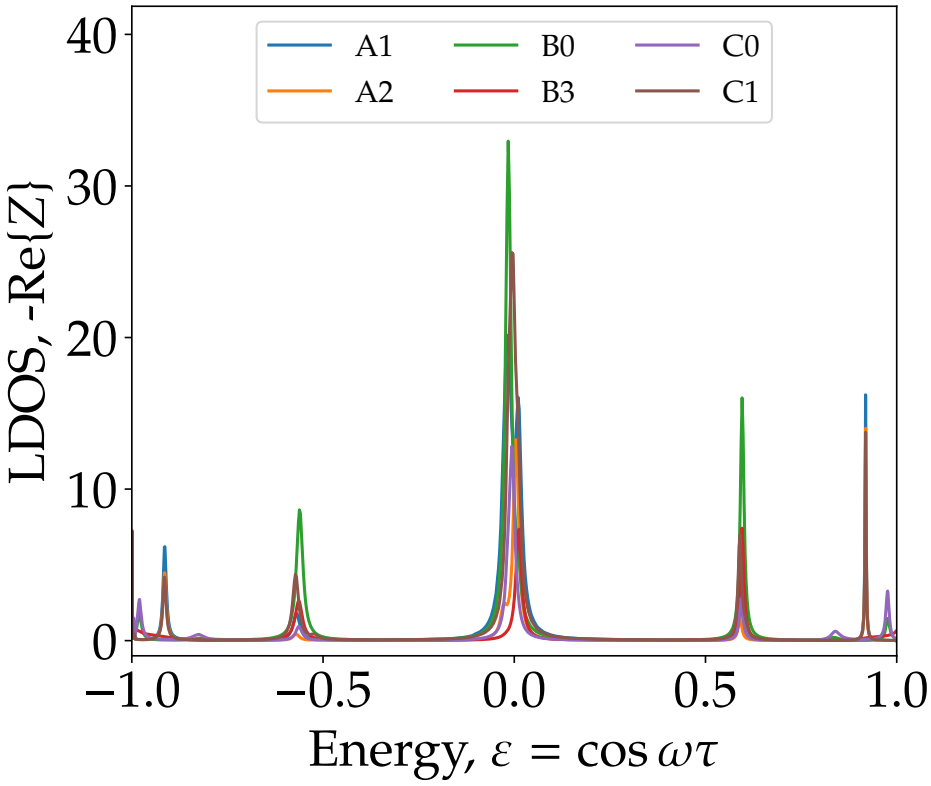

(b)

Figure A.0.8: The structure μ which satisfies all the constraint maps for zero energy states, confirmed by support of nullstates on both sub lattices of each section. As a consequence of the partial ordering of this structure, this confirms there are 6 zero energy states. RG58 cables are indicated with a dashed line, and RG62 cables with a solid line.

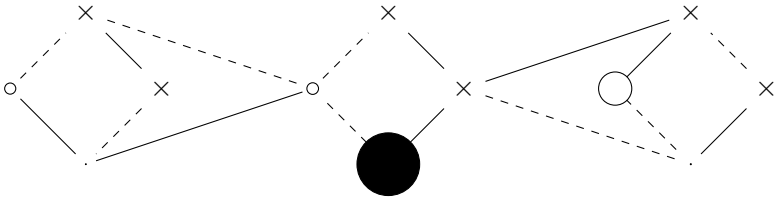

(a)

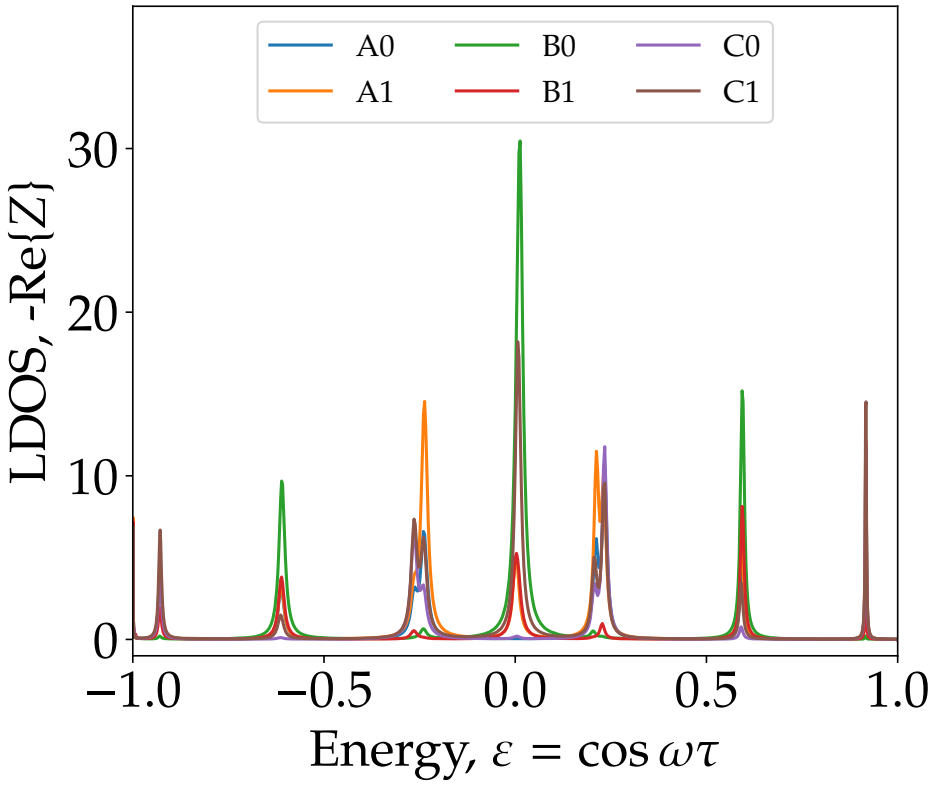

(b)

Figure A.0.9: This is the structure ν in the sequence of zeroth homotopy groups. One section is critical in this structure, resulting in two zero energy states, as indicated by the location where nullstates have support. RG58 cables are indicated with a dashed line, and RG62 cables with a solid line.

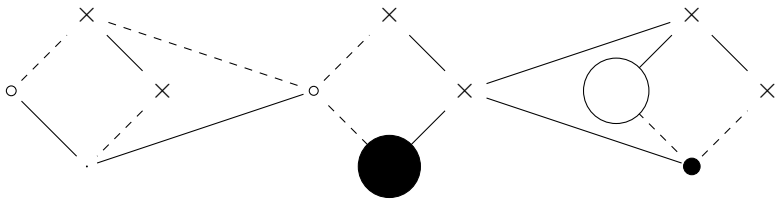

(a)

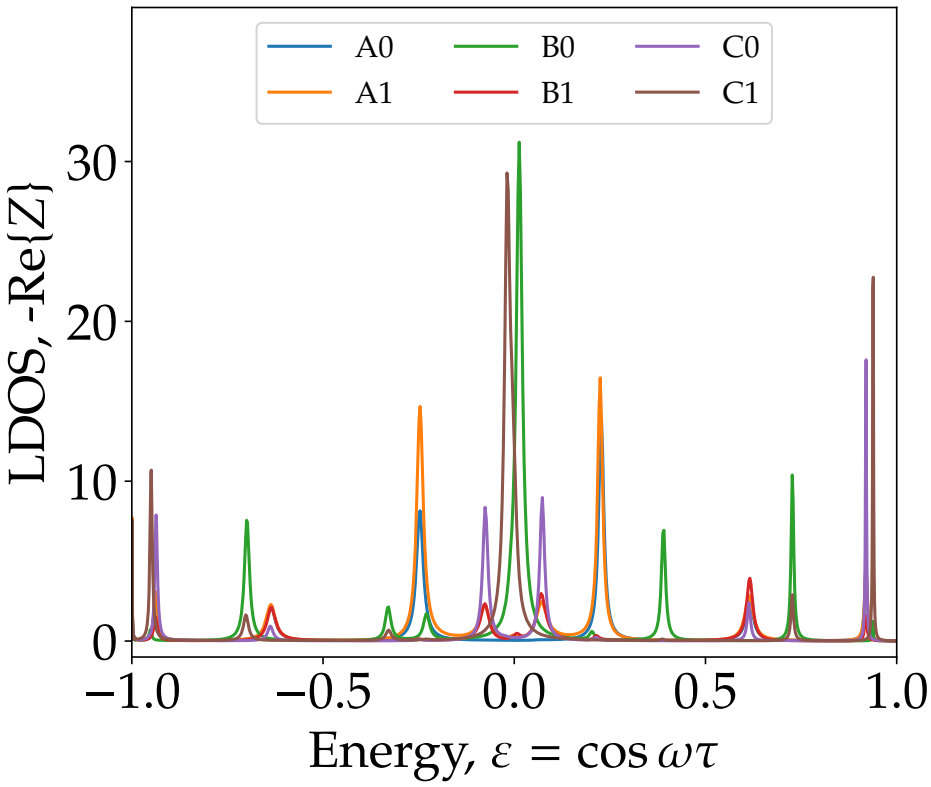

(b)

Figure A.0.10: This is the structure θ in the sequence of zeroth homotopy groups. Two sections are critical in this structure, but they are not equal by the partial ordering and the constraint map for mutual orthogonality is not satisfied. This results in two zero energy states indicated by non-zero support on both sublattices somewhere in the structure, but no one section supports nullstates on both sub lattices. RG58 cables are indicated with a dashed line, and RG62 cables with a solid line.

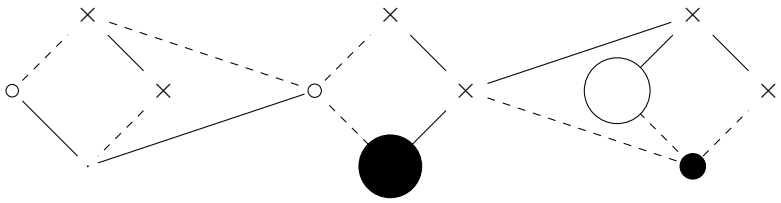

(a)

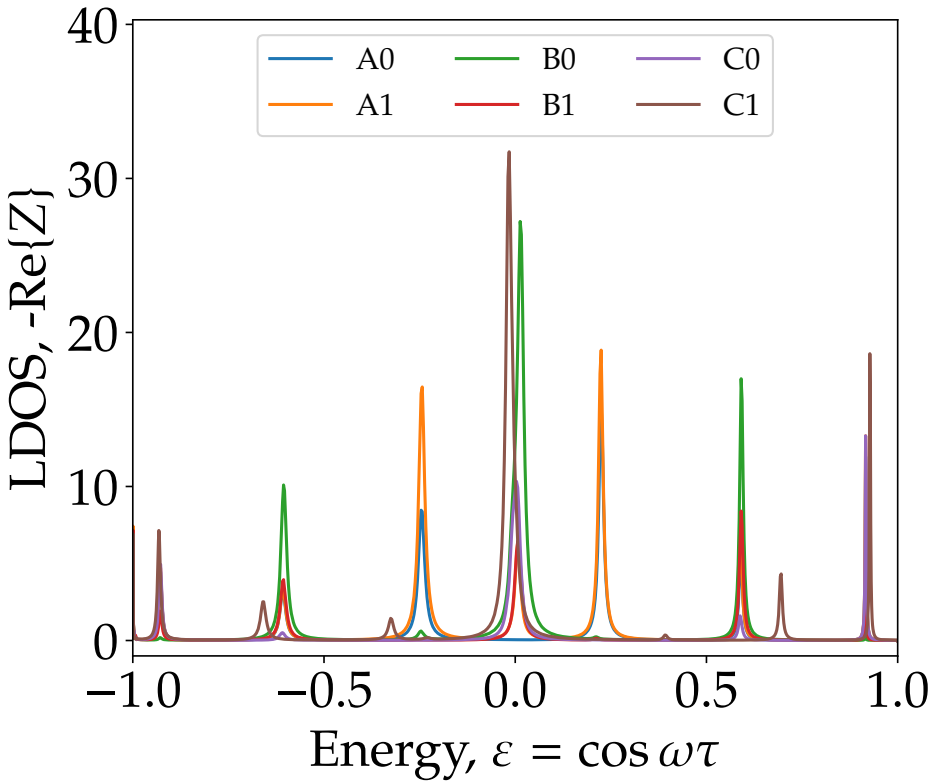

(b)

Figure A.0.11: This is the structure ζ in the sequence of zeroth homotopy groups. Two unequal sections are critical in this structure, and the constraint map for mutual orthogonality is now satisfied. This results in four zero energy states indicated by non-zero support on both sublattices for two sections. RG58 cables are indicated with a dashed line, and RG62 cables with a solid line.

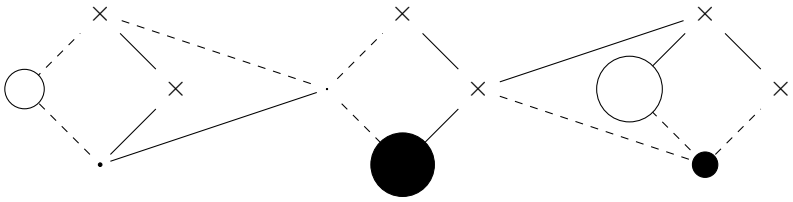

(a)

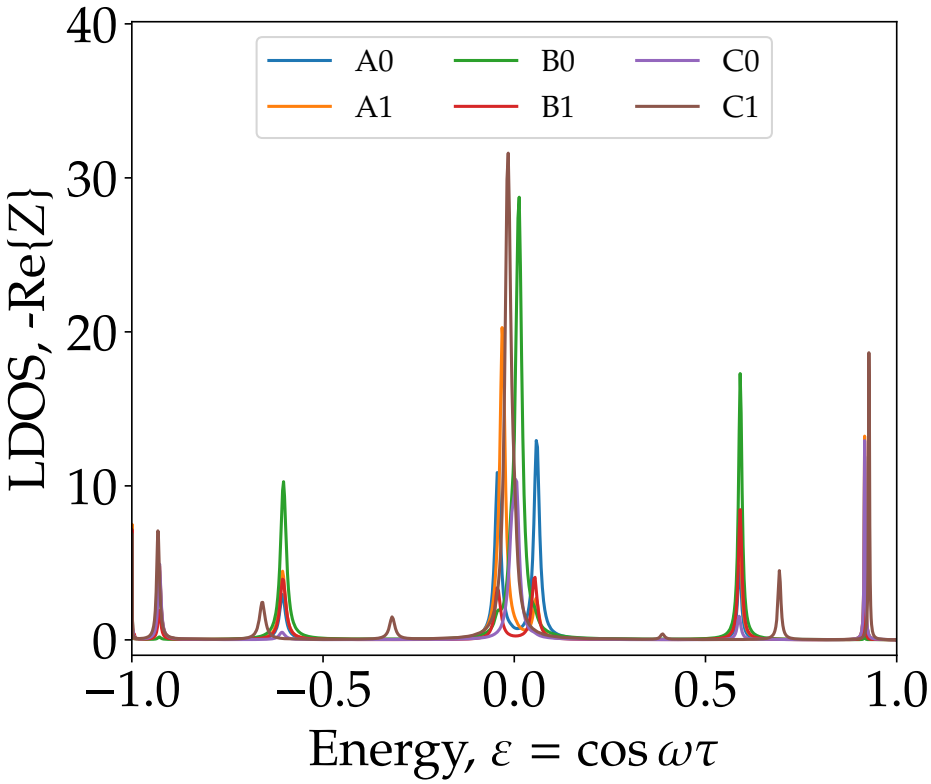

(b)

Figure A.0.12: This is the structure κ in the sequence of zeroth homotopy groups. All sections are critical in this structure, and the constraint map for mutual orthogonality is satisfied for two of the sections. This results in four zero energy states indicated by non-zero support on both sublattices on one section, and support on only one sublattice for each of the two sections where mutual orthogonality is not satisfied. Note that due to the narrow gap for the sites A0 and B1 these data were integrated between $\varepsilon = -0.025$ and $\varepsilon = 0.025$ (113.3MHz and 117MHz). RG58 cables are indicated with a dashed line, and RG62 cables with a solid line.

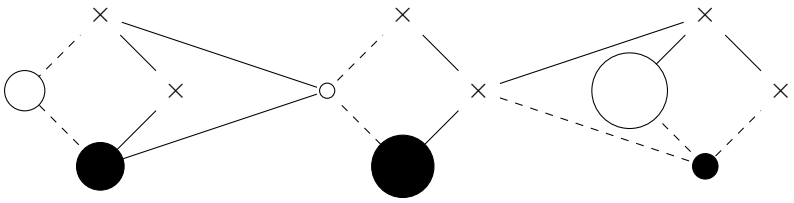

(a)

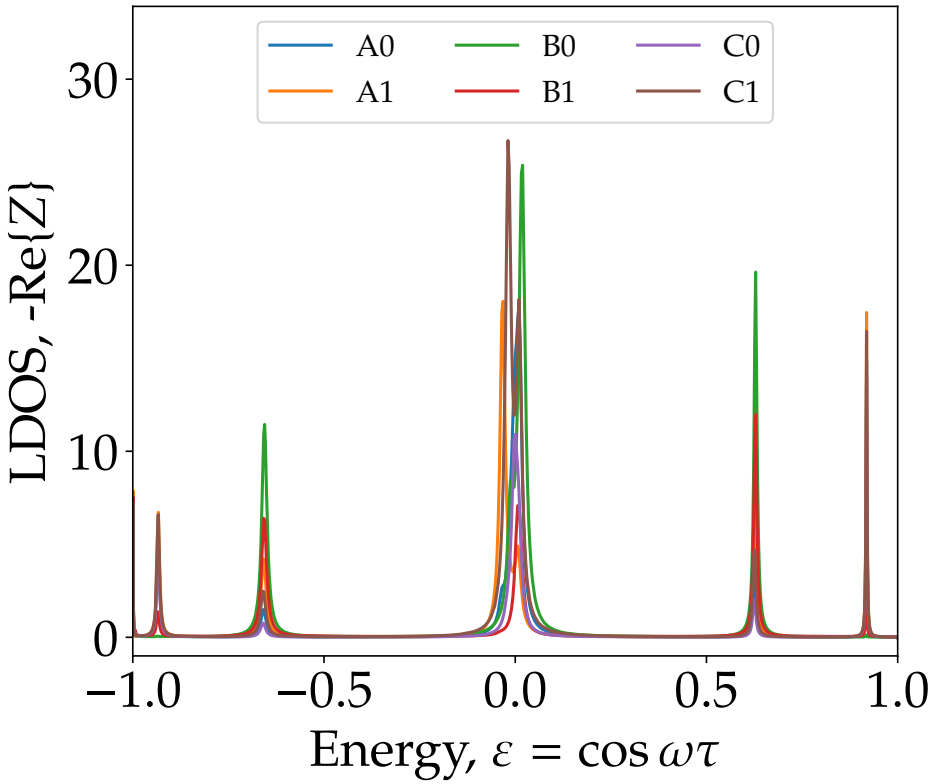

(b)

Figure A.0.13: This is the structure σ in the sequence of zeroth homotopy groups. All sections are critical in this structure, and the constraint map for mutual orthogonality are satisfied. This results in six zero energy states indicated by non-zero support on both sublattices of every section. RG58 cables are indicated with a dashed line, and RG62 cables with a solid line.

Appendix B

Supplementary material from SSH paper

Supplementary Materials: Observation of a Topological Phase Transition in Random Coaxial Cable Structures with Chiral Symmetry

S1 DERIVATION OF TIGHT BINDING HAMILTONIAN

Our system consists of a series of sections of transmission line of length d_n, with transmission speed c_n and impedance Z_n. Wave proagation in such a structure is determined by the telegraph equations. In each section, the voltage $V(x)$ is determined by a Helmholtz equation

$$\frac{d^2V}{dx^2} + \left(\frac{\omega}{c_n}\right)^2 V = 0 \,, \tag{S1}$$

where ω is the frequency. At the boundaries between sections both V and the current,

$$I = -i\frac{c_n}{\omega Z_n}\frac{dV}{dx} \,, \tag{S2}$$

are continuous.

For a piece-wise continuous system, we conventionally solve this equation using transfer matrices. In a given section, the solution can be written

$$V(x) = V(0)\cos(\omega x/c_n) + iZ_nI(0)\sin(\omega x/c_n) \tag{S3}$$

$$I(x) = iZ_n^{-1}V(0)\sin(\omega x/c_n) + I(0)\cos(\omega x/c_n). \tag{S4}$$

Thus, at the end of the section $x = d_n$,

$$\begin{pmatrix} V(d_n) \\ I(d_n) \end{pmatrix} = \mathcal{M}_n \begin{pmatrix} V(0) \\ I(0) \end{pmatrix} = \begin{pmatrix} \cos(\omega d_n/c_n) & iZ_n\sin(\omega d_n/c_n) \\ i/Z_n\sin(\omega d_n/c_n) & \cos(\omega d_n/c_n) \end{pmatrix} \begin{pmatrix} V(0) \\ I(0) \end{pmatrix} \tag{S5}$$

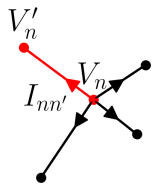

FIG. S1. Site n of the network and its neighbours. $I_{nn'}$ is the current flowing out of site n towards n'.

We next demonstrate that a transmission line network is equivalent to a tight-binding system when each section has the same transit time, $\tau = d_n/c_n$. To show this, let us add to the notation a little so that V_n is the voltage at the n^{th} junction (site), and $I_{nn'}$ is the current flowing out of that junction to connected site n'. $Z_{nn'}$ is the impedance of the section between sites n and n'. Then the transfer matrix gives

$$V_{n'} = V_n\cos\omega\tau + iZ_{nn'}I_{nn'}\sin\omega\tau, \tag{S6}$$

We can use this to find $I_{nn'}$ in terms of V_n and $V_{n'}$, then apply Kirchhoff's junction rule, $\sum_{n'} I_{nn'} = 0$, to get

$$\sum_{n'} Z_{nn'}^{-1}(V_{n'} - V_n\cos\omega\tau) = 0 \,. \tag{S7}$$

Here, the sum over n' includes the sites which are directly connected to n. Identifying $\varepsilon = \cos\omega\tau$, this becomes

$$\sum_{n'} Z_{nn'}^{-1}V_{n'} = \varepsilon\sum_{n'} Z_{nn'}^{-1}\,V_n \,. \tag{S8}$$

This is a generalised eigenvalue problem, but we can turn it into the standard form by defining scaled voltages depending on the impedances of the cables connected to site n:

$$v_n = \left(\sum_{n'} Z_{nn'}^{-1}\right)^{\frac{1}{2}} V_n = \sigma_n^{-1}\,V_n \,. \tag{S9}$$

Then we have the tight binding system

$$\sum_{n'} H_{nn'} v_{n'} = \varepsilon\, v_n \ , \tag{S10}$$

with

$$H_{nn'} = \sigma_n Z^{-1}_{nn'} \sigma'_n \ . \tag{S11}$$

Note that the 'energy', ε is not the frequency, so zero energy corresponds to finite frequency; indeed the spectrum repeats periodically in frequency.

S2 ADDING INPUTS AND OUTPUTS

In this section, we show how to add inputs and outputs to the tight binding model derived above. We shall consider an experiment where we connect an input to site α, which we model as an ideal voltage source with amplitude $V_{\rm in}$ in series with an impedance $Z_{\rm in}$. We measure an output voltage at site β, using a detector which is modelled as an ideal voltmeter in parallel with an impedance $Z_{\rm out}$. The measured output voltage is simply the site voltage $V_{\rm out} = V_\beta$.

We start with the detector. From the circuit point of view, this is simply an impedance $Z_{\rm out}$, which causes an additional current out of the site β, with magnitude $I_{\rm out} = V_\beta / Z_{\rm out}$. The expression from Kirchhoff's rule for site β is then modified to

$$\sum_{n'} Z^{-1}_{\beta n'} V_{n'} + i Z^{-1}_{\rm out} \sqrt{1-\varepsilon^2}\, V_\beta = \varepsilon \sum_{n'} Z^{-1}_{\beta n'}\, V_\beta \ , \tag{S12}$$

since $\sin \omega\tau = \sqrt{1-\varepsilon^2}$. Now scaling the voltages as in Eq.(S9), the tight binding equation for site β becomes

$$\sum_{n'} H_{\beta n'} v_{n'} + i\Gamma_{\rm out} \sqrt{1-\varepsilon^2}\, v_\beta = \varepsilon\, v_\beta \ , \tag{S13}$$

where $\Gamma_{\rm out} = \sigma_\beta^2\, Z^{-1}_{\rm out}$; the finite impedance leads to an on-site imaginary energy for site β.

Doing a similar thing for the source, on site α, we get a slightly more complicated result. If the source voltage is $V_{\rm in}$, and it has an impedance $Z_{\rm in}$, there is an extra current flowing into site α, $I_{\rm in}$, determined by

$$V_\alpha = V_{\rm in} - I_{\rm in} Z_{\rm in} \ . \tag{S14}$$

subtracting this from the Kirchhoff expression gives

$$\sum_{n'} Z^{-1}_{\alpha n'} V_{n'} + i Z^{-1}_{\rm in} \sqrt{1-\varepsilon^2}\, (V_\alpha - V_{\rm in}) = \varepsilon \sum_{n'} Z^{-1}_{\alpha n'}\, V_\alpha \ . \tag{S15}$$

Rearranging, and scaling, we get

$$\sum_{n'} H_{\alpha n'} v_{n'} + i\Gamma_{\rm in} \sqrt{1-\varepsilon^2}\, v_\alpha = \varepsilon\, v_\alpha + i\sqrt{1-\varepsilon^2}\, v_{\rm in} \ , \tag{S16}$$

where $\Gamma_{\rm in} = \sigma_\alpha^2\, Z^{-1}_{\rm in}$ and $v_{\rm in} = \sigma_\alpha\, Z^{-1}_{\rm in}\, V_{\rm in}$. The input adds an on-site imaginary energy and a driving term at site α.

We now have a matrix system which takes the form

$$(H + i\Gamma) v = \varepsilon v + i\,\mathcal{V} \ , \tag{S17}$$

where the 'Hamiltonian' H is the same as in Eq(S10), and Γ is diagonal with the only entries the loss terms $\Gamma_{\rm in}\sqrt{1-\varepsilon^2}$ and $\Gamma_{\rm out}\sqrt{1-\varepsilon^2}$ on sites α and β. The driving term $\mathcal{V}$ has the single entry $\sqrt{1-\varepsilon^2}\, v_{\rm in}$ on site α.

We can diagonalise H to find its eigenvalues ε_k, and eigenvectors $u^{(k)}$. Then $H = UDU^\dagger$ where U is the unitary with matrix elements $U_{ij} = u_i^{(j)}$ and D is a diagonal matrix with $D_{ii} = \varepsilon_i$. This can be used to invert $H - \varepsilon \mathbb{1}$ to get the Green's function

$$g = (H - \varepsilon \mathbb{1})^{-1} = U (D - \varepsilon \mathbb{1})^{-1} U^\dagger, \tag{S18}$$

so that

$$g_{ij} = \sum_k \frac{u_i^{(k)} u_j^{(k)*}}{\varepsilon_k - \varepsilon} \ . \tag{S19}$$

With this, we can relate the output and input voltages for the case where the input and output impedances are infinite, so the loss terms, $\Gamma_{\rm in}$ and $\Gamma_{\rm out}$ are zero:

$$v_{\rm out} = v_\beta = i g_{\beta\alpha} \sqrt{1-\varepsilon^2}\, v_{\rm in} \ . \tag{S20}$$

However, we really want to find $G = (H + i\Gamma - \varepsilon \mathbb{1})^{-1}$, to deal with the case where there are finite losses. Since Γ has only two non-zero entries, this can be calculated using the Sherman Morrison formula twice to obtain

$$G_{\beta\alpha} = \frac{g_{\beta\alpha}}{1 + \Gamma_{\rm in}\Gamma_{\rm out}(1-\varepsilon^2)(g_{\beta\alpha}g_{\alpha\beta} - g_{\alpha\alpha}g_{\beta\beta}) + i\sqrt{1-\varepsilon^2}(\Gamma_{\rm in}g_{\alpha\alpha} + \Gamma_{\rm out}g_{\beta\beta})} \ . \tag{S21}$$

Then

$$v_{\rm out} = i G_{\beta\alpha} \sqrt{1-\varepsilon^2}\, v_{\rm in} \ , \tag{S22}$$

or, in terms of the unscaled physical quantities,

$$V_{\rm out} = i\sigma_\beta\sigma_\alpha\, G_{\beta\alpha}\, Z_{\rm in}^{-1} \sqrt{1-\varepsilon^2}\, V_{\rm in} \ . \tag{S23}$$

For a single port measurement, connecting only to site α and measuring V_α to obtain the complex reflectance, we put $\Gamma_{\rm out} = 0$ and get

$$\frac{V_\alpha}{V_{\rm in}} = i\sigma_\alpha^2\, Z_{\rm in}^{-1} \frac{\sqrt{1-\varepsilon^2}\, g_{\alpha\alpha}}{1 + i\Gamma_{\rm in}\sqrt{1-\varepsilon^2}\, g_{\alpha\alpha}} = \frac{i\sigma_\alpha^2\sqrt{1-\varepsilon^2}\, g_{\alpha\alpha}}{Z_{\rm in} + i\sigma_\alpha^2\sqrt{1-\varepsilon^2}\, g_{\alpha\alpha}} \ . \tag{S24}$$

However, we can also think of the circuit as simply a potential divider, with the input $V_{\rm in}$ connected across the input impedance $Z_{\rm in}$ in series with an effective impedance Z_α representing the network. In these terms, we get

$$\frac{V_\alpha}{V_{\rm in}} = \frac{Z_\alpha}{Z_{\rm in} + Z_\alpha}, \tag{S25}$$

so the network impedance is just

$$Z_\alpha = i\sigma_\alpha^2 \sqrt{1-\varepsilon^2}\, g_{\alpha\alpha} \ . \tag{S26}$$

Hence

$$-\frac{{\rm Re}\{Z_\alpha\}}{\sigma_\alpha^2\sqrt{1-\varepsilon^2}} = {\rm Im}\{g_{\alpha\alpha}\} = \sum_k |u_\alpha^{(k)}|^2\, \delta(\varepsilon - \varepsilon_k) \ , \tag{S27}$$

which is the unbroadened local density of states on site α. In practice, the delta function peaks are broadened by the small resistive losses within the cables.

S3 EXPERIMENTAL DETAILS

We make our experimental structures using two types of coaxial cable: RG58 and RG62, with impedances of, respectively, 50 and 93Ω. In order to obtain the mapping onto the tight binding Hamiltonian, and thus chiral symmetry, it is essential that the transmission time, τ, in each section of the cable is the same. For our choice of zero energy at $\sim$ 114MHz, this corresponds to nominal cable lengths of approximately 41cm and 55cm for the RG58 and RG62 cables, as they have different propagation speeds. However, to obtain the accurate chiral symmetry in our results, it was necessary to consider the contribution of the SMA connectors used to join the cables, which all have 50Ω impedance. To account for these, the RG58 cables were shortened and the RG62 cables lengthened, such that, in a structure where they alternate, the transmission times in the 50Ω and 93Ω sections were the same. However double sections of the same cable type are then the wrong length, and the RG62 doubles contain a pair of 50Ω connectors in the middle. We avoided this problem by using special double length cables of each type. It is clearly possible also to make triple and greater lengths, but instead we restricted our random sequences to those containing no more than pair repeats.

Radio frequency spectra were obtained using a vector network analyser (NanoVNA V2 Plus4). Our results use two types of measurements. We find the impedance, and thus the local density of states, using a single port measurement of the S_{11} parameter. The structure impedance is then given by

$$Z_s = \frac{1 + S_{11}}{1 - S_{11}} Z_{\rm in} \ , \tag{S28}$$

where $Z_{\rm in}$ is the output impedance of the VNA. The value of the transmission amplitude, S_{21}, is obtained directly from a two port measurement between the ends of the cable. The adjustments to the cable lengths to account for the connectors, as described above, moves the effective junctions, and hence the sites in the tight binding model, to the points where the RG62 cables enter their SMA connectors. In the impedance measurements on the terminated chains, we accounted for this by calculating the correction to the impedance due to the transmission through the SMA connector between the physical junction with the VNA and the effective site position. At the opposite end to the measurement, the length of the terminating cable also needed to be modified, so that the final site corresponds to the end of the cable. For an RG62 termination, we simply removed the connector at the end, while in the RG58 case a slightly longer cable accounted for the pair of SMA connectors required to obtain the correct position.

Bibliography

[1] William Thomson. "4. On Vortex Atoms". In: *Proceedings of the Royal Society of Edinburgh* 6 (1869), 94–105. DOI: 10.1017/S0370164600045430.

[2] M. Jayaseelan, Joseph D. Murphree, Justin T. Schultz, Janne Roustekoski, and Nicholas P. Bigelow. "Topological atom optics and beyond with knotted quantum wavefunctions". In: *Commun. Phys.* 7 (7 2024). DOI: 10.1038/s42005-023-01499-0. URL: https://doi.org/10.1038/s42005-023-01499-0.

[3] Bo-Hung Chen and Dah-Wei Chiou. "An elementary rigorous proof of bulk-boundary correspondence in the generalized Su-Schrieffer-Heeger model". In: *Physics Letters A* 384.7 (2020), p. 126168. ISSN: 0375-9601. DOI: https://doi.org/10.1016/j.physleta.2019.126168. URL: https://www.sciencedirect.com/science/article/pii/S0375960119311028.

[4] Dimitrie Culcer, Aydın Cem Keser, Yongqing Li, and Grigory Tkachov. "Transport in two-dimensional topological materials: recent developments in experiment and theory". In: *2D Materials* 7.2 (2020), p. 022007. DOI: 10.1088/2053-1583/ab6ff7. URL: https://dx.doi.org/10.1088/2053-1583/ab6ff7.

[5] Andreas P. Schnyder, Shinsei Ryu, Akira Furusaki, and Andreas W. W. Ludwig. "Classification of topological insulators and superconductors in three spatial dimensions". In: *Phys. Rev. B* 78 (19 2008), p. 195125. DOI: 10.1103/PhysRevB.78.195125. URL: https://link.aps.org/doi/10.1103/PhysRevB.78.195125.

[6] Michael H. Freedman, Alexei Kitaev, Michael J. Larsen, and Zhenghan Wang. *Topological Quantum Computation*. 2002. arXiv: quant-ph/0101025 [quant-ph].

[7] Tsuneya Ando, Yukio Matsumoto, and Yasutada Uemura. "Theory of Hall Effect in a Two-Dimensional Electron System". In: *Journal of the Physical Society of Japan* 39.2 (Aug. 1975), pp. 279–288. DOI: 10.1143/JPSJ.39.279.

[8] Jun Wakabayashi and Shinji Kawaji. "Hall Effect in Silicon MOS Inversion Layers under Strong Magnetic Fields". In: *Journal of the Physical Society of Japan* 44 (1978), pp. 1839–1849. URL: https://api.semanticscholar.org/CorpusID:204177545.

[9] D. J. Thouless, M. Kohmoto, M. P. Nightingale, and M. den Nijs. "Quantized Hall Conductance in a Two-Dimensional Periodic Potential". In: *Phys. Rev. Lett.* 49 (6 1982), pp. 405–408. DOI: 10.1103/PhysRevLett.49.405. URL: https://link.aps.org/doi/10.1103/PhysRevLett.49.405.

[10] C. L. Kane and E. J. Mele. "Quantum Spin Hall Effect in Graphene". In: *Phys. Rev. Lett.* 95 (22 2005), p. 226801. DOI: 10.1103/PhysRevLett.95.226801. URL: https://link.aps.org/doi/10.1103/PhysRevLett.95.226801.

[11] Markus König, Steffen Wiedmann, Christoph Brüne, Andreas Roth, Hartmut Buhmann, Laurens W. Molenkamp, Xiao-Liang Qi, and Shou-Cheng Zhang. "Quantum Spin Hall Insulator State in HgTe Quantum Wells". In: *Science* 318.5851 (2007), pp. 766–770. DOI: 10.1126/science.1148047. eprint: https://www.science.org/doi/pdf/10.1126/science.1148047. URL: https://www.science.org/doi/abs/10.1126/science.1148047.

[12] Jennifer Cano, Barry Bradlyn, Zhijun Wang, L. Elcoro, M. G. Vergniory, C. Felser, M. I. Aroyo, and B. Andrei Bernevig. "Building blocks of topological quantum chemistry: Elementary band representations". In: *Phys. Rev. B* 97 (3 2018), p. 035139. DOI: 10.1103/PhysRevB.97.035139. URL: https://link.aps.org/doi/10.1103/PhysRevB.97.035139.

[13] Jennifer Cano M. G. Vergniory Zhijun Wang C. Felser M. I. Aroyo & B. Andrei Bernevig Barry Bradlyn L. Elcoro. "Topological quantum chemistry". In: *Nature* 547 (2017), p. 298. DOI: 10.1038/nature23268. URL: https://www.nature.com/articles/nature23268.

[14] Claudia Felser Nicolas Regnault B. Andrei Bernevig & Zhijun Wang M. G. Vergniory L. Elcoro. "A complete catalogue of high-quality topological materials". In: *Nature* 566 (2019), p. 480. DOI: 10.1038/s41586-019-0954-4. URL: https://www.nature.com/articles/s41586-019-0954-4.

[15] Emil Prodan. "Bulk and Boundary Invariants for Complex Topological Insulators: From K-Theory to Physics". In: Springer International Publishing, 2016. ISBN: 978-3-319-29350-9. DOI: 10.1007/978-3-319-29351-6. URL: https://link.springer.com/book/10.1007/978-3-319-29351-6#toc.

[16] Raffaello Bianco and Raffaele Resta. "Mapping topological order in coordinate space". In: *Phys. Rev. B* 84 (24 2011), p. 241106. DOI: 10.1103/PhysRevB.84.241106. URL: https://link.aps.org/doi/10.1103/PhysRevB.84.241106.

[17] Urs Gebert, Bernhard Irsigler, and Walter Hofstetter. "Local Chern marker of smoothly confined Hofstadter fermions". In: *Phys. Rev. A* 101 (6 2020), p. 063606. DOI: 10.1103/PhysRevA.101.063606. URL: https://link.aps.org/doi/10.1103/PhysRevA.101.063606.

[18] Abhijeet Alase, Emilio Cobanera, Gerardo Ortiz, and Lorenza Viola. "Wiener–Hopf factorization approach to a bulk-boundary correspondence and stability conditions for topological zero-energy modes". In: *Annals of Physics* 458 (2023), p. 169457. ISSN: 0003-4916. DOI: https://doi.org/10.1016/j.aop.2023.169457. URL: https://www.sciencedirect.com/science/article/pii/S0003491623002592.

[19] Emil Prodan. "Disordered topological insulators: a non-commutative geometry perspective". In: *Journal of Physics A: Mathematical and Theoretical* 44.11 (2011), p. 113001. DOI: 10.1088/1751-8113/44/11/113001. URL: https://dx.doi.org/10.1088/1751-8113/44/11/113001.

[20] R. Flores-Calderon, Roderich Moessner, and Ashley M. Cook. "Time-reversal invariant finite-size topology". In: *Phys. Rev. B* 108 (12 2023), p. 125410. DOI: 10.1103/PhysRevB.108.125410. URL: https://link.aps.org/doi/10.1103/PhysRevB.108.125410.

[21] Ashley M. Cook and Anne E. B. Nielsen. "Finite-size topology". In: *Phys. Rev. B* 108 (4 2023), p. 045144. DOI: 10.1103/PhysRevB.108.045144. URL: https://link.aps.org/doi/10.1103/PhysRevB.108.045144.

[22] Nicola Marzari and David Vanderbilt. "Maximally localized generalized Wannier functions for composite energy bands". In: *Phys. Rev. B* 56 (20 1997), pp. 12847–12865. DOI: 10.1103/PhysRevB.56.12847. URL: https://link.aps.org/doi/10.1103/PhysRevB.56.12847.

[23] Nicola Marzari, Arash A. Mostofi, Jonathan R. Yates, Ivo Souza, and David Vanderbilt. "Maximally localized Wannier functions: Theory and applications". In: *Rev. Mod. Phys.* 84 (4 2012), pp. 1419–1475. DOI: 10.1103/RevModPhys.84.1419. URL: https://link.aps.org/doi/10.1103/RevModPhys.84.1419.

[24] W. P. Su, J. R. Schrieffer, and A. J. Heeger. "Solitons in Polyacetylene". In: *Phys. Rev. Lett.* 42 (25 1979), pp. 1698–1701. DOI: 10.1103/PhysRevLett.42.1698. URL: https://link.aps.org/doi/10.1103/PhysRevLett.42.1698.

[25] Yoichi Ando. "Topological Insulator Materials". In: *Journal of the Physical Society of Japan* 82.10 (2013), p. 102001. DOI: 10.7566/JPSJ.82.102001. eprint: https://doi.org/10.7566/JPSJ.82.102001. URL: https://doi.org/10.7566/JPSJ.82.102001.

[26] Sergey Kruk, Alexey Slobozhanyuk, Denitza Denkova, Alexander Poddubny, Ivan Kravchenko, Andrey Miroshnichenko, Dragomir Neshev, and Yuri Kivshar. "Edge States and Topological Phase Transitions in Chains of Dielectric Nanoparticles". In: *Small* 13.11 (2017), p. 1603190. DOI: https://doi.org/10.1002/smll.201603190. eprint: https://onlinelibrary.wiley.com/doi/pdf/10.1002/smll.201603190. URL: https://onlinelibrary.wiley.com/doi/abs/10.1002/smll.201603190.

[27] Simon Stützer, Yanatan Plotnik, Yaakov Lumer, Paraj Titum, Netanel H. Lindner, Mordechai Segev, Mikael C. Rechtsman, and Alexander Szameit. "Photonic topological Anderson insulators". In: *Nature* 560 (2018), pp. 461–465. DOI: https://doi.org/10.1038/s41586-018-0418-2.

[28] Maciej Pieczarka, Eliezer Estrecho, Sanjib Ghosh, Matthias Wurdack, Mark Steger, David W. Snoke, Kenneth West, Loren N. Pfeiffer, Timothy C. H. Liew, Andrew G. Truscott, and Elena A. Ostrovskaya. "Topological phase transition in an all-optical exciton-polariton lattice". In: *Optica* 8.8 (2021), pp. 1084–1091. DOI: 10.1364/

OPTICA.426996. URL: https://opg.optica.org/optica/abstract.cfm?URI=optica-8-8-1084.

[29] M. Born and R. Oppenheimer. "Zur Quantentheorie der Molekeln". In: *Annalen der Physik* 389.20 (1927), pp. 457–484. DOI: https://doi.org/10.1002/andp.19273892002. eprint: https://onlinelibrary.wiley.com/doi/pdf/10.1002/andp.19273892002. URL: https://onlinelibrary.wiley.com/doi/abs/10.1002/andp.19273892002.

[30] Douglas Rayner Hartree and W. Hartree. "Self-consistent field, with exchange, for beryllium". In: *Proceedings of the Royal Society of London. Series A - Mathematical and Physical Sciences* 150.869 (1935), pp. 9–33. DOI: 10.1098/rspa.1935.0085. eprint: https://royalsocietypublishing.org/doi/pdf/10.1098/rspa.1935.0085. URL: https://royalsocietypublishing.org/doi/abs/10.1098/rspa.1935.0085.

[31] V Fock. "Näherungsmethode zur Lösung des quantenmechanischen Mehrkörperproblems". In: *Z. Physik* 61 (1930), pp. 126–148. DOI: 10.1007/BF01340294. URL: https://doi.org/10.1007/BF01340294.

[32] P. Hohenberg and W. Kohn. "Inhomogeneous Electron Gas". In: *Phys. Rev.* 136 (3B 1964), B864–B871. DOI: 10.1103/PhysRev.136.B864. URL: https://link.aps.org/doi/10.1103/PhysRev.136.B864.

[33] He Li, Zun Wang, Nianlong Zou, Meng Ye, Runzhang Xu, Xiaoxun Gong, Wenhui Duan, and Yong Xu. "Deep-learning density functional theory Hamiltonian for efficient ab initio electronic-structure calculation". In: *Nature Computational Science* 2 (2021), pp. 367 –377. URL: https://api.semanticscholar.org/CorpusID:248887842.

[34] W. Jones and N.H. March. "Theoretical Solid State Physics". In: Dover books on physics and chemistry v. 1. Wiley-Interscience, 1973, pp. 12–15. ISBN: 9780471449003. URL: https://books.google.co.uk/books?id=qyzienNSa2EC.

[35] Erich Hückel. "Quantentheoretische Beiträge zum Benzolproblem". In: *Zeitschrift für Physik* 70 (1931), pp. 204–286. URL: https://api.semanticscholar.org/CorpusID:186218131.

[36] Erich Hückel. "Quantentheoretische Beiträge zum Problem der aromatischen und ungesättigten Verbindungen. III". In: *Zeitschrift für Physik* 76 (1932), pp. 628–648. URL: https://api.semanticscholar.org/CorpusID:121787219.

[37] Felix Bloch. "Über die Quantenmechanik der Elektronen in Kristallgittern". In: *Zeitschrift für Physik* 52 (1929), pp. 555–600. URL: https://api.semanticscholar.org/CorpusID:120668259.

[38] Gregory H. Wannier. "The Structure of Electronic Excitation Levels in Insulating Crystals". In: *Phys. Rev.* 52 (3 1937), pp. 191–197. DOI: 10.1103/PhysRev.52.191. URL: https://link.aps.org/doi/10.1103/PhysRev.52.191.

[39] David S Simon. "Topology and physics: a historical overview". In: *Tying Light in Knots*. 2053-2571. Morgan & Claypool Publishers, 2018, 1–1 to 1–7. ISBN: 978-1-64327-234-4. DOI: 10.1088/2053-2571/aaddd5ch1. URL: https://dx.doi.org/10.1088/2053-2571/aaddd5ch1.

[40] Chen Ning Yang, Mo-Lin Ge, and Yang-Hui He. *Topology and Physics*. WORLD SCIENTIFIC, 2019. DOI: 10.1142/11217. eprint: https://worldscientific.com/doi/pdf/10.1142/11217. URL: https://worldscientific.com/doi/abs/10.1142/11217.

[41] Léon Van Hove. "The Occurrence of Singularities in the Elastic Frequency Distribution of a Crystal". In: *Phys. Rev.* 89 (6 1953), pp. 1189–1193. DOI: 10.1103/PhysRev.89.1189. URL: https://link.aps.org/doi/10.1103/PhysRev.89.1189.

[42] Michael Victor Berry. "Quantal phase factors accompanying adiabatic changes". In: *Proc. R. Soc. Lond. A* 392 (1984), 45–57.

[43] Max Born and Vladimir Fock. "Beweis des Adiabatensatzes". In: *Zeitschrift für Physik* 51 (3 1928), pp. 165–180.

[44] J. Zak. "Berry's phase for energy bands in solids". In: *Phys. Rev. Lett.* 62 (23 1989), pp. 2747–2750. DOI: 10.1103/PhysRevLett.62.2747. URL: https://link.aps.org/doi/10.1103/PhysRevLett.62.2747.

[45] Di Xiao, Ming-Che Chang, and Qian Niu. "Berry phase effects on electronic properties". In: *Rev. Mod. Phys.* 82 (3 2010), pp. 1959–2007. DOI: 10.1103/RevModPhys.82.1959. URL: https://link.aps.org/doi/10.1103/RevModPhys.82.1959.

[46] Barry Simon. "Holonomy, the Quantum Adiabatic Theorem, and Berry's Phase". In: *Phys. Rev. Lett.* 51 (24 1983), pp. 2167–2170. DOI: 10.1103/PhysRevLett.51.2167. URL: https://link.aps.org/doi/10.1103/PhysRevLett.51.2167.

[47] Efton Park. "K-theory". In: *Complex Topological K-Theory*. Cambridge Studies in Advanced Mathematics. Cambridge University Press, 2008, 51–110.

[48] F. D. M. Haldane. "Model for a Quantum Hall Effect without Landau Levels: Condensed-Matter Realization of the "Parity Anomaly"". In: *Phys. Rev. Lett.* 61 (18 1988), pp. 2015–2018. DOI: 10.1103/PhysRevLett.61.2015. URL: https://link.aps.org/doi/10.1103/PhysRevLett.61.2015.

[49] Emil Prodan. "Non-commutative Brillouin Torus". In: *A Computational Non-commutative Geometry Program for Disordered Topological Insulators*. Cham: Springer International Publishing, 2017, pp. 25–48. ISBN: 978-3-319-55023-7. DOI: 10.1007/978-3-319-55023-7_3. URL: https://doi.org/10.1007/978-3-319-55023-7_3.

[50] Terry A. Loring. "K-theory and pseudospectra for topological insulators". In: *Annals of Physics* 356 (2015), pp. 383–416. ISSN: 0003-4916. DOI: https://doi.org/10.1016/j.aop.2015.02.031. URL: https://www.sciencedirect.com/science/article/pii/S0003491615000901.

[51] Alexander Cerjan and Terry A. Loring. "Local invariants identify topology in metals and gapless systems". In: *Phys. Rev. B* 106 (6 2022), p. 064109. DOI: 10.1103/PhysRevB.106.064109. URL: https://link.aps.org/doi/10.1103/PhysRevB.106.064109.

[52] Abhijeet Alase, Emilio Cobanera, Gerardo Ortiz, and Lorenza Viola. "Generalization of Bloch's theorem for arbitrary boundary conditions: Theory". In: *Phys. Rev. B* 96 (19 2017), p. 195133. DOI: 10.1103/PhysRevB.96.195133. URL: https://link.aps.org/doi/10.1103/PhysRevB.96.195133.

[53] Emilio Cobanera, Abhijeet Alase, Gerardo Ortiz, and Lorenza Viola. "Generalization of Bloch's theorem for arbitrary boundary conditions: Interfaces and topological surface band structure". In: *Phys. Rev. B* 98 (24 2018), p. 245423. DOI: 10.1103/PhysRevB.98.245423. URL: https://link.aps.org/doi/10.1103/PhysRevB.98.245423.

[54] Alexander Altland and Martin R. Zirnbauer. "Nonstandard symmetry classes in mesoscopic normal-superconducting hybrid structures". In: *Phys. Rev. B* 55 (2 1997), pp. 1142–1161. DOI: 10.1103/PhysRevB.55.1142. URL: https://link.aps.org/doi/10.1103/PhysRevB.55.1142.

[55] M. Karoubi. *K-Theory: An Introduction*. Classics in Mathematics. Springer, 2008. ISBN: 9783540798897. URL: https://books.google.co.uk/books?id=i3A1T7nhVHMC.

[56] Alexei Kitaev. "Periodic table for topological insulators and superconductors". In: *AIP Conference Proceedings* 1134.1 (May 2009), pp. 22–30. ISSN: 0094-243X. DOI: 10.1063/1.3149495. eprint: https://pubs.aip.org/aip/acp/article-pdf/1134/1/22/11584243/22_1_online.pdf. URL: https://doi.org/10.1063/1.3149495.

[57] Hosho Katsura and Tohru Koma. "The noncommutative index theorem and the periodic table for disordered topological insulators and superconductors". In: *Journal of Mathematical Physics* 59.3 (Mar. 2018), p. 031903. ISSN: 0022-2488. DOI: 10.1063/1.5026964. eprint: https://pubs.aip.org/aip/jmp/article-pdf/doi/10.1063/1.5026964/14040818/031903_1_online.pdf. URL: https://doi.org/10.1063/1.5026964.

[58] Hoi Chun Po, Haruki Watanabe, and Ashvin Vishwanath. "Fragile topology and Wannier obstructions". In: *Physical review letters* 121.12 (2018), p. 126402. DOI: 10.1103/PhysRevLett.121.126402. URL: https://link.aps.org/doi/10.1103/PhysRevLett.121.126402.

[59] Wladimir A. Benalcazar, B. Andrei Bernevig, and Taylor L. Hughes. "Quantized electric multipole insulators". In: *Science* 357.6346 (2017), pp. 61–66. DOI: 10.1126/science.aah6442. eprint: https://www.science.org/doi/pdf/10.1126/science.aah6442. URL: https://www.science.org/doi/abs/10.1126/science.aah6442.

[60] Max Geier, Luka Trifunovic, Max Hoskam, and Piet W. Brouwer. "Second-order topological insulators and superconductors with an order-two crystalline symmetry". In: *Phys. Rev. B* 97 (20 2018), p. 205135. DOI: 10.1103/PhysRevB.97.205135. URL: https://link.aps.org/doi/10.1103/PhysRevB.97.205135.

[61] Christian Brouder, Gianluca Panati, Matteo Calandra, Christophe Mourougane, and Nicola Marzari. "Exponential Localization of Wannier Functions in Insulators". In: *Phys. Rev. Lett.* 98 (4 2007), p. 046402. DOI: 10.1103/PhysRevLett.98.046402. URL: https://link.aps.org/doi/10.1103/PhysRevLett.98.046402.

[62] Raffaello Bianco and Raffaele Resta. "Mapping topological order in coordinate space". In: *Phys. Rev. B* 84 (24 2011), p. 241106. DOI: 10.1103/PhysRevB.84.241106. URL: https://link.aps.org/doi/10.1103/PhysRevB.84.241106.

[63] Frank Harary. "The Determinant of the Adjacency Matrix of a Graph". In: *SIAM Review* 4.3 (1962), pp. 202–210. ISSN: 00361445. URL: http://www.jstor.org/stable/2027712 (visited on 02/29/2024).

[64] Hörst Sachs. "Beziehungen zwischen den in einem Graphen enthaltenen Kreisen und seinem charakteristischen Polynom." In: *Publ. Math. Debrecen* 11 (1964), pp. 119–134.

[65] Irene Sciriha. "Maximal core size in singular graphs". In: *Ars Math. Contemp.* 2 (2009), pp. 217–229. URL: https://api.semanticscholar.org/CorpusID:54867540.

[66] Irene Sciriha and Ivan Gutman. "Nut graphs: Maximally extending cores". In: *Util. Math.* 54 (Nov. 1998), pp. 257–272.

[67] I. Sciriha. "On the construction of graphs of nullity one". In: *Discrete Math.* 181 (Feb. 1998), pp. 193–211.

[68] Patrick W. Fowler, Tomaž Pisanski, and Nino Bašić. "Charting the Space of Chemical Nut Graphs". In: *Physical chemistry chemical physics : PCCP* (2019).

[69] Irene Sciriha and Patrick W. Fowler. "On nut and core singular fullerenes". In: *Discrete Mathematics* 308.2 (2008). Combinatorics04, pp. 267–276. ISSN: 0012-365X. DOI: https://doi.org/10.1016/j.disc.2006.11.040. URL: https://www.sciencedirect.com/science/article/pii/S0012365X07003652.

[70] Irene Sciriha and Patrick W. Fowler. "Nonbonding Orbitals in Fullerenes: Nuts and Cores in Singular Polyhedral Graphs". In: *Journal of Chemical Information and Modeling* 47.5 (2007). PMID: 17691719, pp. 1763–1775. DOI: 10.1021/ci700097j. eprint: https://doi.org/10.1021/ci700097j. URL: https://doi.org/10.1021/ci700097j.

[71] P. W. Fowler, B. T. Pickup, T. Z. Todorova, Martha Borg, and Irene Sciriha. "Omni-conducting and omni-insulating molecules". In: *The Journal of Chemical Physics* 140.5 (Feb. 2014), p. 054115. ISSN: 0021-9606. DOI: 10.1063/1.4863559. eprint: https://pubs.aip.org/aip/jcp/article-pdf/doi/10.1063/1.4863559/15471788/054115_1_online.pdf. URL: https://doi.org/10.1063/1.4863559.

[72] Felix Hausdorff. “Grundzüge der Mengenlehre”. In: 1914.

[73] Oscar Zariski. “The compactness of the Riemann manifold of an abstract field of algebraic functions”. English. In: *Bull. Am. Math. Soc.* 50 (1944), pp. 683–691. ISSN: 0002-9904. DOI: 10.1090/S0002-9904-1944-08206-2.

[74] S.D. Cutkosky. *Introduction to Algebraic Geometry*. Graduate Studies in Mathematics. American Mathematical Society, 2018. Chap. 2. ISBN: 9781470435189. URL: https://books.google.co.uk/books?id=jAxJswEACAAJ.

[75] M. Yan and H.E. Press. *Introduction to Topology*. De Gruyter Textbook. De Gruyter, 2016. Chap. 4. ISBN: 9783110378160. URL: https://books.google.co.uk/books?id=DY2lCwAAQBAJ.

[76] D. M. Whittaker, Maxine M. McCarthy, and Qingqing Duan. *Observation of a Topological Phase Transition in Random Coaxial Cable Structures with Chiral Symmetry*. 2023. arXiv: 2311.11040 [cond-mat.dis-nn].

[77] D. M. Whittaker and R. Ellis. *Topological Protection in Disordered Photonic Multilayers and Transmission Lines*. 2021. arXiv: 2102.03641 [physics.optics].

[78] T. Jiang, M. Xiao, W.J. Chen, L. Yang, Y. Fang, W. Y. Tam, and C. T. Chan. “Experimental demonstration of angular momentum-dependent topological transport using a transmission line network”. In: *Nat Commun* 10 (434 2019). DOI: 10.1038/s41467-018-08281-9. URL: https://www.nature.com/articles/s41467-018-08281-9.

[79] Christopher Oliver, Denis Nabari, Hannah M. Price, Leonardo Ricci, and Iacopo Carusotto. *Photonic lattices of coaxial cables: flat bands and artificial magnetic fields*. 2023. arXiv: 2310.18325 [physics.optics].

[80] Su-Yang Xu, Y. Xia, L. A. Wray, S. Jia, F. Meier, J. H. Dil, J. Osterwalder, B. Slomski, A. Bansil, H. Lin, R. J. Cava, and M. Z. Hasan. “Topological Phase Transition and Texture Inversion in a Tunable Topological Insulator”. In: *Science* 332.6029 (2011), pp. 560–564. DOI: 10.1126/science.1201607. eprint: https://www.science.org/doi/pdf/10.1126/science.1201607. URL: https://www.science.org/doi/abs/10.1126/science.1201607.

[81] Youngwook Kim, Patrick Herlinger, Pilkyung Moon, Mikito Koshino, Takashi Taniguchi, Kenji Watanabe, and Jurgen H. Smet. “Charge Inversion and Topological Phase Transition at a Twist Angle Induced van Hove Singularity of Bilayer Graphene”. In: *Nano Letters* 16.8 (2016). PMID: 27387484, pp. 5053–5059. DOI: 10.1021/acs.nanolett.6b01906. eprint: https://doi.org/10.1021/acs.nanolett.6b01906. URL: https://doi.org/10.1021/acs.nanolett.6b01906.

[82] Si-Yu Li, Zhengwen Wang, Yucheng Xue, Yingbo Wang, Shihao Zhang, Jianpeng Liu, Zheng Zhu, Kenji Watanabe, Takashi Taniguchi, Hong-Jun Gao, Yuhang Jiang, and Jinhai Mao. “Imaging topological and correlated insulating states in twisted monolayer-bilayer graphene”. In: *Nature communications* 13.1 (2022), p. 4225. ISSN:

2041-1723. DOI: 10.1038/s41467-022-31851-x. URL: https://europepmc.org/articles/PMC9307793.

[83] Matthieu Bellec, Ulrich Kuhl, Gilles Montambaux, and Fabrice Mortessagne. "Topological Transition of Dirac Points in a Microwave Experiment". In: *Phys. Rev. Lett.* 110 (3 2013), p. 033902. DOI: 10.1103/PhysRevLett.110.033902. URL: https://link.aps.org/doi/10.1103/PhysRevLett.110.033902.

[84] Junjie Lu, Jiongning Che, Xiaodong Zhang, and Barbara Dietz. "Experimental and numerical investigation of parametric spectral properties of quantum graphs with unitary or symplectic symmetry". In: *Phys. Rev. E* 102 (2 2020), p. 022309. DOI: 10.1103/PhysRevE.102.022309. URL: https://link.aps.org/doi/10.1103/PhysRevE.102.022309.

[85] A. Rehemanjiang, M. Allgaier, C. H. Joyner, S. Müller, M. Sieber, U. Kuhl, and H.-J. Stöckmann. "Microwave Realization of the Gaussian Symplectic Ensemble". In: *Phys. Rev. Lett.* 117 (6 2016), p. 064101. DOI: 10.1103/PhysRevLett.117.064101. URL: https://link.aps.org/doi/10.1103/PhysRevLett.117.064101.

[86] Afshin Akhshani, Małgorzata Białous, and Leszek Sirko. "Quantum graphs and microwave networks as narrow-band filters for quantum and microwave devices". In: *Phys. Rev. E* 108 (3 2023), p. 034219. DOI: 10.1103/PhysRevE.108.034219. URL: https://link.aps.org/doi/10.1103/PhysRevE.108.034219.

[87] Oleh Hul, Szymon Bauch, Prot Pakoński, Nazar Savytskyy, Karol Życzkowski, and Leszek Sirko. "Experimental simulation of quantum graphs by microwave networks". In: *Phys. Rev. E* 69 (5 2004), p. 056205. DOI: 10.1103/PhysRevE.69.056205. URL: https://link.aps.org/doi/10.1103/PhysRevE.69.056205.

[88] Zeyun Fu, Trystan Koch, Thomas M. Antonsen, Edward Ott, and Steven Mark Anlage. "Experimental Study of Quantum Graphs with Simple Microwave Networks: Non-Universal Features". In: *Acta Physica Polonica A* 132 (2017), pp. 1655–1660. URL: https://api.semanticscholar.org/CorpusID:41306657.

[89] I. C. Fulga, F. Hassler, and A. R. Akhmerov. "Scattering theory of topological insulators and superconductors". In: *Phys. Rev. B* 85 (16 2012), p. 165409. DOI: 10.1103/PhysRevB.85.165409. URL: https://link.aps.org/doi/10.1103/PhysRevB.85.165409.

[90] Maxine M. McCarthy and D. M. Whittaker. *A Topological Classification of Finite Chiral Structures using Complete Matchings.*

[91] Raul A. Monsalve, Alan E. E. Rogers, Thomas J. Mozdzen, and Judd D. Bowman. "One-Port Direct/Reverse Method for Characterizing VNA Calibration Standards". In: *IEEE Transactions on Microwave Theory and Techniques* 64.8 (2016), pp. 2631–2639. DOI: 10.1109/TMTT.2016.2580141.

[92] Rakesh Kumar Malakar and Asim Kumar Ghosh. “Engineering topological phases of any winding and Chern numbers in extended Su–Schrieffer–Heeger models”. In: *Journal of Physics: Condensed Matter* 35.33 (2023), p. 335401. DOI: 10.1088/1361-648X/acd15d. URL: https://dx.doi.org/10.1088/1361-648X/acd15d.

[93] AIM Minimum Rank – Special Graphs Work Group. “Zero forcing sets and the minimum rank of graphs”. In: *Linear Algebra and its Applications* 428.7 (2008), pp. 1628–1648. ISSN: 0024-3795. DOI: https://doi.org/10.1016/j.laa.2007.10.009. URL: https://www.sciencedirect.com/science/article/pii/S0024379507004624.

[94] Yu Jing, Wenqian Zhang, and Shengjin Ji. “The Zero Forcing Number of Graphs with the Matching Number and the Cyclomatic Number”. In: *Graphs and Combinatorics* 39 (2023), p. 72. DOI: https://doi.org/10.1007/s00373-023-02664-6.

[95] E. Clar and C.C. Mackay. “Circobiphenyl and the attempted synthesis of 1:14, 3:4, 7:8, 10:11-tetrabenzoperopyrene”. In: *Tetrahedron* 28.24 (1972), pp. 6041–6047. ISSN: 0040-4020. DOI: https://doi.org/10.1016/0040-4020(72)88138-9. URL: https://www.sciencedirect.com/science/article/pii/0040402072881389.

[96] S.J. Cyvin and I. Gutman. “Kekulé Structures and their Symmetry Properties”. In: *Symmetry*. Ed. by István Hargittai. Pergamon, 1986, pp. 859–876. ISBN: 978-0-08-033986-3. DOI: https://doi.org/10.1016/B978-0-08-033986-3.50061-6. URL: https://www.sciencedirect.com/science/article/pii/B9780080339863500616.

[97] Aug. Kekulé. “Sur La Constitution Des Substances Aromatiques”. In: *Bull. Soc. Chim. Fr.* 3 (1865), pp. 98–111.

[98] Aug. Kekulé. “Untersuchungen über aromatische Verbindungen Ueber die Constitution der aromatischen Verbindungen. I. Ueber die Constitution der aromatischen Verbindungen.” In: *European Journal of Organic Chemistry* 137 (1866), pp. 129–196. URL: https://api.semanticscholar.org/CorpusID:94935559.

[99] Shantanu Mishar, Doreen Beyer, Kristjan Eimre, Shawulienu Kezilebieke, Reinhard Berger, Oliver Gröning, Carlo A. Pignedoli, Klaus Müllen, Peter Liljeroth, Pascal Ruffieux, Xinliang Feng, and Roman Fasel. “Topological frustration induces unconventional magnetism in a nanographene”. In: *Nat. Nanotechnol.* 15 (2020), pp. 22–28.

[100] Irene Sciriha, Xandru Mifsud, and James L. Borg. “Nullspace vertex partition in graphs”. In: *Journal of Combinatorial Optimization* 42 (2020), pp. 310 –326. URL: https://api.semanticscholar.org/CorpusID:210473039.

[101] Barry T. Pickup. *Private communication.*

[102] Elliott Lieb and Daniel Mattis. “Ordering Energy Levels of Interacting Spin Systems”. In: *Journal of Mathematical Physics* 3.4 (July 1962), pp. 749–751. ISSN: 0022-2488. DOI: 10.1063/1.1724276. eprint: https://pubs.aip.org/aip/jmp/article-pdf/3/4/749/19167430/749_1_online.pdf. URL: https://doi.org/10.1063/1.1724276.

[103] Elliott H. Lieb. "Two theorems on the Hubbard model". In: *Phys. Rev. Lett.* 62 (10 1989), pp. 1201–1204. DOI: 10.1103/PhysRevLett.62.1201. URL: https://link.aps.org/doi/10.1103/PhysRevLett.62.1201.

[104] Elliott Lieb, Theodore Schultz, and Daniel Mattis. "Two soluble models of an antiferromagnetic chain". In: *Annals of Physics* 16.3 (1961), pp. 407–466. ISSN: 0003-4916. DOI: https://doi.org/10.1016/0003-4916(61)90115-4. URL: https://www.sciencedirect.com/science/article/pii/0003491661901154.

[105] A.A. Ovchinnikov. "Multiplicity of the ground state of large alternant organic molecules with conjugated bonds". In: *Theoret. Chim. Acta* (1978), pp. 297–304. DOI: 10.1007/BF00549259. URL: https://doi.org/10.1007/BF00549259.

[106] A. García-Fuente, D. Carrascal, G. Ross, and J. Ferrer. "Full analytical solution of finite-length armchair/zigzag nanoribbons". In: *Phys. Rev. B* 107 (11 2023), p. 115403. DOI: 10.1103/PhysRevB.107.115403. URL: https://link.aps.org/doi/10.1103/PhysRevB.107.115403.

[107] Ian Mondragon-Shem, Taylor L. Hughes, Juntao Song, and Emil Prodan. "Topological Criticality in the Chiral-Symmetric AIII Class at Strong Disorder". In: *Phys. Rev. Lett.* 113 (4 2014), p. 046802. DOI: 10.1103/PhysRevLett.113.046802. URL: https://link.aps.org/doi/10.1103/PhysRevLett.113.046802.

[108] Barry T. Pickup and Patrick W. Fowler. "An analytical model for steady-state currents in conjugated systems". In: *Chemical Physics Letters* 459 (2008), pp. 198–202. URL: https://api.semanticscholar.org/CorpusID:98386414.

[109] Zhida Song, Zhong Fang, and Chen Fang. "$(d-2)$-Dimensional Edge States of Rotation Symmetry Protected Topological States". In: *Phys. Rev. Lett.* 119 (24 2017), p. 246402. DOI: 10.1103/PhysRevLett.119.246402. URL: https://link.aps.org/doi/10.1103/PhysRevLett.119.246402.

[110] Wladimir A. Benalcazar and Alexander Cerjan. "Chiral-Symmetric Higher-Order Topological Phases of Matter". In: *Phys. Rev. Lett.* 128 (12 2022), p. 127601. DOI: 10.1103/PhysRevLett.128.127601. URL: https://link.aps.org/doi/10.1103/PhysRevLett.128.127601.

[111] Frank Schindler, Ashley M. Cook, Maia G. Vergniory, Zhijun Wang, Stuart S. P. Parkin, B. Andrei Bernevig, and Titus Neupert. "Higher-order topological insulators". In: *Science Advances* 4.6 (2018), eaat0346. DOI: 10.1126/sciadv.aat0346. eprint: https://www.science.org/doi/pdf/10.1126/sciadv.aat0346. URL: https://www.science.org/doi/abs/10.1126/sciadv.aat0346.

[112] Eslam Khalaf. "Higher-order topological insulators and superconductors protected by inversion symmetry". In: *Phys. Rev. B* 97 (20 2018), p. 205136. DOI: 10.1103/PhysRevB.97.205136. URL: https://link.aps.org/doi/10.1103/PhysRevB.97.205136.

[113] Hong Wang and Xiaoyu Zhu. "Higher-order topological superconductors characterized by Fermi level crossings". In: *Phys. Rev. B* 108 (12 2023), p. 125426. DOI: 10.1103/PhysRevB.108.125426. URL: https://link.aps.org/doi/10.1103/PhysRevB.108.125426.

[114] Sayed Ali Akbar Ghorashi, Tianhe Li, and Taylor L. Hughes. "Higher-Order Weyl Semimetals". In: *Phys. Rev. Lett.* 125 (26 2020), p. 266804. DOI: 10.1103/PhysRevLett.125.266804. URL: https://link.aps.org/doi/10.1103/PhysRevLett.125.266804.

[115] Luka Trifunovic and Piet W. Brouwer. "Higher-Order Bulk-Boundary Correspondence for Topological Crystalline Phases". In: *Phys. Rev. X* 9 (1 2019), p. 011012. DOI: 10.1103/PhysRevX.9.011012. URL: https://link.aps.org/doi/10.1103/PhysRevX.9.011012.

[116] Eslam Khalaf, Hoi Chun Po, Ashvin Vishwanath, and Haruki Watanabe. "Symmetry Indicators and Anomalous Surface States of Topological Crystalline Insulators". In: *Phys. Rev. X* 8 (3 2018), p. 031070. DOI: 10.1103/PhysRevX.8.031070. URL: https://link.aps.org/doi/10.1103/PhysRevX.8.031070.

[117] F.D.R. Santos and R.G. Dias. "Methods for the construction of interacting many-body Hamiltonians with compact localized states in geometrically frustrated clusters". In: *Sci Rep* 10 (2020), p. 4532. DOI: https://doi.org/10.1038/s41598-020-60975-7. URL: https://www.nature.com/articles/s41598-020-60975-7.

[118] Elena Garuccio, Margherita Lalli, and Diego Garlaschelli. "Multiscale network renormalization: Scale-invariance without geometry". In: *Phys. Rev. Res.* 5 (4 2023), p. 043101. DOI: 10.1103/PhysRevResearch.5.043101. URL: https://link.aps.org/doi/10.1103/PhysRevResearch.5.043101.

[119] Pablo Villegas, Tommaso Gili, Guido Caldarelli, and Andrea Gabrielli. "Laplacian renormalization group for heterogeneous networks". In: *Nat. Phys.* 19 (2023), pp. 445–450. DOI: 10.1038/s41567-022-01866-8. URL: https://doi.org/10.1038/s41567-022-01866-8.

[120] B Barzel and A L Barabáso. "Universality in network dynamics". In: *Nat. Phys.* 9 (2013), pp. 673–681. DOI: 10.1038/nphys2741. URL: https://doi.org/10.1038/nphys2741.